A TRIDENT SCHOLAR PROJECT REPORT

NO. 240

THE EFFECTS OF INLET DUCTING GEOMETRIES ON THE
PERFORMANCE CHARACTERISTICS OF WATERJET ENGINES
PHASE I: MEASUREMENT OF PRESSURE DISTRIBUTIONS

UNITED STATES NAVAL ACADEMY
ANNAPOLIS, MARYLAND

20000406 053

REPORT DOCUMENTATION PAGE

Public reporting burden for this collection of information is estimated to average 1 hour per response, including the time for reviewing instructions, searching existing data sources, gathering and maintaining the data needed, and completing and reviewing the collection of information. Send comments regarding this burden estimate or any other aspect of this collection of information, including suggestions for reducing this burden, to Washington Headquarters Services, Directorate for Information Operations and Reports, 1215 Jefferson Davis Highway, Suite 1204, Arlington, VA 22202-4302, and to the Office of Management and Budget Paperwork Reduction Project (0704-0188), Washington, DC 20503.

1. AGENCY USE ONLY (*Leave Blank*)	2. REPORT DATE 1996	3. REPORT TYPE AND DATES COVERED

4. TITLE AND SUBTITLE

The effects of inlet ducting geometries on the performance characteristics of waterjet engines
Phase 1: Measurement of pressure distributions

5. FUNDING NUMBERS

6. AUTHOR(S)

Loustaunau, Shelly M.

7. PERFORMING ORGANIZATION NAME(S) AND ADDRESS(ES)

8. PERFORMING ORGANIZATION REPORT NUMBER

9. SPONSORING/MONITORING AGENCY NAME(S) AND ADDRESS(ES)

United States Naval Academy
Annapolis, MD 21402

10. SPONSORING/MONITORING AGENCY REPORT NUMBER

USNA Trident Scholar report; no. 240 (1996)

11. SUPPLEMENTARY NOTES

Accepted by the U.S.N.A. Trident Scholar Committee

12a. DISTRIBUTION/AVAILABILITY STATEMENT

Approved for public release; distribution unlimited.

12b. DISTRIBUTION CODE

UL

13. ABSTRACT (*Maximum 200 words*)

Currently, the U.S. military has shown interest in developing landing craft with waterjet engines. To date, little is known about the best shape for the inlet of the waterjet. The shape of the inlet is important, as separation effects and two phase flow can result in decreased efficiency of the engine. This project is the first of several phases involved in designing efficient waterjet engines. The main goal of the initial phase of the project is to develop an experimental technique to determine the pressure distribution under the hull of a ship near the inlet of the engines. Pressure readings from measuring devices are used to determine the pressure distribution under the aft section of the hull. The resultant pressure distribution can be used to design hulls with differently shaped inlets for the waterjet with a high degree of confidence. The technique for determining the pressure distribution can be used to test other hulls, providing information on the velocity distribution over the aft section of the hull.

14. SUBJECT TERMS

Waterjet; Pressure distribution on an hull; Hamilton cutter; Hydrodynamics; External flow; Design of ship hulls

15. NUMBER OF PAGES

173

16. PRICE CODE

17. SECURITY CLASSIFICATION OF REPORT	18. SECURITY CLASSIFICATION OF THIS PAGE	19. SECURITY CLASSIFICATION OF ABSTRACT	20. LIMITATION OF ABSTRACT
UNCLASSIFIED	UNCLASSIFIED	UNCLASSIFIED	UL

NSN 7540-01-280-5500

THE EFFECTS OF INLET DUCTING GEOMETRIES ON THE PERFORMANCE CHARACTERISTICS OF WATERJET ENGINES PHASE I: MEASUREMENT OF PRESSURE DISTRIBUTIONS
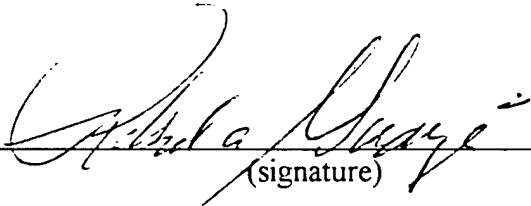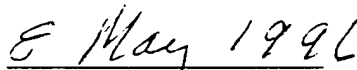
by

Midshipman Shelly M. Loustaunau, Class of 1996
United States Naval Academy
Annapolis, Maryland
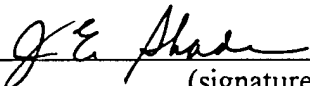
_____
(signature)

Certification of Adviser Approval

Professor Robert Granger
Department of Mechanical Engineering

_____
(signature)

_____
(date)

Acceptance for the Trident Scholar Committee

Professor Joyce E. Shade
Chair, Trident Scholar Committee

_____
(signature)

_____
(date)

USNA - 1531 - 2

ABSTRACT

Currently, the U.S. military has shown interest in developing landing craft with waterjet engines. To date, little is known about the best shape for the inlet of the waterjet. The shape of the inlet is important, as separation effects and two phase flow can result in decreased efficiency of the engine. This project is the first of several phases involved in designing efficient waterjet engines. The main goal of the initial phase of the project is to develop an experimental technique to determine the pressure distribution under the hull of a ship near the inlet of the engines. Pressure readings from measuring devices are used to determine the pressure distribution under the aft section of the hull. The resultant pressure distribution can be used to design hulls with differently shaped inlets for the waterjet with a high degree of confidence. The technique for determining the pressure distribution can be used to test other hulls, providing information on the velocity distribution over the aft section of the hull.

ACKNOWLEDGEMENTS

I would like to thank the members of the USNA Hydromechanics Lab staff for all the time they dedicated to this project. It would not have been successful without the expertise of Mr. Don Bunker, Mr. Steve Enzinger, and Mr. Norm Tyson. I would also like to express my gratitude to Mr. Tom Price of the USNA model shop for his enthusiasm for this project. His efforts were the key factor in the completion of the hull model. Finally, I feel the need to thank Professor Robert Granger of the Mechanical Engineering Department for his guidance throughout this year. He has offered suggestions and inspiring words that have been essential to the completion of the project.

TABLE OF CONTENTS

LIST OF FIGURES

LIST OF TABLES

1. INTRODUCTION

Since the end of the Cold War, the major threats to the United States and the world have changed drastically. The decreasing possibility of a global war, and the increase in regional conflicts have caused a major shift in the focus of the military. The need to quickly send troops into an area in response to a military crisis has become extremely important, as was shown in the fairly recent Desert Storm. The Marine Corps' response to this need has been through the use of amphibious landings. An effective landing requires that as many troops as possible get to the beach quickly, so there is always interest in developing faster and more efficient landing craft to accomplish this. One such vehicle, the Advanced Amphibious Assault Vehicle (AAAV), is currently being used. As always, the performance of vehicle is meticulously evaluated, and research is constantly being done to improve the effectiveness of the vehicle.

The AAAV uses a waterjet engine, which allows for speeds in excess of 30 knots, as well as higher maneuverability at low speeds and higher efficiency than propeller driven ships[1]. A waterjet engine can be thought of as a jet engine that uses water rather than air as the working fluid. The waterjet takes water in through an inlet located on the hull and pushes it through a series of impellers in a pump which in turn thrusts it out the back of the ship at extremely high speed (See Figure 1). An engine of this type is capable of very high speeds, as proven by the *Destriero*, the Italian super yacht which averaged more than 61 mph while crossing the Atlantic[1]. The water jet is more efficient than propeller driven ships, and it leaves less wake, thereby producing less fluidborne noise than a propeller. Since no external propellers are required, the vehicle can have a shallower draft, allowing it to

operate in shallow waters. There is also less chance of being damaged by any floating objects since all the propulsion equipment is contained within the vehicle, and the inlet is below the free surface of the water.

Essential to the efficient performance of the waterjet engines is knowledge of the pressure distribution at the pump inlet. Such a pressure distribution is dependent upon the velocity field across the waterjet inlet on the hull and on the ramp geometry. A major problem is that little is known about the best shape for the inlet. There has been very little testing of the pressure profiles or velocity fields surrounding the inlet, so it is currently difficult to design an efficient waterjet propulsion system.

The 21st International Towing Tank Conference Waterjet Group, composed of the world's leading experts on the subject of waterjets, has called the problem a very high risk task, one that has historically been filled with great uncertainty[2]. There are several reasons for this. First, the technology is highly proprietary, making it very difficult to find any literature on the subject. The privately owned corporations have worked with waterjet technology, but they are concerned with patent rights. Second, the subject is complex due to the enormous problems of measuring the pressure distributions around the hull and water entry inlets. This is partly due to cross flows, and partly due to secondary effects. In addition, there is the uncertainty of the precise description of the turbulent boundary layer. To make matters even more complicated, there is separation and cavitation that must be considered, plus the possibility the flow could be two-phase. In summary, though the task has been well defined, previous measurement techniques and procedures simply do not exist. This project requires going back to the fundamentals in order to devise a procedure[3]. The

present procedure itself is at high risk. There is no certainty for its success, since there is no information from previous investigations with which to make comparisons. It is interesting to point out that many companies (such as Hydrodynamics, Inc.) have spent thousands of man hours performing a similar investigation. The Hydrodynamics Inc. engineers tried to interpret their pressure data, with only partial success, yet for its time, their results and techniques were the best available.

The complexity of designing a waterjet engine requires that it be split into several phases, only one of which, the initial phase, is completed in this project. The goal of this project, therefore, is to study solely the pressure distributions on the aft section of a ship model. This information is necessary for the design of the ramp of the inlet, allowing minimum drag and maximum efficiency. A 1/36 scale model of a Hamilton class cutter is used to run through a series of baseline tests in order to determine the normal pressure distribution and subsequent velocity fields on the wetted surface of the aft section of the model. After studying these pressure distributions, it will then be possible to fit the stern with a bustle that represents the new geometry for the housing of the waterjet inlet, and measure the resultant form drag for various speeds. The data would then be compared to the baseline testing to determine how the performance characteristics change when an inlet is added. Another experimental phase would follow, where a method for collecting data will be used to test a model which has the bustle containing the newly designed ramp. This should provide accurate data showing exactly what the pressure and velocity distributions are under the hull when the waterjet engine is in use.

2. FACILITY

The experimental portion of this project takes place in the USNA 380-foot Hydrodynamics Tow Tank in Rickover Hall. A schematic of the facility is shown in Figure 2. Since the entire experiment is conducted in still water, the waveboard and the beach of Figure 2 are not used. The drydock and the fingerpier allow for the setup of the model in the water. From this area, the model can be easily moved into position under the carriage. The primary mover is the low speed carriage. It is capable of running at a constant speed along the rails running the length of the tank, requiring only small distances to accelerate and decelerate. The distance required to accelerate and decelerate varies with the desired speed, but for this experiment, the constant speed portion of the run is approximately 200 to 250 ft long.

The scale model is attached to the carriage using pitch and heave potentiometers, that allow the model to move freely in the vertical plane. Figure 3 shows the heave potentiometer as well as a block gage underneath it. The pitch potentiometer is under the block gage, but is not in view in the figure. The heave potentiometer is connected to the carriage. The ability to move in the vertical plane allows the pitch and heave to be consistent with what would be expected for the same type of ship at that speed. The model is constrained in the horizontal plane, thereby preventing the model from yawing. The Tow Tank facility uses a specially designed data acquisition system (Hydromechanics Laboratory System, HLS) for data acquisition. Pressure transducers convert the mechanical force into an electrical signal, which can be transmitted to the HLS computer. The computer has preassigned channels for each signal, so it can distinguish one signal from another. Twenty-

eight channels are available on the HLS system, so a maximum of twenty-eight data points can be gathered for each run.

When the transducer measures a pressure, it does not always return to the zero point, a phenomena called drifting. Prior to each run, all twenty-eight channels must be rezeroed in order to eliminate the effects of the drifting that may have occurred. When the model is stationary, the pressures measured by the transducers are not zero, but they are defined as zero so data can be compared. The zeroing is done by taking a reading in still water. The computer reads a voltage that corresponds to the pressure on the transducer. This voltage is correlated to zero pressure, so any change from the corresponding pressure will result in a pressure measurement. The computer receives data from the pressure transducers at a specified sampling rate of 50 HZ during the test. When the run is complete, the computer has acquired several data points for each channel. The data is truncated, meaning that the portions of the run when the carriage is accelerating and decelerating are ignored, and an average value of the remaining pressures is taken and used in defining the pressure distribution to be presented later in the report. Since the computer acquires data in voltages, calibration is required to transform the voltages into pressures.

3. HAMILTON MODEL

The model used in all the testing for this experiment was constructed in the Model Shop in Rickover Hall. Using the lines of form, the measurements for a 1/36 scale model are calculated, and a computer machines a block of foam to the measurements of different

stations in the model. This leaves a block of foam with the general shape of the hull, but ridges remain because the machine only cuts at discrete locations. The foam must be sanded to get a smooth hull shape. A fiberglass cast is then placed over the hull shape. When the cast has hardened, the foam can be removed, leaving a smooth mold from which to make the model. The model is constructed by laying fiberglass sheets soaked in resin inside the mold. It is important that the sheets are flat, allowing no wrinkles or air bubbles. Several layers of fiberglass are used to make the hull walls. Once it has hardened, the model is removed from the mold. The skeg is constructed separately, also made from fiberglass, and attached to the hull at the geometrically similar location to the prototype.

The finished model is 116.67 in. long with a beam width of 14 in. The final steps of the finishing process include painting the outside hull, adding a grid with the waterline appropriately marked, and installing the pressure measurement devices.

4. CALIBRATION OF EQUIPMENT

Several different types of instruments are used in this experiment, including Honeywell pressure transducers, a Validyne pressure transducer, a boundary layer rake, a Pitot-static tube, a block gage, a pitch potentiometer, and a heave potentiometer.

It is very important that all the instruments are carefully calibrated prior to being installed in the model to insure that the readings from each instrument are reliable. Calibration of the each pressure sensor became a time consuming project because no one at the Naval Academy has ever dealt with Honeywell transducers before or tried to measure pressure distributions on the hulls of ship models.

The Honeywell transducer is a type of strain-gage transducer, which means that the pressure applied to it causes a diaphragm to deform. The change in resistance of a strain-gage connected to the diaphragm is measured by a Wheatstone bridge circuit[4]. The changed resistance causes a changed voltage output according to Ohm's law. The voltage is measured by a voltmeter. A calibration curve must be created which will enable the voltage to be converted to a pressure.

In order to use the transducers, static calibration curves must be created for the Honeywell transducers. Two different transducers are used: one with a range of +/- 5 psi, and three with a range of 0 to 5 in. of water. The set-up for the static calibration is shown in Figure 4. A bucket of water connected to the transducer by a small piece of Tygon tubing can be raised or lowered to produce different pressures. Like all pressure transducers, there must be a reference. In this case, the reference port is open to the atmosphere, so the pressure measured is with respect to atmospheric pressure. To avoid the possible effects of any compressibility of the air inside the tubes leading to the transducer, the tubes must be completely filled with water. In the configuration shown in Figure 4, this is done by simply opening the valve between the bucket and the tubing and holding the tube lower than the bucket so water flows all the way through it. When no air bubbles are left in the tube, it can be connected to the transducer, while still being held below the bucket. To begin the calibration, a zero point must be established. The transducer is located as close as possible to the surface of the water in the bucket when the bucket is at its lowest point. In this configuration, the pressure is defined as zero. When the bucket is elevated one inch from its original position, the pressure on the transducer should read one inch of water. Using

this method, the voltages corresponding to different pressures are recorded using the HLS computer. Figure 5 shows the static calibration curves for both types of Honeywell transducers. The 5-in. of water sensor proves to be very consistent with that given by the manufacturer, with a change of one volt corresponding to the change in pressure of one inch of water. Note, the static calibration curve is linear, as expected. The manufacturer's value of repeatability is +/- 0.25 % of the full scale, which means this transducer should be accurate to +/- 0.01 in of water. The same method is used to find the static calibration for the +/- 5 psi transducers. The results of the calibration show in Figure 5 that one volt corresponds to 2 psi. It is important at this point to note the difference in the voltages for the two transducers. The 5 in. of water transducer has a much smaller range than the +/- 5 psi transducer, so each volt represents a smaller difference in pressure, making it useful in resolving very small differences in pressure. In the +/- 5 psi transducers, the manufacturer's value for repeatability is 0.15 % of the full scale, so they are accurate to the nearest 0.01-psi.

The Validyne transducer is also calibrated using a bucket method. Since the reference port of this transducer may be exposed to water, the set-up is slightly different than used above. Two buckets are required for this calibration. The first bucket acts as a reference. It is connected to the reference port. The second bucket is used to change the pressure. Before the calibration can begin, the levels of water in the buckets are equalized in order to obtain a zero reading. This is done by connecting the valves on the bottom of each bucket with a piece of Tygon tubing and allowing the water to flow freely between them. Once the water levels reach static equilibrium, the pressure reading from the

transducer is recorded as zero, and one of the valves is closed to prevent water from continuing to flow between the buckets. The static calibration of Figure 5 shows one volt equals 5 psi. The transducer has a range of +/- 0.5 psi and a repeatability of 0.5 % of full scale. This means that it is accurate to 0.0025 psi.

For the dynamic calibration, a rectangular airfoil with a 1/64 in. diameter hole on the leading edge is constructed and set up on the towing carriage as shown in Figure 6. A hypodermic tube connects the hole on the leading edge to the transducer. As the airfoil is pulled through the water in the USNA 120-ft Tow Tank, the stagnation pressure is measured using both of the Honeywell and the Validyne transducers. To avoid any effects of trapped air in the tube between the leading edge and the transducer, the tube must be carefully filled with water. Filling the tube requires a syringe, which is used to push water through the tube , thereby pushing the air out. When the tube is then connected to the transducer, a negligible volume of air is left inside the port.

To obtain positive pressure readings for the 0 to 5 in. of water Honeywell transducer, it is necessary to have the transducer at the same level or lower than the height of the pressure port it is reading, in this case, the small hole on the leading edge of the airfoil. Again, this is due to the fact that the reference port is open to the atmosphere. To position the transducer where it can measure positive pressures, a coffee can is clamped behind the airfoil with the can's bottom in the water. The transducer is then placed inside the can. This setup is slightly different than the one shown in Figure 6, as the coffee can would be suspended from a separate strut several inches behind the airfoil.

The results of this test for the Honeywell transducer yield the dynamic calibration

curve of Figure 7. The figure shows the pressure measured at different speeds. The data

points in these figures are compared against theoretical values obtained using

Bernoulli's equation:

$$P_1 + \frac{1}{2}\rho V_1^2 + \gamma z_1 = P_2 + \frac{1}{2}\rho V_2^2 + \gamma z_2 \qquad (1)$$

In this equation, P is the static pressure (the familiar pressure of a fluid), the term $\frac{1}{2}\rho V^2$ is

the dynamic pressure (pressure caused by motion) where ρ is the density and V is the

velocity, and the term γz is the hydrostatic pressure (the pressure due to the weight of the

fluid) where γ is the specific weight and z is the height. The subscripts 1 and 2 represent

different locations along the same streamline. Bernoulli's equation is simplified by assuming

that there is no significant change in height. The static pressure, P_1, is set at zero before the

test is conducted. Since the stagnation pressure, P_2, is being measured, the stagnation

velocity, V_2, is also zero. These assumptions result in the equation:

$$\frac{1}{2}\rho V_1^2 = P_2 \qquad (2)$$

When the stagnation pressures found using Equation (2) are plotted in Figure 7, the

experimental data are very close to that predicted by theory. The experimental

measurements are lower than the theoretical values, but they are within the experimental

accuracy of 7%.

The dynamic test must be performed one more time using the Validyne transducer.

Since the reference port on the Validyne transducer is a wet port, it is not referenced to

atmospheric pressure. Instead, it can be referenced to the static pressure of the water at the hole in the leading edge of the airfoil. This is done using a column of water to provide the same amount of pressure. The coffee can is filled with water and attached to the same strut as the airfoil. A tube from the transducer to the coffee can is adjusted so the transducer gives a zero reading when the airfoil is stationary. The Validyne transducer dynamic calibration curve of Figure 8 shows that this transducer is accurate to 7 %.

The boundary layer rake, shown in Figure 9, is designed and built specifically for this project. The calibration of the boundary layer rake is more difficult than the calibrations of the other instruments. Figure 10 shows a schematic of the boundary layer rake. It has 7 probes, numbered 1 - 7, each at a different vertical distance from the ship's hull. The bottom of the rake is flush with the hull, so the probes are exposed to the water moving past the hull as shown in Figure 9. The purpose of the boundary layer rake is to measure the fluid velocity at different vertical distances from the hull. The fluid velocity distribution in a steady, laminar boundary layer flow past a thin flat plate is well-known theoretically[5]. As water flows past a boundary, shear stresses cause the water to flow at different velocities near the surface than it does in the free stream. Figure 11 shows the laminar velocity distribution past a stationary flat plate obtained experimentally, using dye to visualize the flow[6]. The flow of Figure 11 is not what the boundary layer on the hull looks like. It is presented merely to show what a typical laminar boundary layer looks like. On the hull, the boundary layer is found not to be laminar. In the present experiment, the fluid velocity at the hull surface is the same as the velocity of the hull, and decreases nonlinearly outward to zero velocity far from the hull surface.

To study a boundary layer, a long flat plate with a sharp leading edge is constructed and placed in the USNA 120-ft Tow Tank as shown in Figure 12a. The boundary layer rake mentioned earlier, is inserted into the plate as shown in Figure 12b. Towing a flat plate at low speeds, the goal is to measure the vertical pressure distribution and thus determine the velocity at different depths in the boundary layer. This requires that several of the ports be within the boundary layer, which is not the case when the plate is towed at a speeds of 2 -5 ft/s. There are two ways to create a thicker boundary layer: one is to tow at a lower speed, and the other is to use a longer plate. At low speeds, the pressures measured are expected to be extremely small, and in fact, they are so small that they are beyond the sensitivity of the transducers. Even when a larger plate is constructed, the speed still must be so low that the transducers cannot measure the pressure with any degree of accuracy. At a speed to create a thick enough boundary layer, the difference in the pressures is still within the tolerance of the transducer, so it cannot be read with any degree of accuracy. Since the model runs at much higher speeds than any used in previous testing, the pressure readings should be greater and thus easier to resolve.

Assuming ports 3 - 7 are in the free stream, they provided for very accurate pressure measurements. Figure 13 is an example of the measured pressure versus the towed velocity, for the case of port 6. The figure shows that the measurements from the probes are accurate, correlating extremely well with the theoretical values. Hence, the rake is an effective and reliable measuring instrument when it is used in the model.

The next phase of calibration involves the set-up of the model in the 380-ft Tow Tank. The model is mounted using a block gage that measures drag, a pitch potentiometer

that measures pitch, and a heave potentiometer that measures heave. The operation of the block gage is as follows. When the gage is acted upon by a shear force, the resistance of a strain gage changes, causing a change in the output voltage. The block gage is calibrated using predetermined weights. The calibration curve for the block gage is linear as seen in Figure 14. The pitch and heave potentiometers work in much the same way as the transducers. A change in angle or elevation of the model causes deformation in the potentiometer which, in turn, causes movement of a brush on a variable resistor, thereby changing the resistance of the potentiometer. Again, a changed resistance causes a change in voltage output, which can be correlated with the calibration of the instrument to yield a useful reading.

With the calibration of all the instrumentation complete, the techniques used to measure different pressures can now be developed.

5. MEASUREMENT TECHNIQUES

The Hamilton model has three different types of pressure sensors installed to give a variety of information on the different pressures existing under the hull. There are 42 pressure taps covering the port side aft section. Each port is flush with the hull, resulting in a static pressure at that point. Each port is numbered and laid out at certain prescribed positions on the hull as shown in Figure 15. The location of each port is descibed using x and y coordinates, where x is the distance from the bow of the model and y is the distance from the centerline. For each run, twenty-two of the ports are selected and hooked up to Honeywell pressure transducers mounted inside the hull. The connection of the static ports

to the pressure transducers is done the same way as discussed above in the calibration section.

The boundary layer rake of Figure 9 is also mounted on the starboard side. It is capable of being rotated +/- 15 degrees from the centerline. Due to the orientation of the rake in the model, the only way to physically adjust the angle of the rake when the model is in the water is to use a mirror in order to see the rake and an angular scale that had been sketched on the hull. The ability to rotate the rake allows a cross flow to be detected. The boundary layer rake measures the vertical pressure distribution near the hull at the axial location where the inlet to the ramp occurs. Knowing this pressure distribution leads to the determination of the velocity profile at the entrance to the ramp. Since only one pressure reading can be taken from each port on the rake, Honeywell transducers are used. With no reference static pressure, the pressure measured by the rake is the total pressure at a specific point. Since the pressures very close to the hull are expected to be on the order of + 0.1 psi, the Honeywell transducers with a range of 0 to 5 inches of water are used to obtain the necessary accuracy.

On the starboard side, located 97.5 in. from the bow and 1.5 in. outboard of the skeg, the Pitot-static tube of Figure 16 is mounted so that it is also capable of rotating +/- 15 degrees, as well as moving vertically. The Pitot-static tube is mounted with a fixed card at the top end, which shows the angle of the tube with respect to a line parallel of the centerline. The depth of the tube is determined by vernier marks on the tube that are referenced to a fixed support of known vertical position. Knowing the exact depth and angle of the Pitot-static tube allows the stagnation pressure to be measured at different

depths and in different directions to determine the velocity profile and thereby provide an alternate means to detect cross flow. The Pitot-static tube requires two wet ports, one for the stagnation pressure, and one for the static pressure, so a Validyne transducer is required to measure the dynamic pressure. The static pressure is attached to the reference port, and the stagnation pressure is attached to the remaining port. This set up allows the Pitot-static tube to be unaffected by any change in the waterline's height.

Each run yields 28 data points. All the desired parameters to be measured for each run are presented in Table 1. Because of the overwhelming amount of data, only a few parametric changes occur throughout the experiment.

Tests are run at the upper and lower limits of normal operation for a prototype waterjet propelled ship. Because the speed of an actual ship is not equal to that of a model, the speeds are scaled using Froude numbers, Fr:

$$Fr = \frac{V}{\sqrt{gl}} \tag{3}$$

In Equation (3), V is the velocity, g is the gravitational acceleration, and 'l' is a reference length. The desired speeds for the actual ship, 50.0 ft/s and 42.5 ft/s, correspond to Froude numbers of 0.47 and 0.40, respectively, which represent the upper and lower limits of normal operation for a waterjet propelled ship. By equating the Froude number for the actual ship with that of the model, the velocity of the model is found. The model speeds are 8.62 ft/s and 7.33 ft/s, corresponding to Froude numbers of 0.47 and 0.40, respectively.

The angles of the boundary layer rake and Pitot-static tube are between + and - 15 degrees, at five degree increments. Fifteen degrees on both sides are chosen because the

flow is expected to be normal to the rake at some angle in between those two extremes. The angular sign convention is arbitrarily assigned. The only important thing is that it is known and consistent throughout the experiment. A positive angle indicates that the tube is pointing inboard, and a negative angle indicates that it is pointing outboard as seen in Figure 17. The same sign convention is used for the boundary layer rake angles. The depth of the Pitot-static tube varies from 0 to 3 inches, in increments of 0.5 inches. The Pitot-static tube is deep enough to penetrate beneath the boundary layer and into the free stream.

Since most of the readings are independent of each other, (i.e. the depth of the Pitot-static tube does not effect the measurements of the static ports or boundary layer rake) fewer combinations than one may expect are possible. The test matrix in Table 2 shows all the runs necessary to get the data for all the test parameters. With the techniques for measurement laid out, the next step is developing a procedure to actually take measurements.

6. EXPERIMENTAL PROCEDURE

The following is the procedure used for making the measurements described in the Measurement Techniques section:

STEP 1: Adjust the Pitot-static tube to a desired depth and angle. Set the boundary layer rake at a desired angle.

STEP 2: Using the existing tow tank computer program for data acquisition, rezero all 28 channels. This requires the computer to read each value while the model is stationary, and assigning the prescribed amount of voltage as the zero point. Zeroing every channel

each time ensures that the reading found during the run is not offset in either direction.

STEP 3:   Set the desired speed on the tow tank control panel and start the run. The model accelerates to the predetermined velocity, and once there, data is acquired until the carriage decelerates to 0 velocity. The run at constant velocity is between 200 and 250 ft long, depending on the prescribed velocity.

STEP 4:   Once the run is complete, truncate the pressure data so that only the time when the carriage is running at its steady-state speed is considered. The pressure data collected during the acceleration and deceleration phases is ignored.

STEP 5:   Repeat steps 1 through 4 for each run on the test matrix. Due to the limited time allowed for use in the Tow Tank facility, the test matrix was modified slightly. All angles and depths of the Pitot-static tube were run, but some of the repetitive measurements of the static ports and the boundary layer rake ports had to be omitted.

7. DATA ANALYSIS

Once the data is collected, it must be put into a useable format. In this case, this is accomplished by transferring the data from the computer to a disk after each run. Then the data can be retrieved and recorded on worksheets, allowing maximum time in the tow tank to be spent making experimental runs. The data can be divided into three basic categories: data from the static ports, from the boundary layer rake, and from the Pitot-static tube. Each must be handled separately.

7.1) Static Port Analysis

Examining the test matrix of Table 2, one notes that numerous repetitive readings for the static ports are collected during the experiment. This is due to the fact that some of the test parameters remain fixed. There is nothing to change on the ports, so each run is repetitive. For each port with the exception of 36 and 38, approximately 20 readings were made. Chauvenet's criterion[7], a statistical method of rejecting spurious data points, is used to reject points in each set. The remaining pressure measurements are organized into spanwise (Figures 18 - 43), and chordwise (Figures 44 - 50) sets, and the pressure is plotted. The spanwise plots show the spread of data for all the ports at any given distance, y, from the centerline for each Froude number. The chordwise plots give the same information for all the ports for all the ports a given distance, x, from the bow of the ship. From this range of data, an average is taken to be used in further calculations. An uncertainty analysis for the static pressure ports is shown in Appendix A.

The average pressures must be corrected. This is due to the fact that the height of the waterline changes when the model moves through the water. To find the height of the waterline over the entire hull, a grid is painted on the port side of the model. During the first runs, the waterline is videotaped at each speed. When the tape is played in slow motion, the height of the waterline at each speed can be easily determined by projecting the video onto a screen, and reading the waterline height referenced to the grid. A 4th order best fit curve of the points collected represents the shape of the free surface along the side of the hull. Figures 58 and 59 show the resultant curves for the waterline. Substituting the x-coordinate of the static port, yields the height of the waterline at that port. Once the height of the waterline is known, a simple calculation gives the correction factor for that

port. By treating the amount of water above or below the static waterline as a column, the following hydrostatic equation can be applied:

$$P = \rho g h \qquad (4)$$

P is the pressure caused by a column of water at that height, h, which is what is being called the correction factor. If the waterline for the moving ship is lower than the static waterline, the correction factor is added to the measured pressure, and vice versa if the dynamic waterline is higher than the static waterline.

For each Froude number, the average pressure is taken and used in fitting three-dimensional surfaces to give a representation of the pressure distribution under the after part of the hull. Figure 60 shows the plots of the 7th order surfaces. The figures mentioned here are discussed more thoroughly in the Results section.

7.2) Boundary Layer Rake Analysis

With the data collected using the boundary layer rake, all spurious data points are omitted. The pressures at all the ports at each angle are plotted in Figures 61 - 74, as well as the pressures at all the angles for each port in Figures 75 - 86. The average pressure for each port must be corrected for the waterline variation, using the method discussed above, in Part 7.1 for the static port analysis..

Since the total pressure is measured at the boundary layer rake ports, the corrected value is the stagnation pressure. Using Bernoulli's Equation (1), the pressure is transformed into a velocity. Velocity profiles are shown in Figures 87 - 100 and are plotted for each

angle and each depth. The velocity profiles are then compared to a turbulent theoretical

velocity profile in the boundary layer, obtained using the Prandtl 1/7th law. The comparison

of the two is discussed further in the Results section.

To obtain a theoretical turbulent velocity profile, the bottom of the hull is assumed

to be a flat plate. The Reynolds number is found using:

$$Re = U_\infty \frac{x}{\nu} \qquad (5)$$

In Equation (5), U_∞ is the free stream velocity, x is the distance from the bow of the model,

and ν is the kinematic viscosity. For this case, the Reynolds number is $5*10^6$, which is ten

times greater than the transitional value of $5*10^5$. Therefore, the flow is assumed to be

turbulent at the position of the boundary layer rake. The thickness of the boundary layer,

δ, at this point is found using:

$$\delta = 0.37 x \left(\frac{1}{Re_x}\right)^{\frac{1}{5}} \qquad (6)$$

In Equation (6), Re_x is the local Reynolds number. At the boundary layer rake, the layer is

theoretically 1.65-in. thick when the model is towed at 7.33 ft/s (Fr = 0.40). This means

that all seven of the ports on the rake fall within the boundary layer. The velocity ratio

between the velocity at a given point and the towed velocity is related to the distance from

the port to the hull according to the turbulent boundary layer theory in Granger's Fluid

Mechanics[8]

$$\frac{u}{U_\infty} = \left(\frac{z}{\delta}\right)^{\frac{1}{7}} \qquad (7)$$

In Equation (7), u is the local mean velocity, U_∞ is the free stream velocity, z is the distance from the hull, and δ is the thickness of the boundary layer. Comparison between the experimental and theoretical plots at the different angles are shown in Figures 87 - 100. The results show that for a Froude number of 0.40, the 0 degree angle is considered to be closest to having results agreeing with the theoretical curve. For the Froude number of 0.47, the -5 degree angle result agrees closest to theory. This result confirms the existence of cross flow under the hull at high speeds. This is further discussed in the Results section.

7.3) Pitot-static Tube Analysis

The Pitot-static tube is different than the previous two categories in that since it had so many settings, only two measurements are acquired for each angle and depth, so no spread of data is possible and no error analysis can be made. Therefore, there is no justifiable way to reject certain data points. The two pressures and their average are plotted on two different plots. Figures 101 - 114 show every angle at a single depth, and Figures 115 - 128 show every depth at a certain angle. The spurious points become very noticeable. This technique allows for easy identification of the spurious data points. Because the Pitot-static tube has a reference static port, it does not need to be corrected for the waterline, but it does need to be corrected for the static pressure head. The static pressure head is measured using the static ports on the port side of the model. Since there is no static port in the exact position of the Pitot-static tube, approximations are made using the equations for the 3D surfaces of Figure 60 generated for the static ports.

Once the static head is subtracted from the actual readings, the stagnation pressures

remain. These pressures can be converted to velocities using Bernoulli's Equation (1). The resulting velocities are plotted in the same manner as the boundary layer rake profiles. It is interesting to note that in Figures 129 and 130, the edge of the boundary layer is apparent. The velocities are very different closer to the hull when the tube is in the boundary layer, but then fall on top each other when the tube is in the free stream.

8. RESULTS

The results obtained in this experiment far exceeded any expectations, because working with pressure readings is such a delicate and complex task, requiring a great deal of repeatability and accuracy. The results can be divided into the same three categories as the data analysis.

8.1) Static Port Analysis Results

The static pressure distributions under the hull are plotted in Figure 60 for both Froude numbers. These figures show that there is no uniform pressure distribution under the hull. Instead, there is a very complex flow in which the velocity varies not only with time, but also with location. Moving outboard from the centerline, the velocity is relatively constant until it hits the region of curvature toward the side of the hull. This is true for both Froude numbers. The exception to this trend is the region very close to the centerline, where the pressure is much lower than the surrounding area. This is possibly a result of the water flowing around the skeg, because separation, cavitation, and other effects may be present. Moving aft from the bow, the pressure drops considerably. This indicates that the

water is flowing more quickly at the stern than anywhere else. Figure 48 is a good example of how the flow varies at each location. The spread of data points at a given location is the effect of separation and turbulent flow. At port 30, which is right on the centerline, directly behind the skeg, a large variation of pressure is noticeable, due to flow irregularities caused by the skeg. Comparing the distributions for the two Froude numbers, one can see that they both follow similar trends. The noticeable difference is that at the higher Froude number, which corresponds to a higher velocity, the distribution has lower pressures. This is exactly what was expected.

At this point, there is unfortunately no theoretical data to compare and help validate these results. A computer simulation may be useful, but even with a computer it is extremely difficult to model such a complex flow, as was attempted. Any theoretical data obtained would be from a laminar approximation, since there exists no valid turbulent flow model. At best, the three-dimensional Navier-Stokes numerical code could only validate the trends. In the opinion of the investigator, this has been accomplished through experimentation.

From the pressure measurements, a velocity field can be calculated, as part of the next phase of the project. Knowing the velocity in that region allows, for example, the determination of the flowrate of the water into the inlet and through the waterjet. This is used in calculating the power of the waterjet, and other performance characteristics.

8.2) Boundary Layer Rake Analysis Results

Since the flow in the boundary layer is turbulent, the Prandtl 1/7th law is used to

calculate the theoretical velocity profile. The boundary layer should be approximately 1.65-in. thick for Fr = 0.40, and 1.60-in. thick for Fr = 0.47. The experimental data and best fit lines from the boundary layer rake are compared against the theoretical profile as shown in Figures 87 - 100. Since the rake does not have a port from which to read the velocity in the free stream, only the local velocities within the boundary layer can be compared. It is important to note that the Prandtl 1/7th law is based on flow over a flat plate. The bottom of the hull is not completely flat. While these lines have a definite correlation, it is likely that the 1/7th law is not the best description.

The velocity profile at the boundary layer rake is extremely important to those involved in the development of the waterjet because they need to know the exact velocity profile in order to design an efficient ramp.

8.3) Pitot-static Tube Analysis Results

The Pitot-static tube analysis is similar to that of the boundary layer rake in that both are used to measure velocity profiles. For the Pitot-static tube, the depth has a much larger range so some measurements are actually taken outside of the boundary layer. The slower velocities at the lower depths are the ones inside the boundary layer, and the profiles that fall very close to each other at the higher velocities are in the free stream as can be seen in Figures 129 and 130. The velocity profiles shown in these two figures are also very useful in determining whether or not cross flow exists. Plotting the towed velocity using the dotted lines of Figures 129 and 130 shows which angle is the closest to being directly in line with the flow. For either Froude numbers, the cross flow is seen to occur at about 10

degrees. A positive 10 degrees means that the water is flowing from inboard to outboard with respect to the centerline.

The method for measuring pressures under the hull is very useful. All three types of measurements yielded much better trends and correlations than anyone expected. These techniques will be very useful in further research on waterjet propulsion, especially in the design of an efficient ramp.

9. CONCLUSIONS

The following are the primary conclusions of this project:

1) A technique to measure the pressure distribution under the hull of a ship was developed in the USNA 380-ft Tow Tank facility.

2) The pressure distribution on the aft section of the hull was identified. It will lead to a full description of the velocity field, which will enable the calculation of the vorticity field, shear stress distribution, type and behavior of the boundary layer, location of separation and the separation line, contribution of drag due to the pressure field, and baseline data that will allow the inlet and ramp to be designed.

Date:

Run #:

Froude #:

PRESSURE SENSORS	
Number	Pressure
1	
2	
3	
4	
5	
6	
7	
8	
9	
10	
11	
12	
13	
14	
15	
16	
17	
18	
19	
20	
21	
22	
23	
24	
25	
26	
27	
28	
29	
30	
31	
32	
33	
34	
35	
36	
37	
38	
39	
40	
41	
42	
43	
44	
45	

BOUNDARY LAYER RAKE		
Setting	Port #	Pressure
	1	
	2	
	3	
	4	
	5	
	6	
	7	

PITOT TUBE		
Depth	Setting	Pressure

OTHER FACTORS			
Velocity	Pitch	Drag	Heave

Table 1   Readings taken on each run

TEST MATRIX FOR BASELINE TESTING

FROUDE # = 0.47

RUN #	B. L. RAKE Setting (deg)	PITOT TUBE Depth (in)	Setting (deg)
1	0	0	0
2	+5		+5
3	+10		+10
4	+15		+15
5	-5		-5
6	-10		-10
7	-15		-15
8	0	0.5	0
9	+5		-5
10	+10		+10
11	+15		+15
12	-5		-5
13	-10		-10
14	-15		-15
15	0	1	0
16	-5		-5
17	+10		+10
18	+15		+15
19	-5		-5
20	-10		-10
21	-15		-15
22	0	1.5	0
23	-5		-5
24	+10		+10
25	+15		+15
26	-5		-5
27	-10		-10
28	-15		-15
29	0	2	0
30	+5		+5
31	+10		+10
32	+15		+15
33	-5		-5
34	-10		-10
35	-15		-15
36	0	2.5	0
37	+5		+5
38	+10		+10
39	+15		+15
40	-5		-5
41	-10		-10
42	-15		-15
43	0	3	0
44	+5		+5
45	+10		+10
46	+15		+15
47	-5		-5
48	-10		-10
49	-15		-15

FROUDE # = 0.40

RUN #	B. L. RAKE Setting (deg)	PITOT TUBE Depth (in)	Setting (deg)
50	0	0	0
51	+5		-5
52	+10		+10
53	+15		+15
54	-5		-5
55	-10		-10
56	-15		-15
57	0	0.5	0
58	+5		-5
59	+10		+10
60	+15		+15
61	-5		-5
62	-10		-10
63	-15		-15
64	0	1	0
65	+5		-5
66	+10		+10
67	+15		+15
68	-5		-5
69	-10		-10
70	-15		-15
71	0	1.5	0
72	+5		-5
73	+10		+10
74	+15		+15
75	-5		-5
76	-10		-10
77	-15		-15
78	0	2	0
79	+5		+5
80	+10		+10
81	+15		+15
82	-5		-5
83	-10		-10
84	-15		-15
85	0	2.5	0
86	+5		+5
87	+10		+10
88	+15		+15
89	-5		-5
90	-10		-10
91	-15		-15
92	0	3	0
93	+5		+5
94	+10		+10
95	+15		+15
96	5		5
97	10		10
98	-15		+5

Table 2: Test matrix.
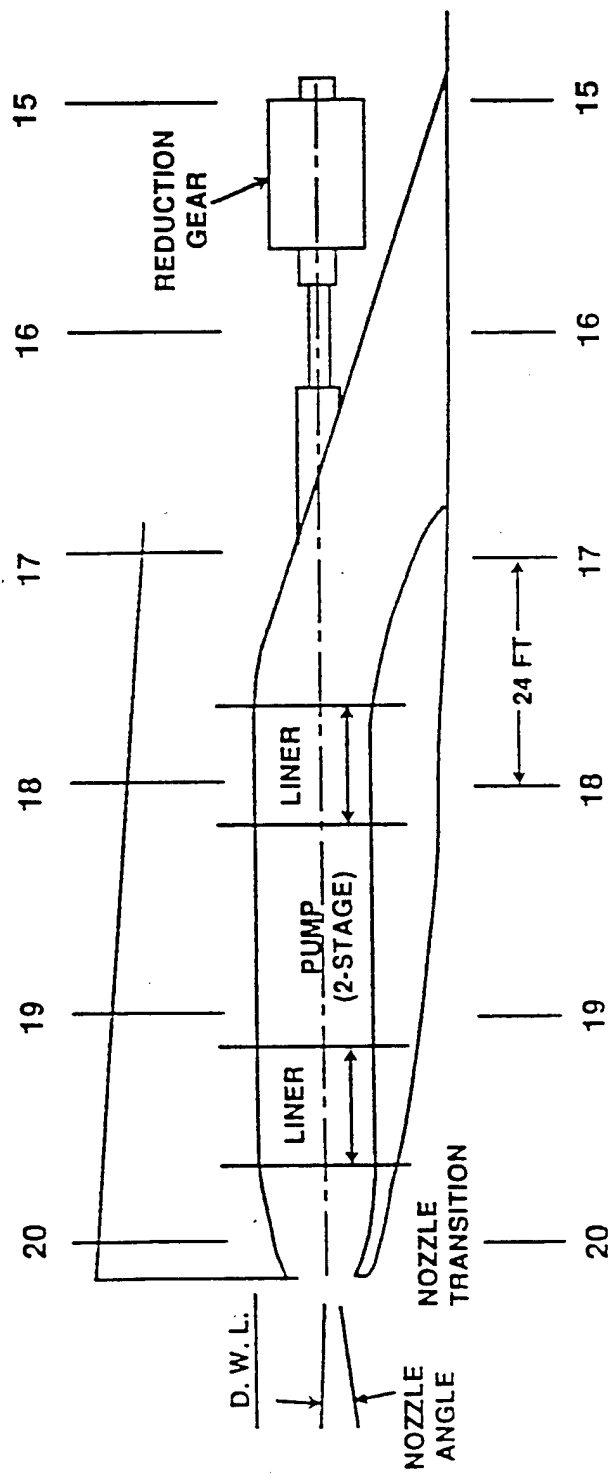
Figure 1: Baseline design of a waterjet engine.

U.S. NAVAL ACADEMY HYDROMECHANICS LABORATORY
380 FT TOWING TANK
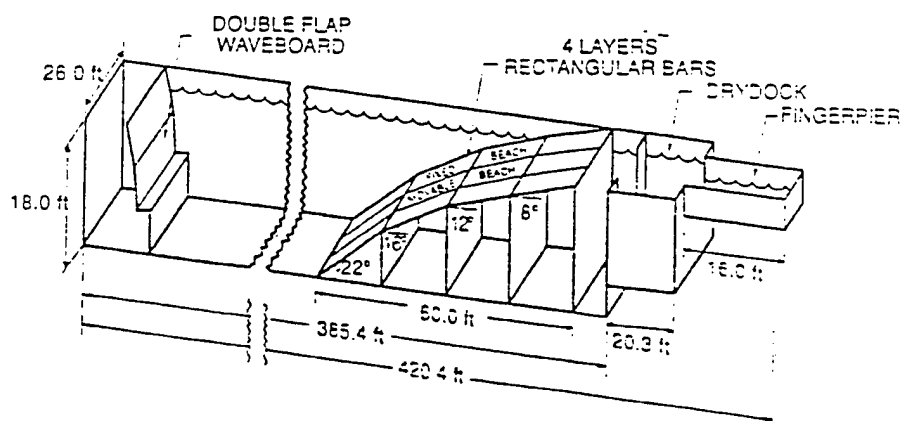
Notes: (1) Not to scale
        (2) All dimensions are inside measurements
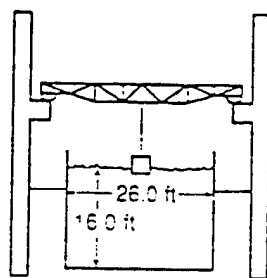
Figure 2 Schematic of USNA 380 ft Tow Tank.
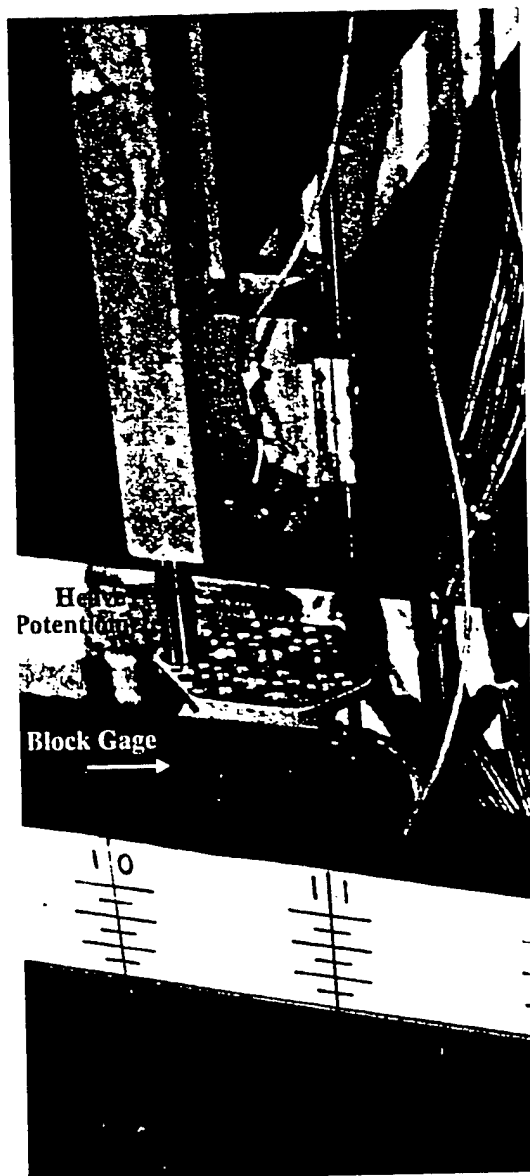
Figure 3: Photograph showing the model mounted to the carriage.
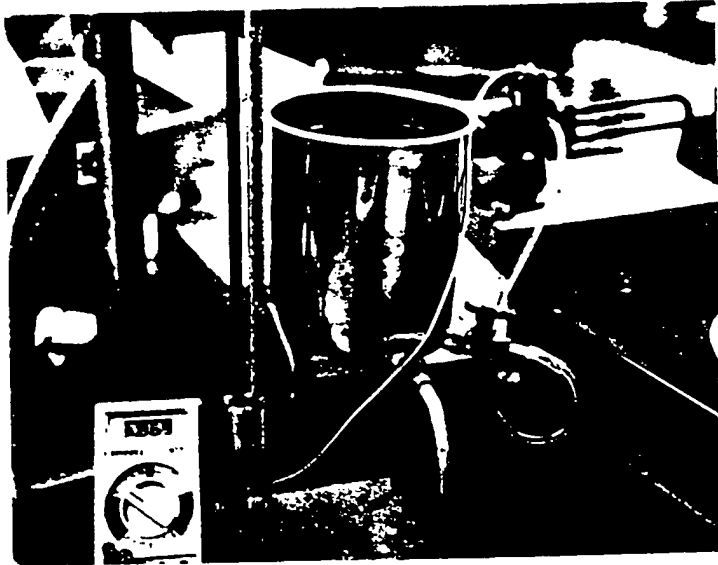
Figure 4 Static calibration set-up for Honeywell transducers
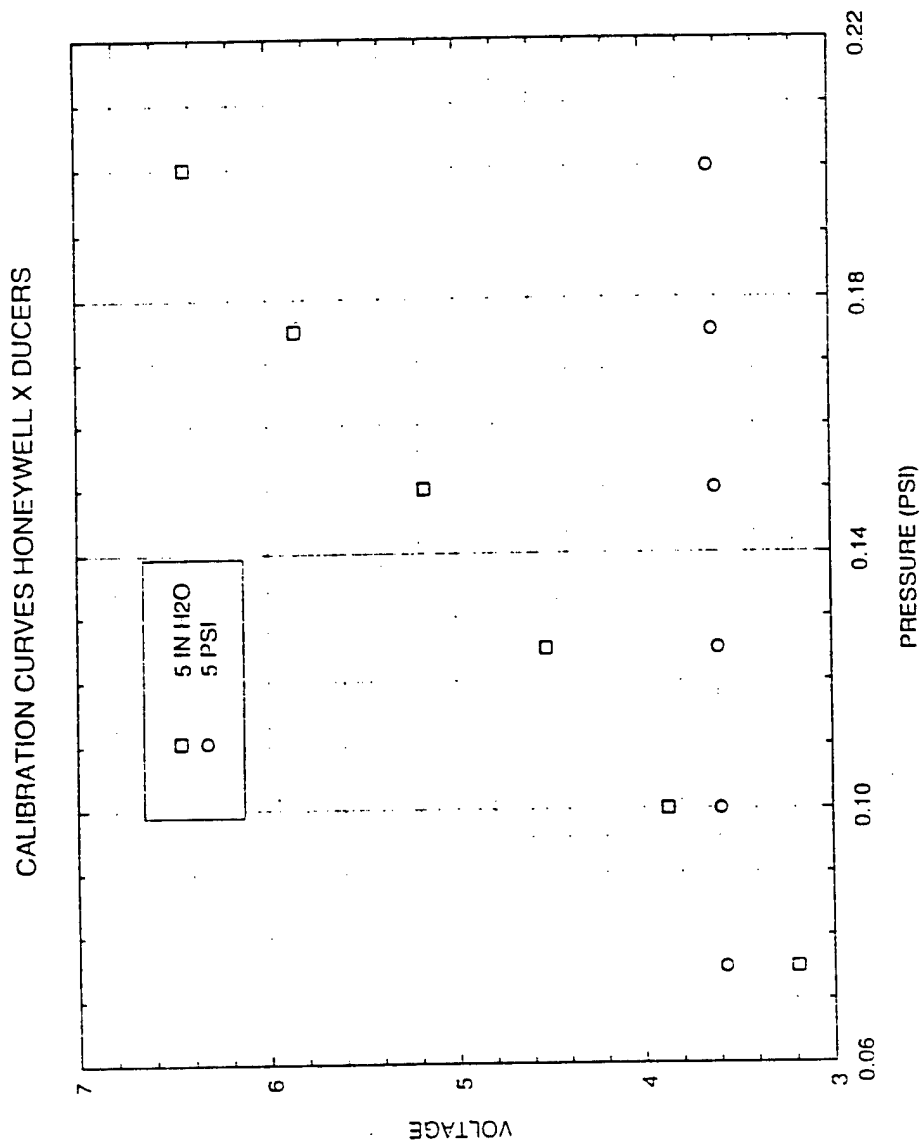
Figure 5: Static calibration curves for Honeywell transducers.
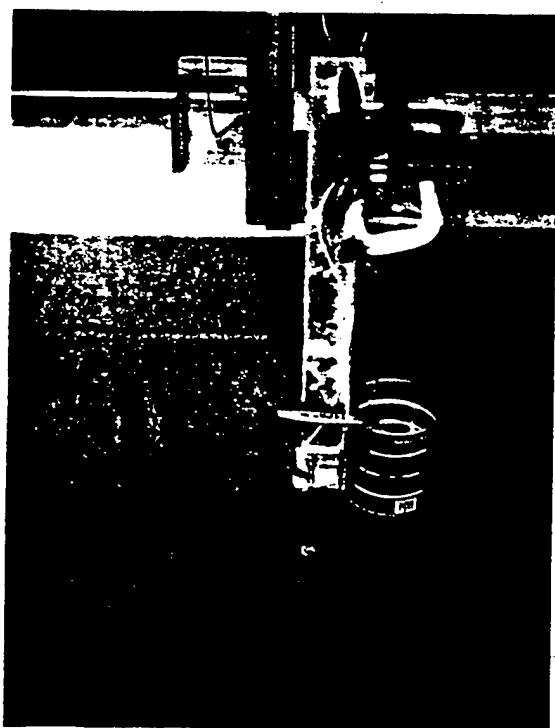
Figure 6 Dynamic calibration set-up for Validyne transducer.
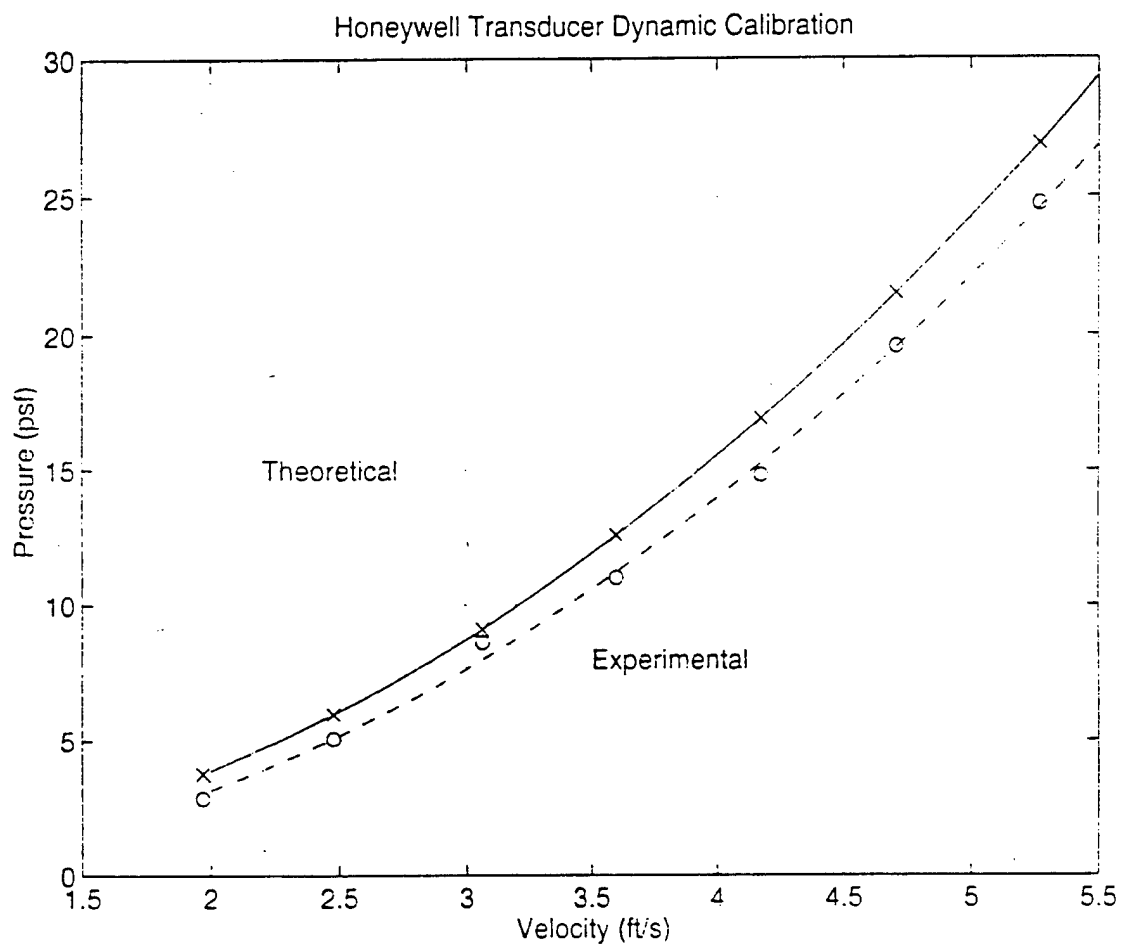
Figure 7 Dynamic calibration curve for Honeywell transducer
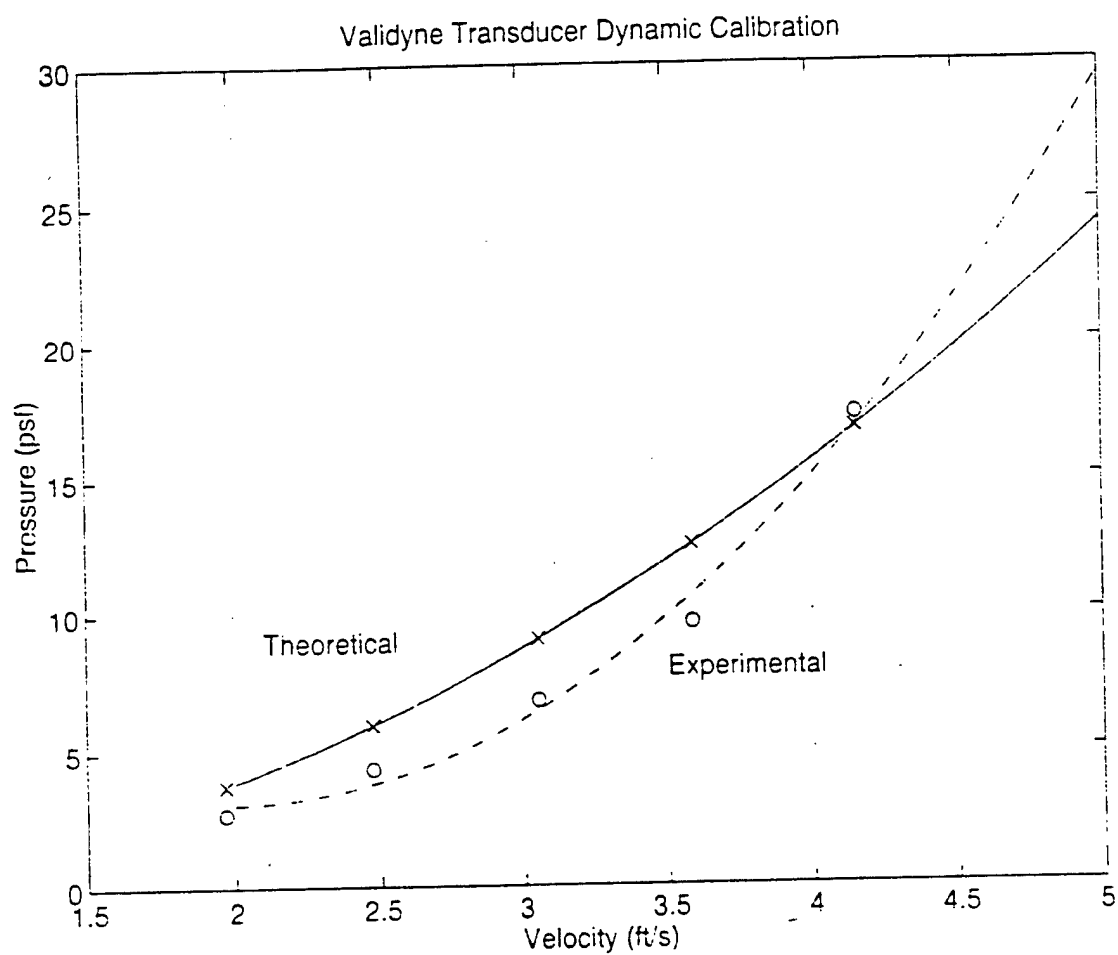
Figure 8 Dynamic calibration curve for Validyne transducer

Figure 9: The boundary layer rake.

Figure 10: Schematic of the boundary layer rake
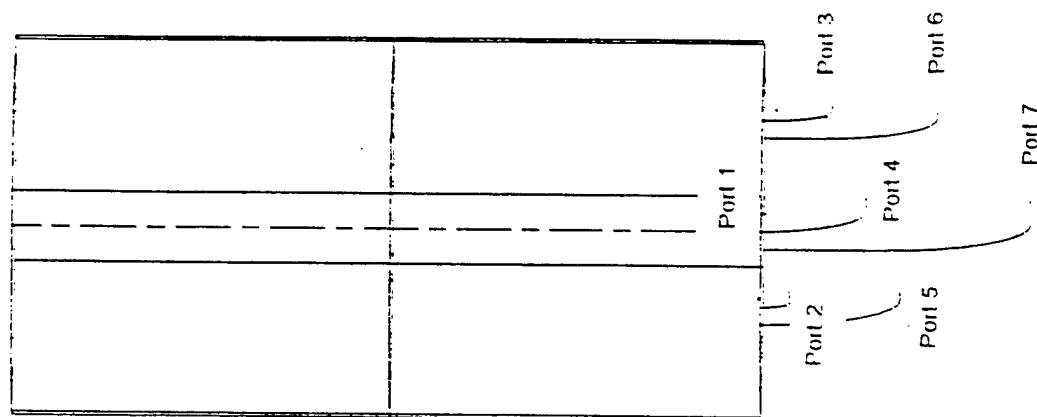
Boundary Layer Rake	
Port #	Depth (in)
1	0.015
2	0.078
3	0.188
4	0.281
5	0.375
6	0.469
7	0.719
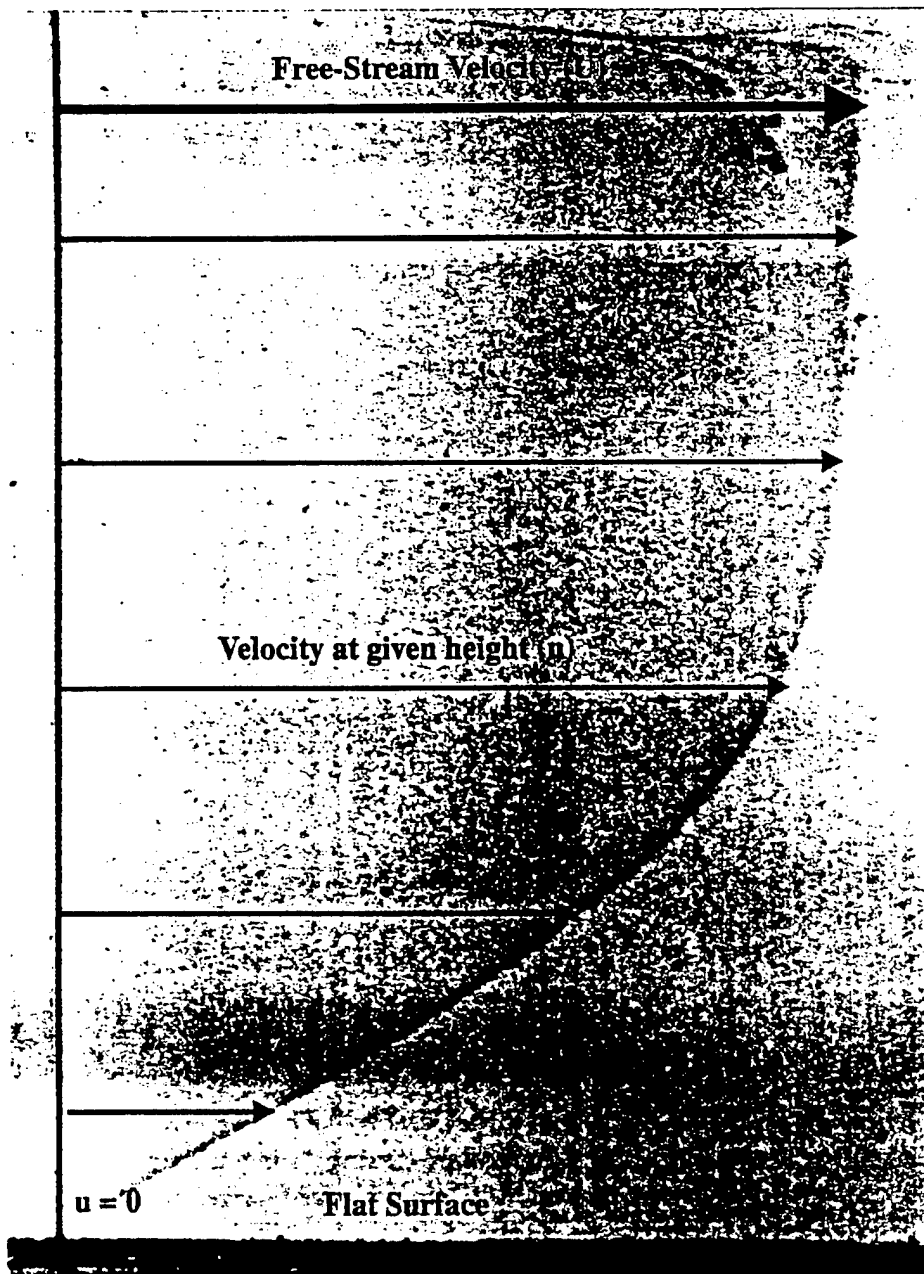
Figure 11: Boundary layer for laminar flow over a flat plate.
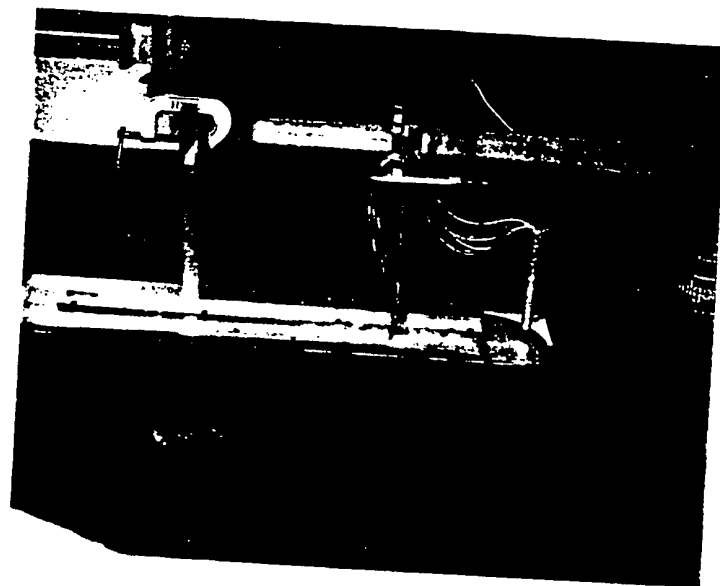
Figure 12a Set-up for calibration of the boundary layer rake.
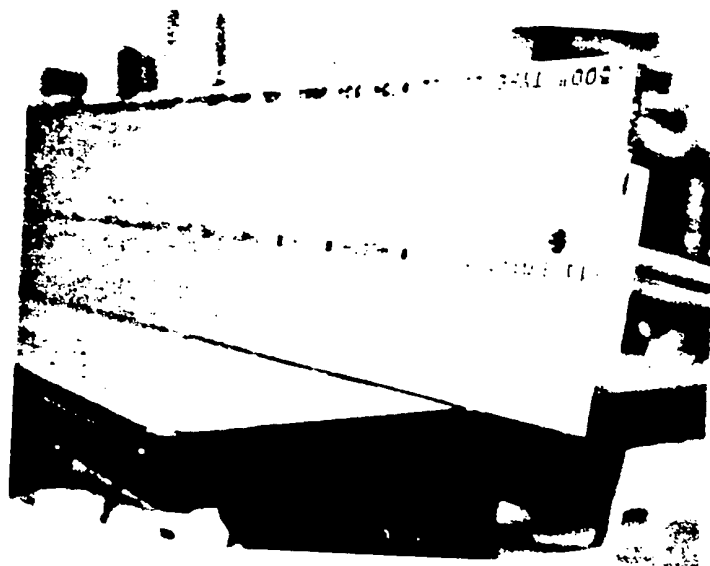
Figure 12b Boundary layer rake mounted in flat plate
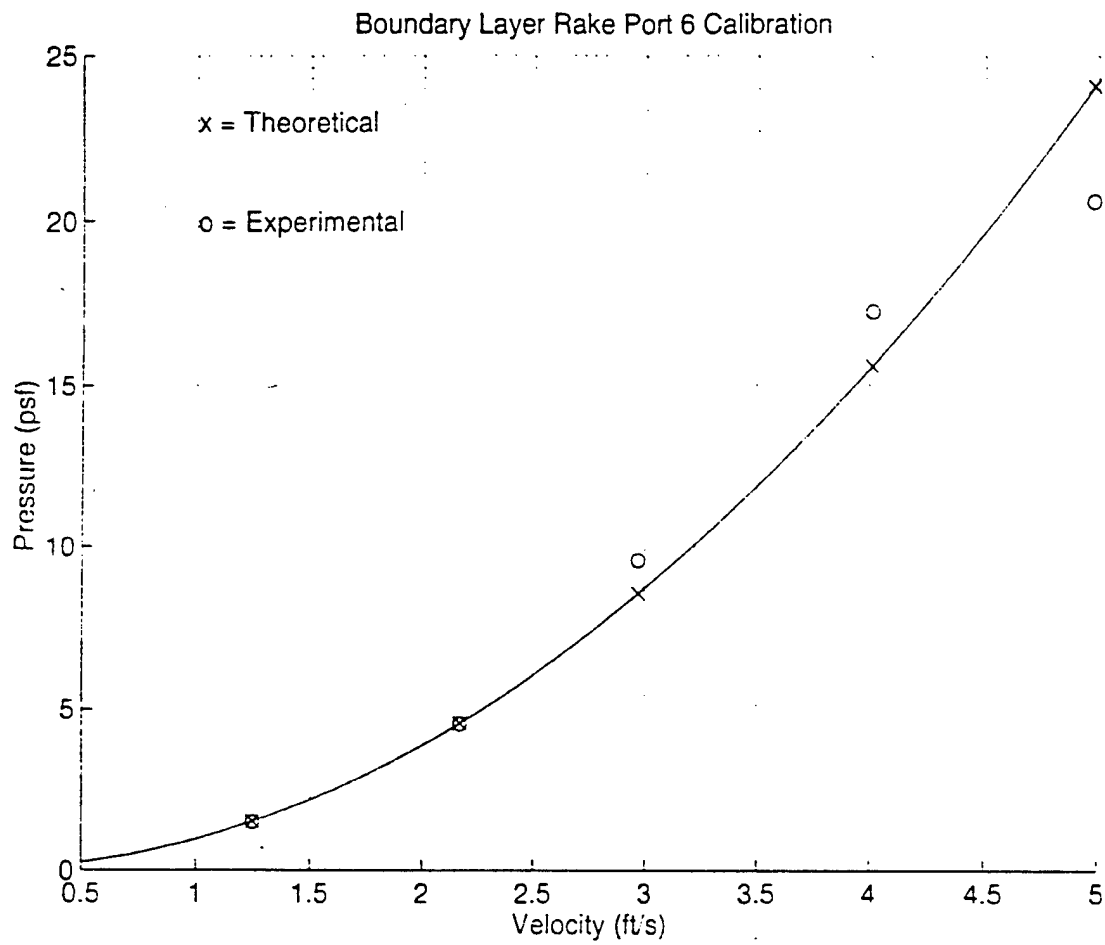
Figure 13. Calibration curve for port 6 of the boundary layer rake

Y=-.3152E-01+.2030E-02(X)   01/24/96 09:37:35
CHI SQUARE = 0.2485E-02

TRUE LOAD-LB

A/D HEADING
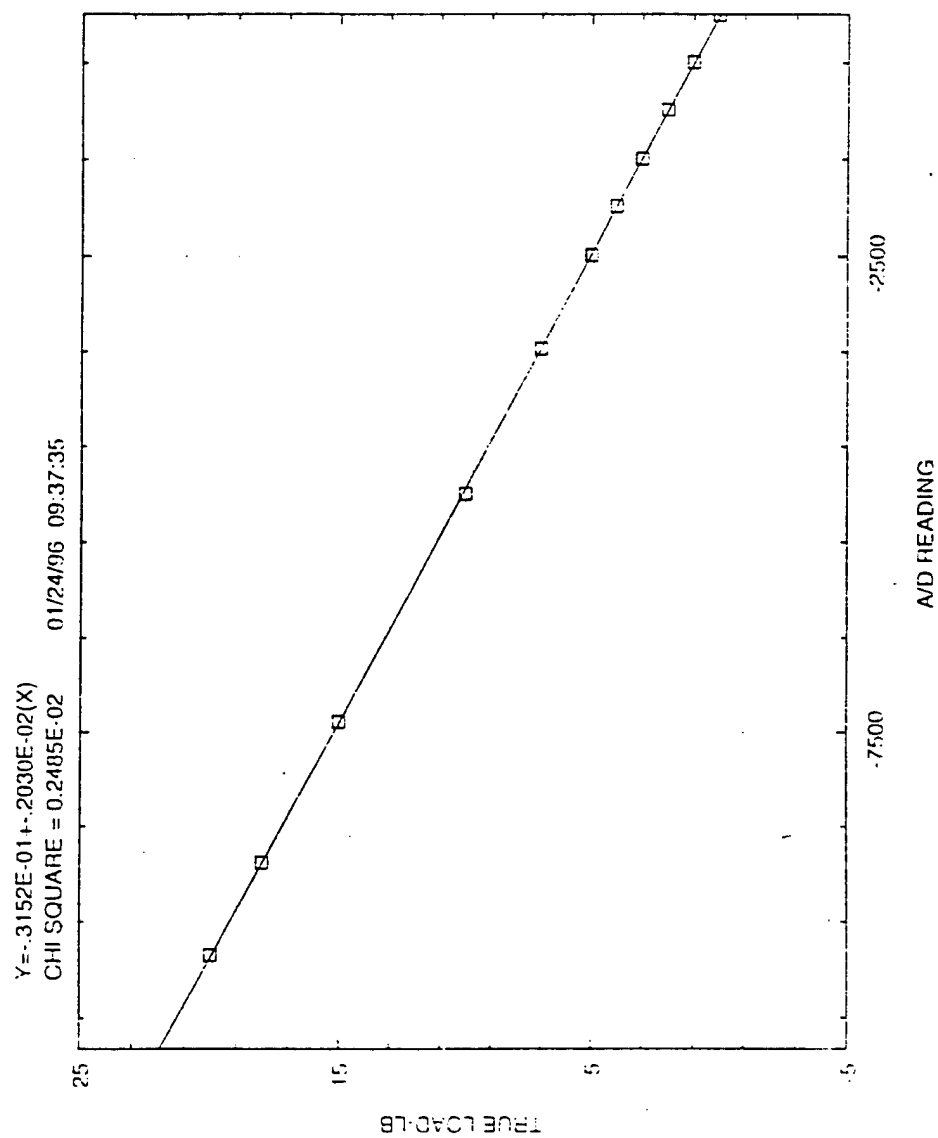
Figure 14: Calibration curve for the block gage.
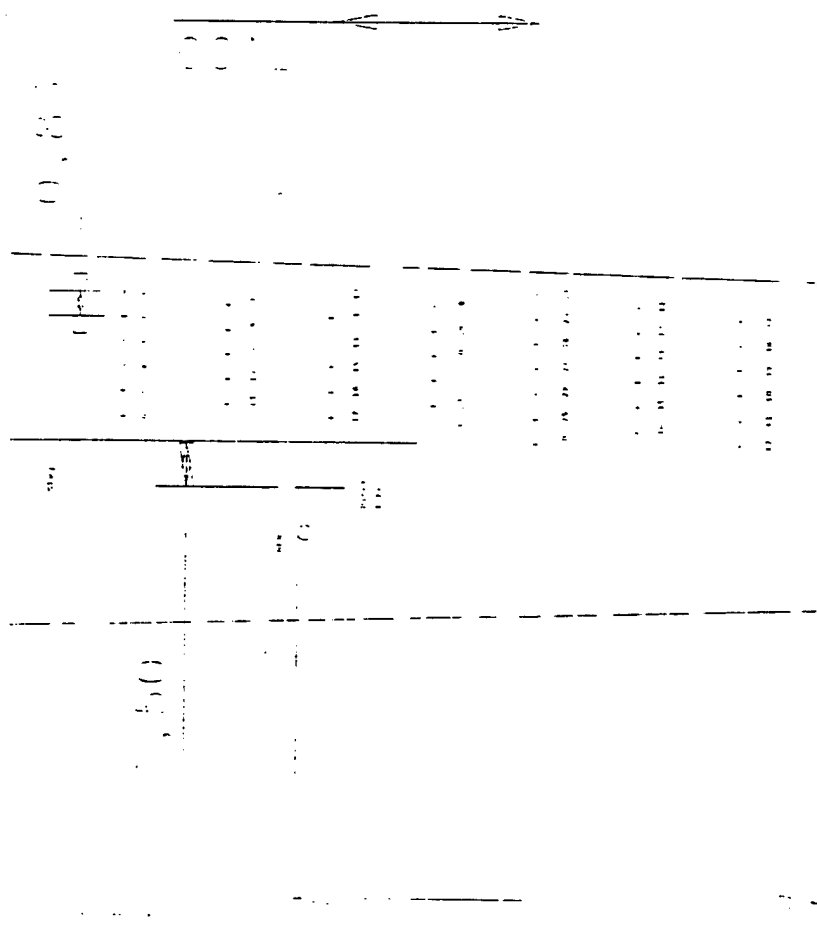
Figure 15: Location of 42 static ports, boundary layer rake, and Pitot-static tube.
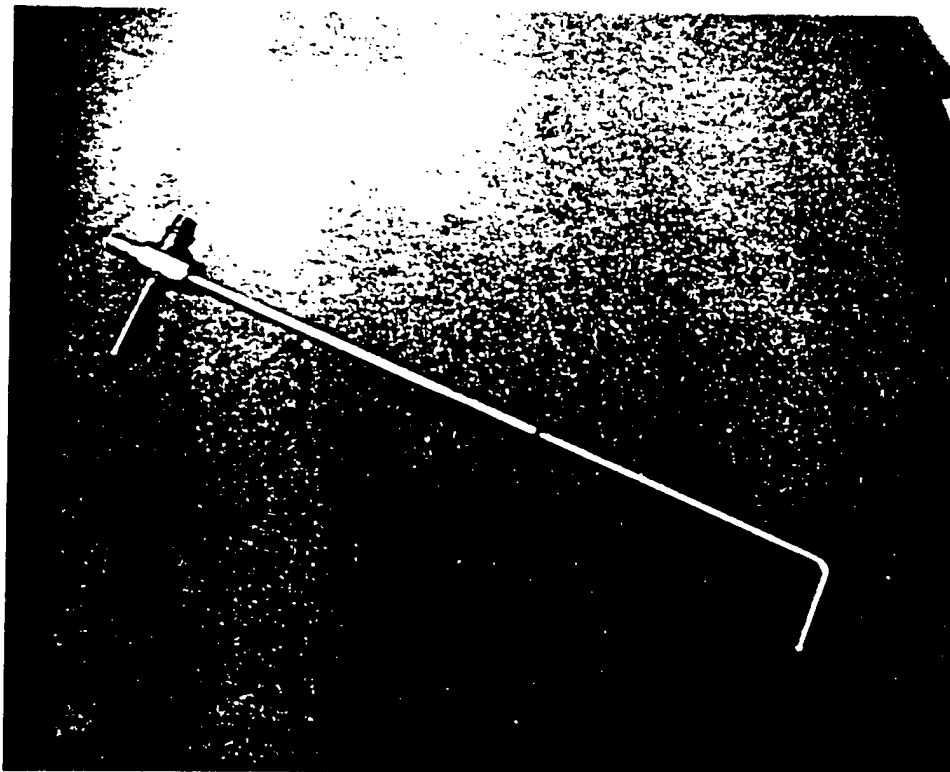
Figure 16: Pitot-static tube.
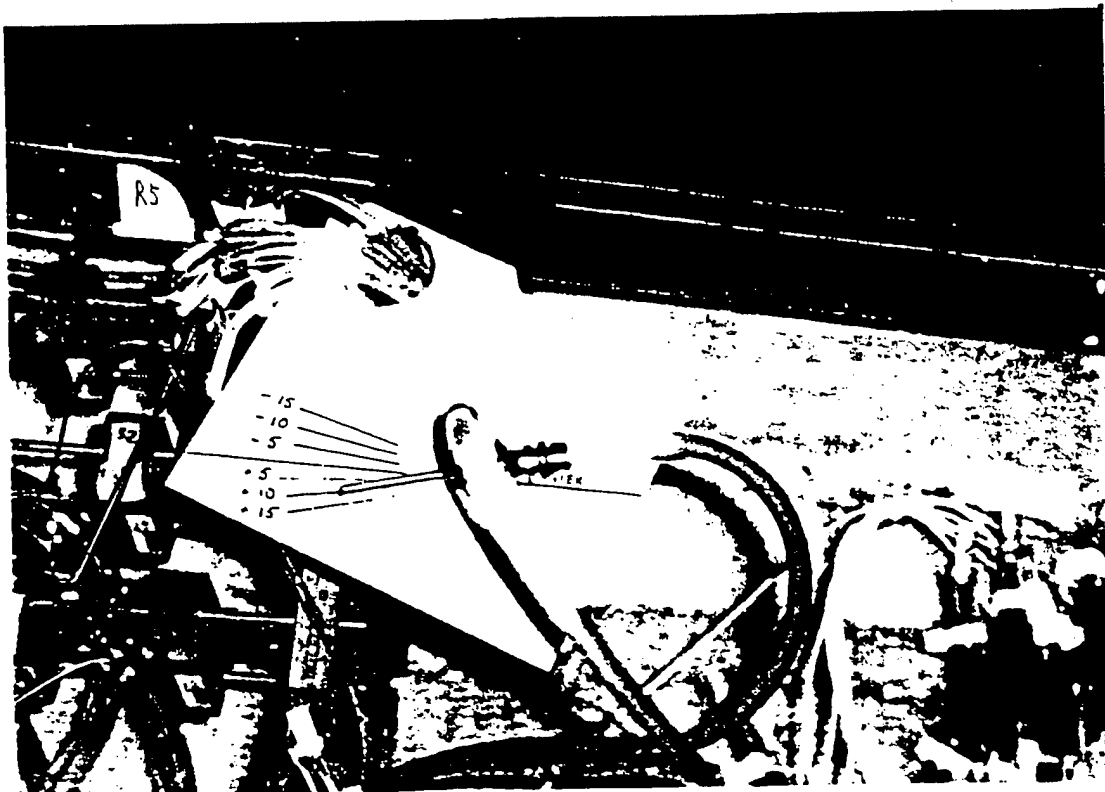
Figure 17 Angle measurements for Pitot-static tube

- Run 50
- Run 51
- Run 52
- Run 53
- Run 54
- Run 55
- Run 56
- Run 57
- Run 58
- Run 59
- Run 60
- Run 61
- Run 62
- Run 63
- Run 64
- Run 65
- Run 66
- Run 67
- Run 68
- Run 69
- Run 70
- Run 78
- Run 78a
- Run 79
- Run 79a
- Run 80
- Run 80a
- Run 81
- Run 81a
- Run 81b
- Run 82
- Run 82a
- Run 83
- Run 83a
- Run 84
- Run 84a
- Run 92
- Run 93
- Run 94
- Run 95
- Run 96
- Run 97
- Run 98

Legend for Figures 18 - 57

Static Pressure Ports 1, 12, 24
Fr=0.40. y=4.998 in.
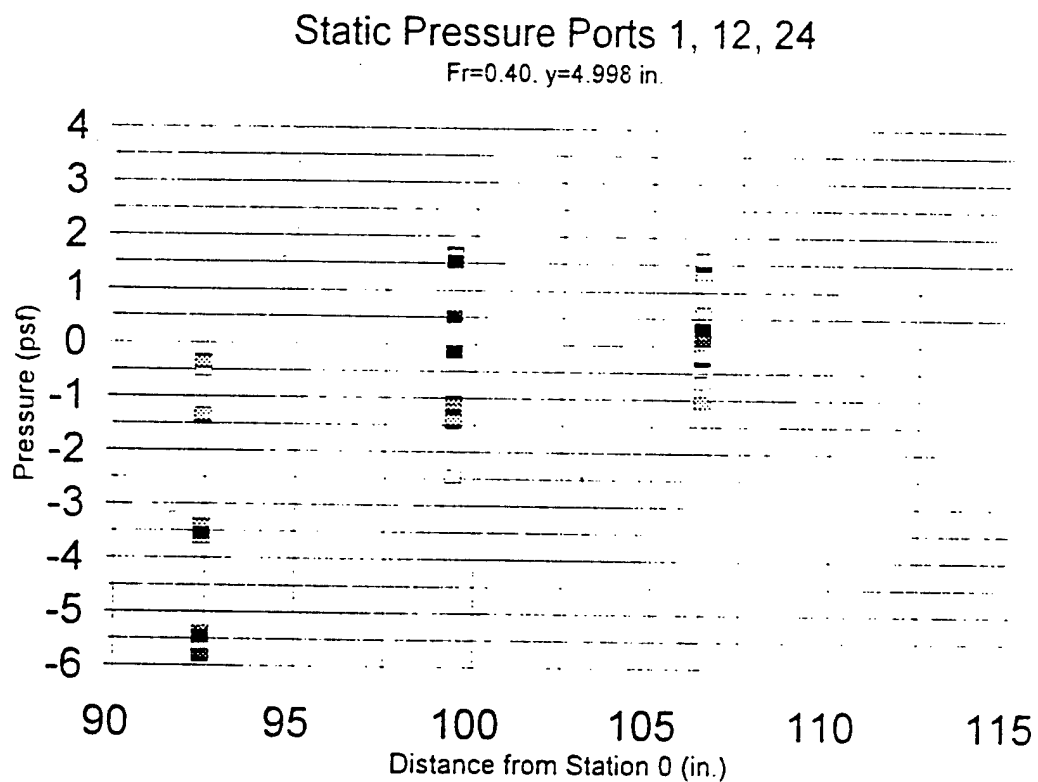
Figure 18 Spanwise distribution of data for static ports 1, 12, 24, at Fr = 0.40

Static Pressure Ports 2,13,25,37

Fr=0.40. y=4.165 in.
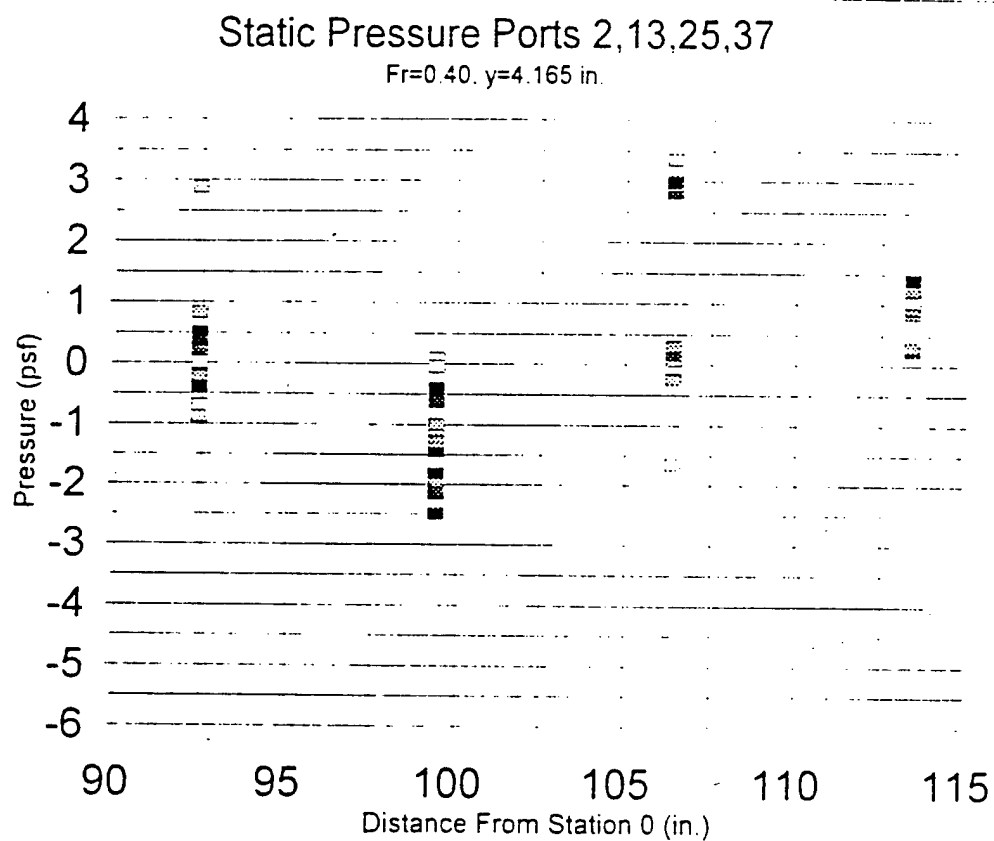
Figure 19 Spanwise distribution of data for static ports 2. 13. 25. 37 at Fr = 0 40
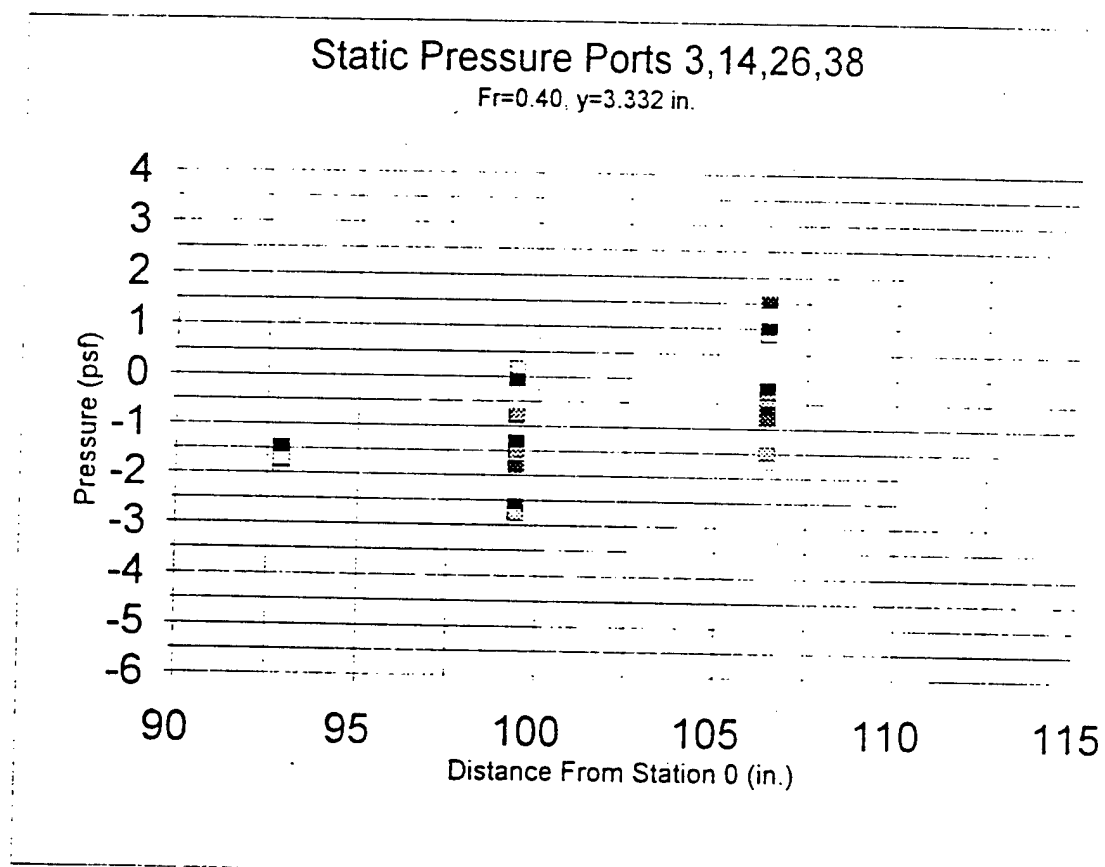
Figure 20 Spanwise distribution of data for static ports 3, 14, 26, 38 at Fr = 0.40
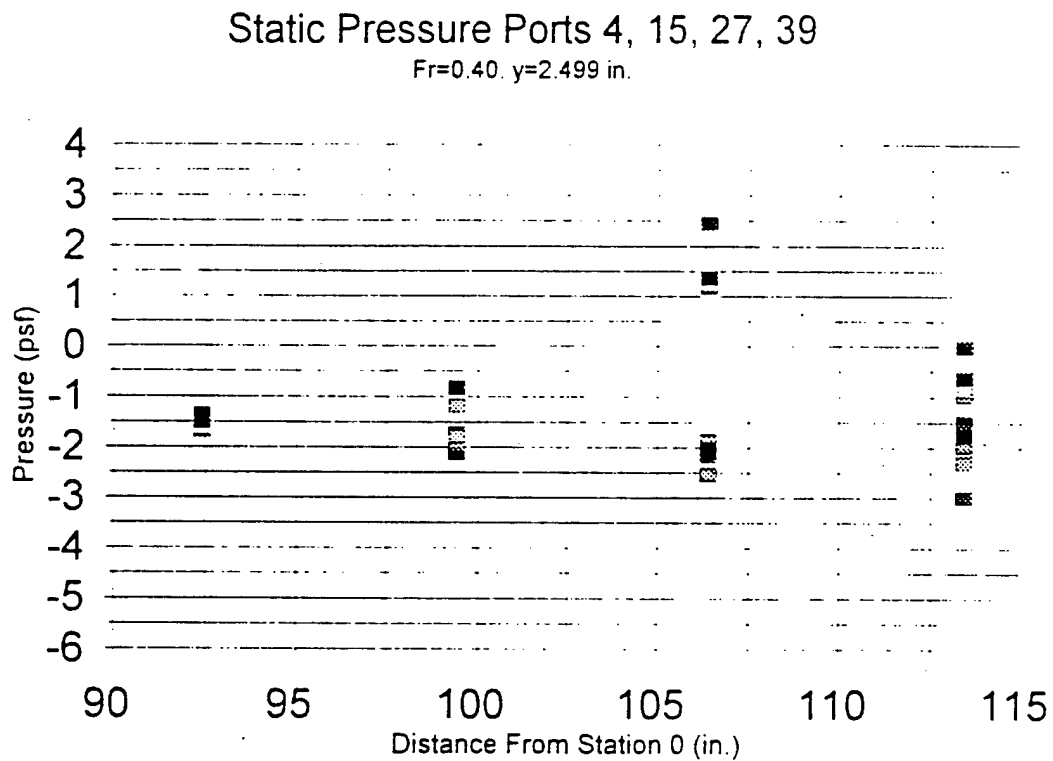
Figure 21: Spanwise distribution of data for static ports 4. 15. 27. 39 at Fr = 0.40
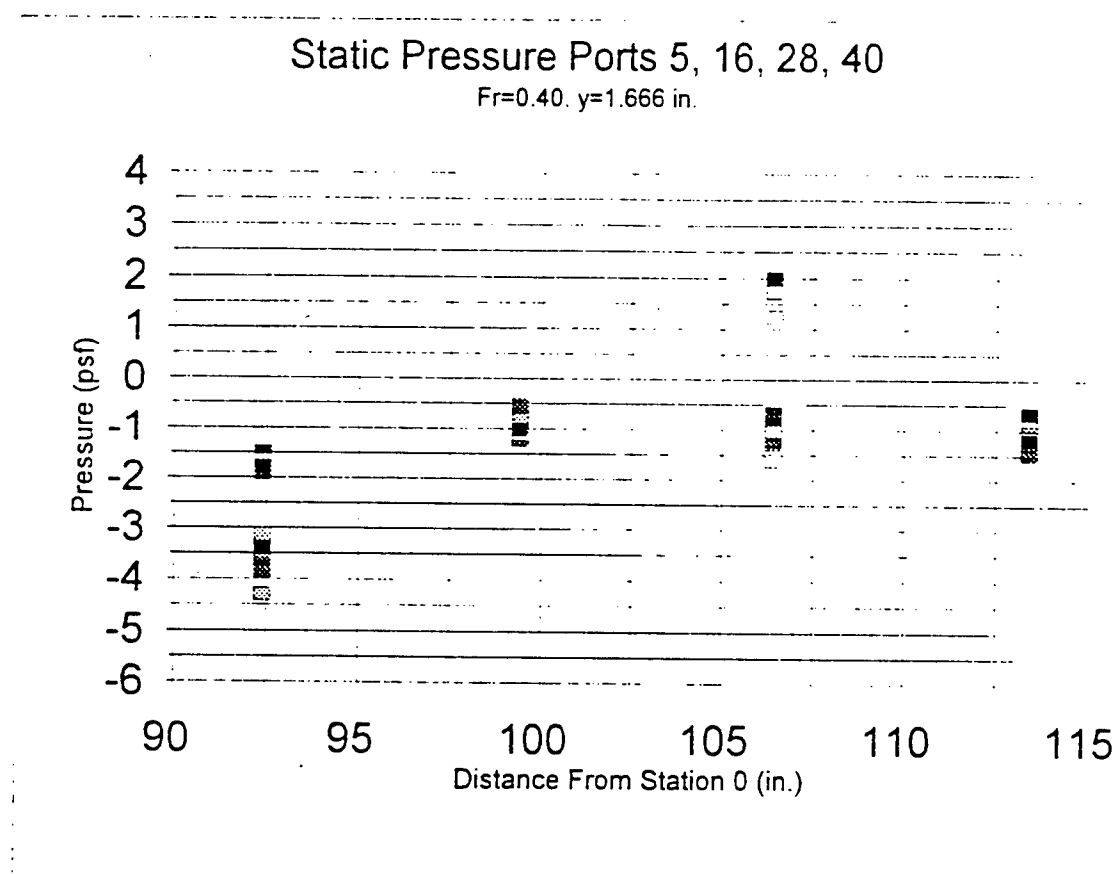
Figure 22 Spanwise distribution of data for static ports 5, 16, 28, 40 at Fr = 0.40
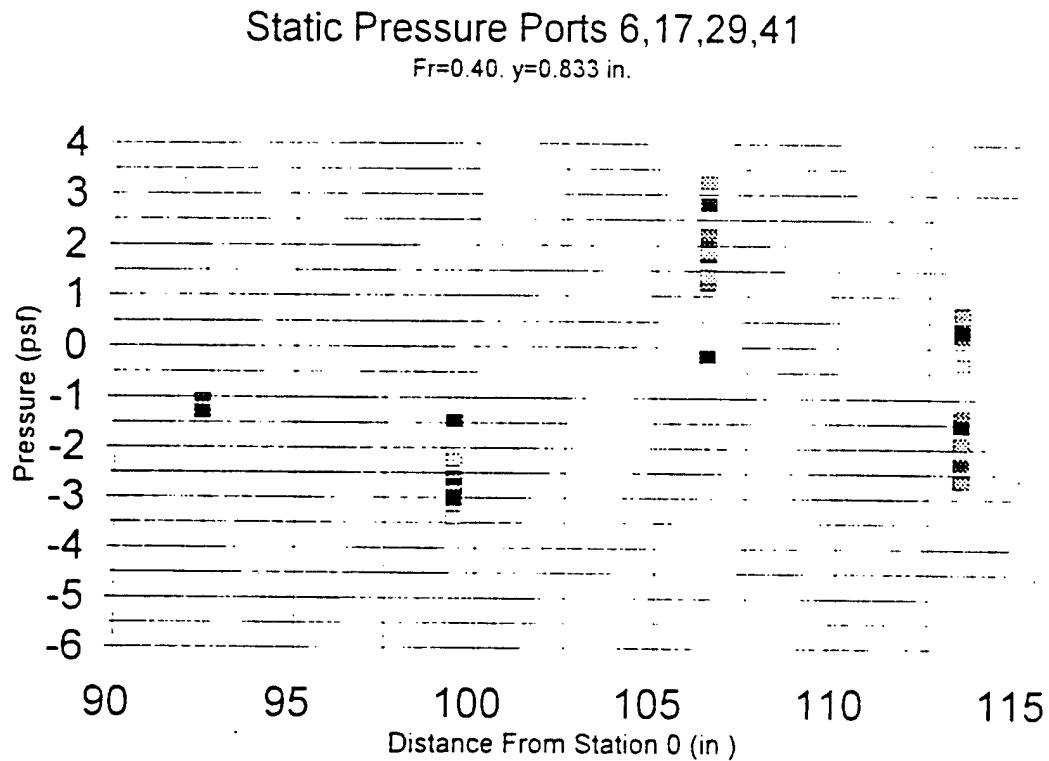
Figure 23 Spanwise distribution of data for static ports 6, 17, 29, 41 at Fr = 0.40
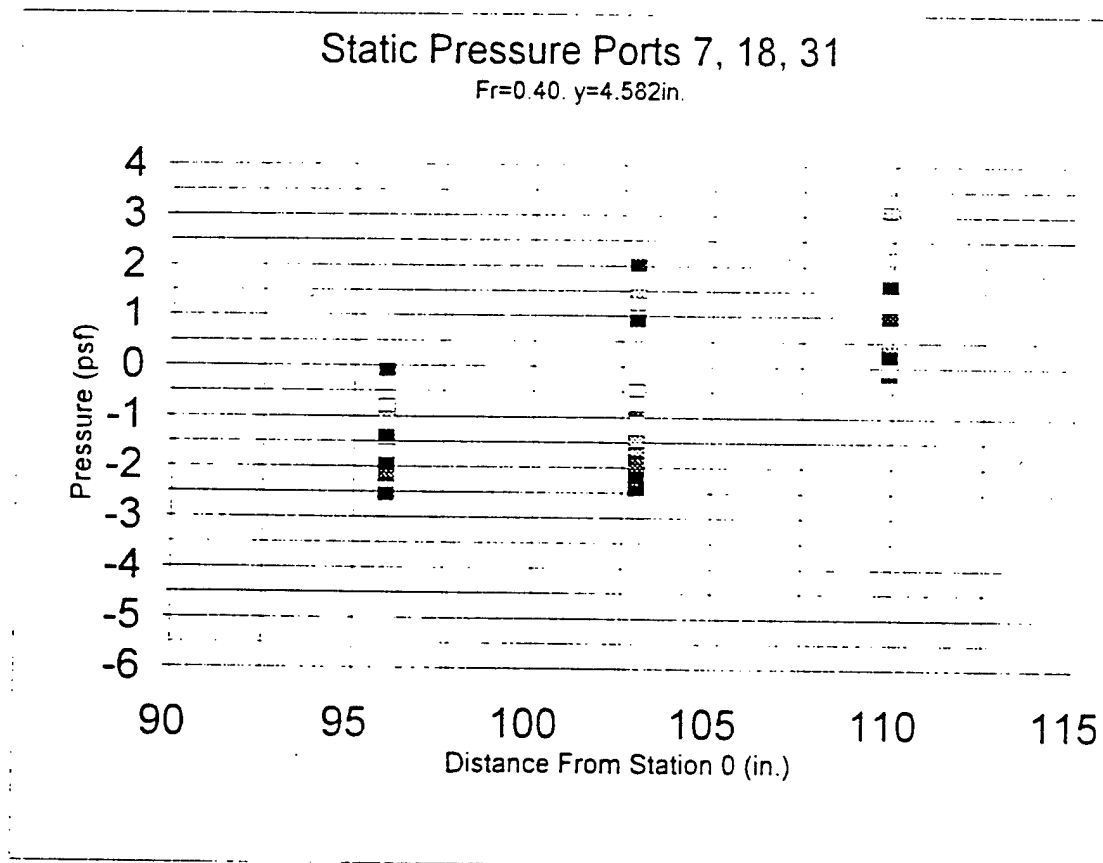
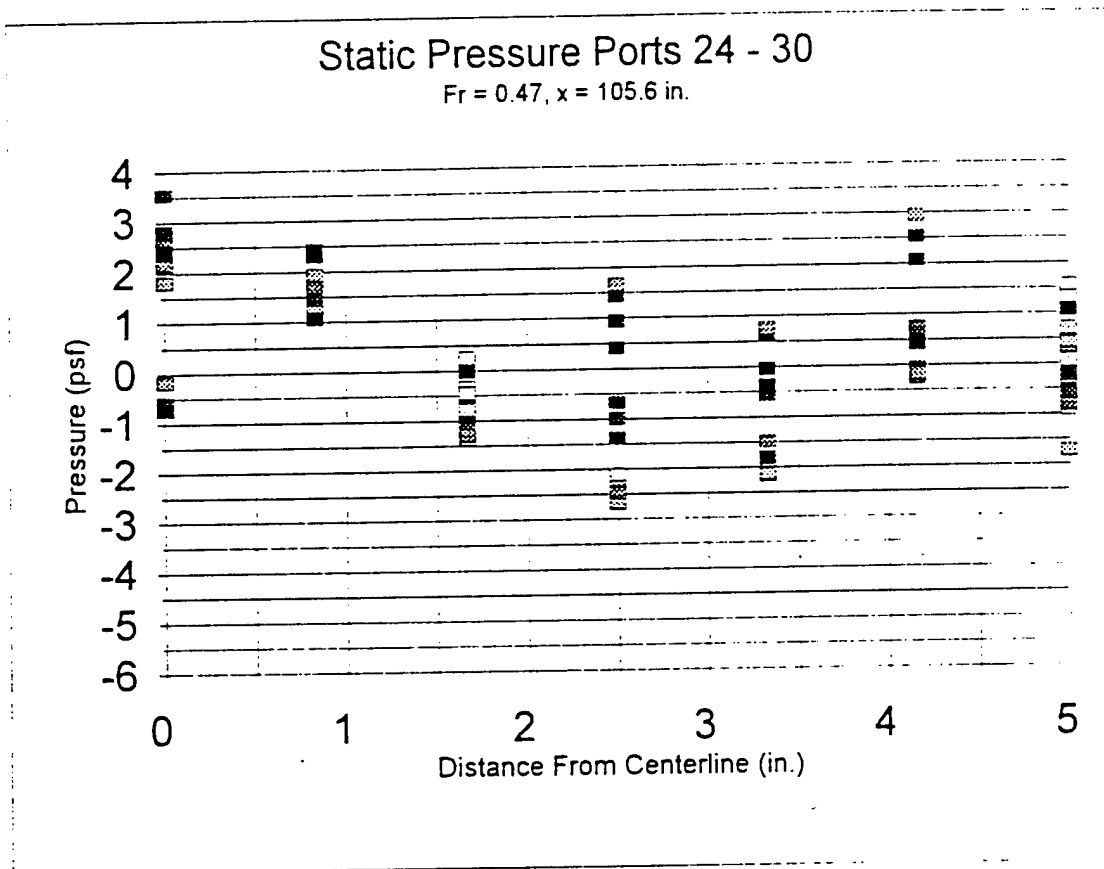Figure 24 Spanwise distribution of data for static ports 7, 18, 31 at Fr = 0.40
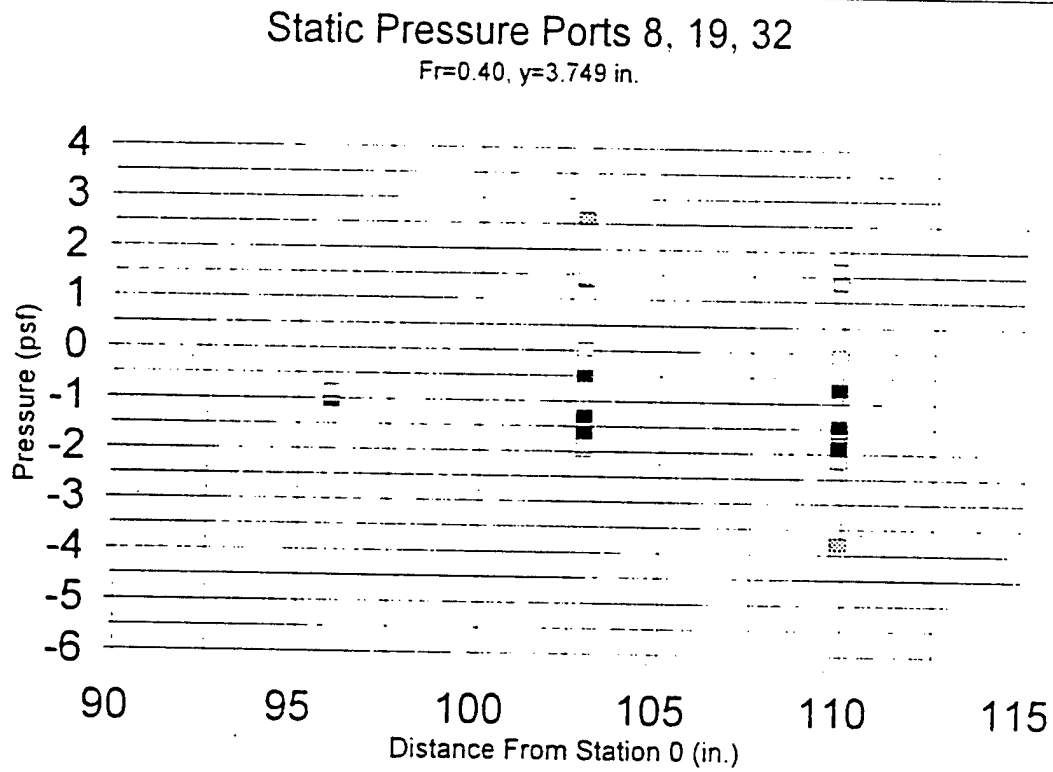
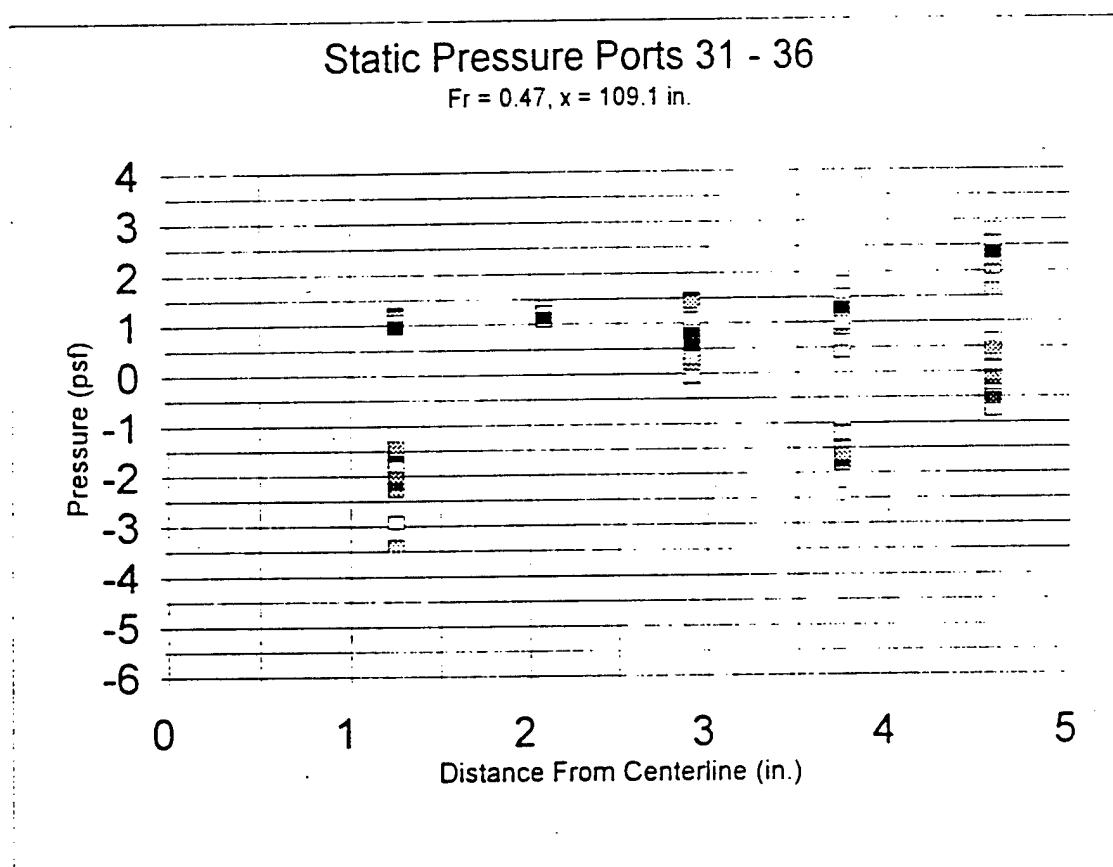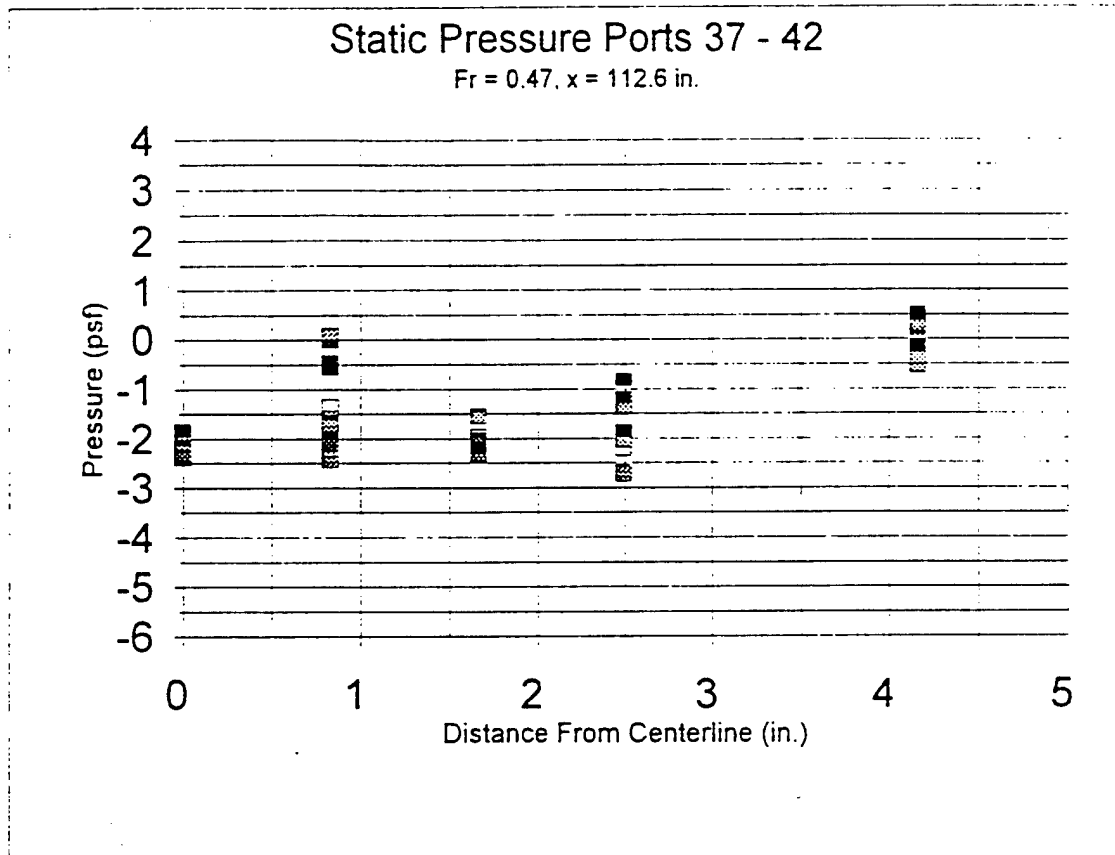Figure 25 Spanwise distribution of data for static ports 8, 19, 32 at Fr = 0.40
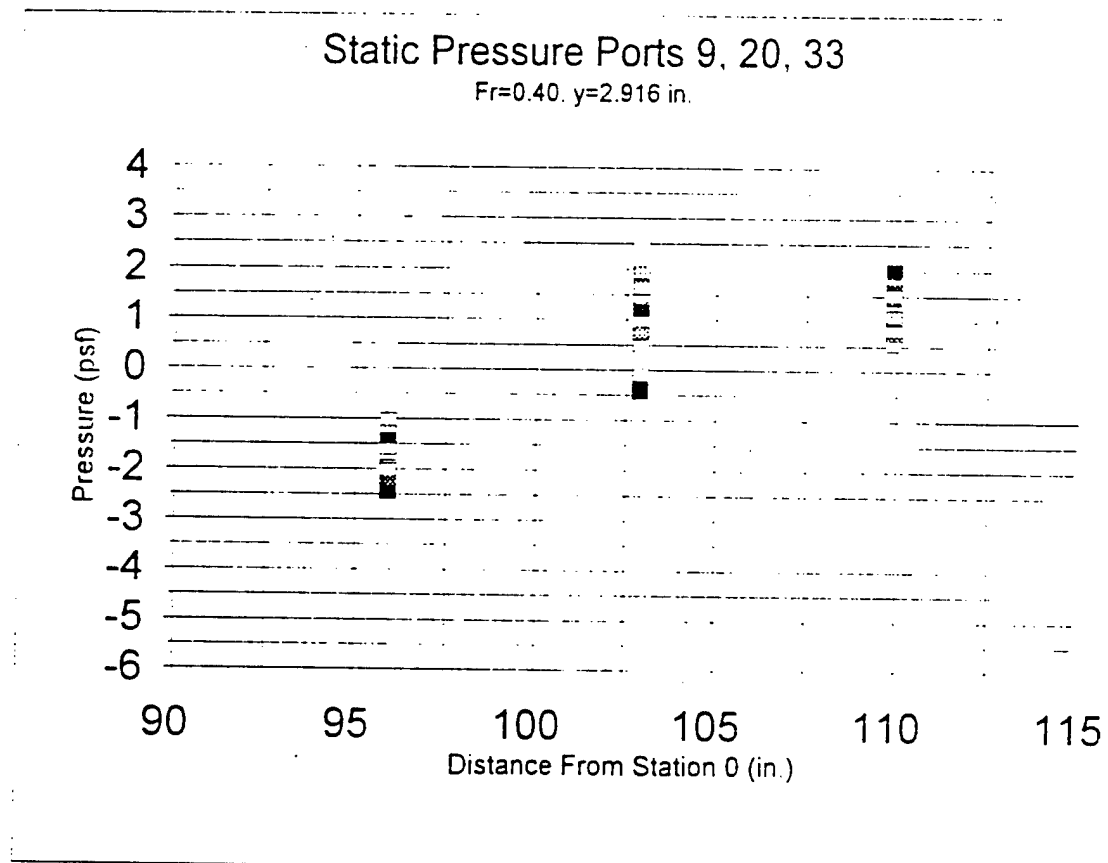
Figure 26 Spanwise distribution of data for static ports 9, 20, 33 at Fr = 0.40

Static Pressure Ports 10, 21, 34
Fr=0.40, y=2.083 in.
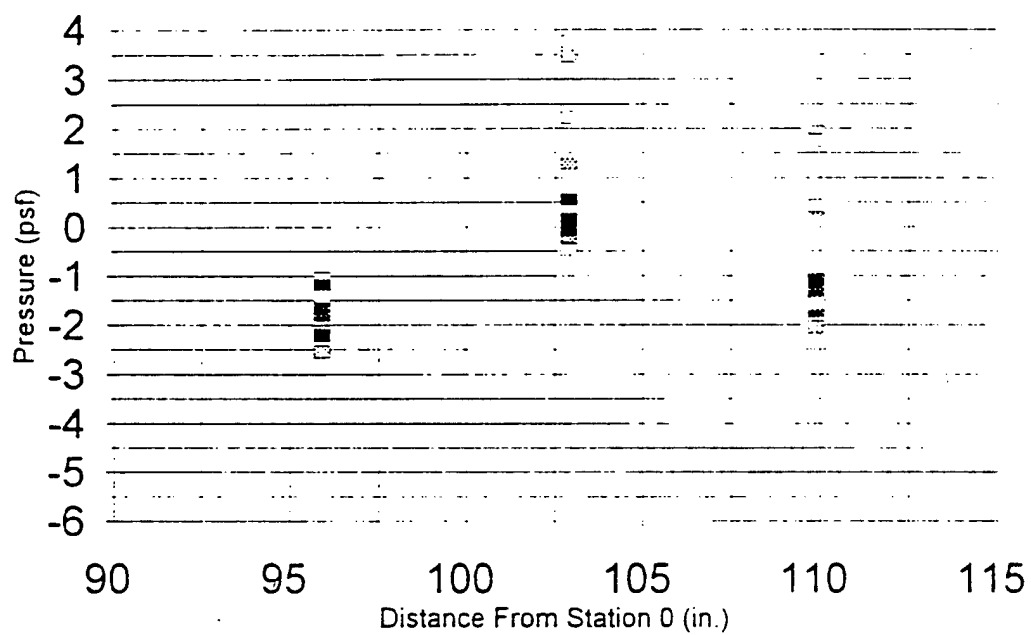
Figure 27. Spanwise distribution of data for static ports 10, 21, 34 at Fr = 0.40

Static Pressure Ports 11,22,35
Fr=0.40. y=1.250 in
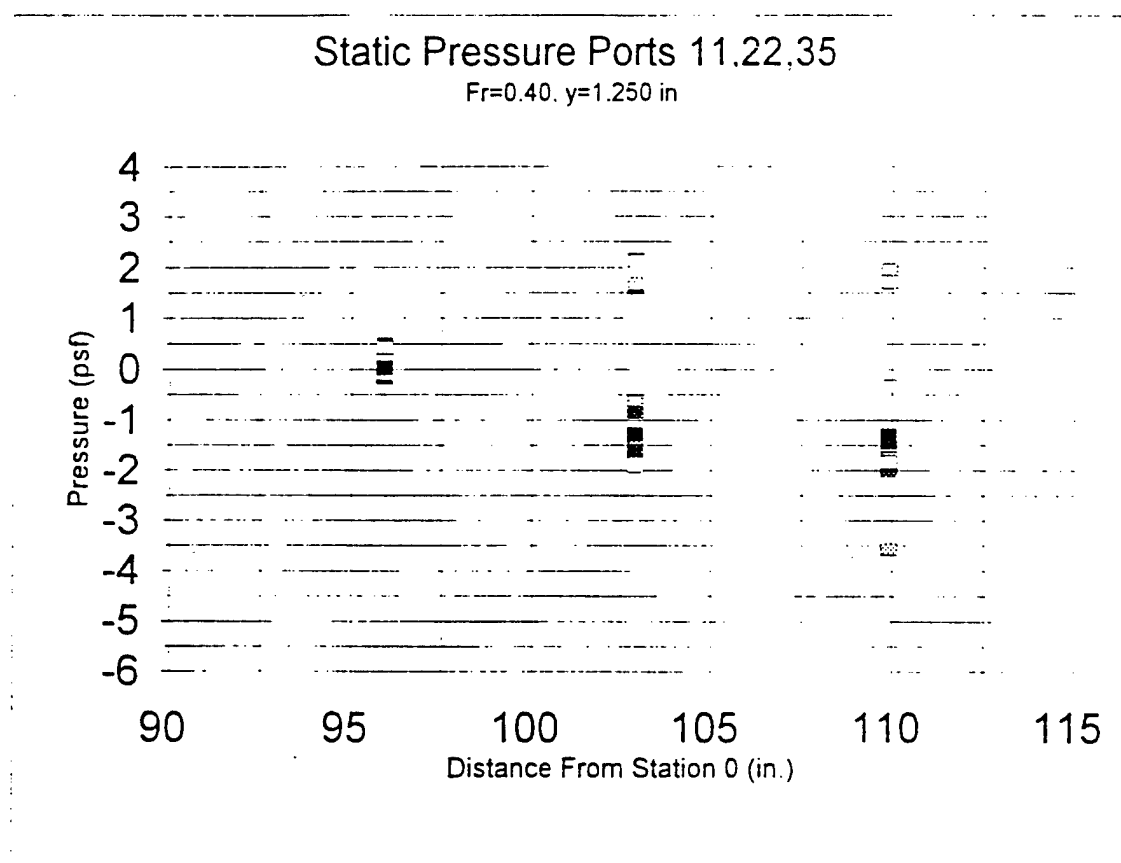
Figure 28 Spanwise distribution of data for static ports 11, 22, 35 at Fr = 0.40
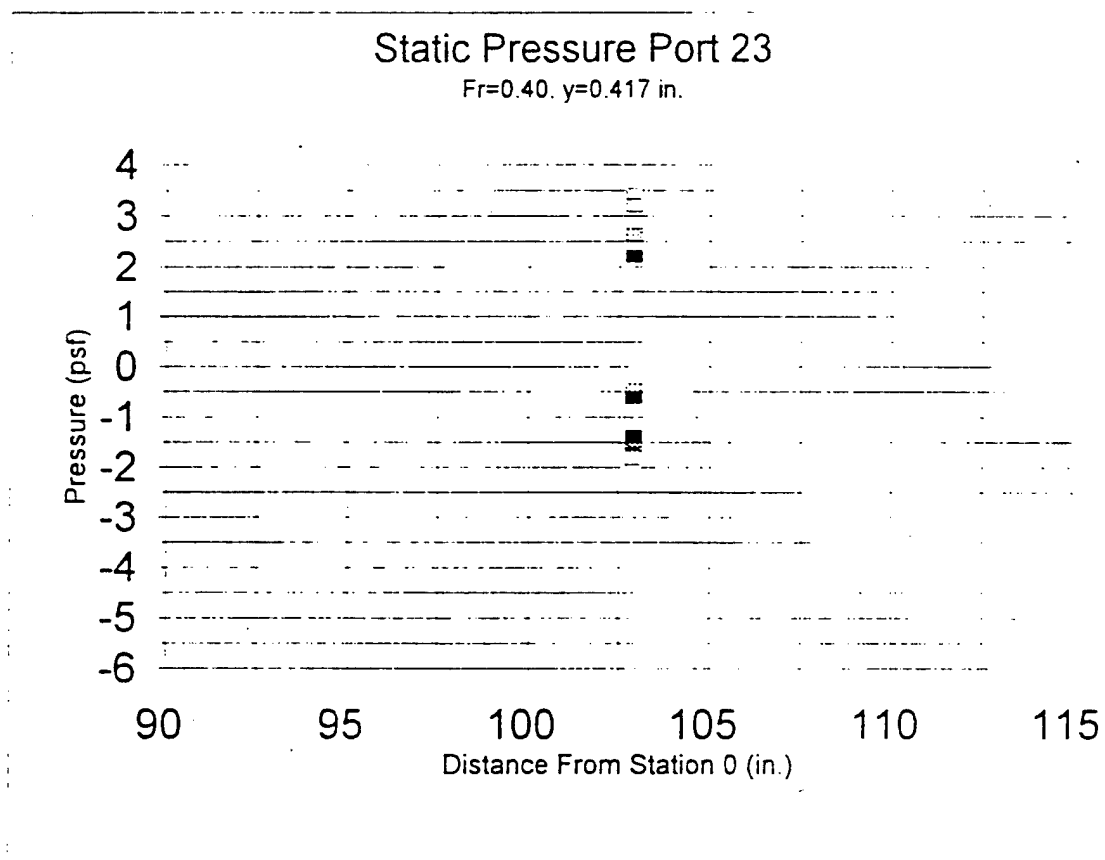
Figure 29 Spanwise distribution of data for static port 23 at Fr = 0.40
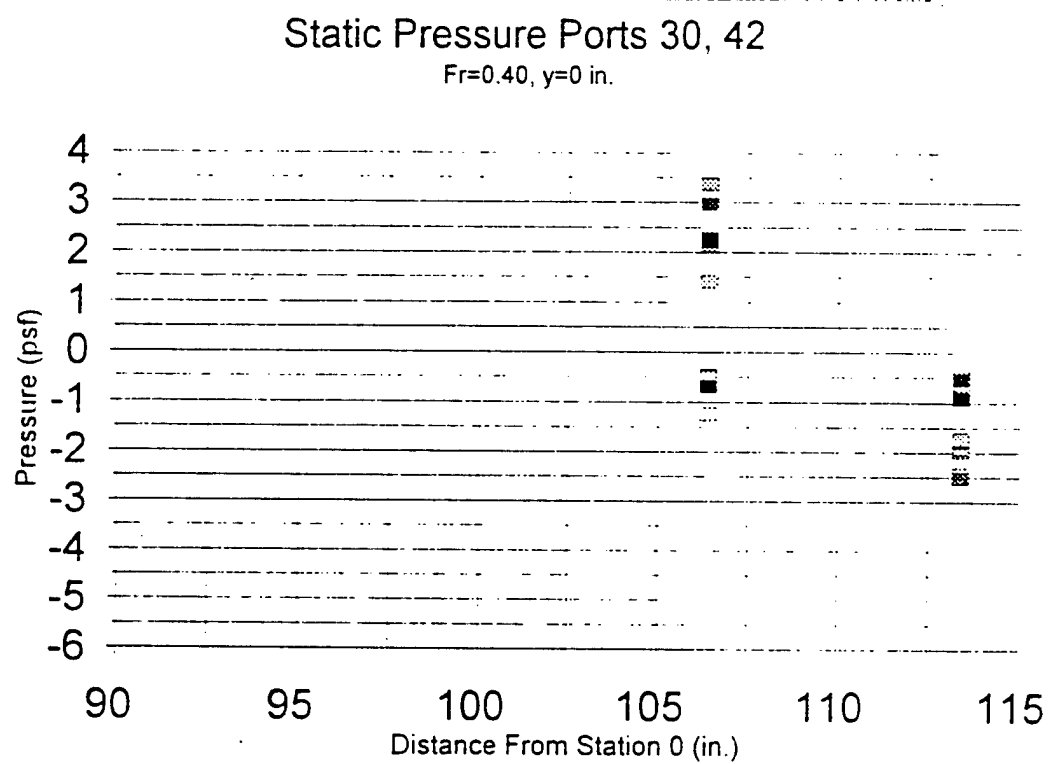
**Figure 30** Spanwise distribution of data for static ports 30, 42 at Fr = 0.40
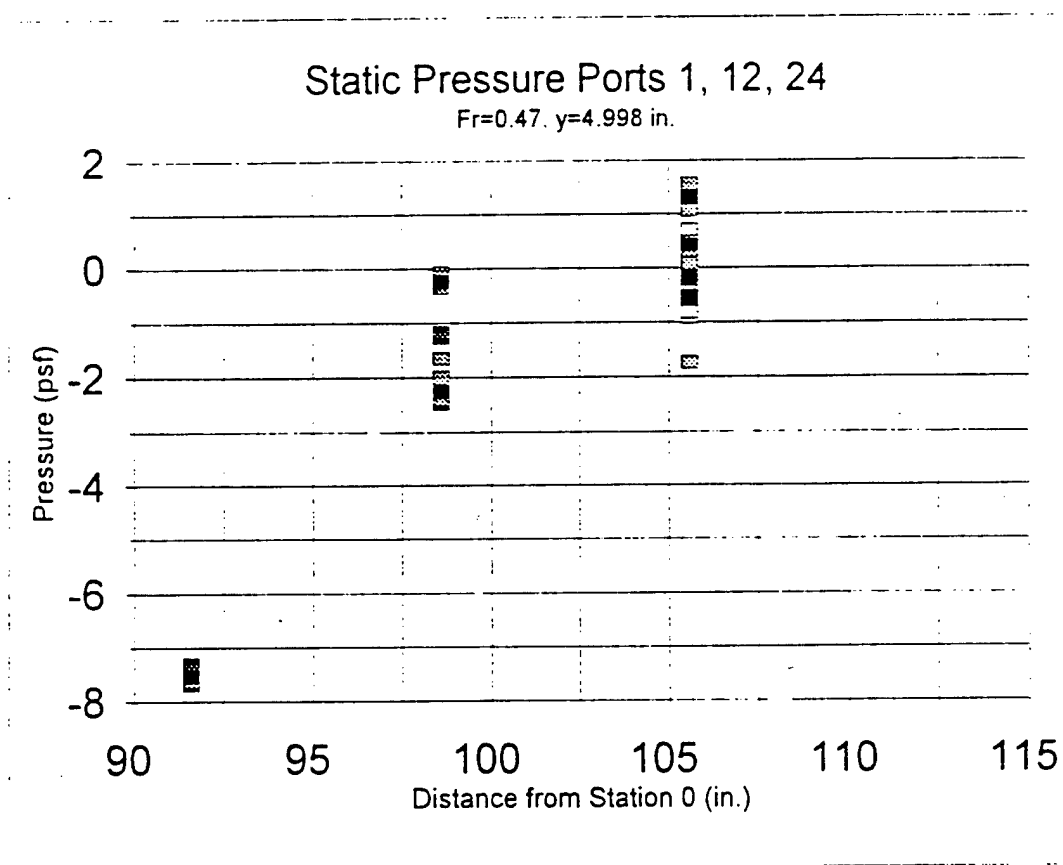
Figure 31: Spanwise distribution of data for static ports 1, 12, 24 at Fr = 0.47
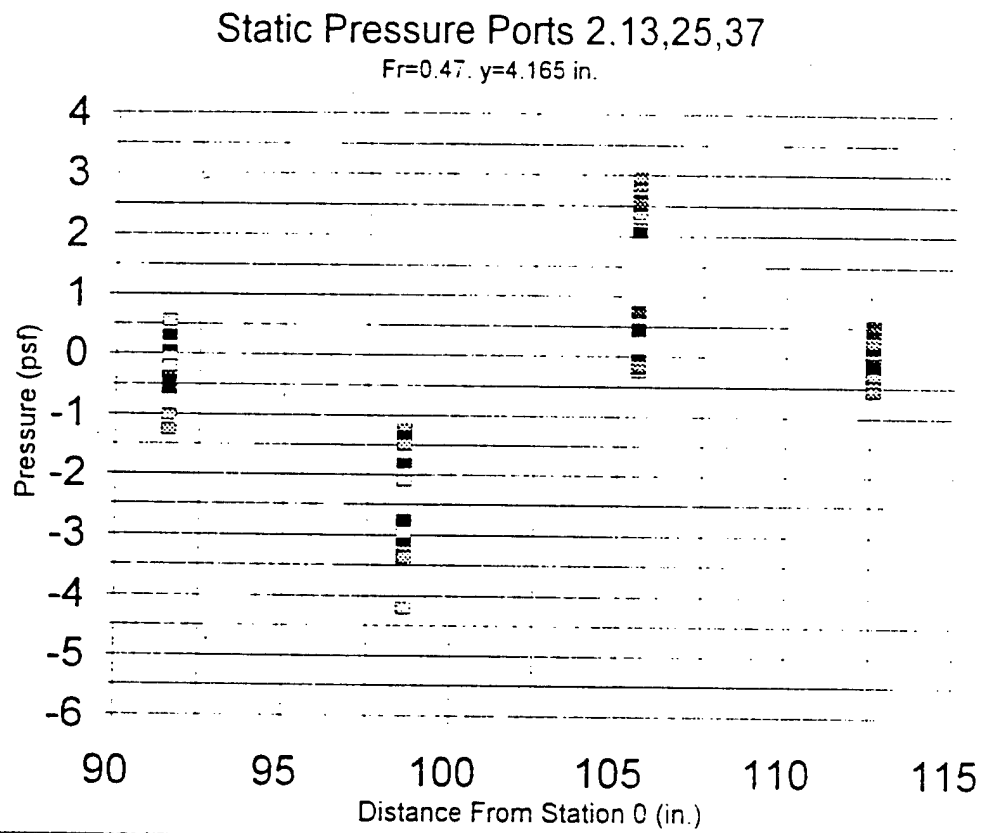
Figure 32 Spanwise distribution of data for static ports 2, 13, 25, 37 at Fr = 0.47
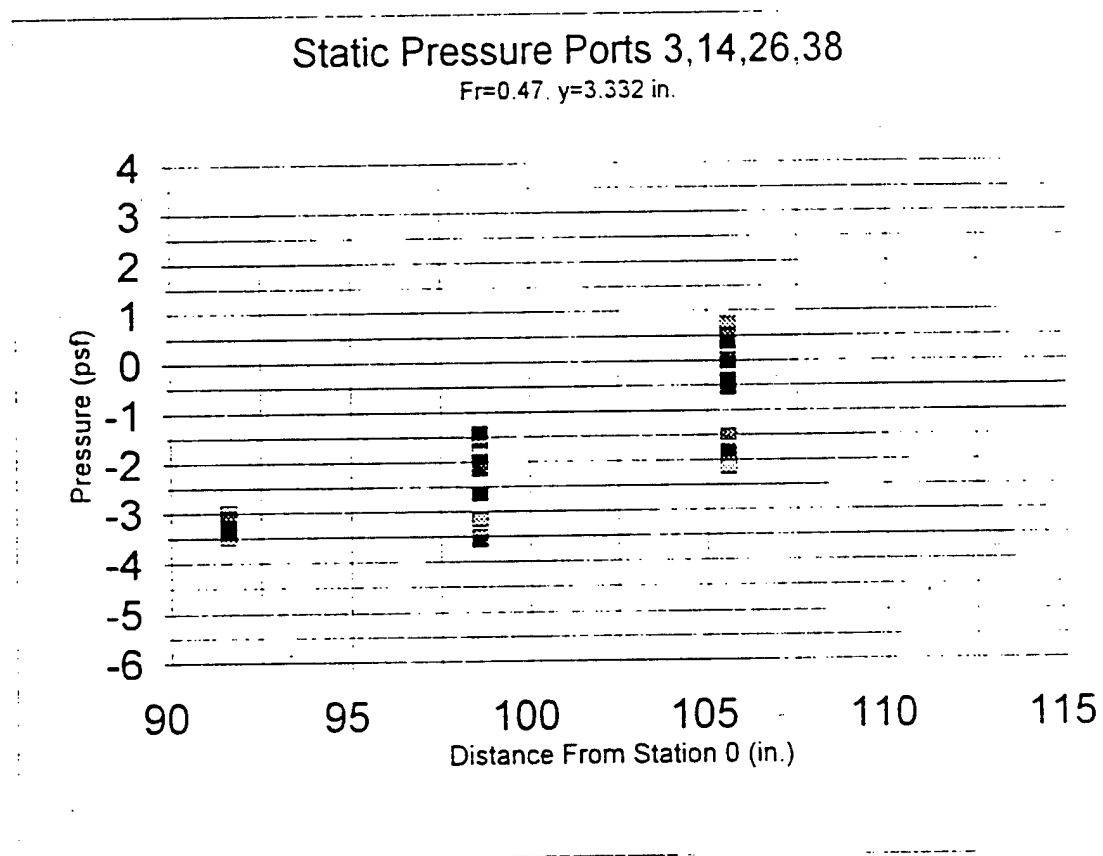
Figure 33 Spanwise distribution of data for static ports 3, 14, 26, 38 at Fr = 0.47.
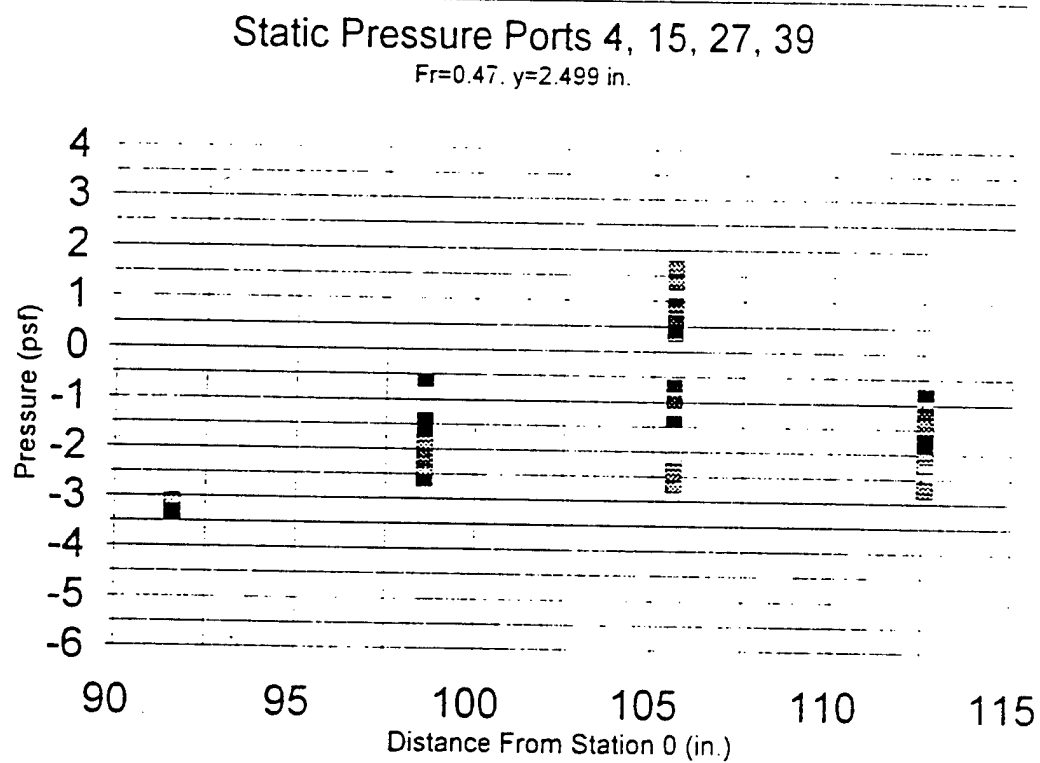
Figure 34 Spanwise distribution of data for static ports 4, 15, 27, 39 at Fr = 0.47.
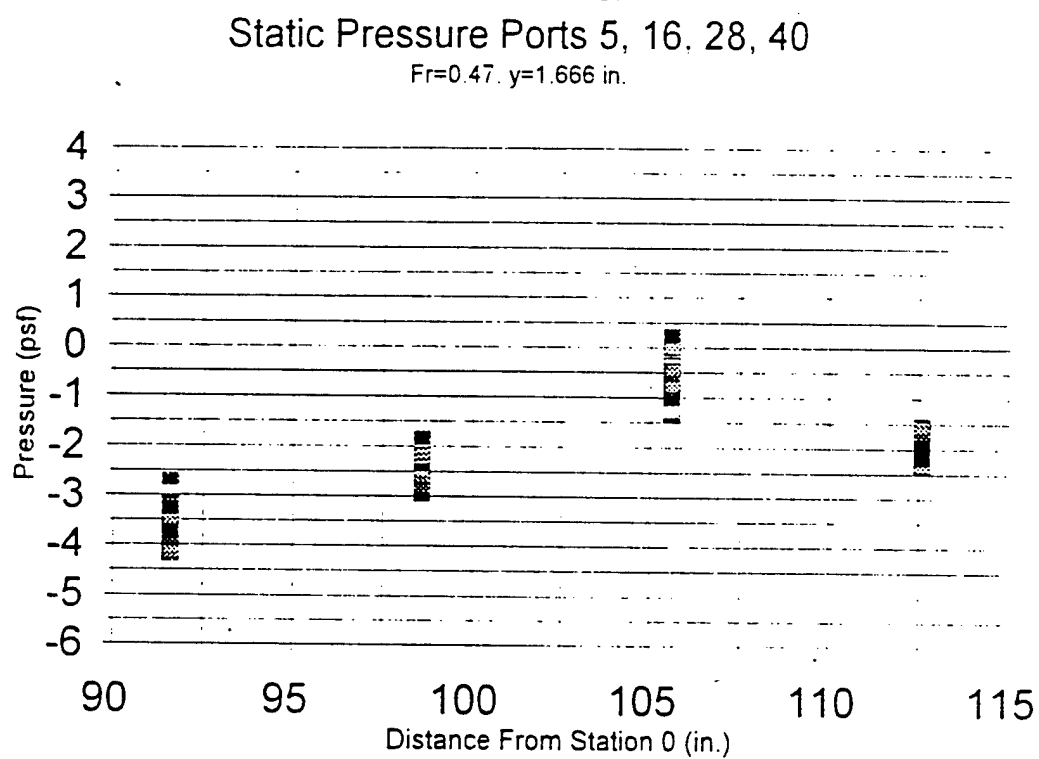
Figure 35: Spanwise distribution of data for static ports 5, 16, 28, 40 at Fr = 0.47.
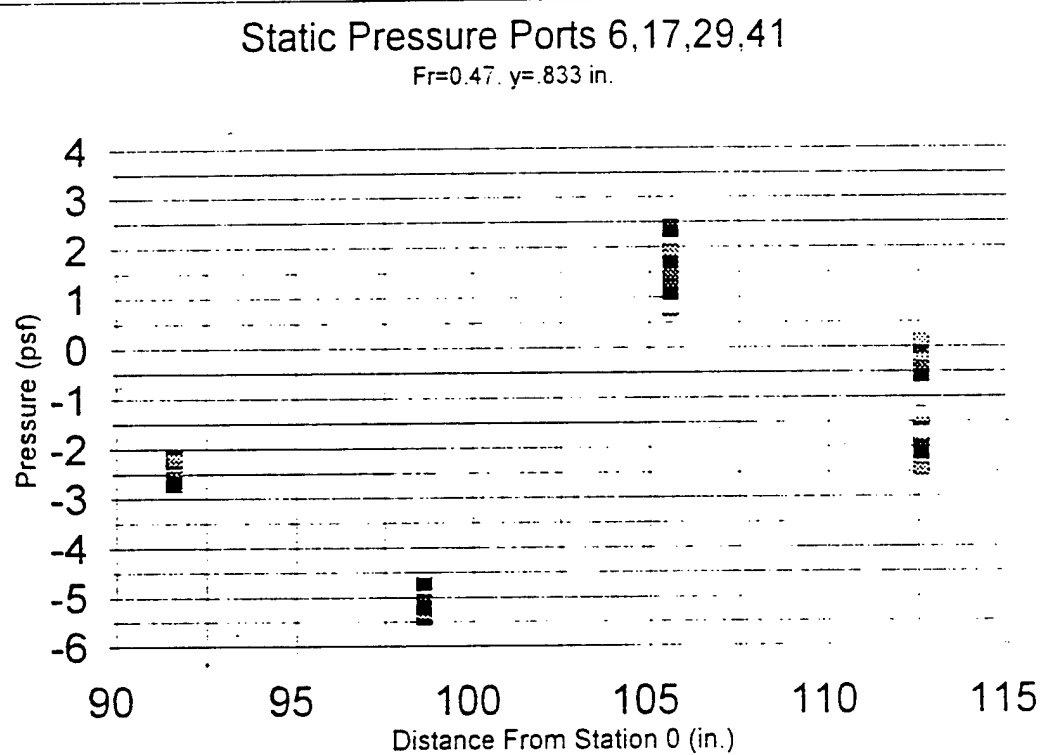
Figure 36. Spanwise distribution of data for static ports 6, 17, 29, 41 at Fr = 0.47
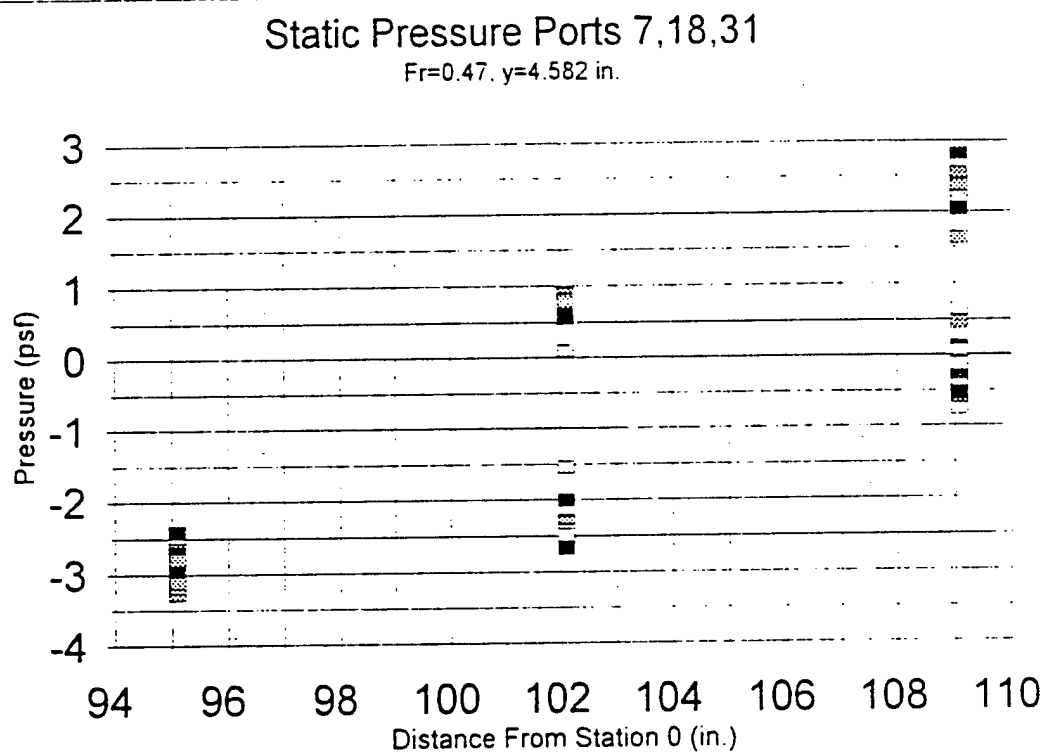
Figure 37: Spanwise distribution of data for static ports 7, 18, 31 at Fr = 0.47
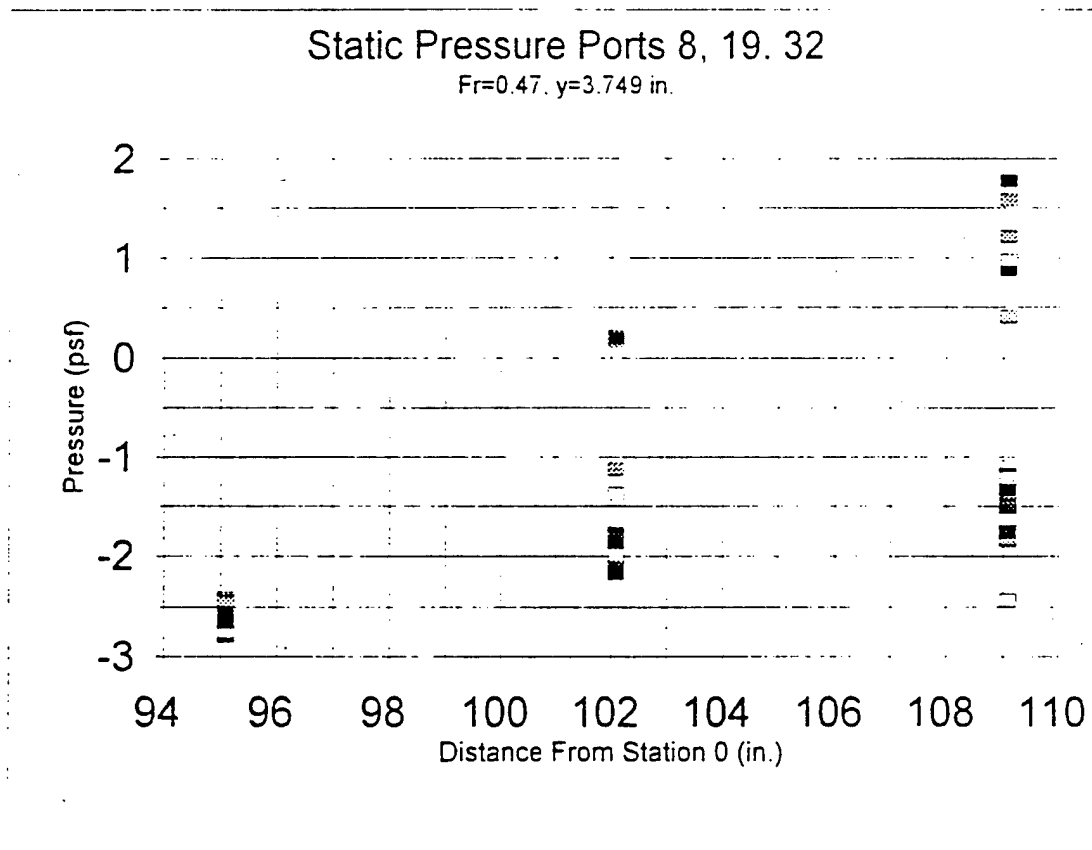
Figure 38. Spanwise distribution of data for static ports 8, 19, 32 at Fr = 0.47
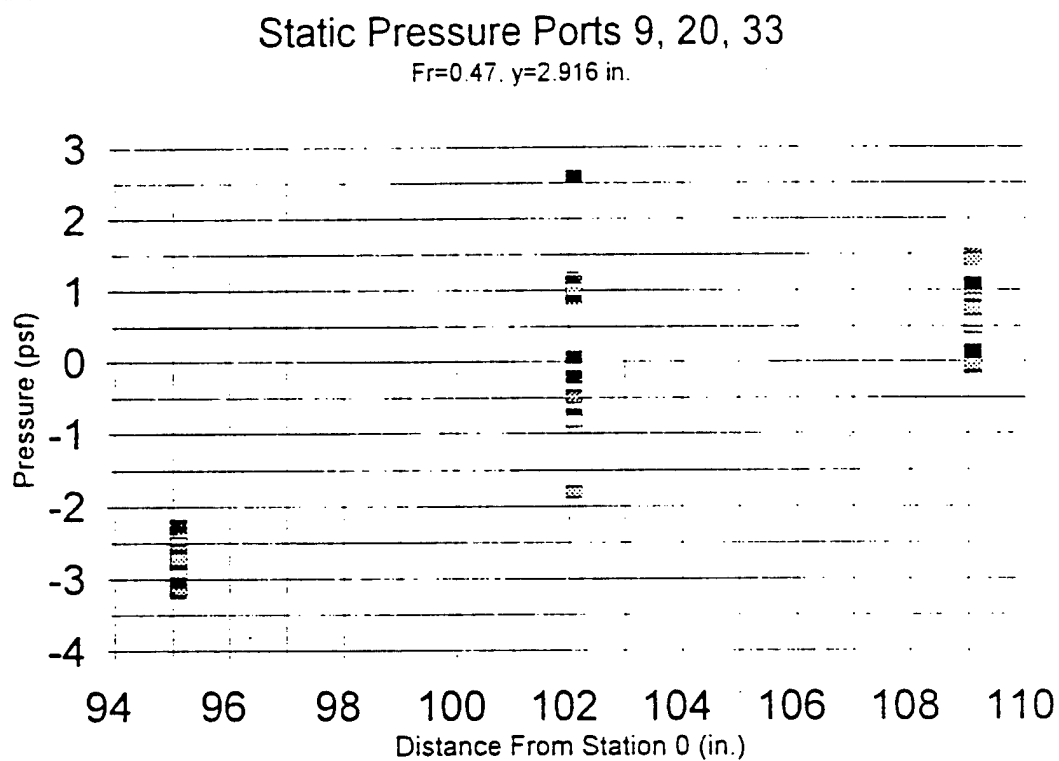
Figure 39 Spanwise distribution of data for static ports 9, 20, 33 at Fr = 0.47

Static Pressure Ports 10. 21, 34

Fr=0.47. y=2.083 in
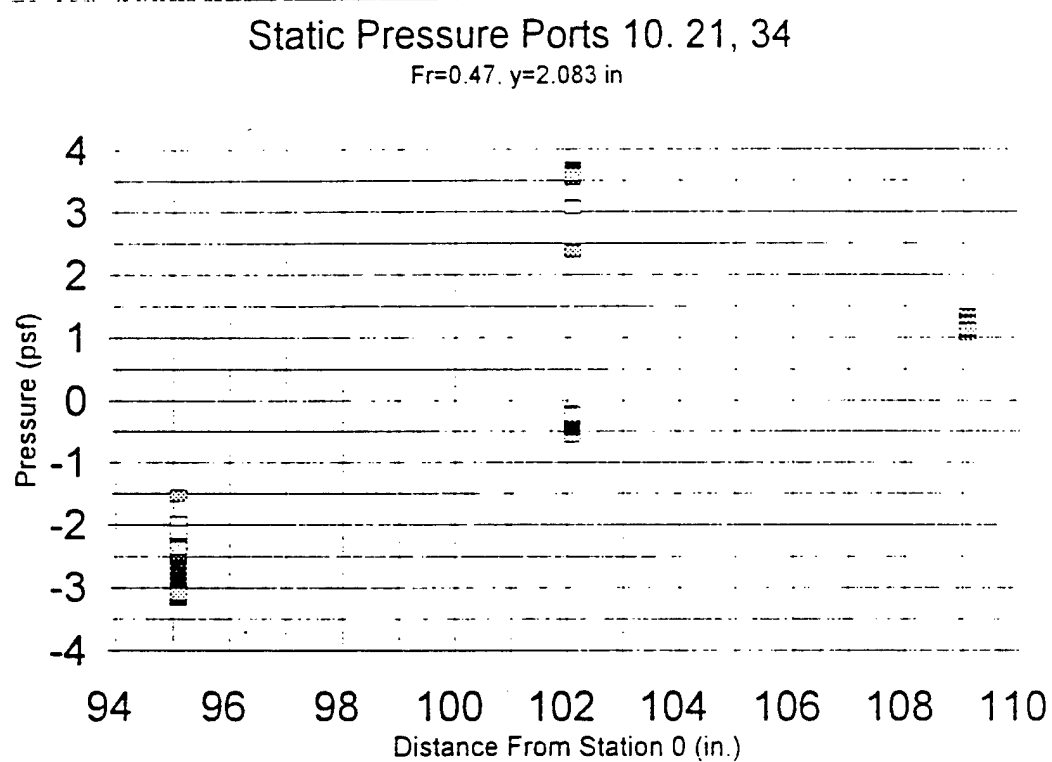
Figure 40 Spanwise distribution of data for static ports 10. 21. 34 at Fr = 0.47.
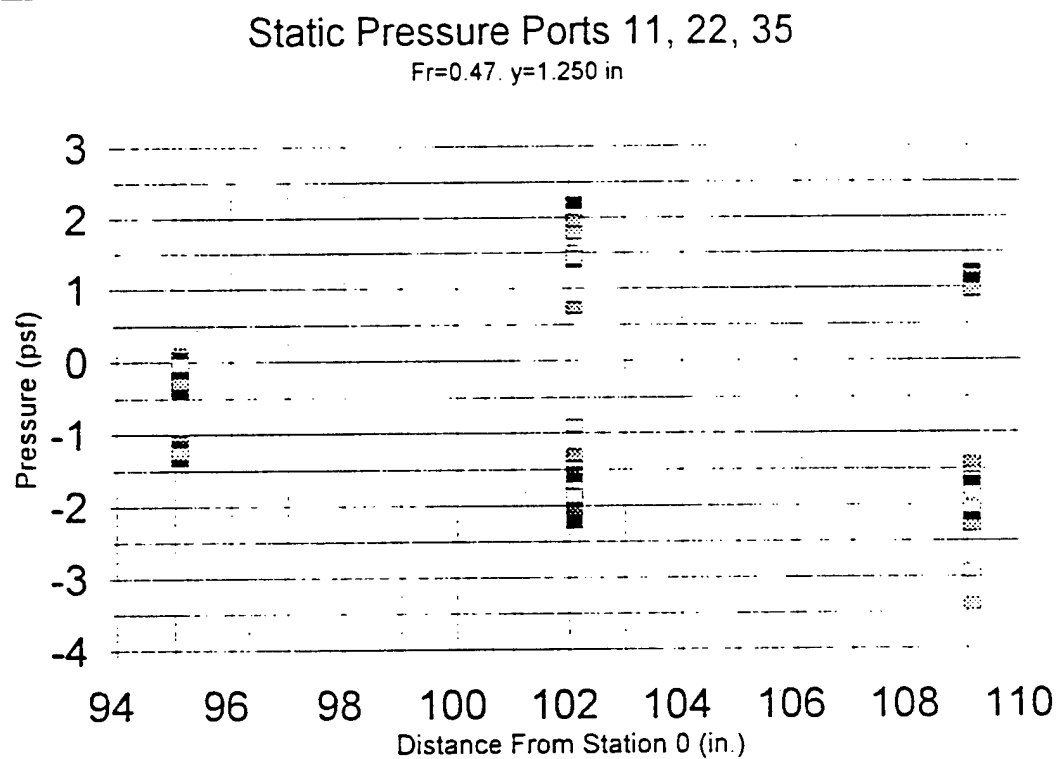
Figure 41 Spanwise distribution of data for static ports 11, 22, 35 at Fr = 0.47.
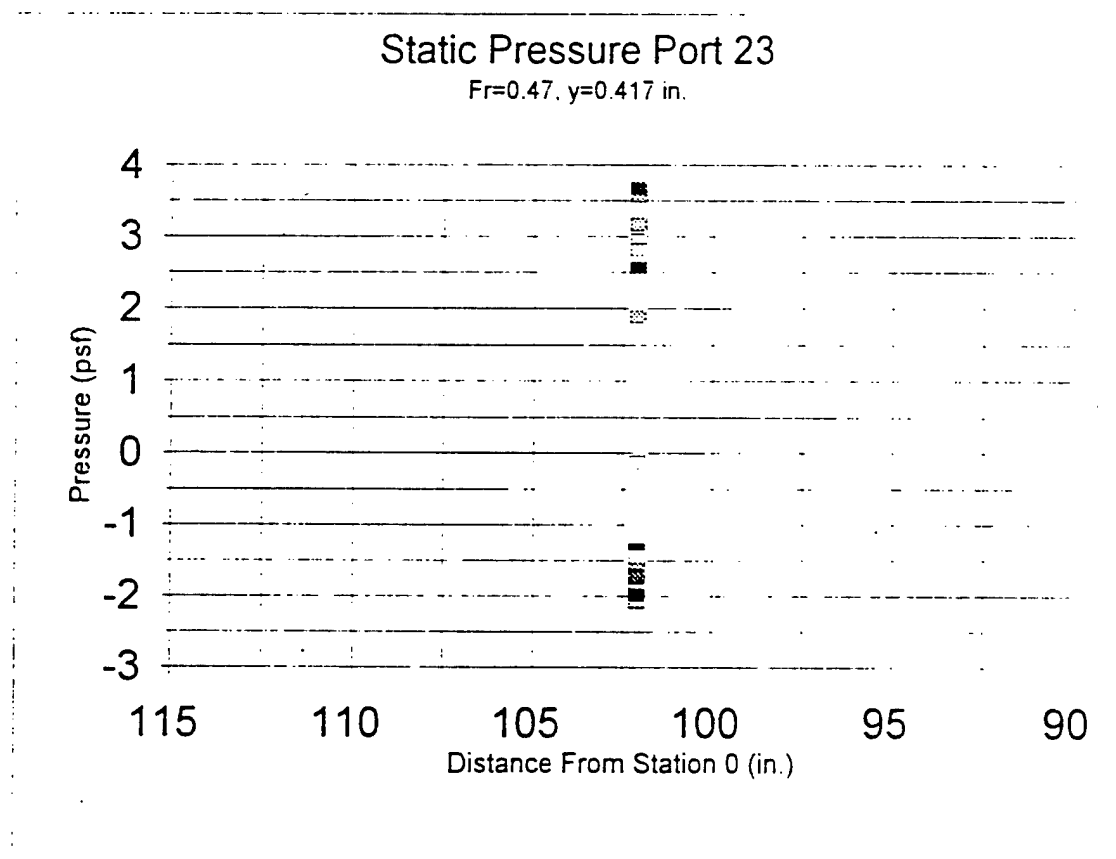
Figure 42 Spanwise distribution of data for static port 23 at Fr = 0.47

Static Pressure Ports 30, 42
Fr=0.47, y=0 in.
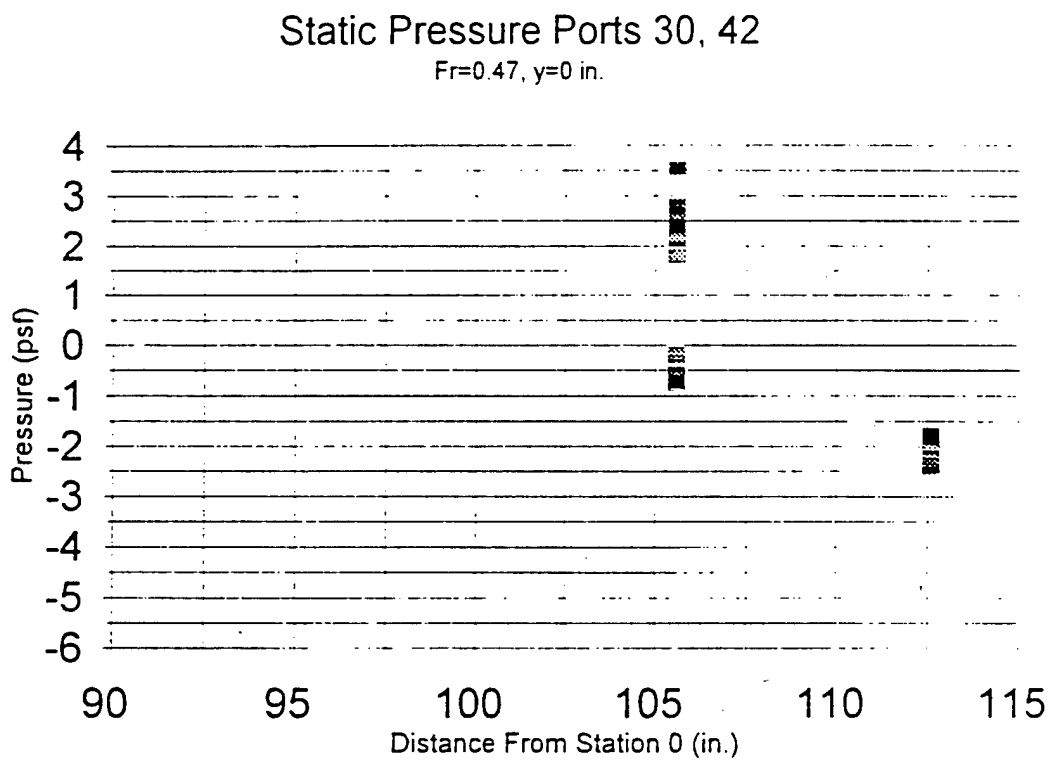
Figure 43 Spanwise distribution of data for static ports 30, 42 at Fr = 0.47

Static Pressure Ports 1 - 6
Fr=0.40. x=91.6 in.
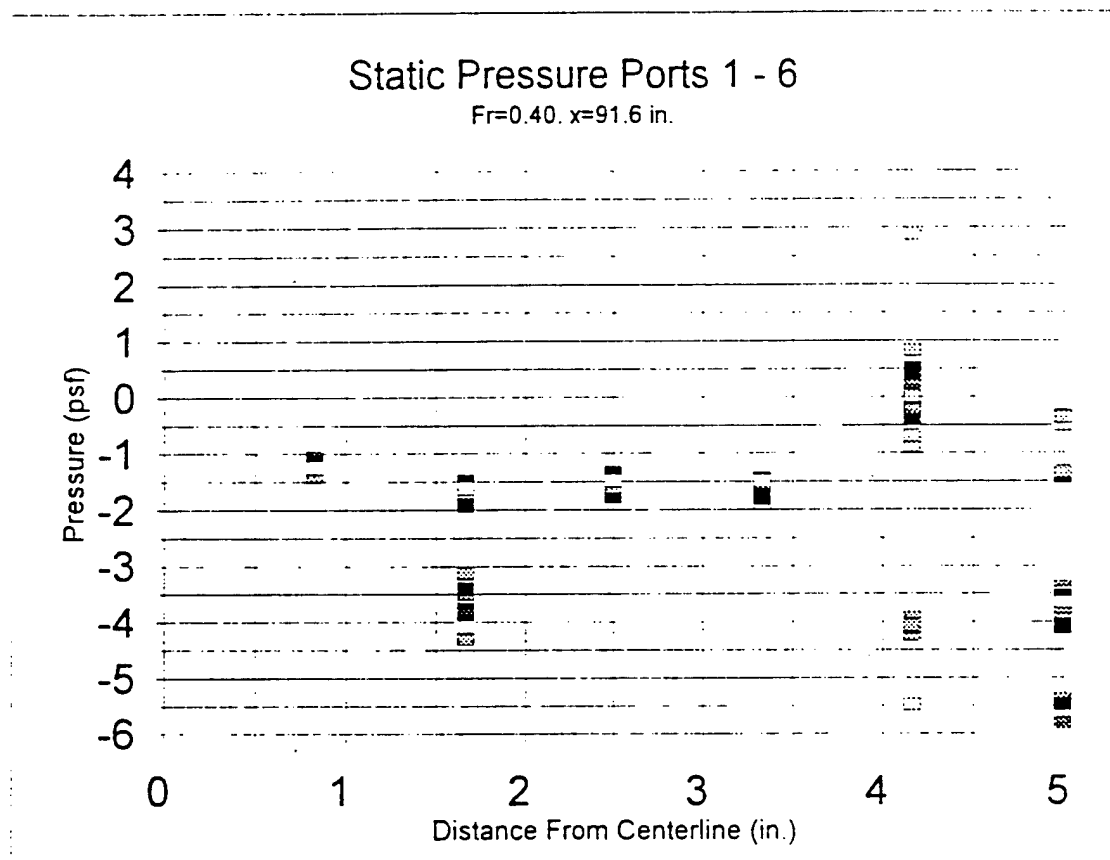
Figure 44 Chordwise distribution of data for static ports 1 - 6 at Fr = 0.40
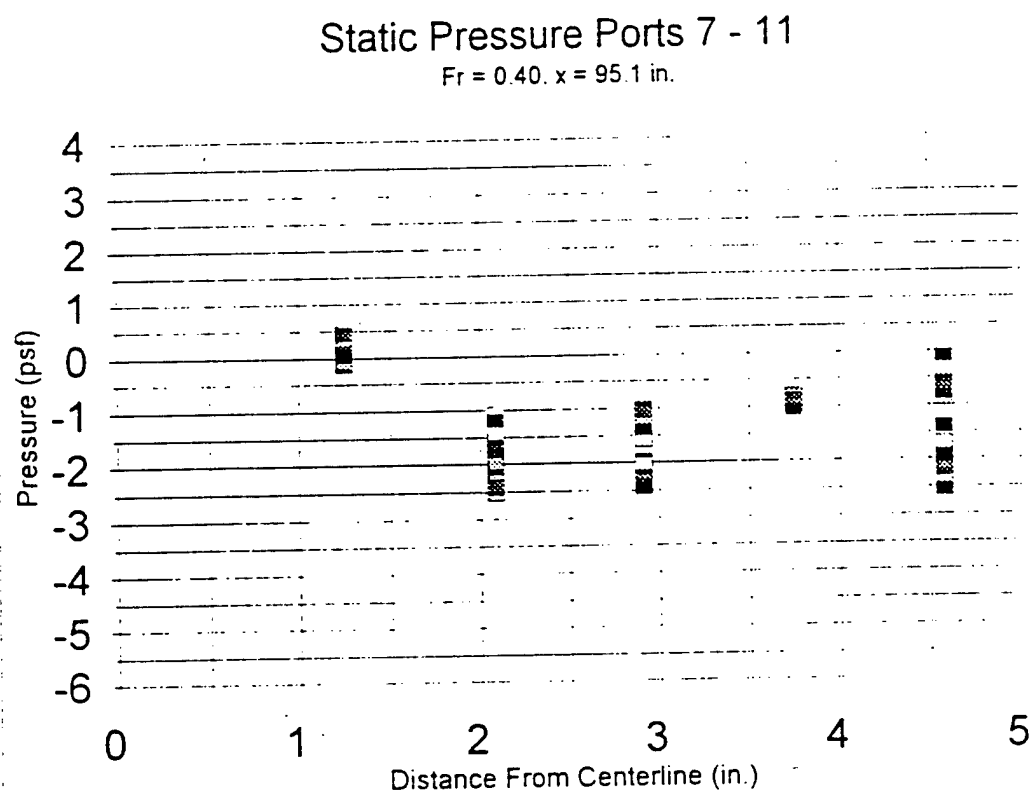
Figure 45 Chordwise distribution of data for static ports 7 - 11 at Fr = 0.40

Static Pressure Ports 12 - 17
Fr=0.40. x=98.6 in.
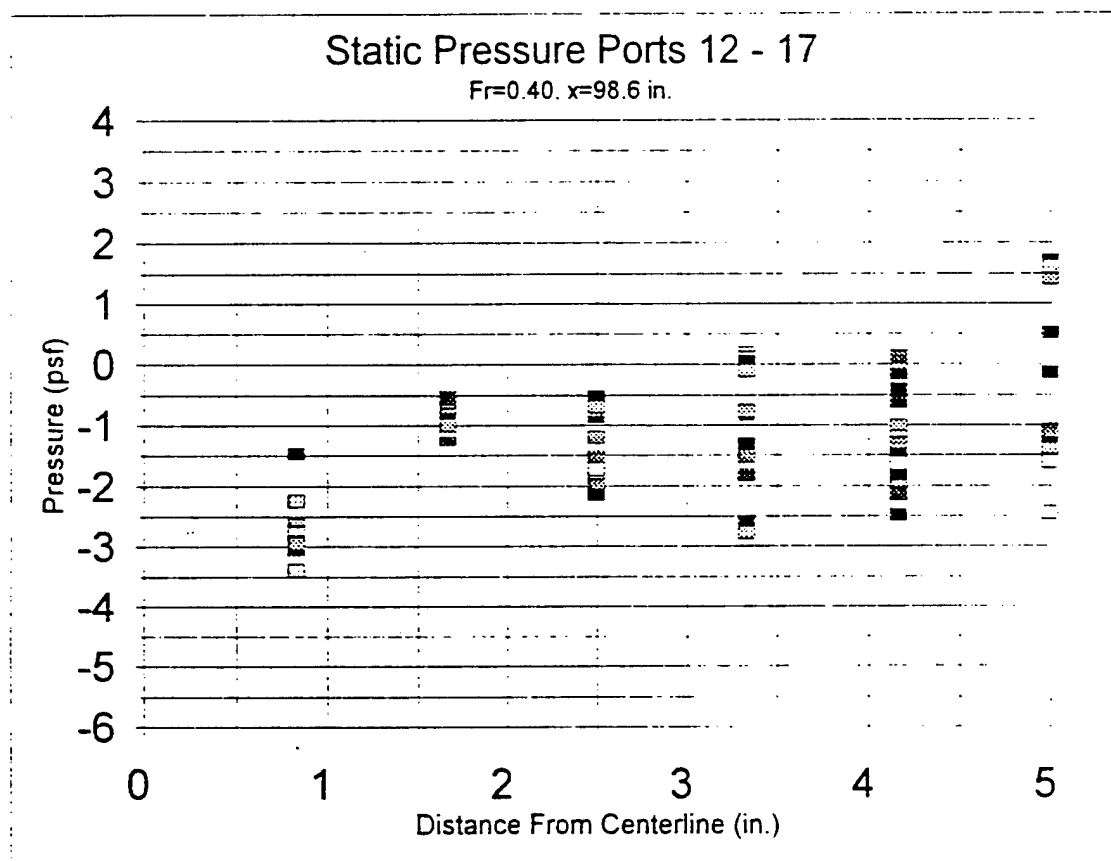
Figure 46 Chordwise distribution of data for static ports 12 - 17 at Fr = 0.40
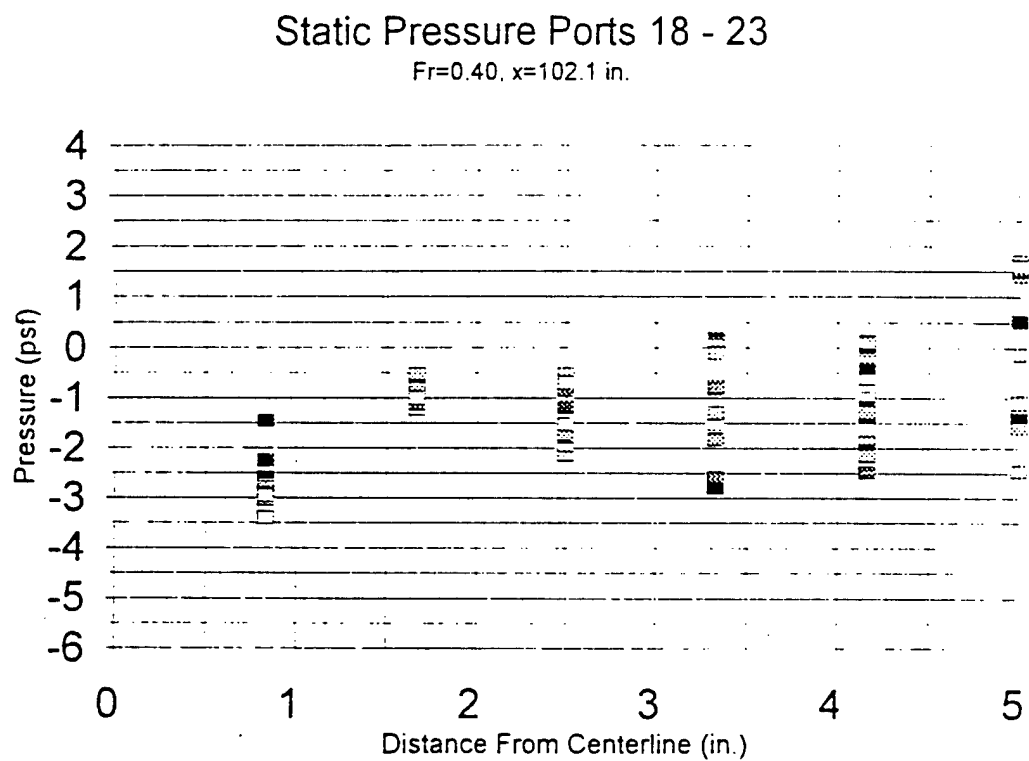
Figure 47 Chordwise distribution of data for static ports 18 - 23 at Fr = 0 40

Static Pressure Ports 24 - 30
Fr=.40. x=105.6 in.
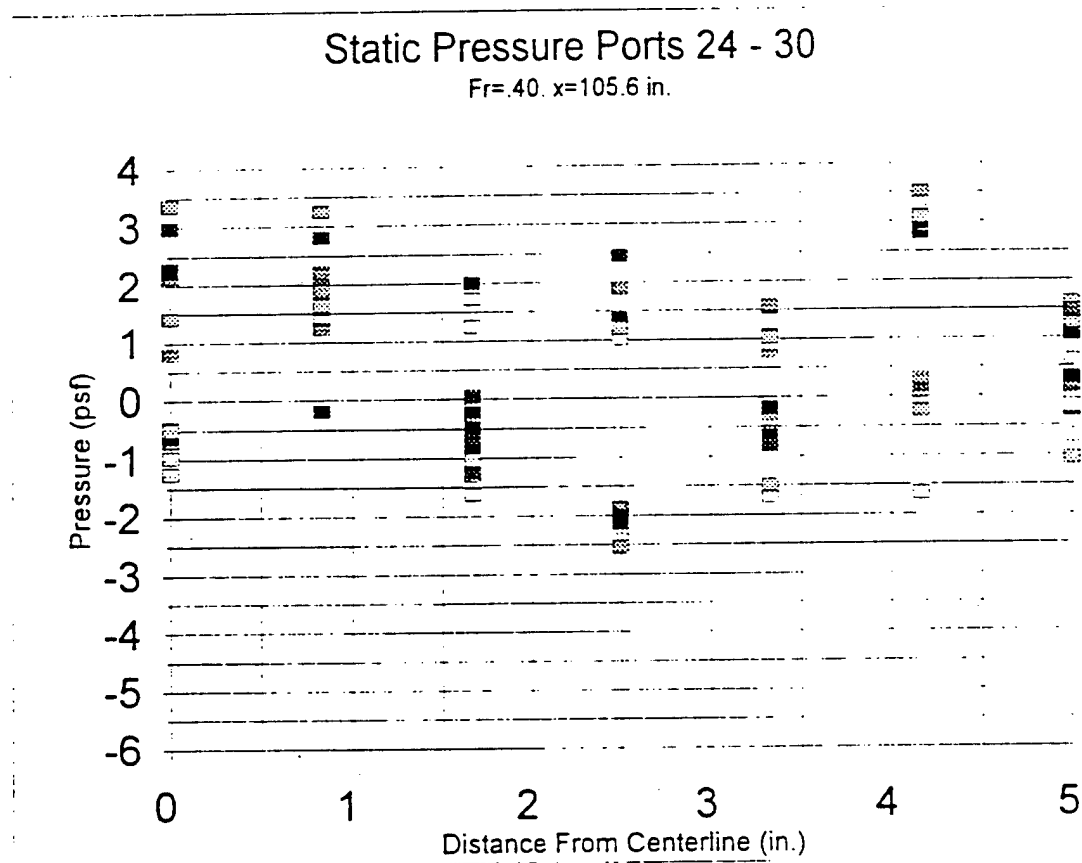
Figure 48 Chordwise distribution of data for static ports 24 - 30 at Fr = 0.40.

Static Pressure Ports 31 - 36
Fr=0.40, x=109.1 in.
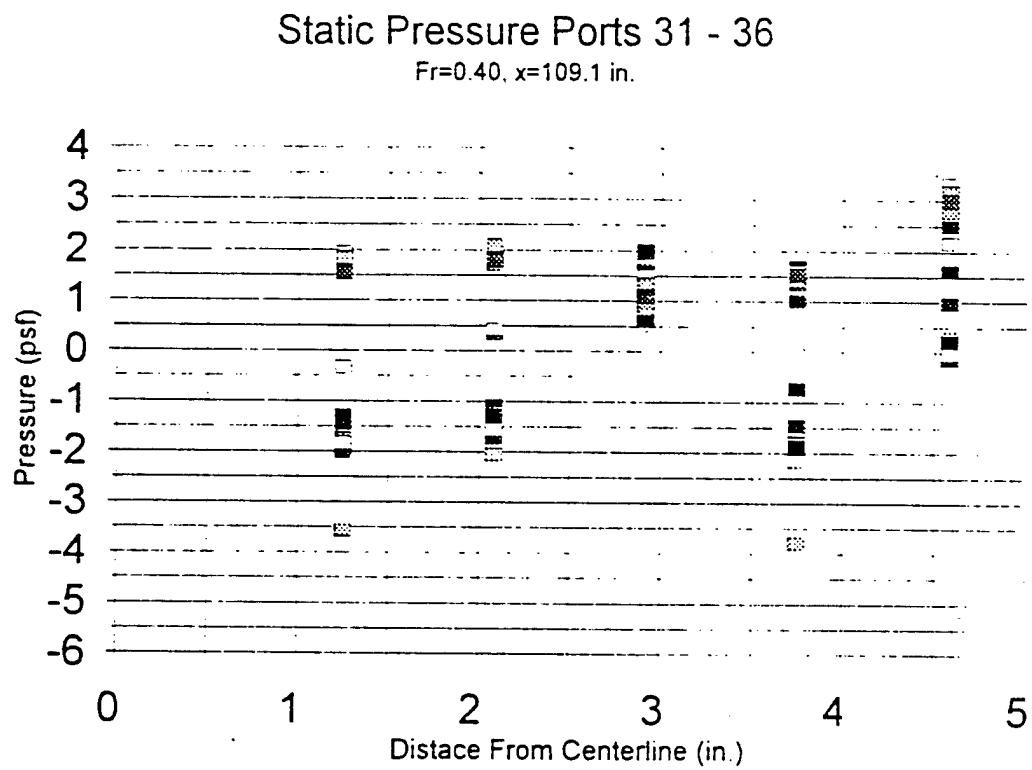
Figure 49 Chordwise distribution of data for static ports 31 - 36 at Fr = 0.40

Static Pressure Ports 37 - 42

Fr = 0.40, x = 112.6 in.
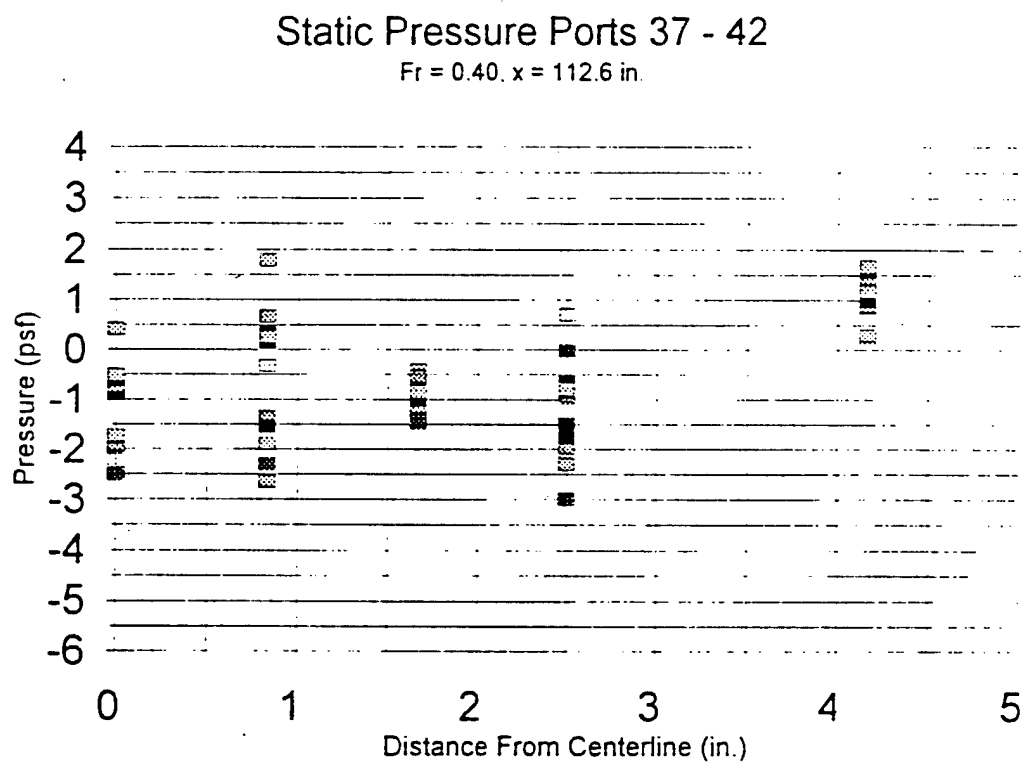
Figure 50 Chordwise distribution of data for static ports 37 - 42 at Fr = 0.40

Static Pressure Ports 1 - 6
Fr = 0.47, x = 91.6 in.
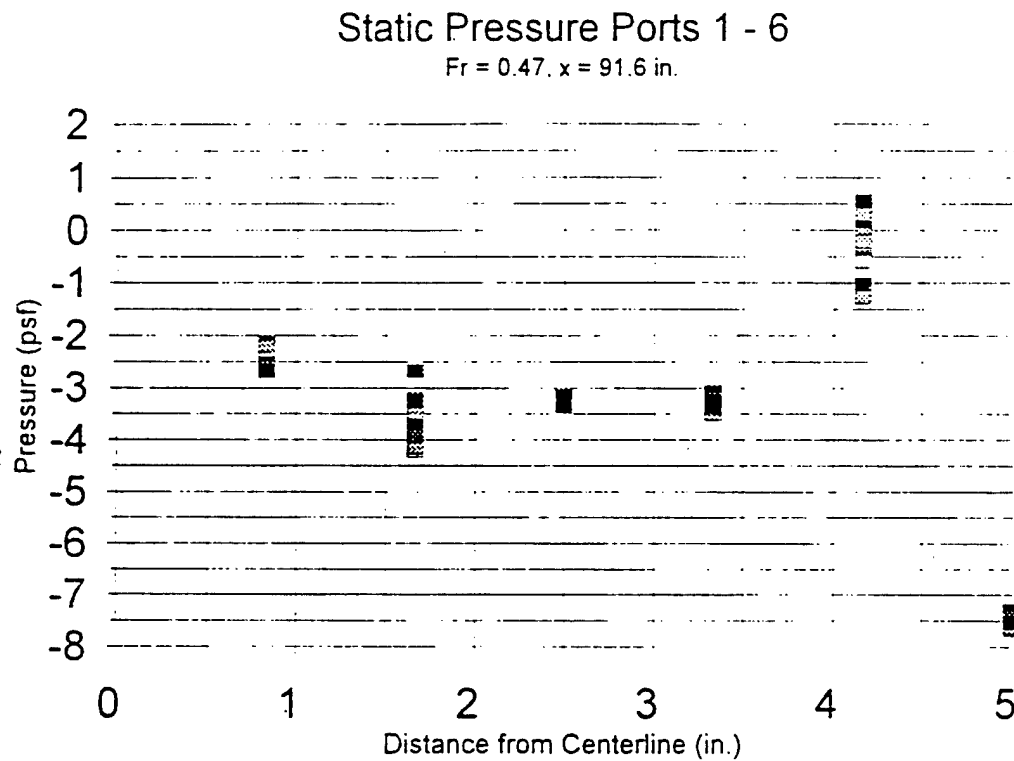
Figure 51 Chordwise distribution of data for static ports 1 - 6 at Fr = 0.47

Static Pressure Ports 7 - 11
Fr = 0.47, x = 95.1 in.
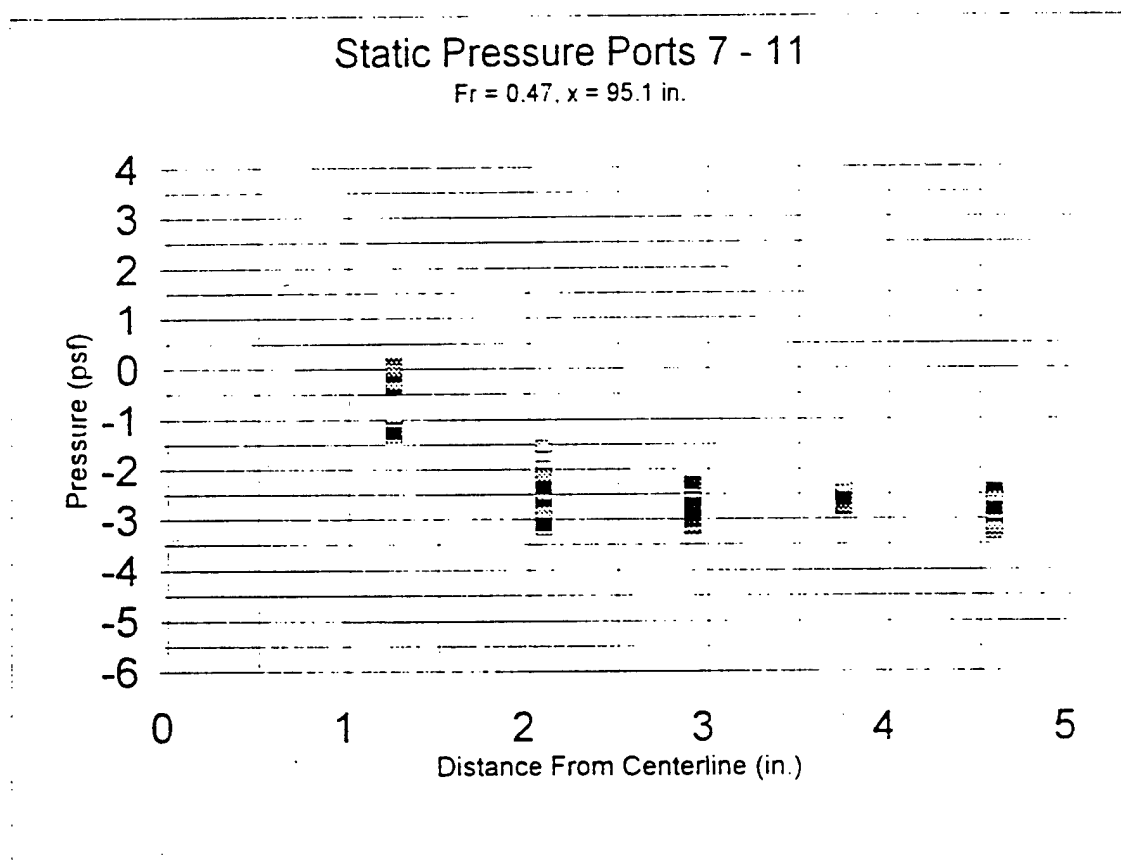
Figure 52 Chordwise distribution of data for static ports 7 - 11 at Fr = 0.47

Static Pressure Ports 12 - 17

Fr = 0.47. x = 98.6 in.
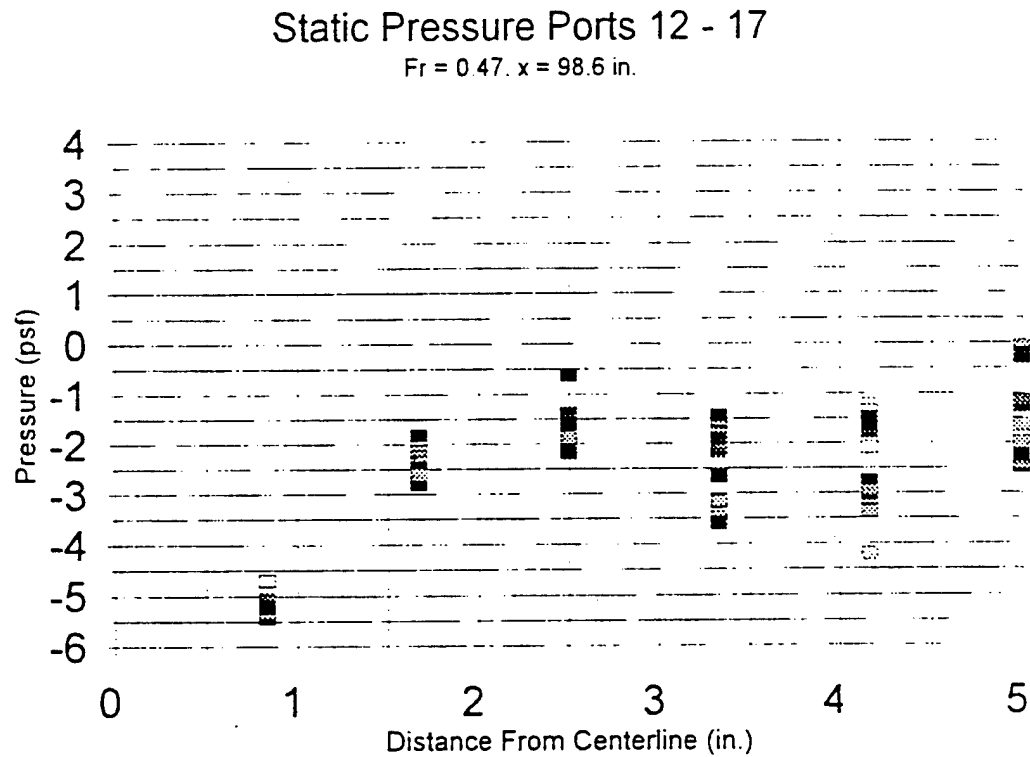
Figure 53 Chordwise distribution of data for static ports 12 - 17 at Fr = 0 47
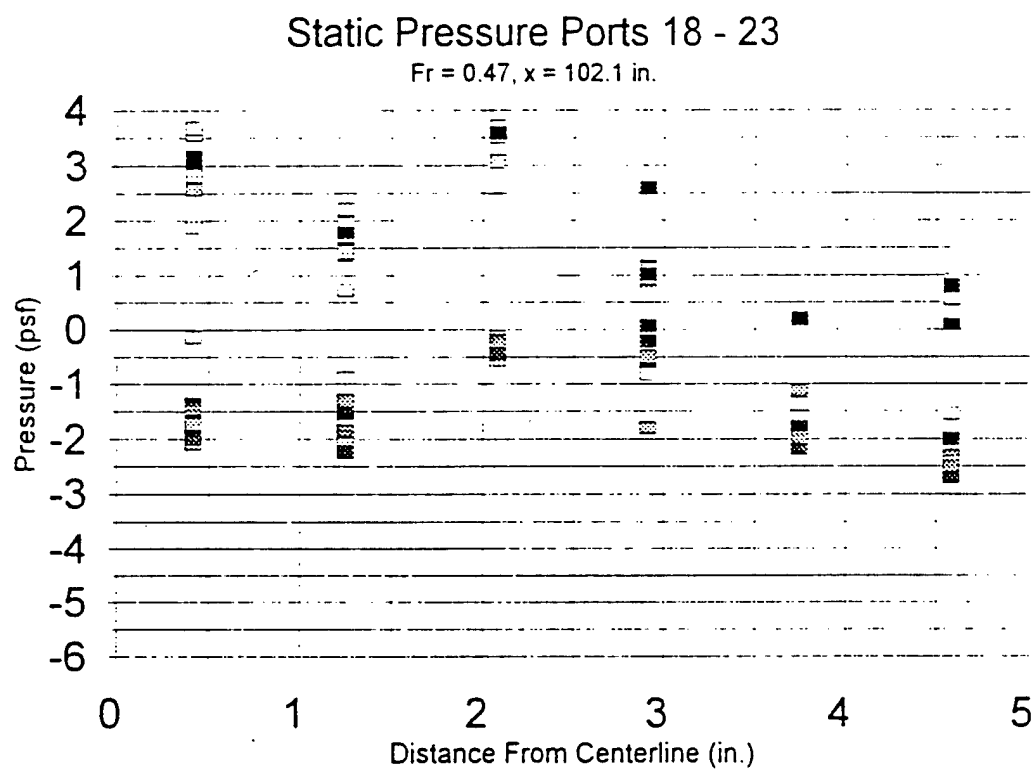
Figure 54 Chordwise distribution of data for static ports 18 - 23 at Fr = 0.47

Static Pressure Ports 24 - 30

Fr = 0.47, x = 105.6 in.

Figure 55: Chordwise distribution of data for static ports 24 - 30 at Fr = 0.47.

Figure 56. Chordwise distribution of data for static ports 31 - 36 at Fr = 0.47

Figure 57: Chordwise distribuiton of data for static ports 37 - 42 at Fr = 0.47.
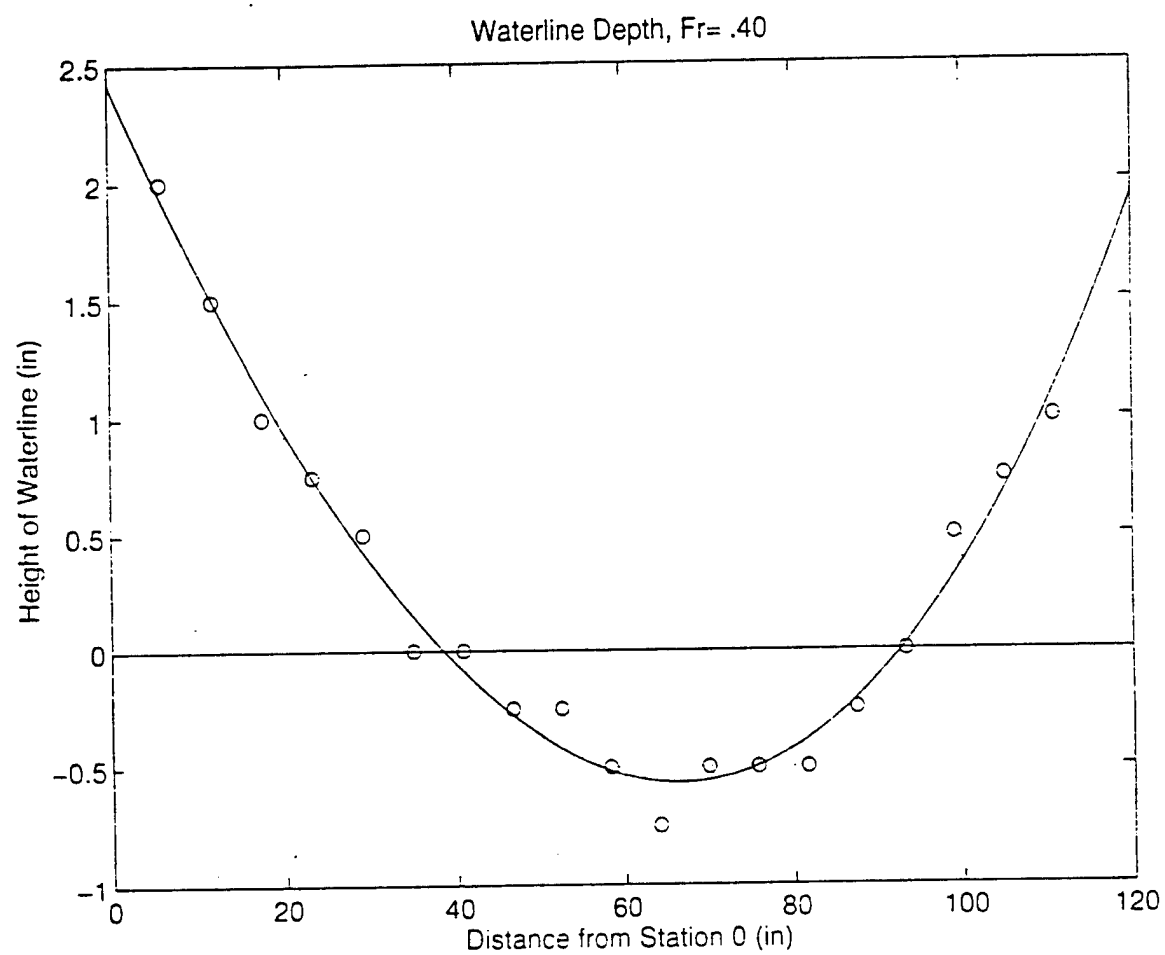
Figure 58: Waterline height at Fr = 0.40
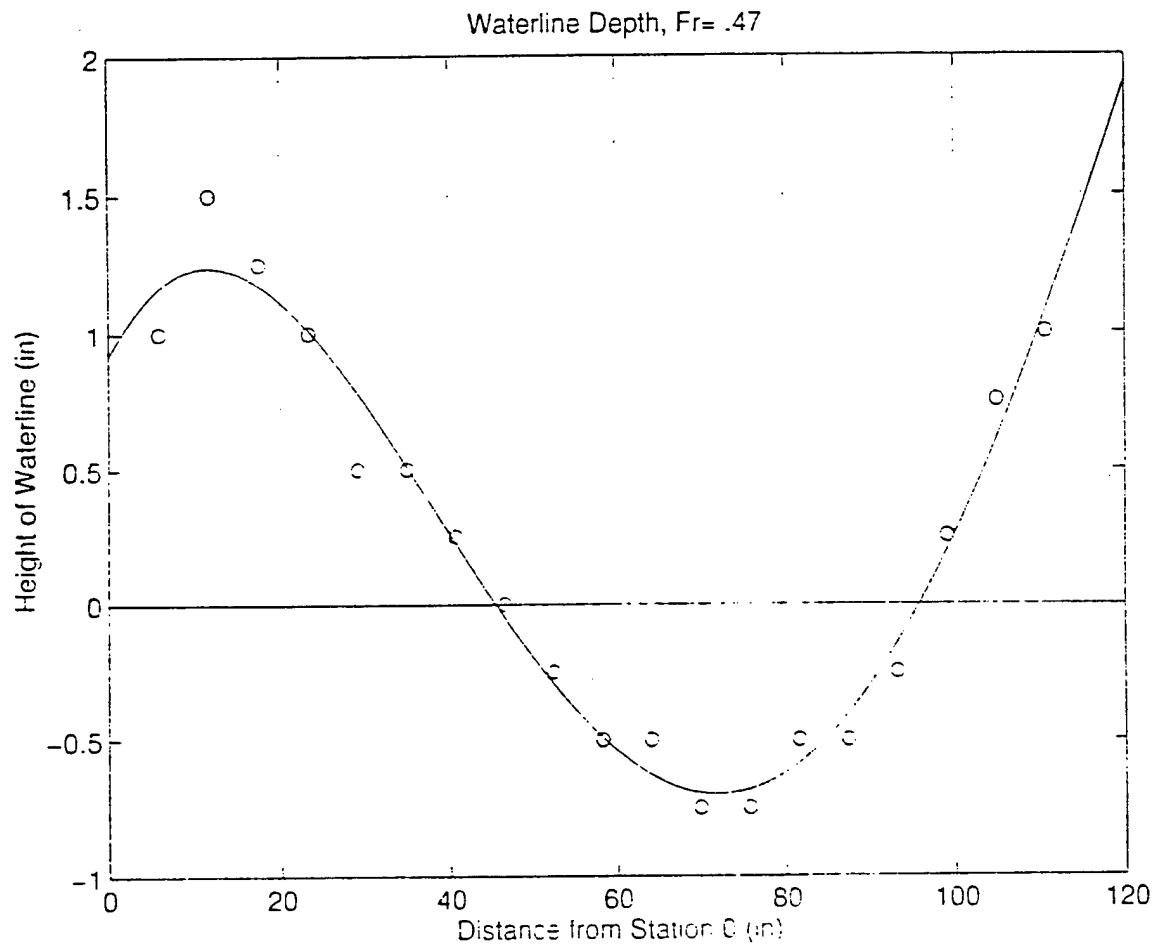
Figure 59: Waterline height at Fr = 0.47

Pressure Distribution on the Aft Section of the Hull
Fr = .47

Pressure (psf)

Distance from
Centerline (in)

Distance from
Bow (in)

Pressure Distribution on the Aft Section of the Hull
Fr = .40

Pressure (psf)

Distance from
Centerline (in)

Distance from
Bow (in)
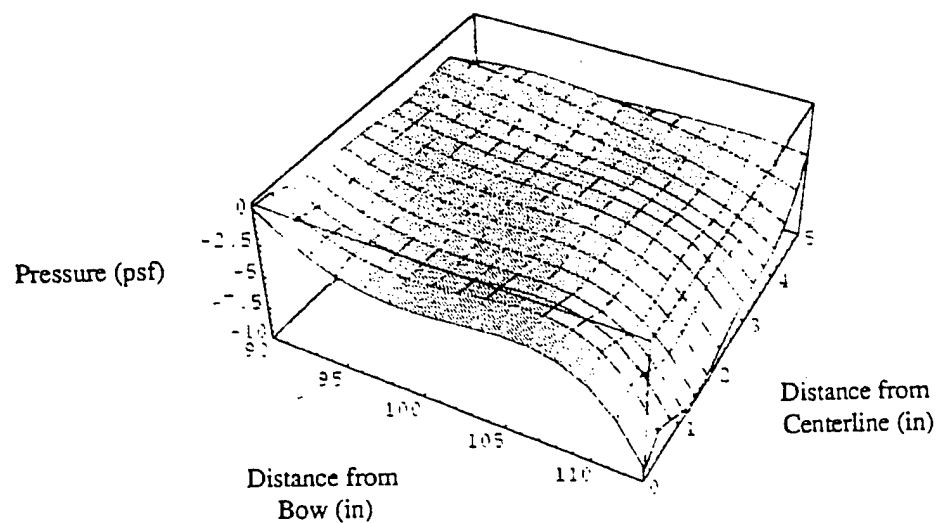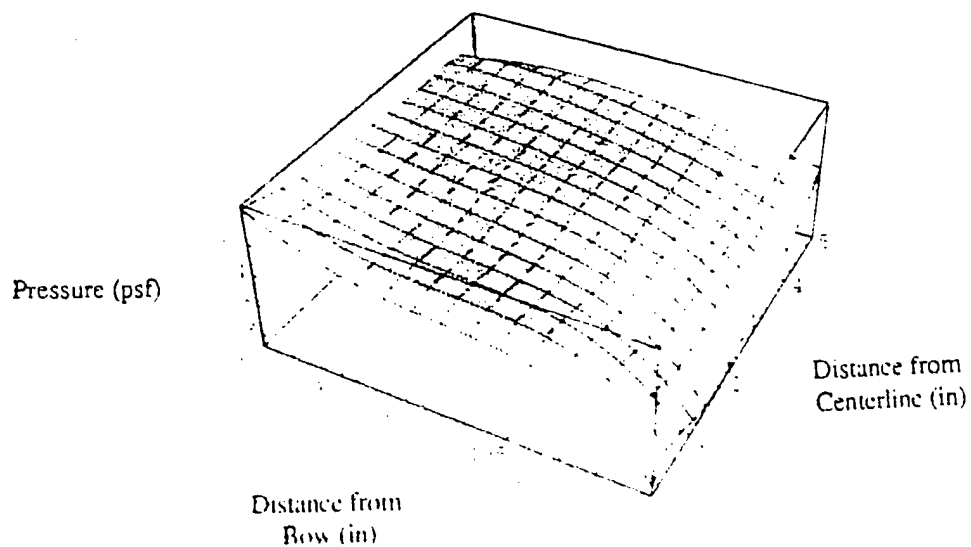
Figure 60: Surface plots of pressure distribution.
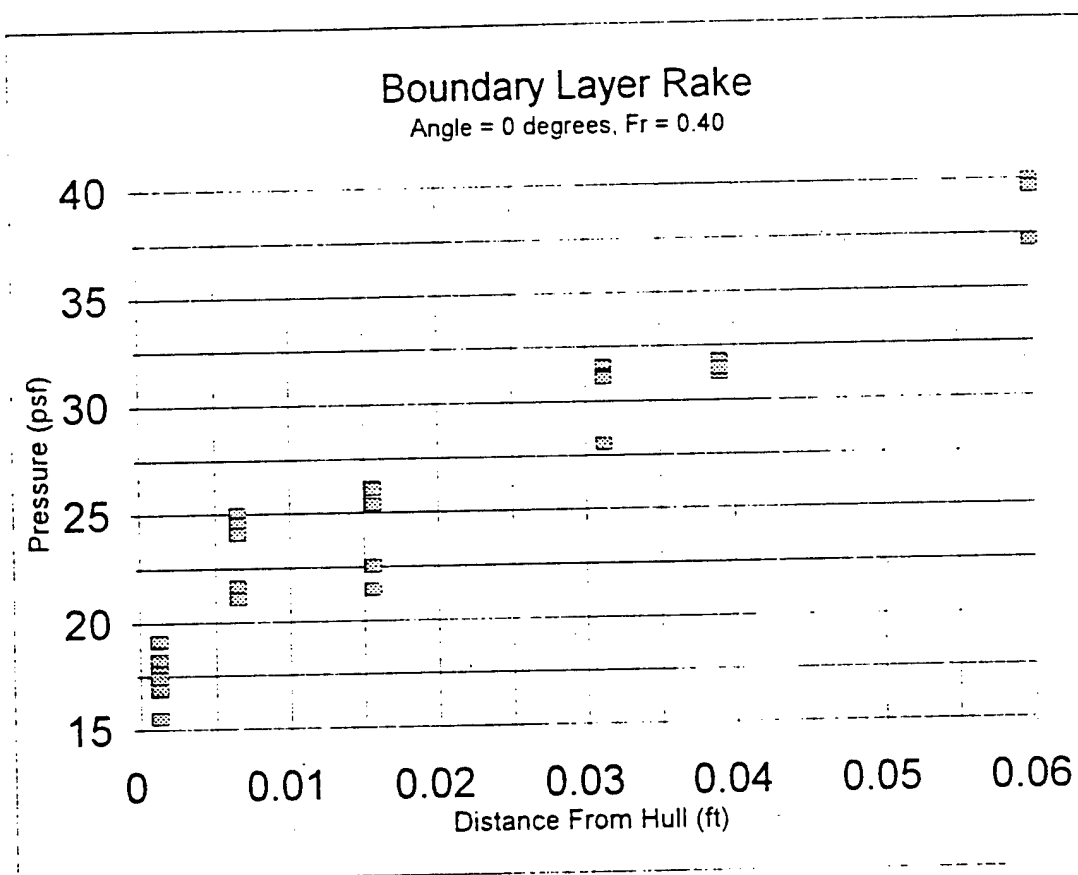
Figure 61. Boundary layer rake data for angle 0 degrees at Fr = 0.40.
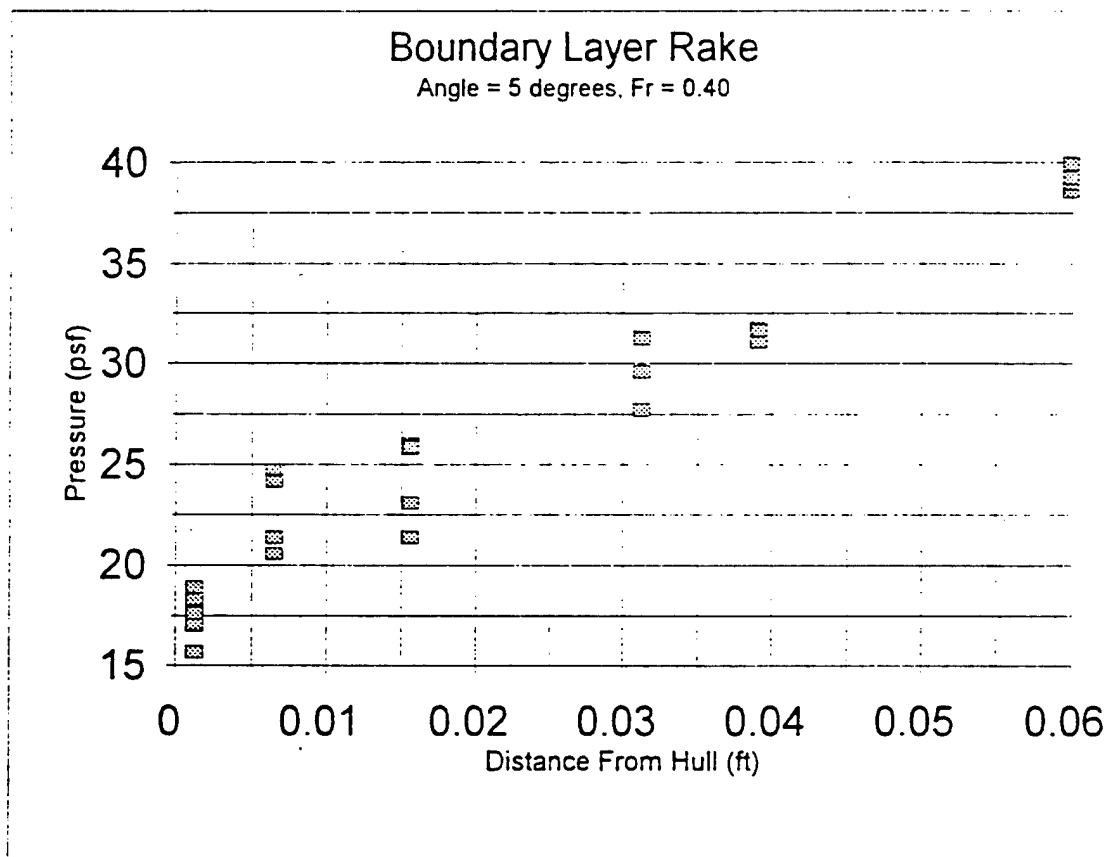
Figure 62: Boundary layer rake data for angle 5 degrees at Fr = 0.40.

# Boundary Layer Rake
Angle = 10 degrees. Fr = 0.40
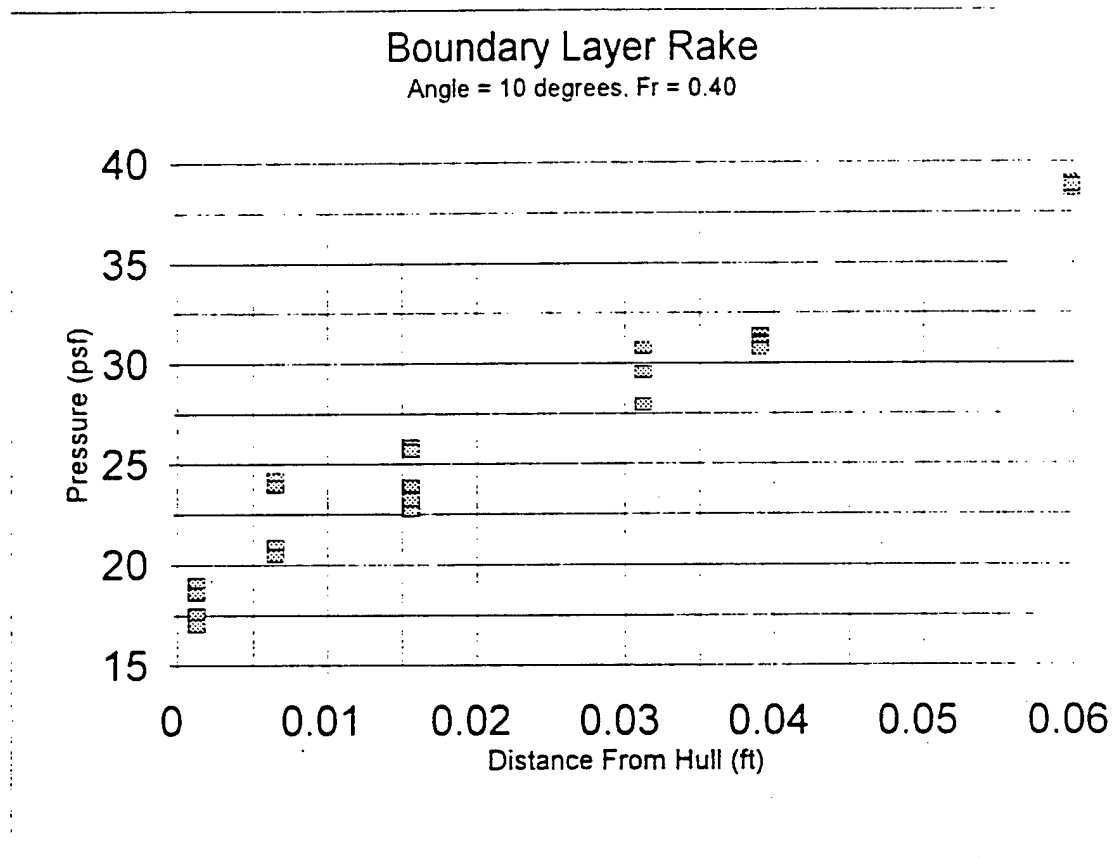
Figure 63 Boundary layer rake data for angle 10 degrees at Fr = 0.40.
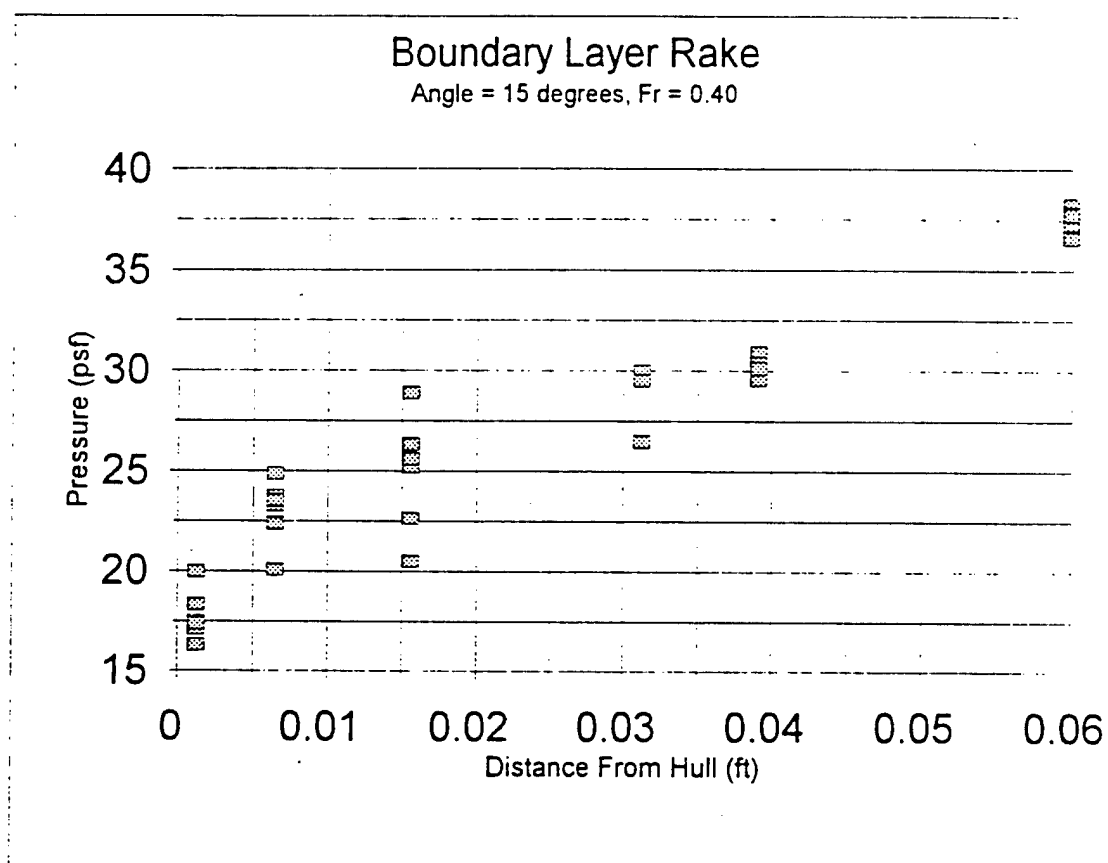
Figure 64. Boundary layer rake data for angle 15 degrees at Fr = 0.40.
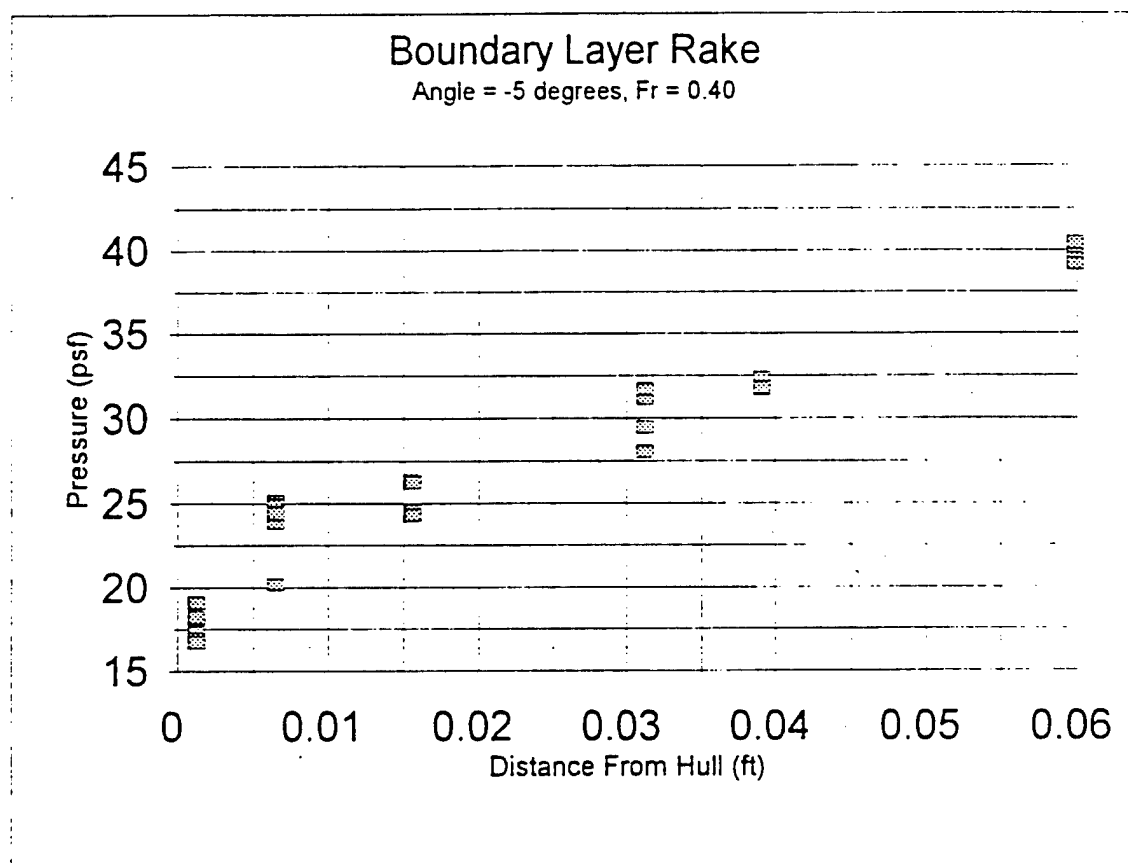
Figure 65 Boundary layer rake data for angle -5 degrees at Fr = 0.40.
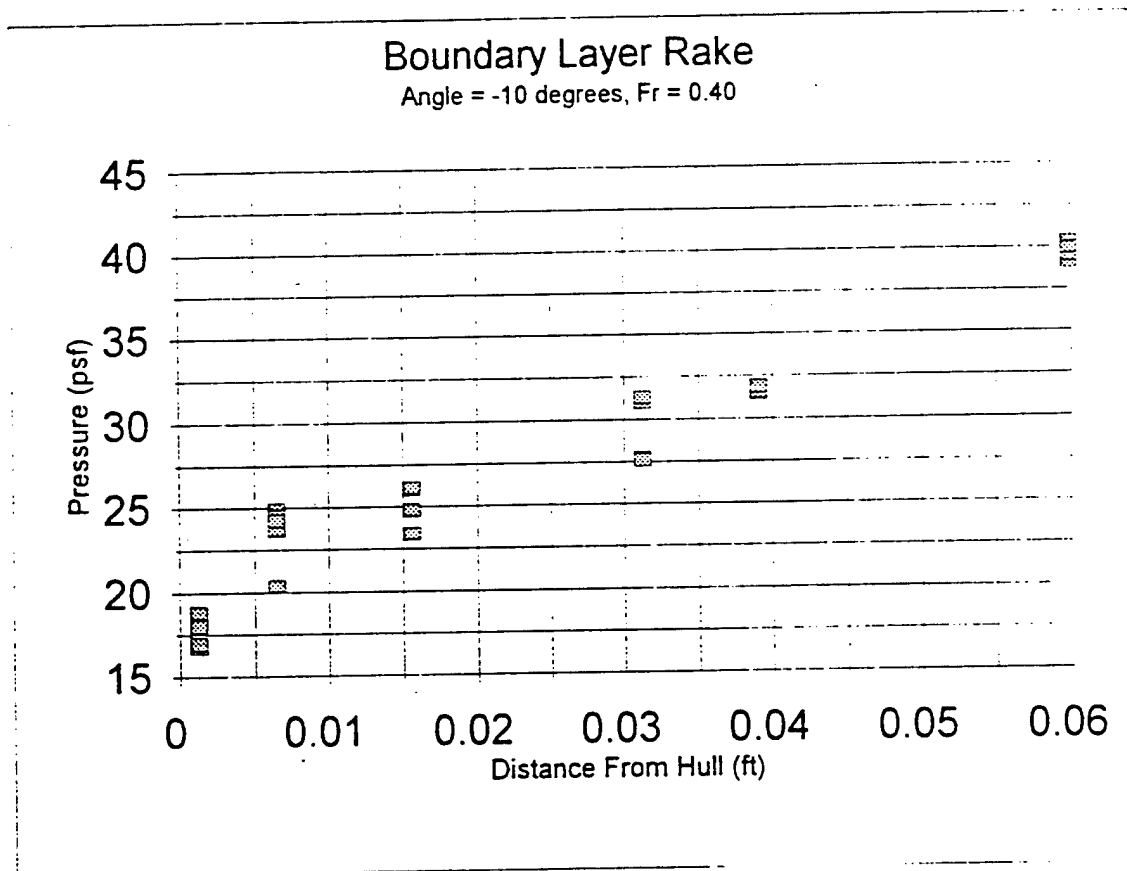
Figure 66: Boundary layer rake data for angle -10 degrees at Fr = 0.40.

Boundary Layer Rake

Angle = -15 degrees, Fr = 0.40
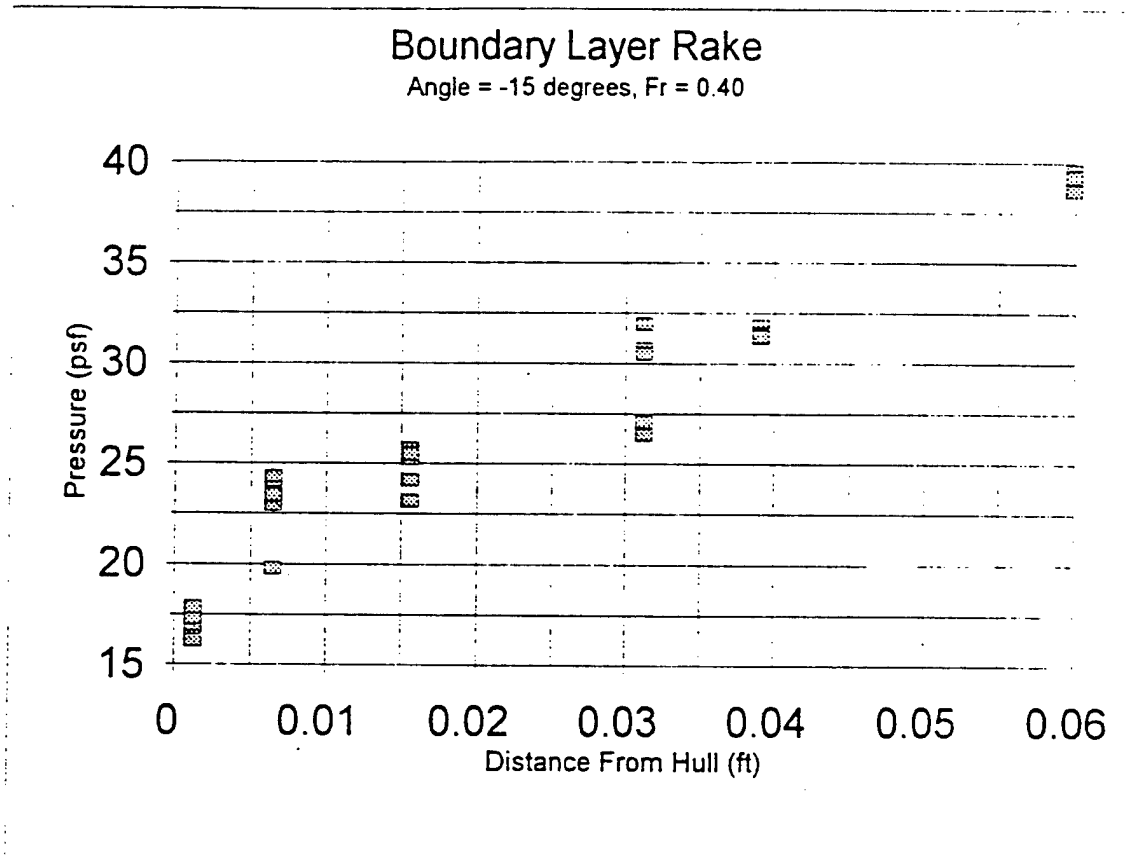
Figure 67. Boundary layer rake data for angle -15 degrees at Fr = 0.40
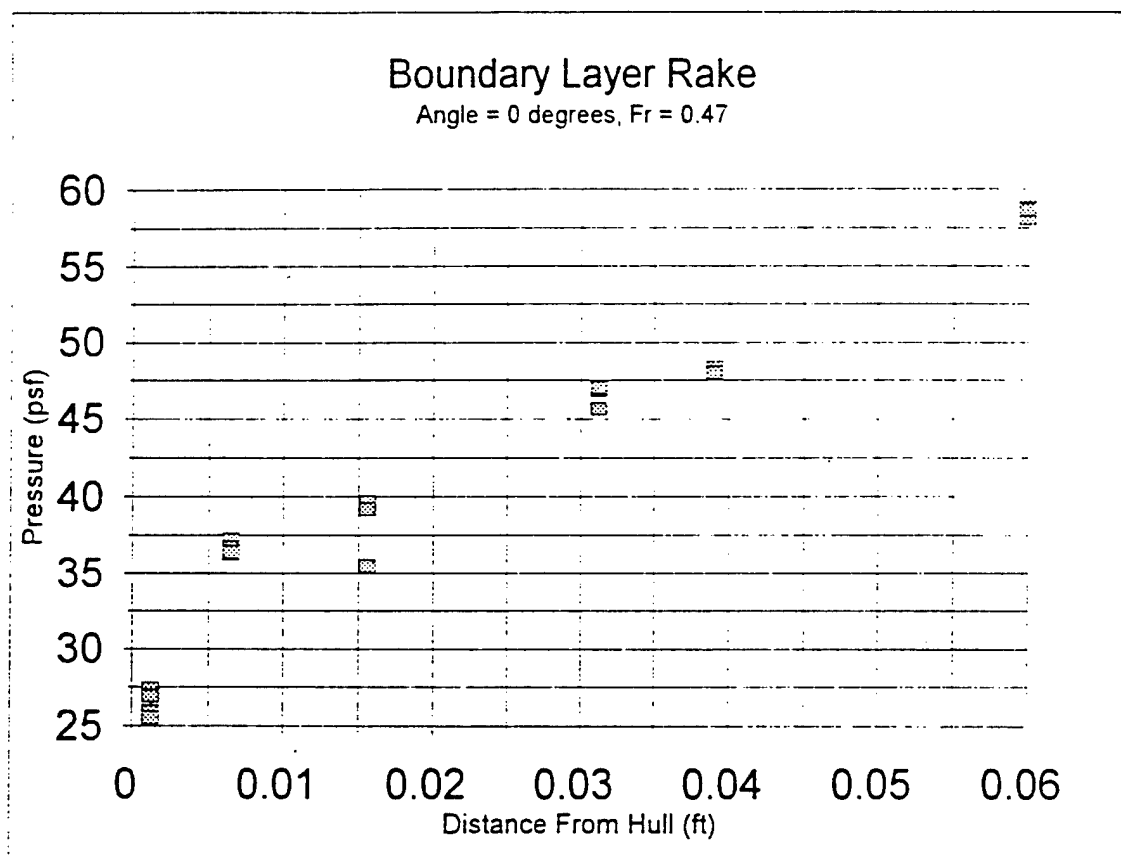
Figure 68 Boundary layer rake data for angle 0 degrees at Fr = 0.47
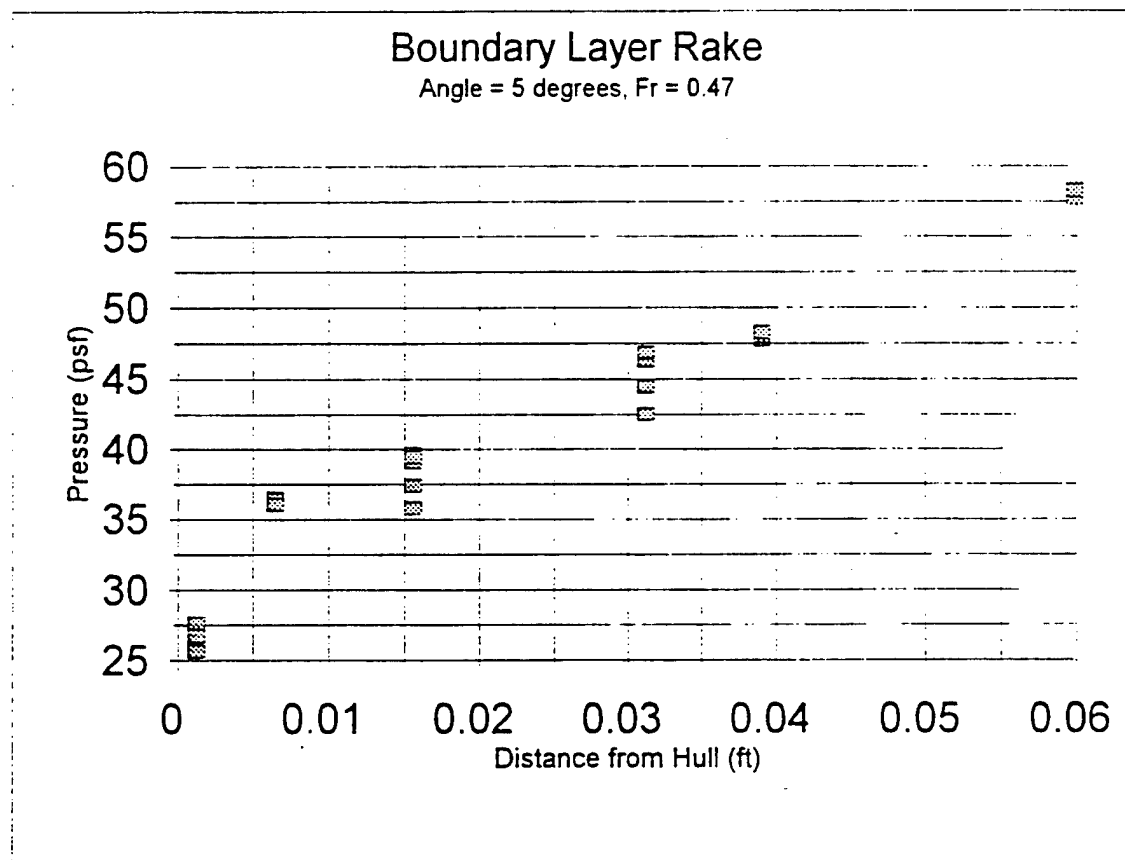
Figure 69: Boundary layer rake data for angle 5 degrees at Fr = 0.47
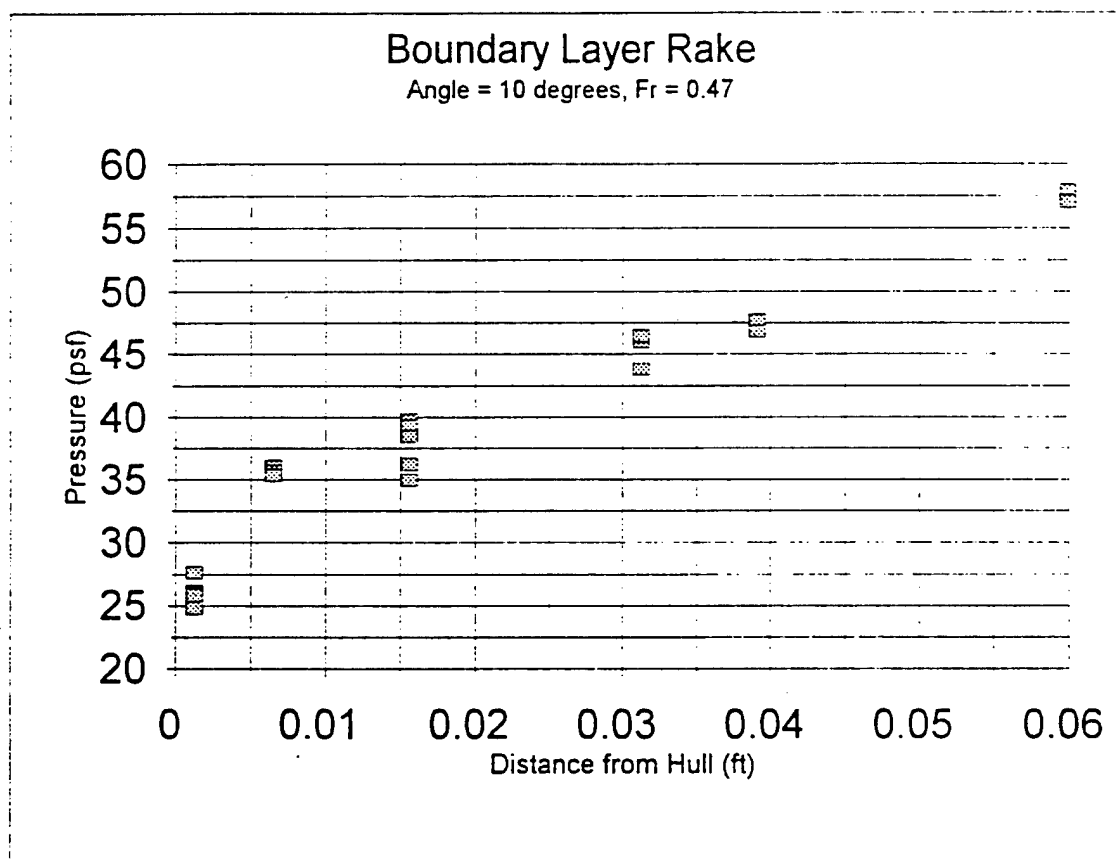
Figure 70. Boundary layer rake data for angle 10 degrees at Fr = 0.47.
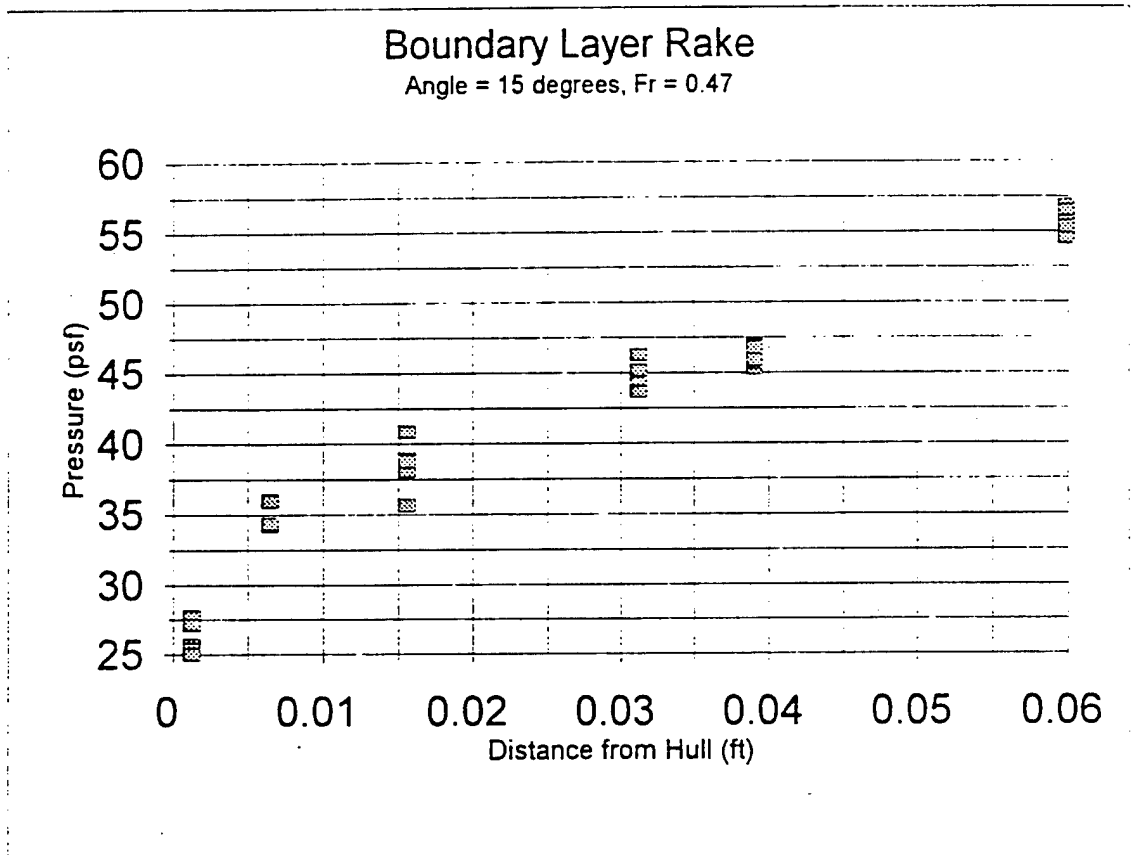
Figure 71: Boundary layer rake data for angle 15 degrees at Fr = 0.47.
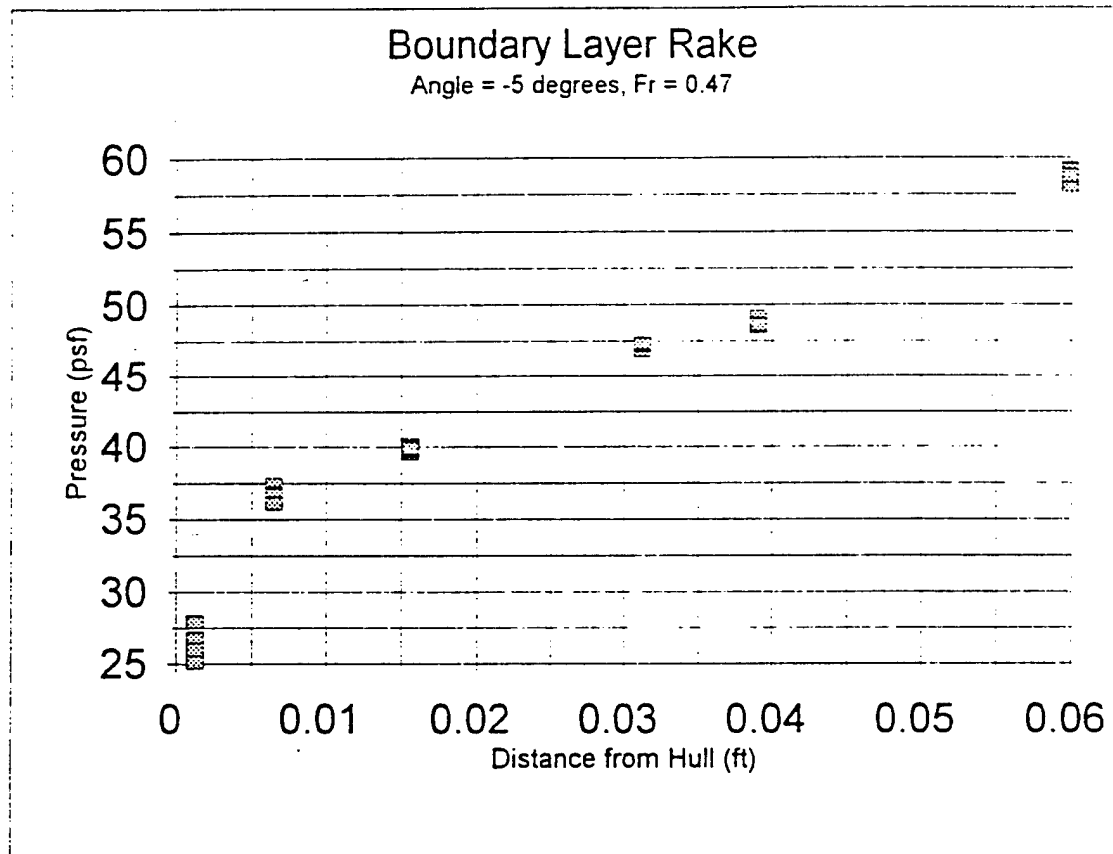
Figure 72: Boundary layer rake data for angle -5 degrees at Fr = 0 47.
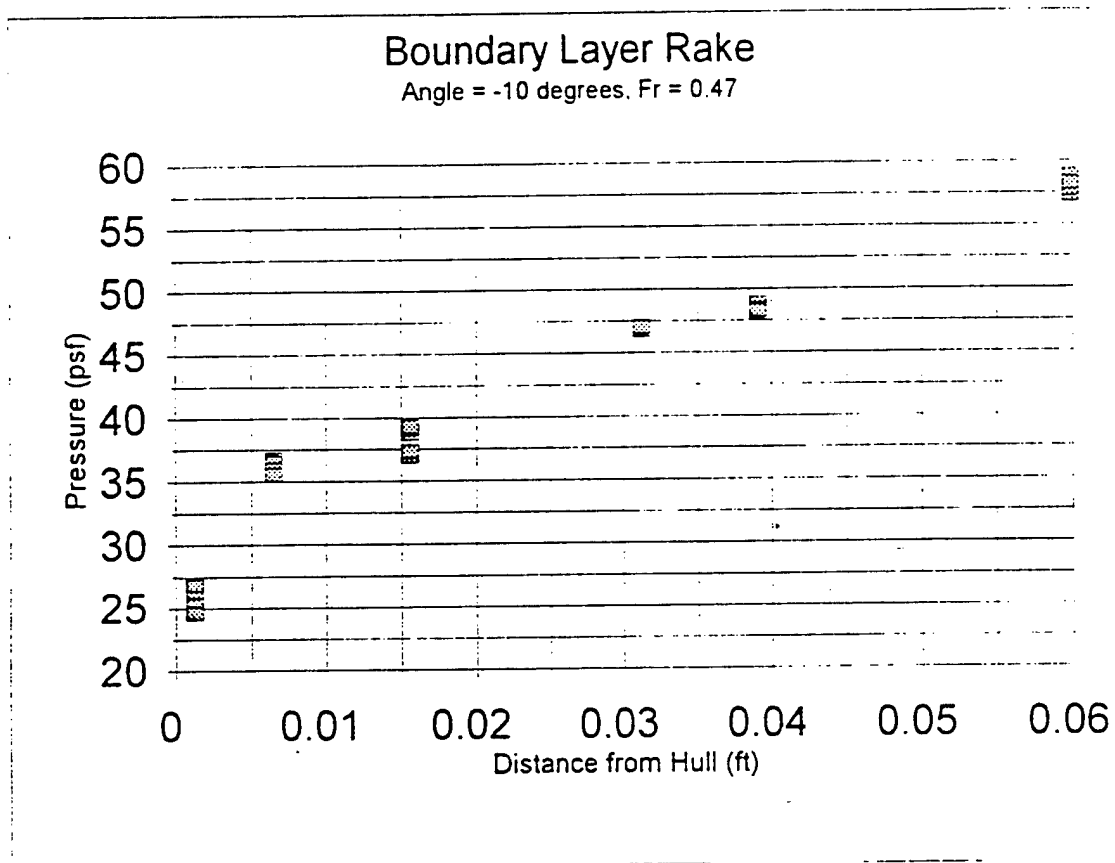
Figure 73: Boundary layer rake data for angle -10 degrees at Fr = 0.47.

Boundary Layer Rake

Angle = -15 degrees, Fr = 0.47

Pressure (psf) vs Distance from Hull (ft)
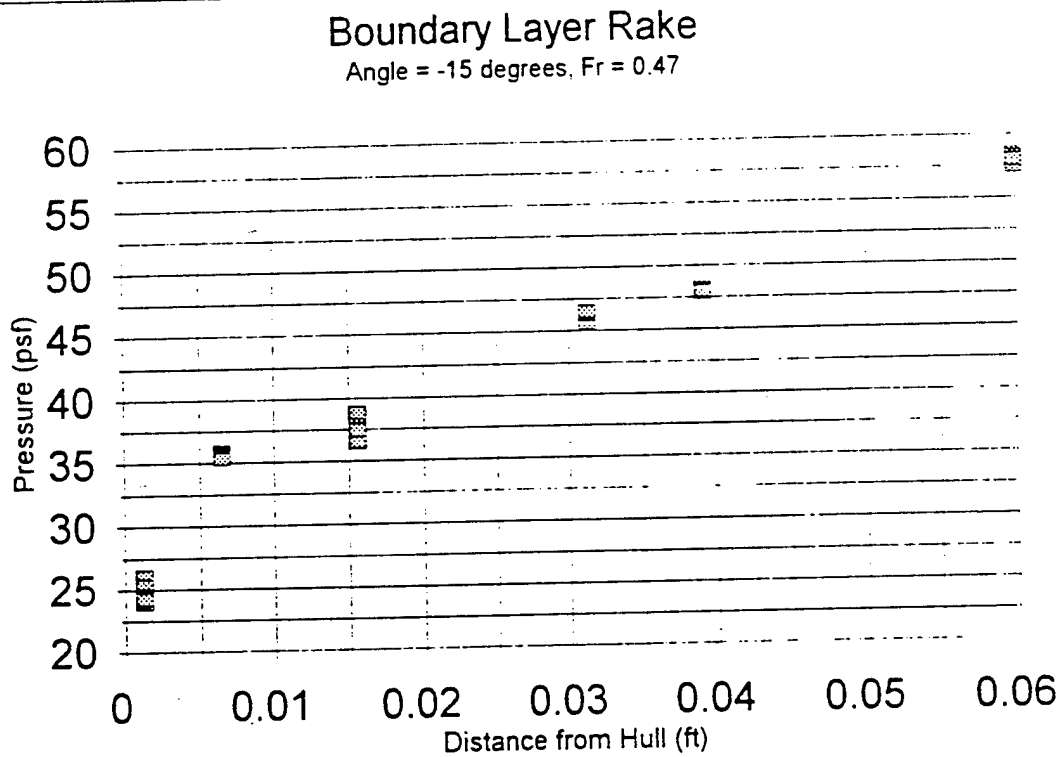
Figure 74 Boundary layer rake data for angle -15 degrees at Fr = 0.47.

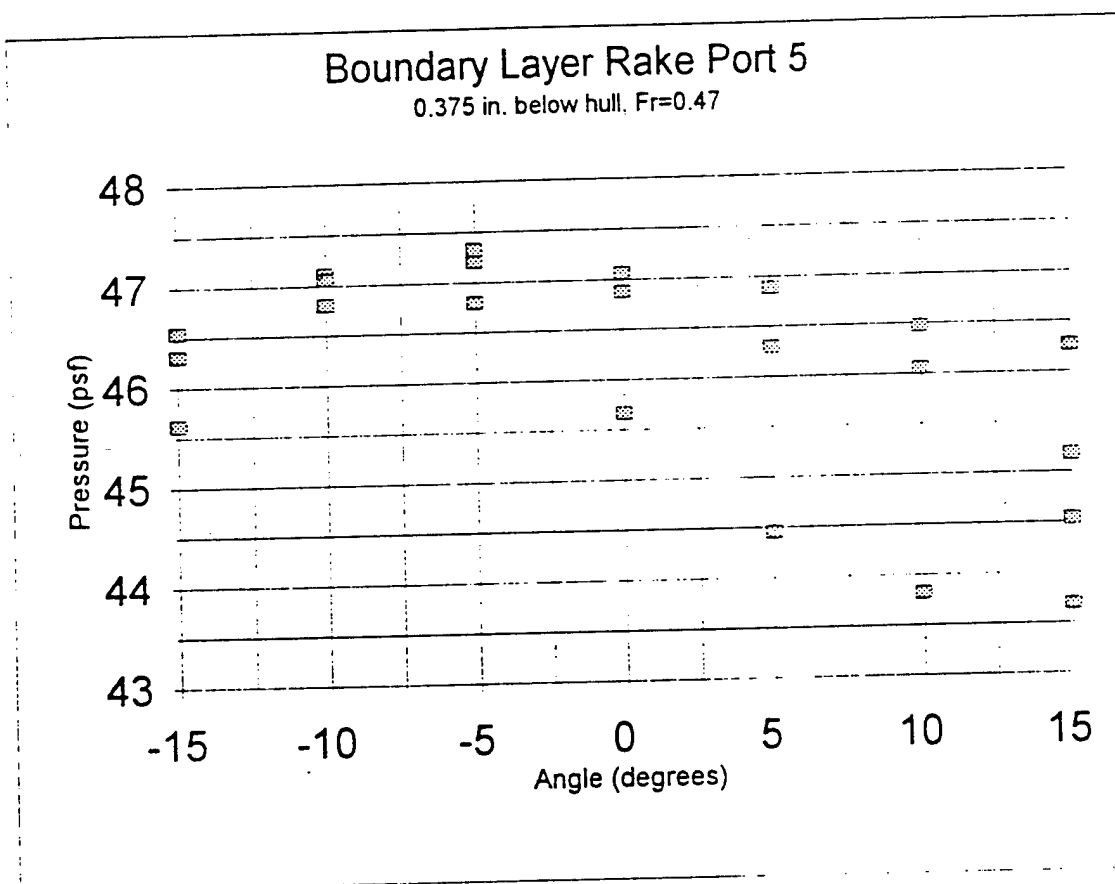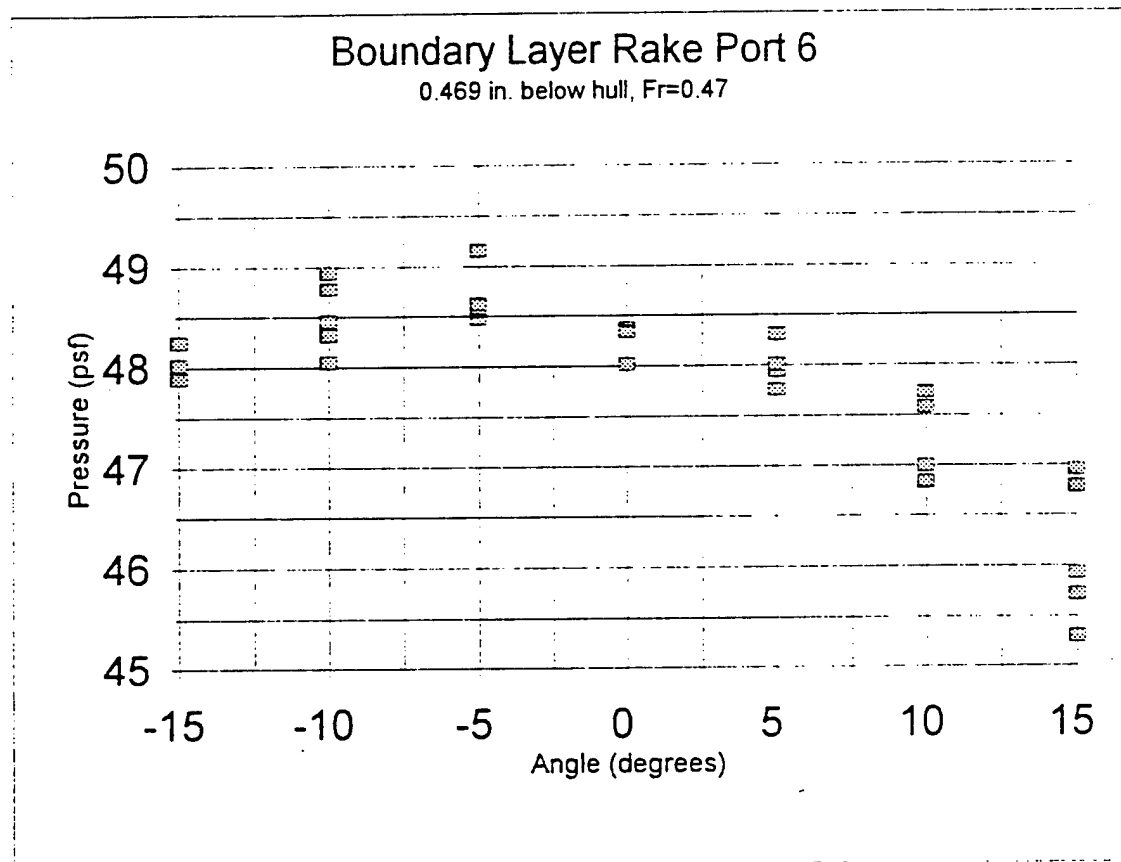## Boundary Layer Rake Port 1
0.015 in. below hull. Fr=0.40
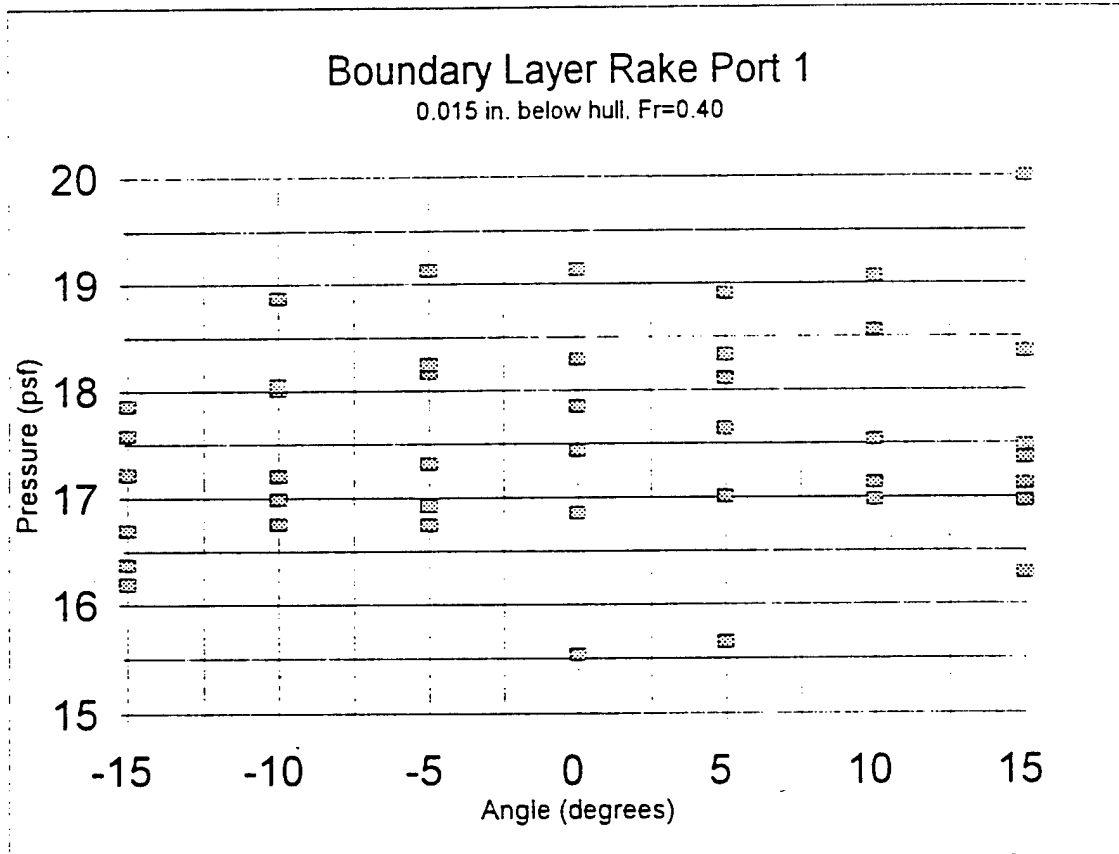
Figure 75: Boundary layer rake data for port 1 at Fr = 0.40.
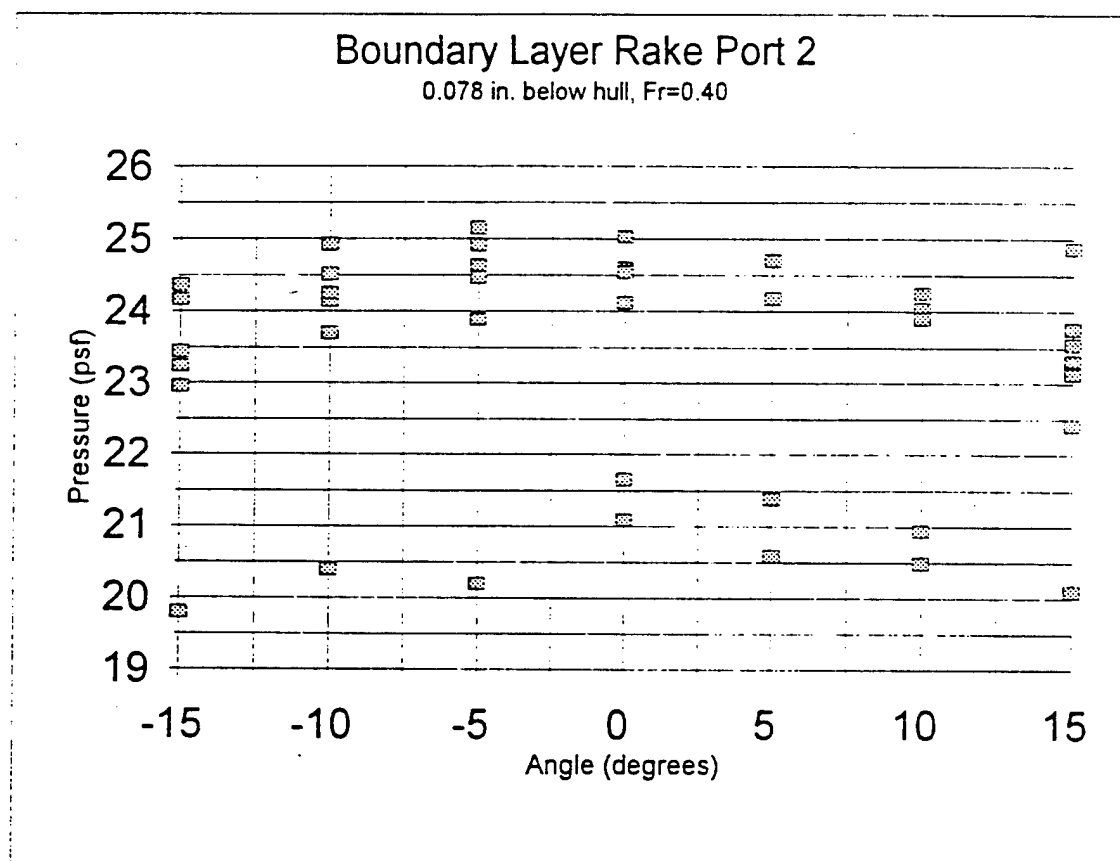
Figure 76: Boundary layer rake data for port 2 at Fr = 0.40.
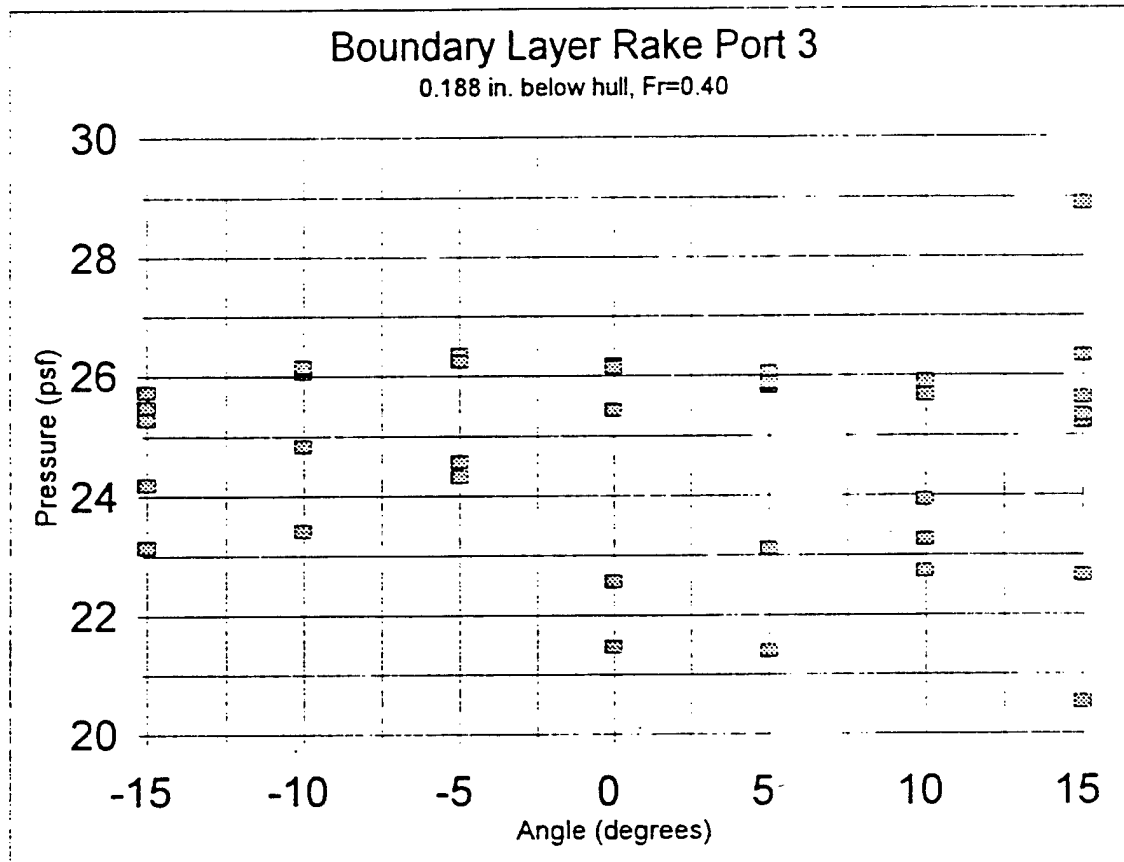
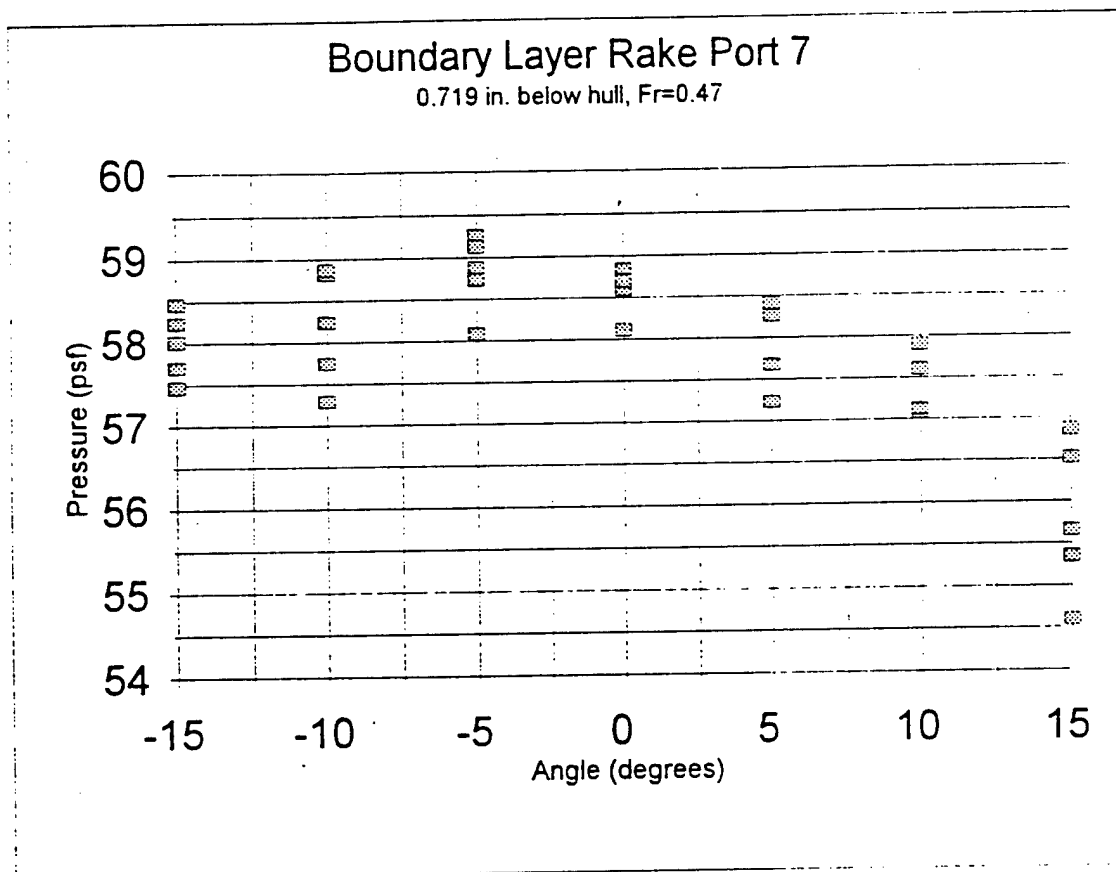Figure 77: Boundary layer rake data for port 3 at Fr = 0.40.

Boundary Layer Rake Port 5

0.375 in. below hull, Fr=0.40
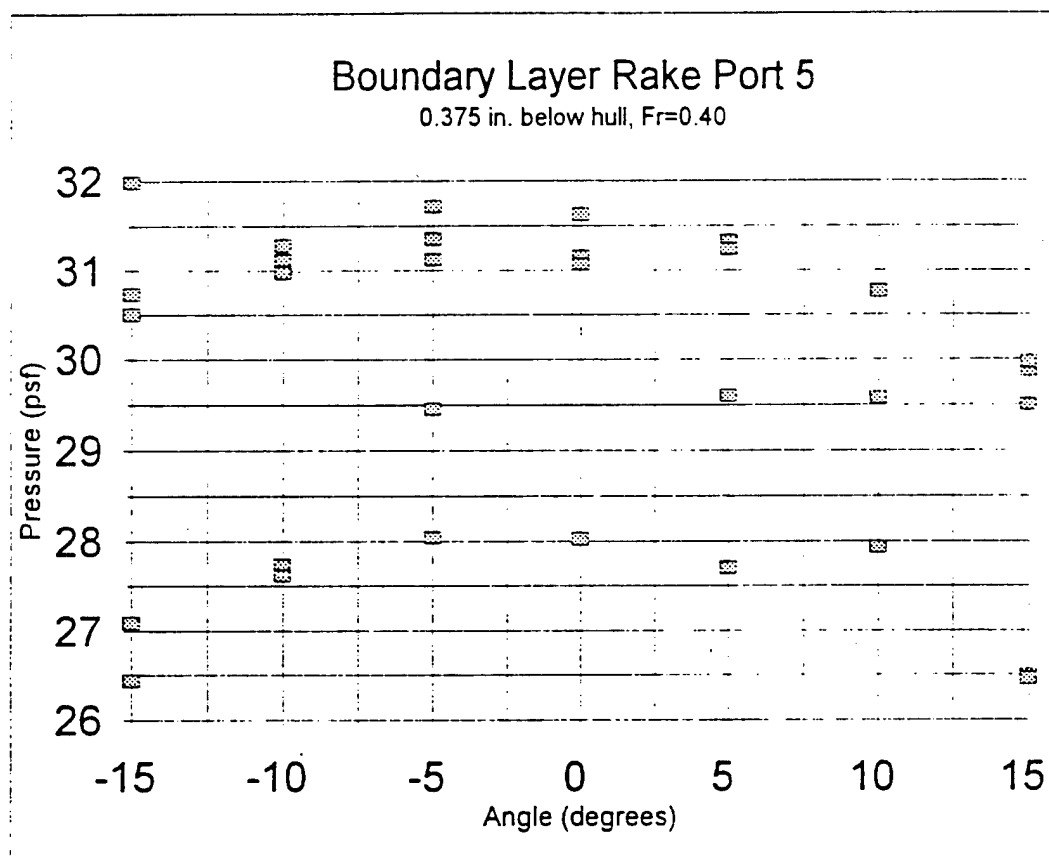
Figure 78 Boundary layer rake data for port 5 at Fr = 0.40.
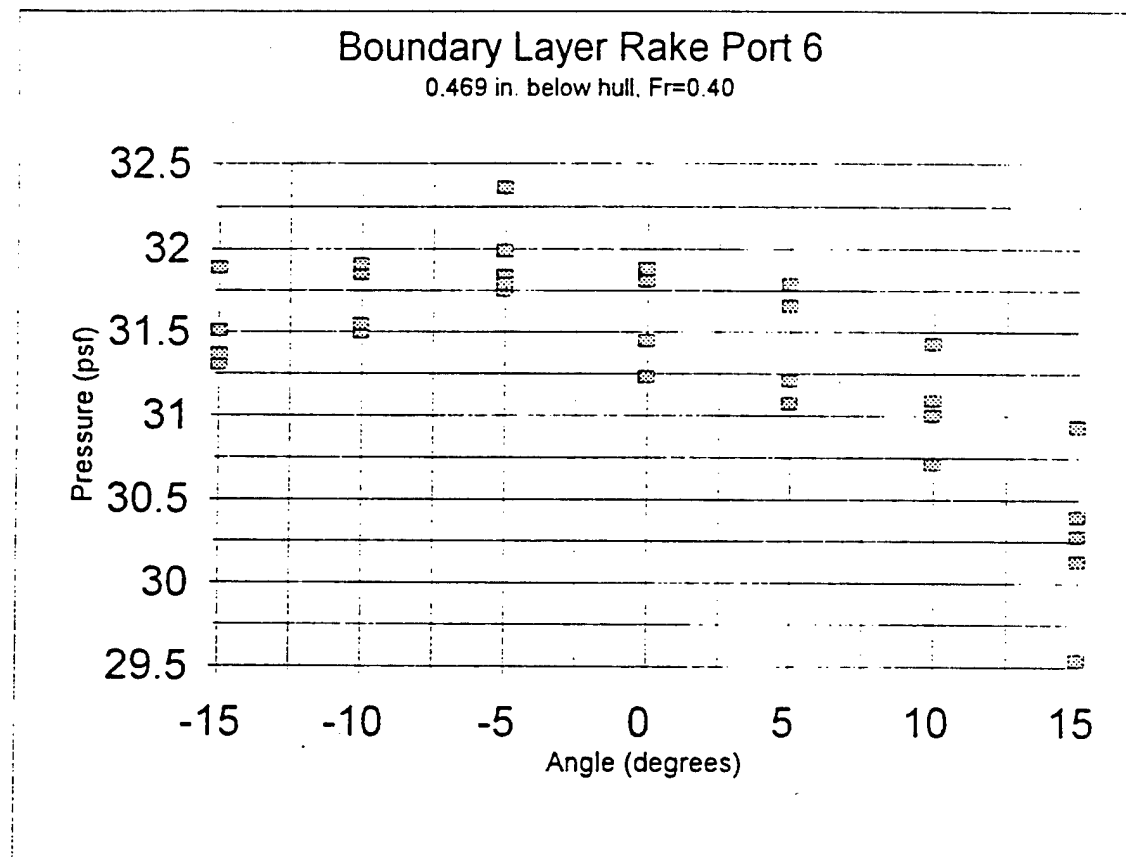
Figure 79. Boundary layer rake data for port 6 at Fr = 0.40
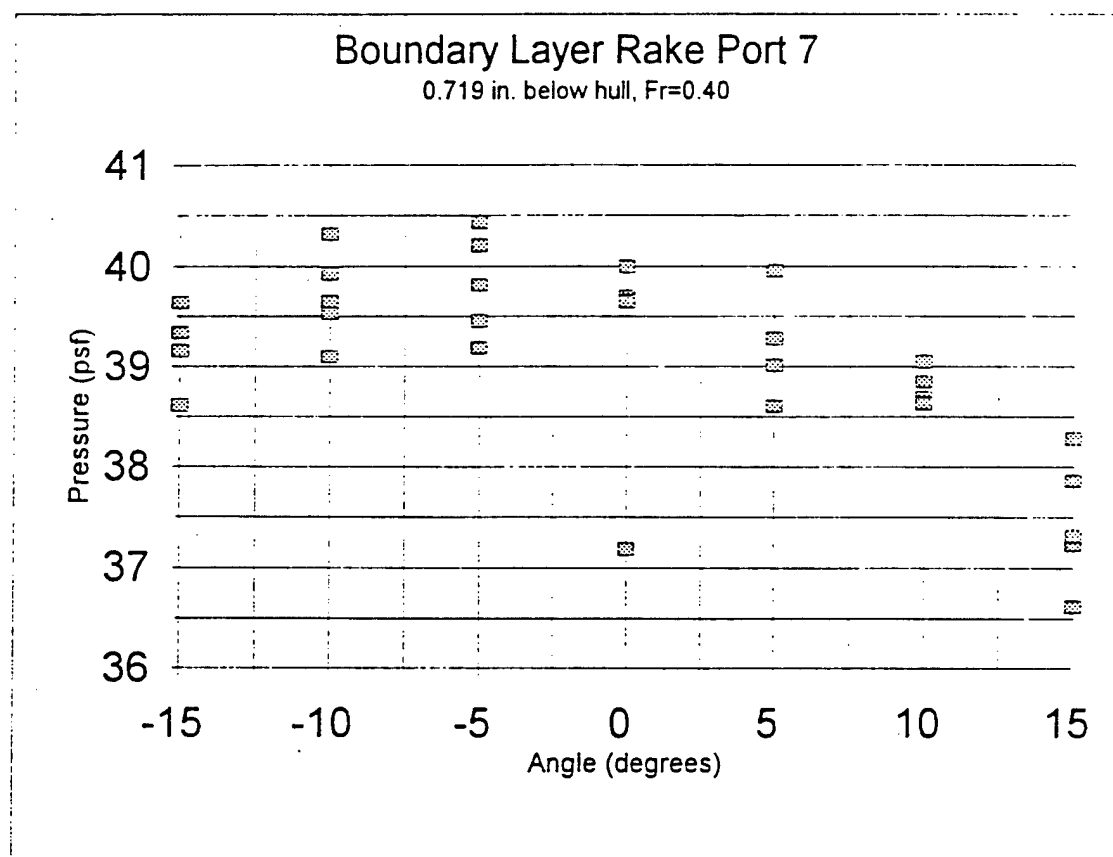
Figure 80 Boundary layer rake data for port 7 at Fr = 0 40

Boundary Layer Rake Port 1
0.015 in. below hull, Fr=0.47
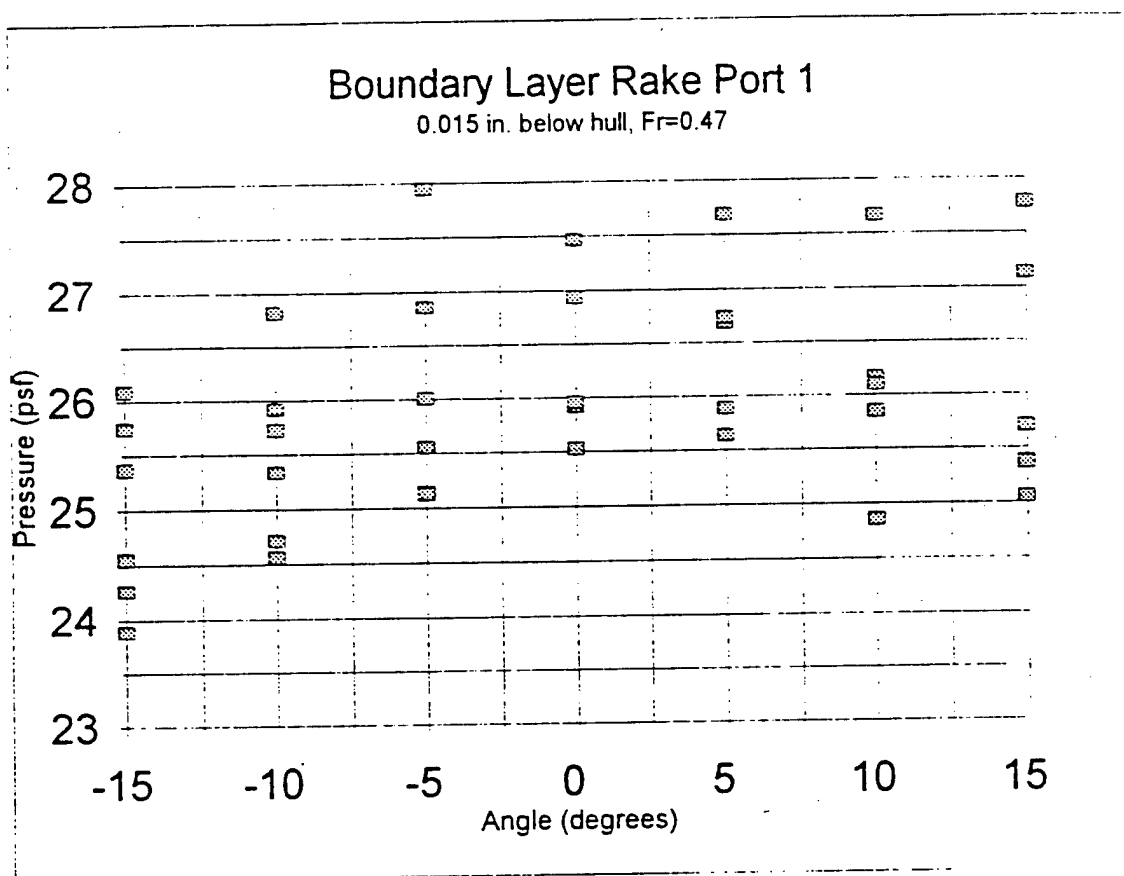
Figure 81. Boundary layer rake data for port 1 at Fr = 0.47.
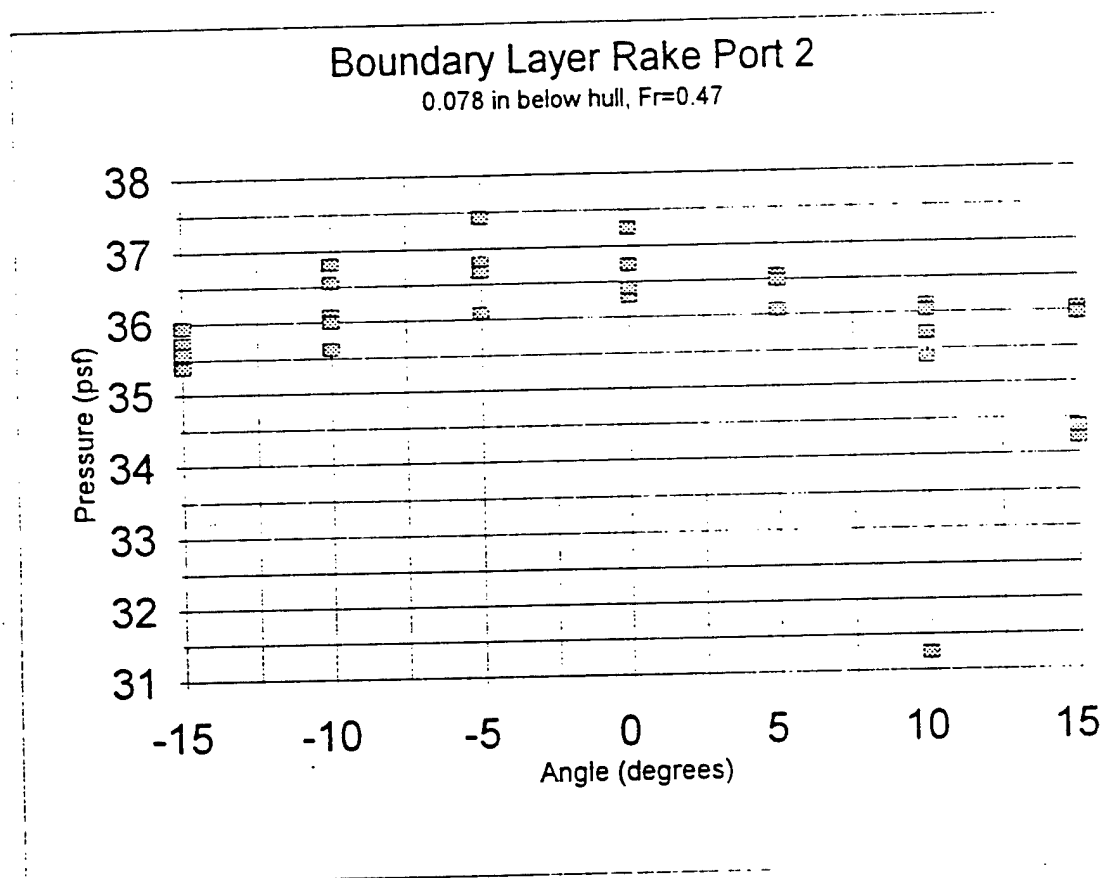
Figure 82. Boundary layer rake data for port 2 at Fr = 0.47

Boundary Layer Rake Port 3
0.188 in. below hull, Fr=0.47
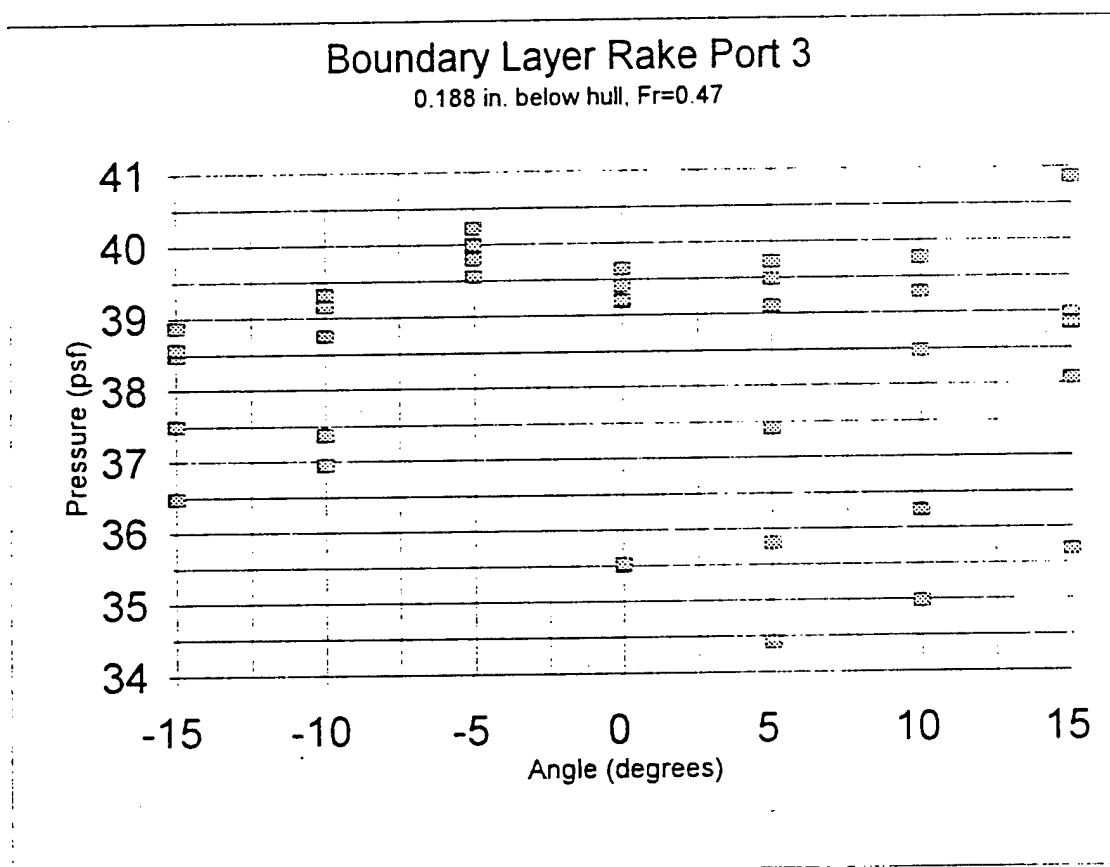
Figure 83: Boundary layer rake data for port 3 at Fr = 0.47.

Figure 84. Boundary layer rake data for port 5 at Fr = 0.47.

Boundary Layer Rake Port 6
0.469 in. below hull, Fr=0.47

Figure 85: Boundary layer rake data for port 6 at Fr = 0.47.

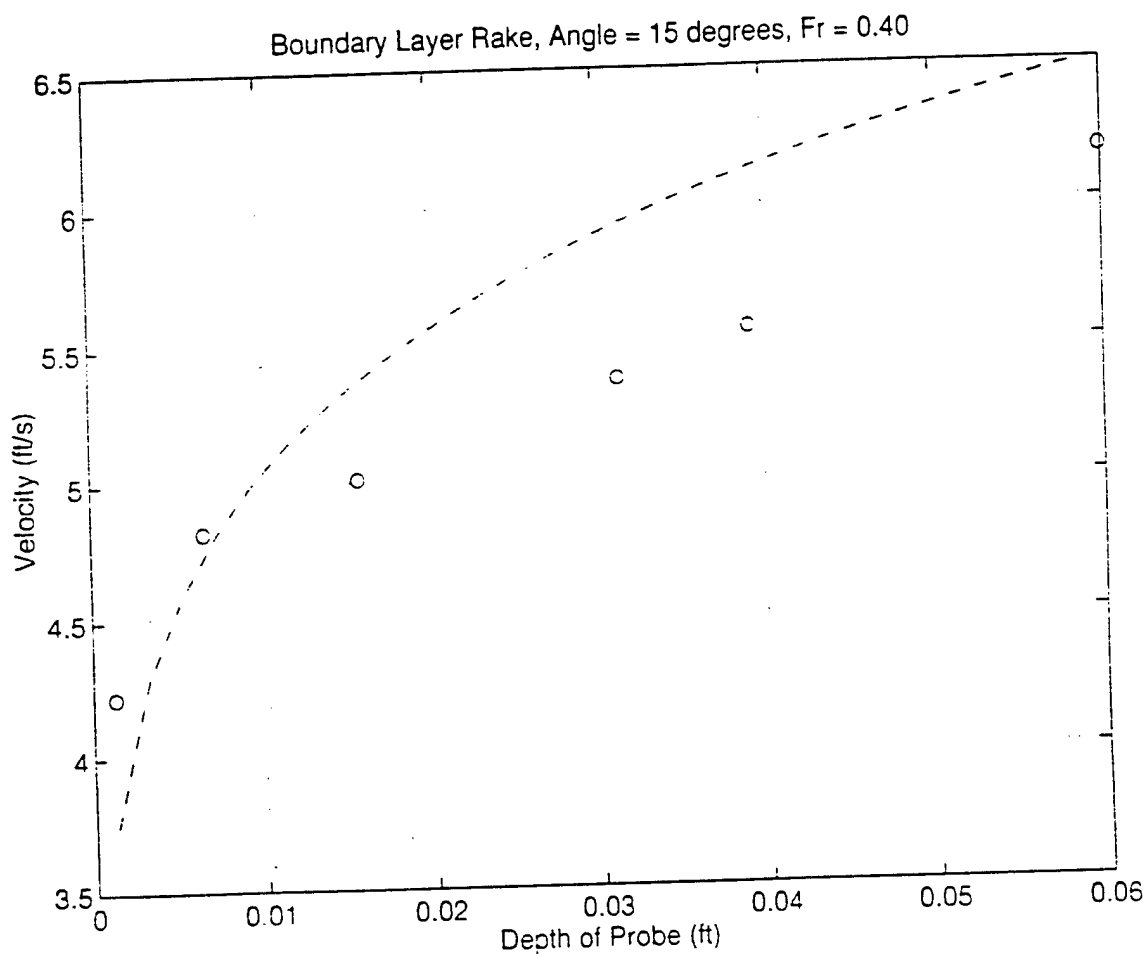Figure 86 Boundary layer rake data for port 7 at Fr = 0.47.
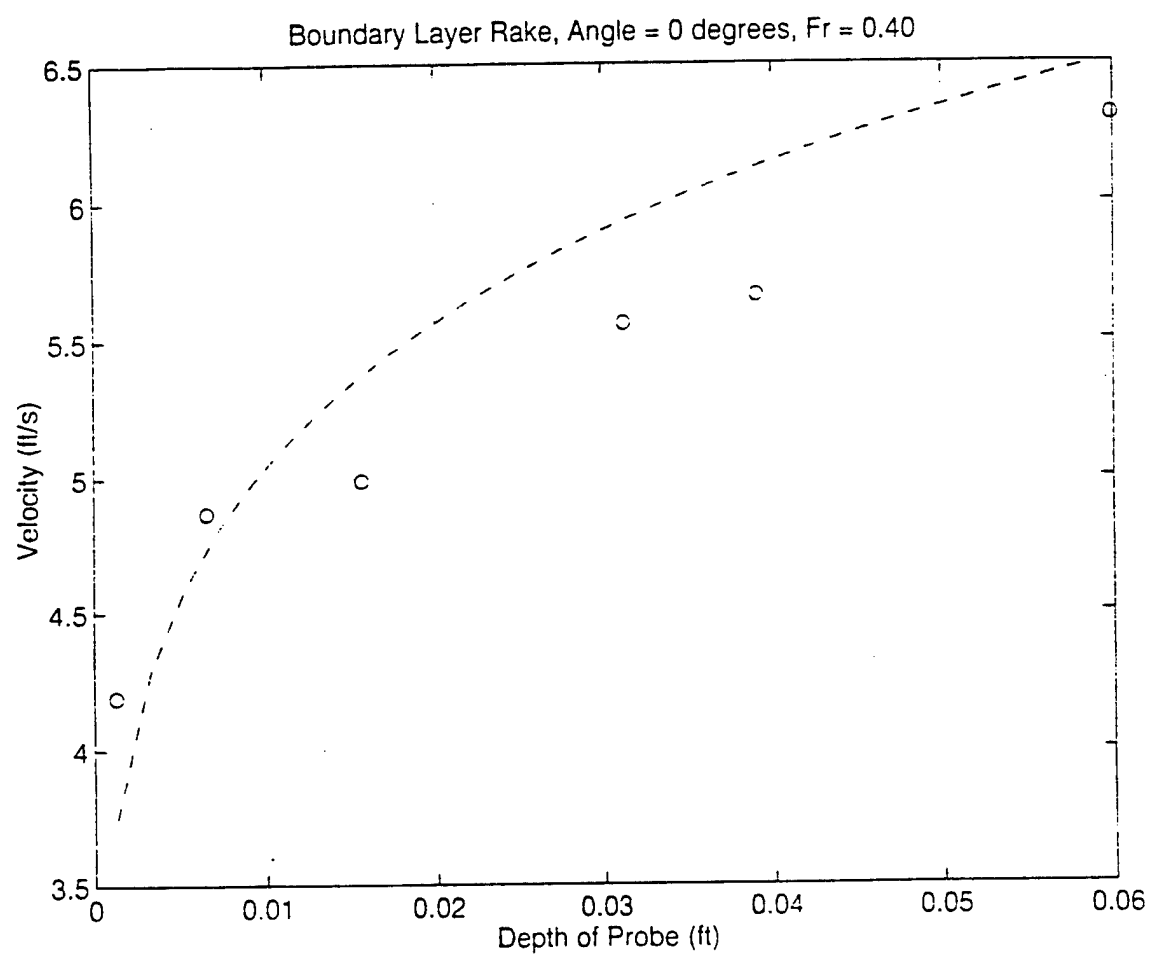
Figure 87 Boundary layer velocity profile for angle 0 degrees at Fr = 0.40.
Dotted line represents theoretical velocity profile
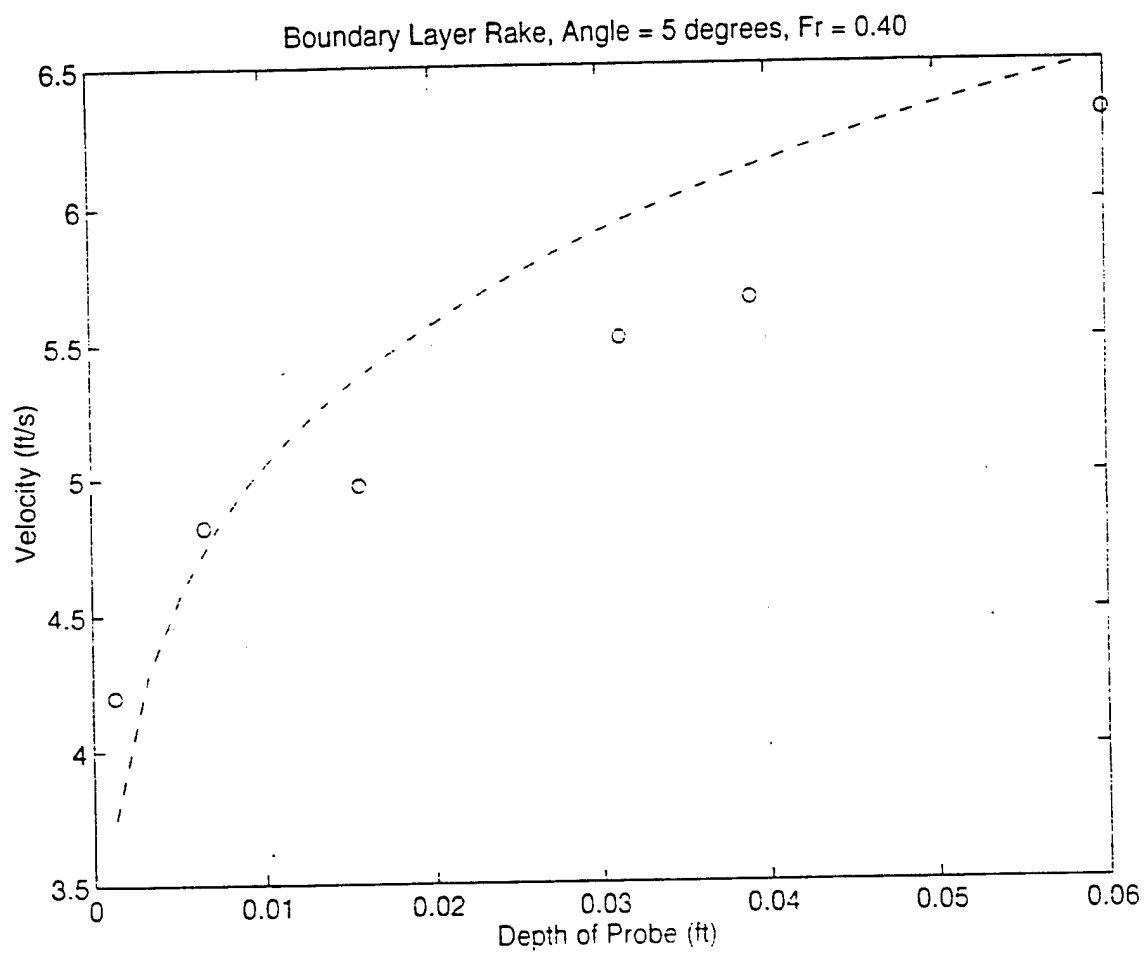
Figure 88: Boundary layer profile for angle 5 degrees at Fr = 0.40.
Dotted line represents theoretical velocity profile
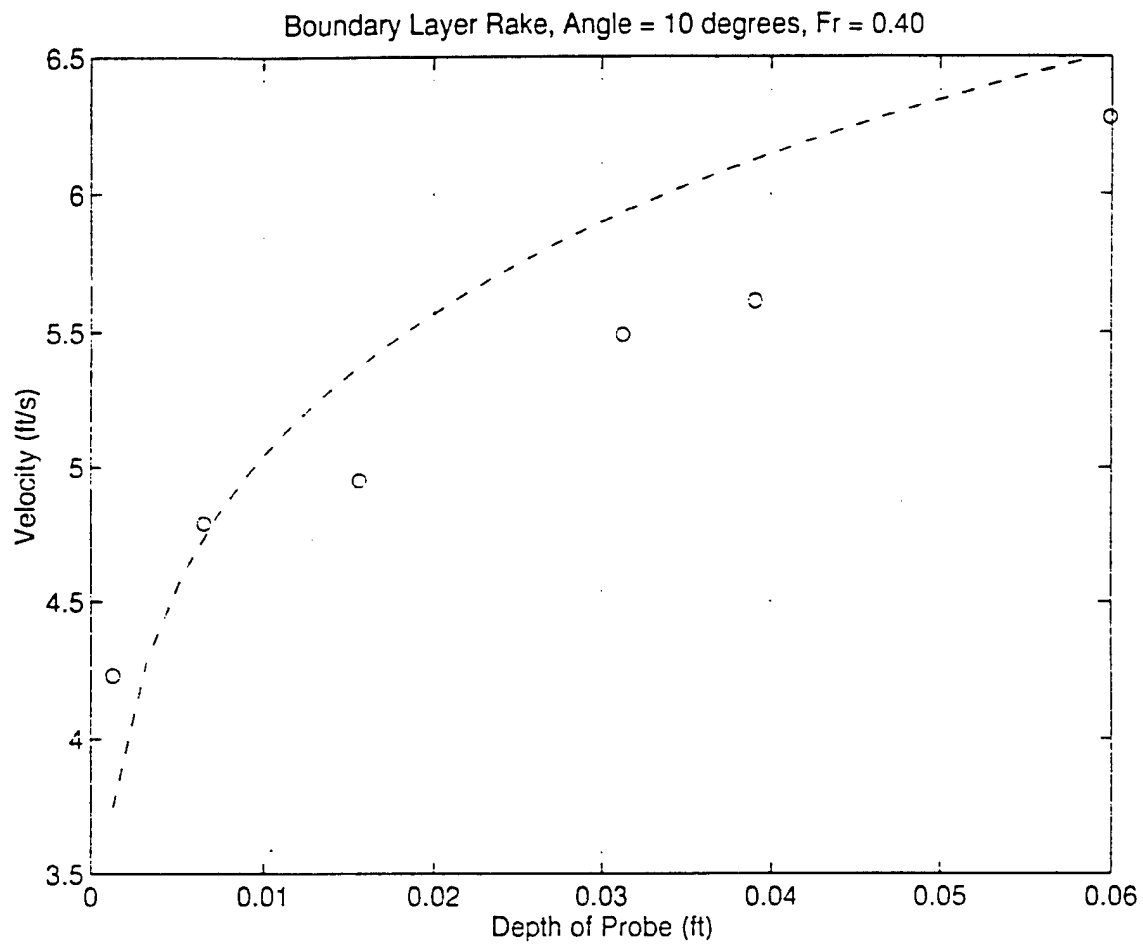
Figure 89: Boundary layer velocity profile for angle 10 degrees at Fr = 0.40.
Dotted line represents theoretical velocity profile.

Figure 90. Boundary layer velocity profile for angle 15 degrees at Fr = 0.40. Dotted line represents theoretical velocity profile.
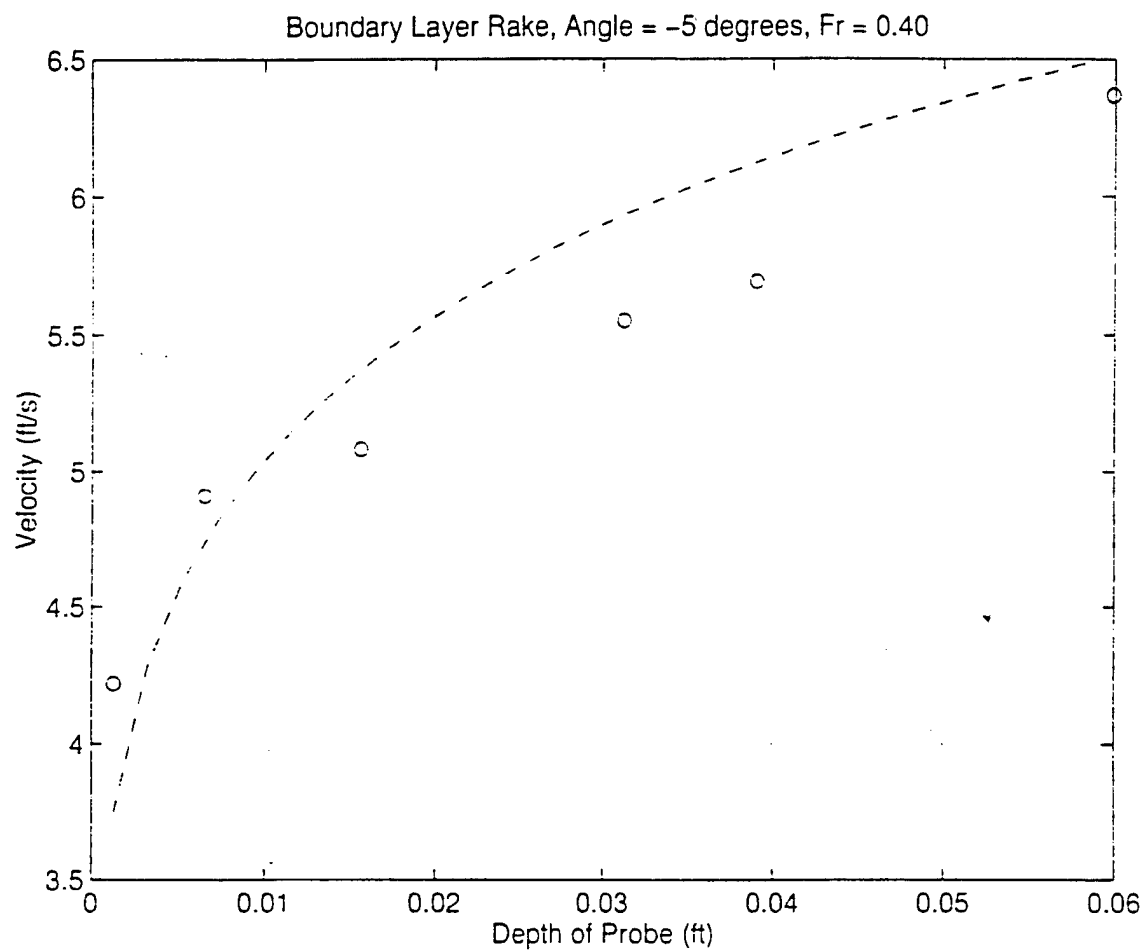
Figure 91 Boundary layer velocity profile for angle -5 degrees at Fr = 0.40.
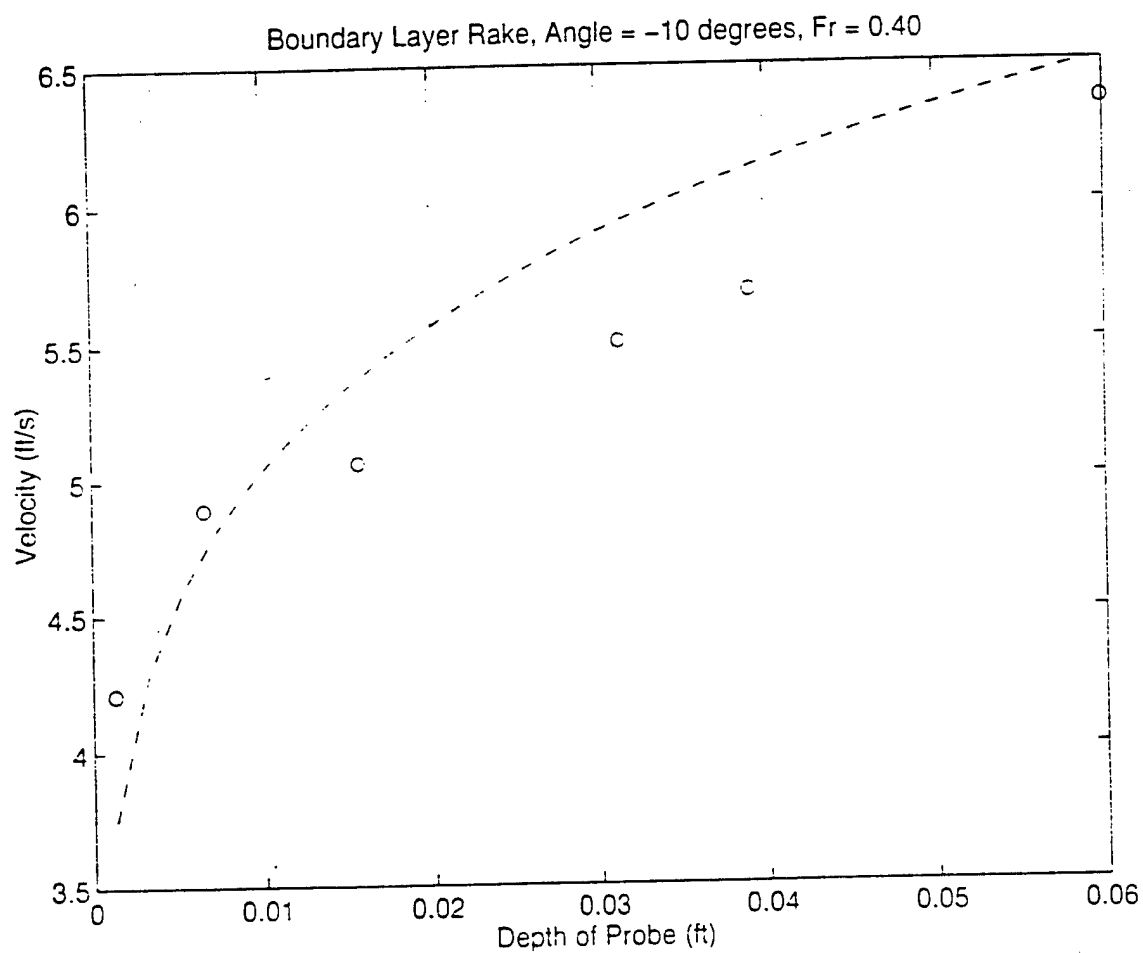Dotted line represents theoretical velocity profile

Figure 92. Boundary layer velocity profile for angle -10 degrees at Fr = 0.40
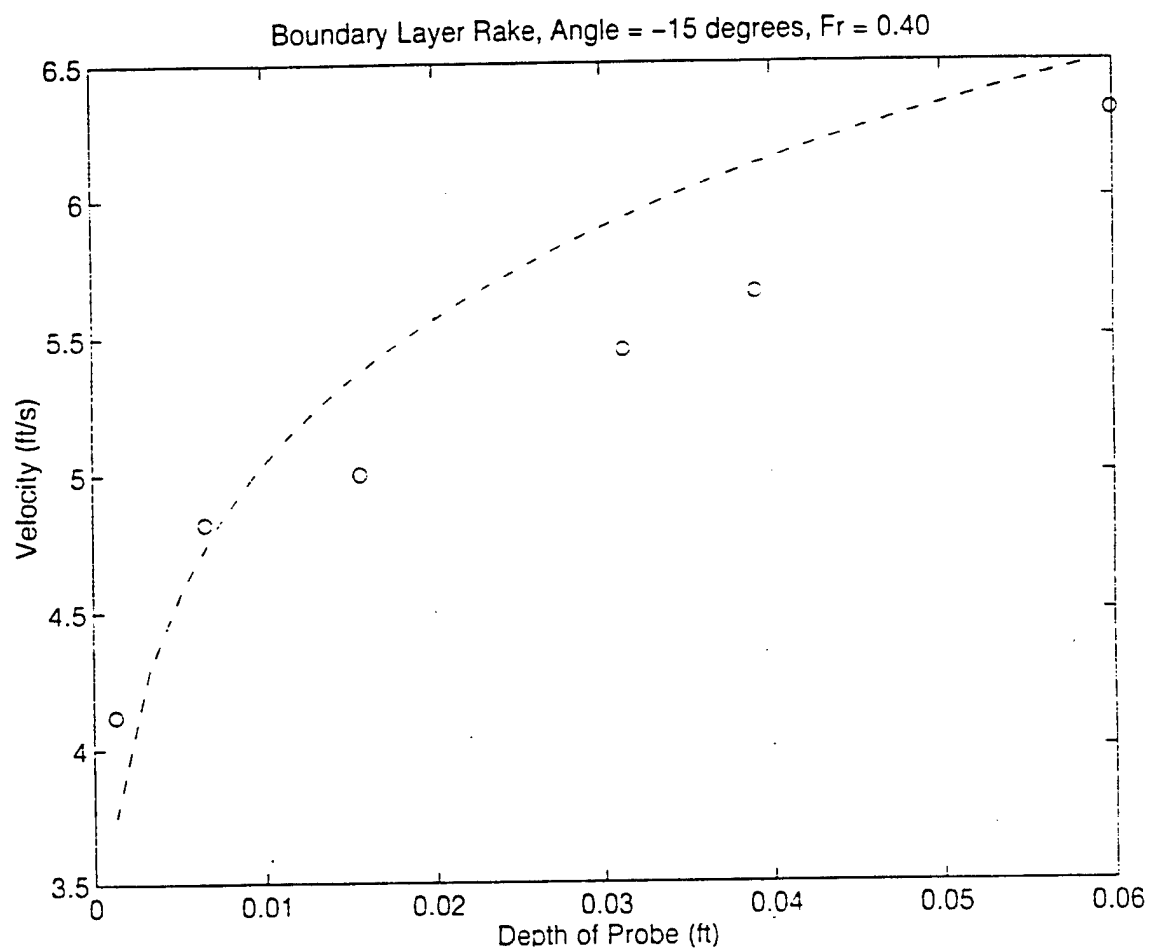Dotted line represents theoretical velocity profile.

Figure 93 Boundary layer velocity profile for angle -15 degrees at Fr = 0.40.
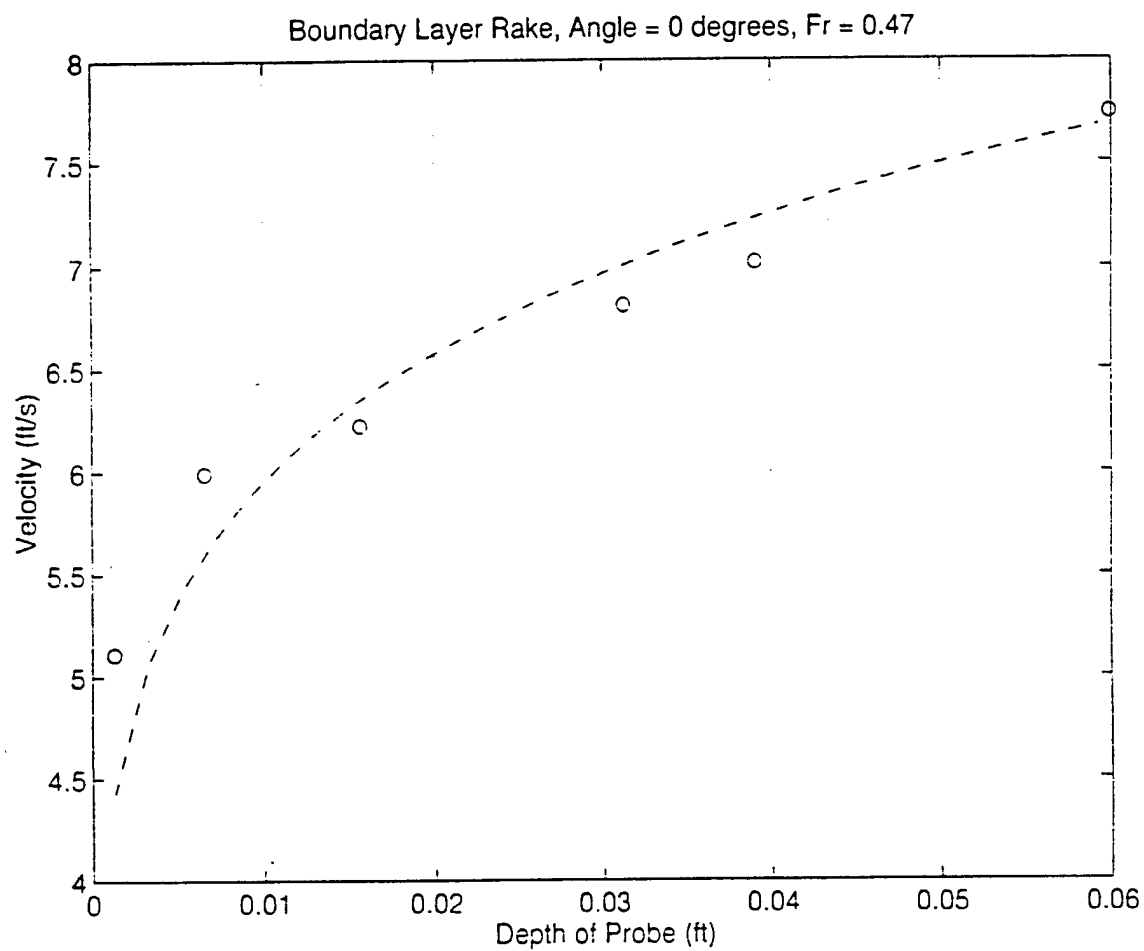Dotted line represents theoretical velocity profile

Figure 94. Boundary layer velocity profile for angle 0 degrees at Fr = 0.47
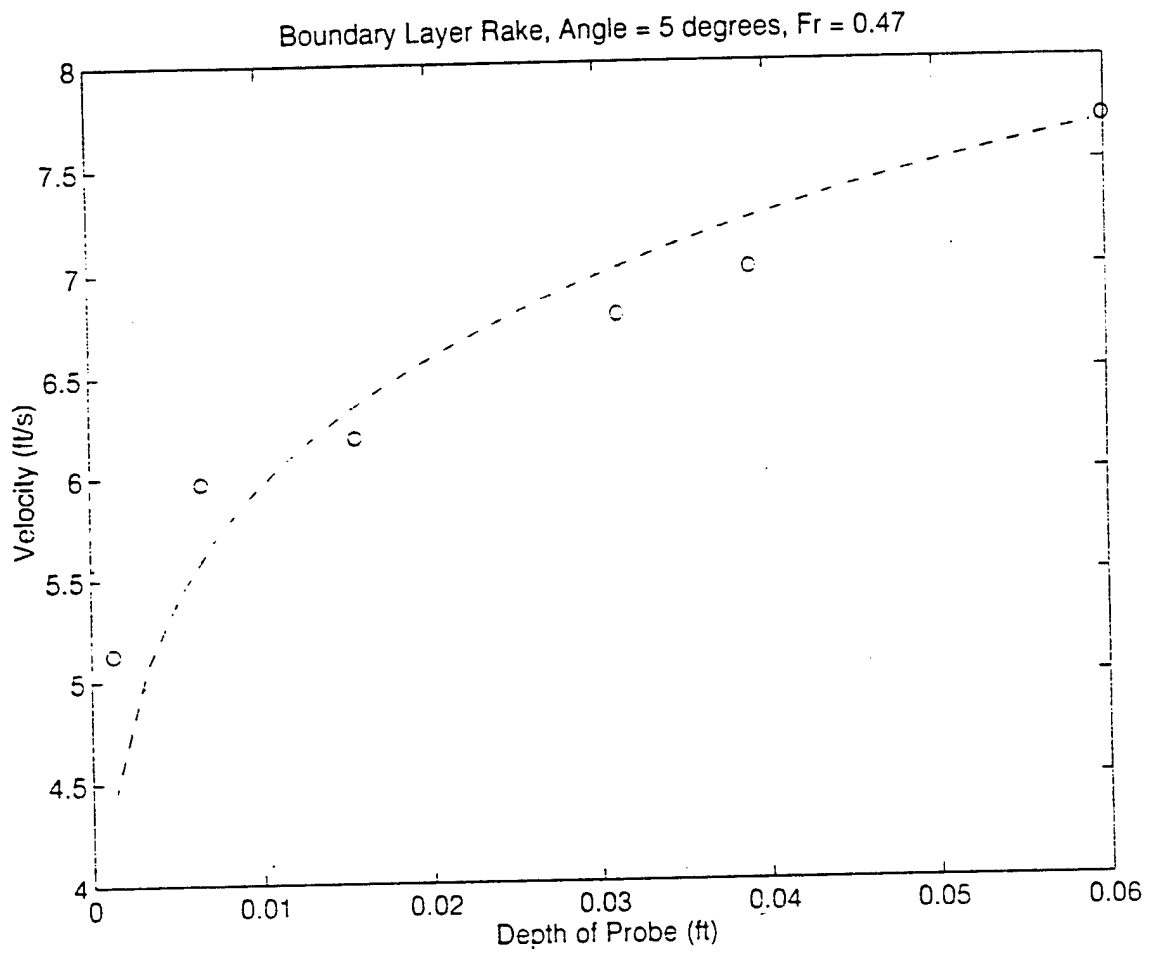Dotted line represents theoretical velocity profile

Figure 95 Boundary layer velocity profile for angle 5 degrees at Fr = 0.47.
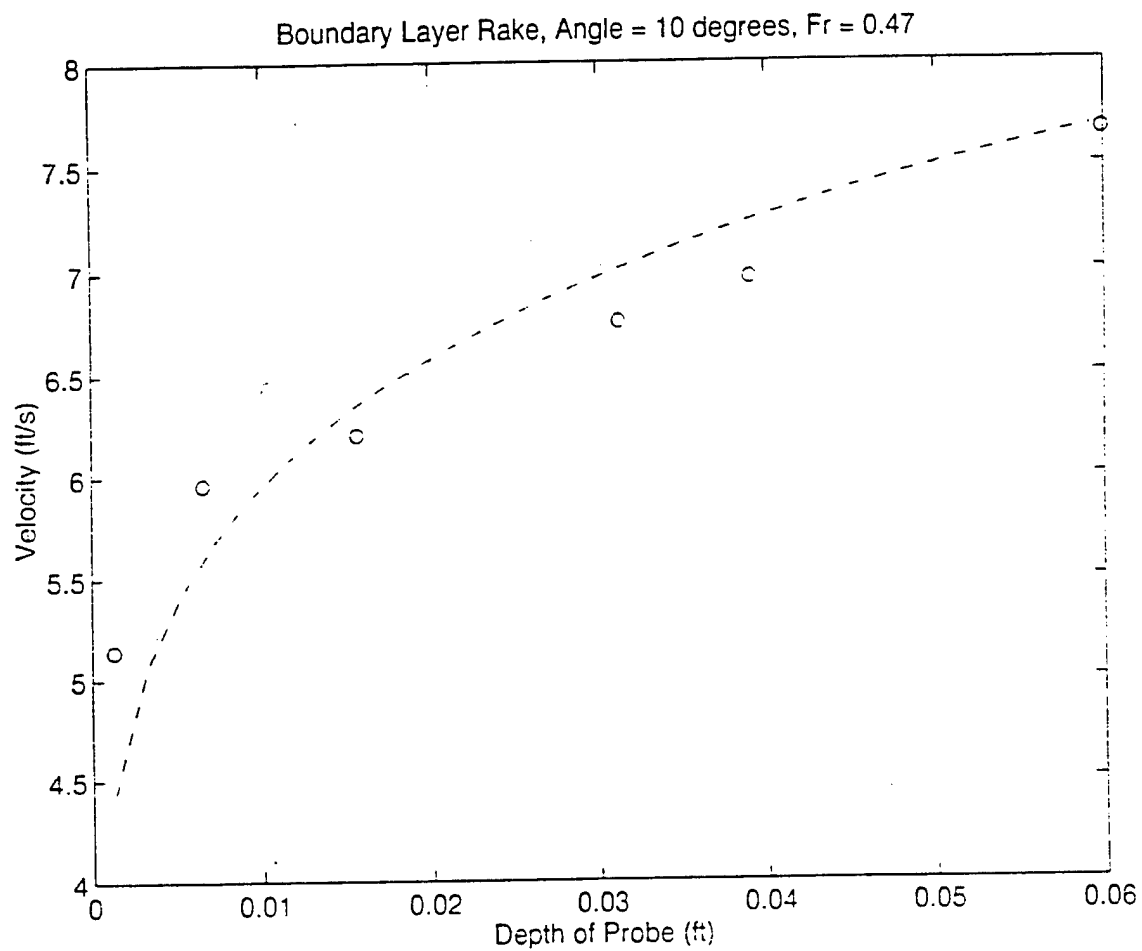Dotted line represents theoretical velocity profile.

Figure 96 Boundary layer velocity profile for angle 10 degrees at Fr = 0.47
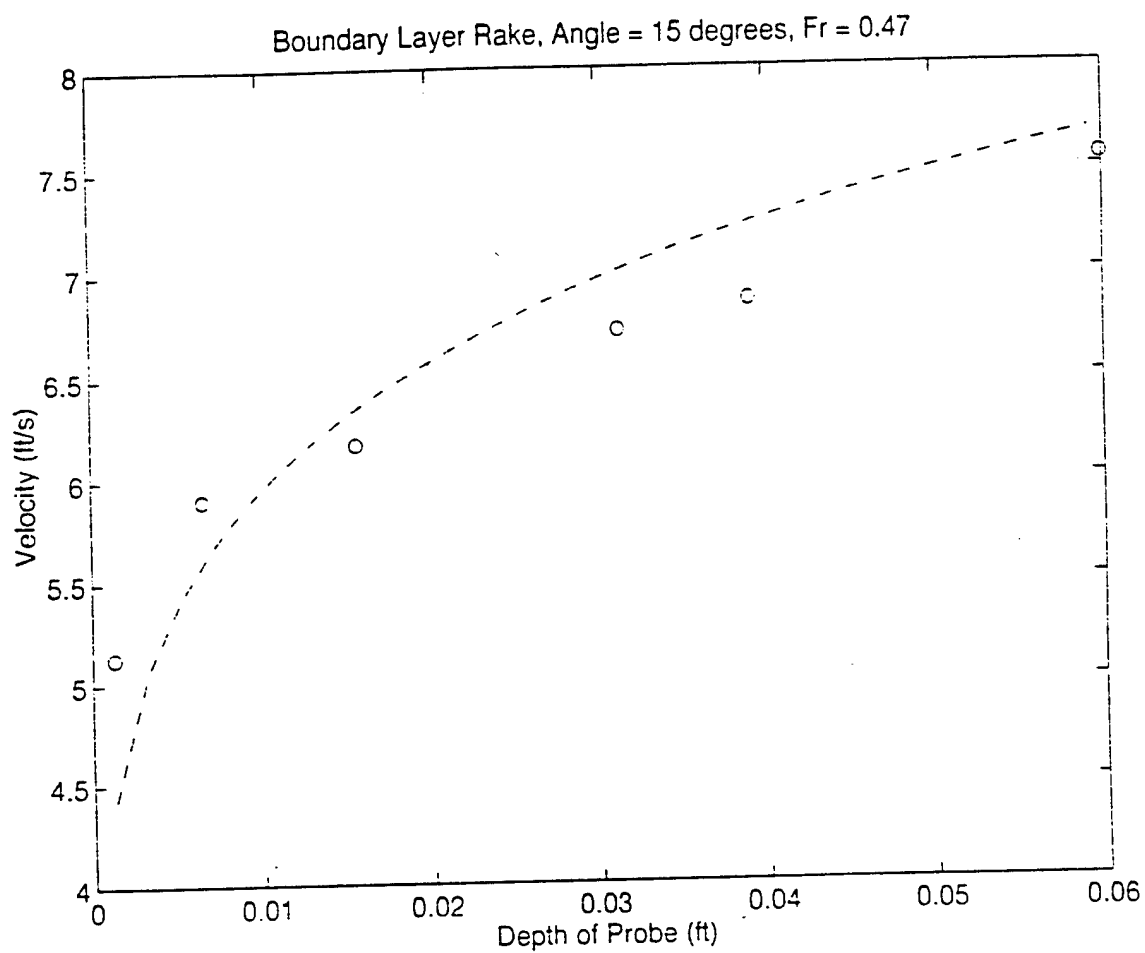Dotted line represents theoretical velocity profile

Figure 97. Boundary layer velocity profile for angle 15 degrees at Fr = 0.47. Dotted line represents theoretical velocity profile.
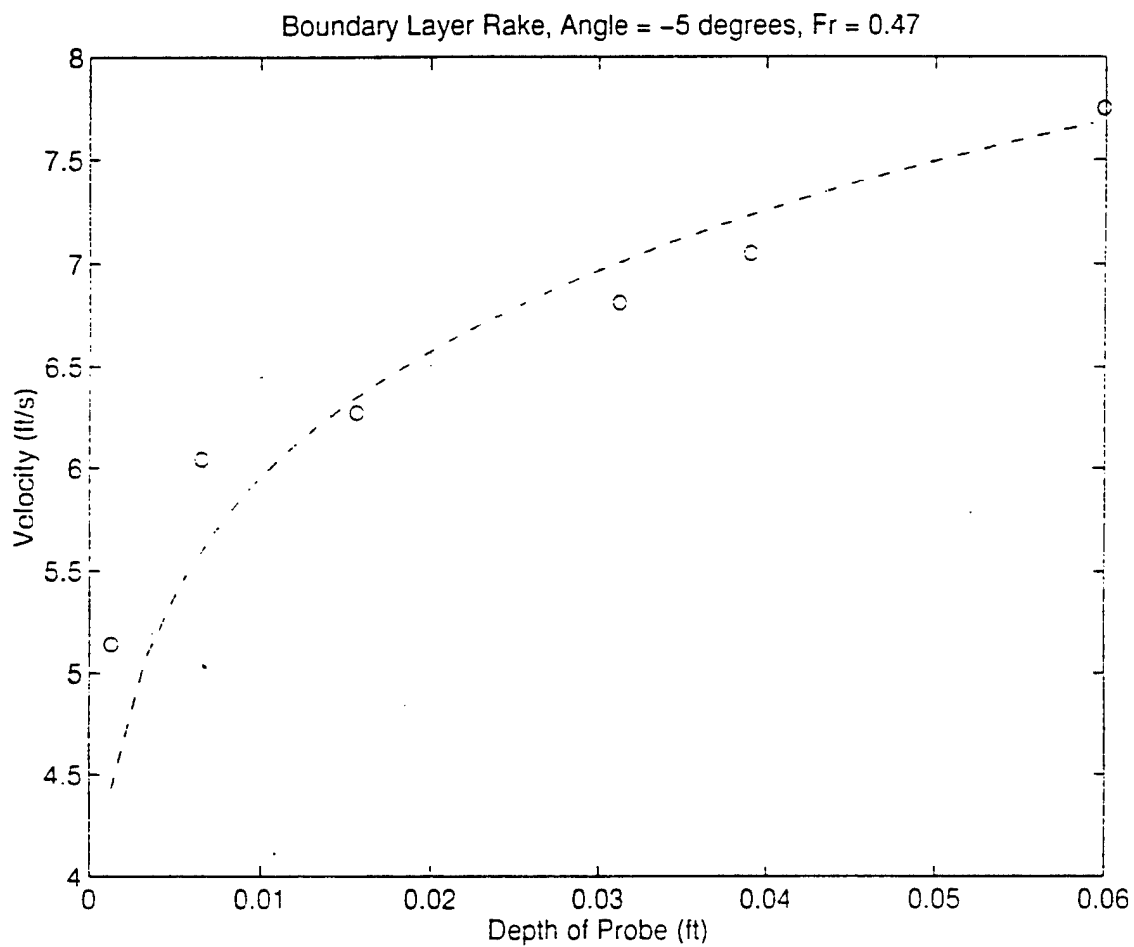
Figure 98. Boundary layer velocity profile for angle -5 degrees at Fr = 0.47.
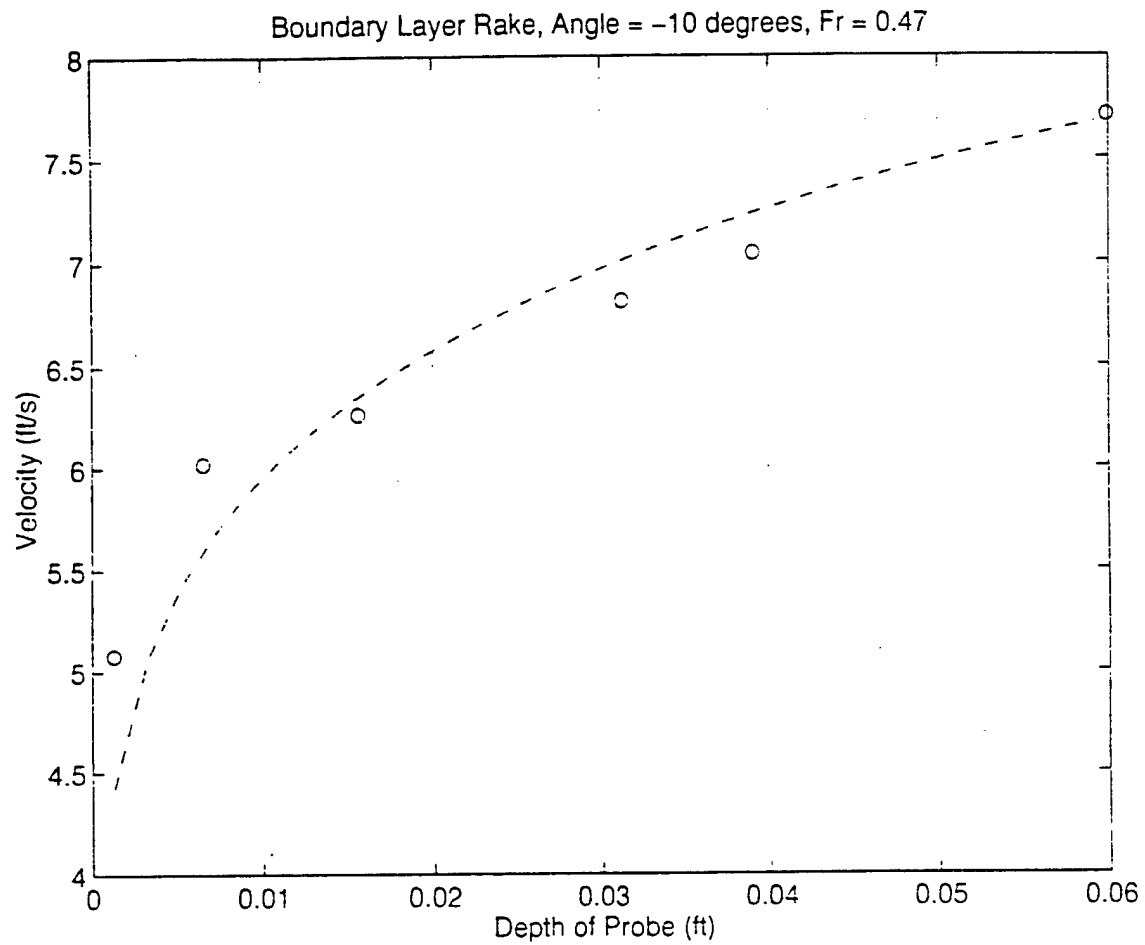Dotted line represents theoretical velocity profile

Figure 99 Boundary layer velocity profile for angle -10 degrees at Fr = 0.47.
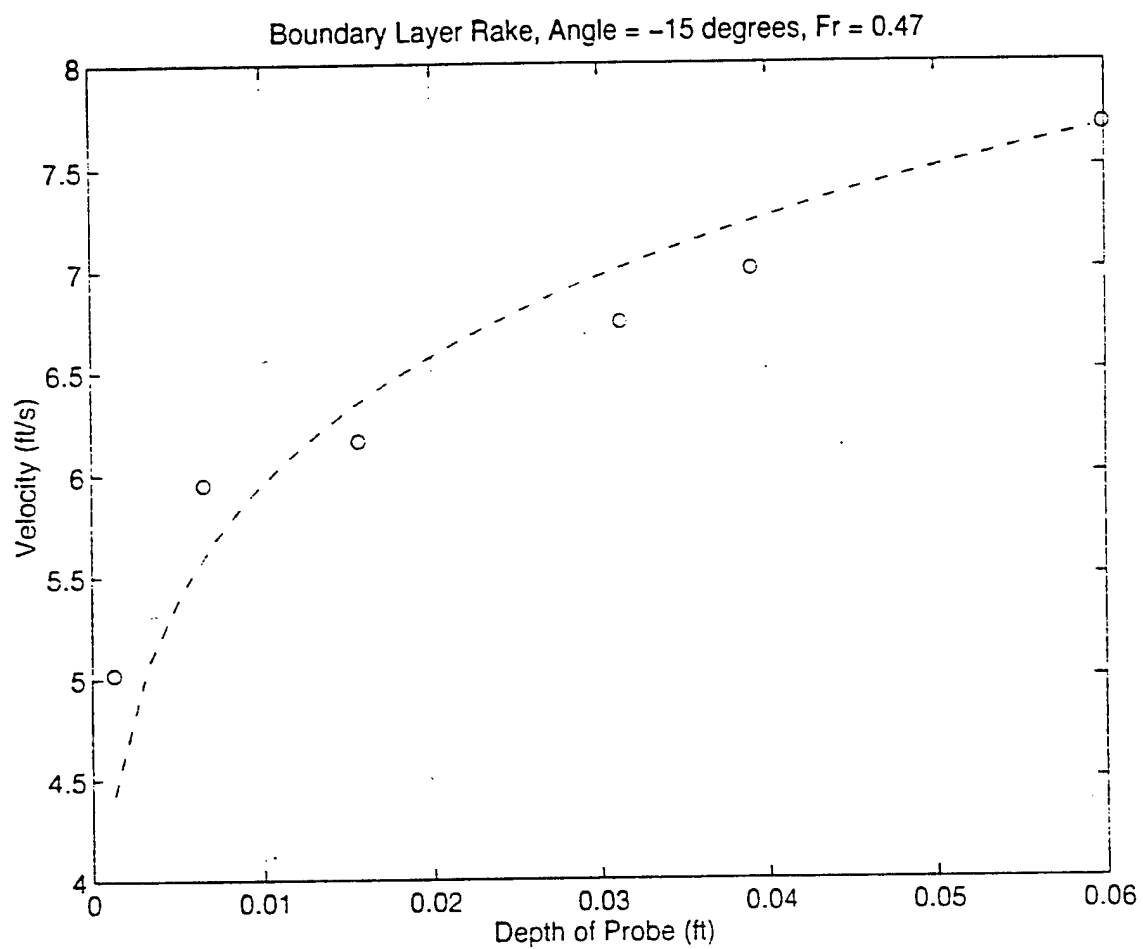Dotted line represents theoretical velocity profile.

Figure 100. Boundary layer velocity profile for angle -15 degrees at Fr = 0.47.
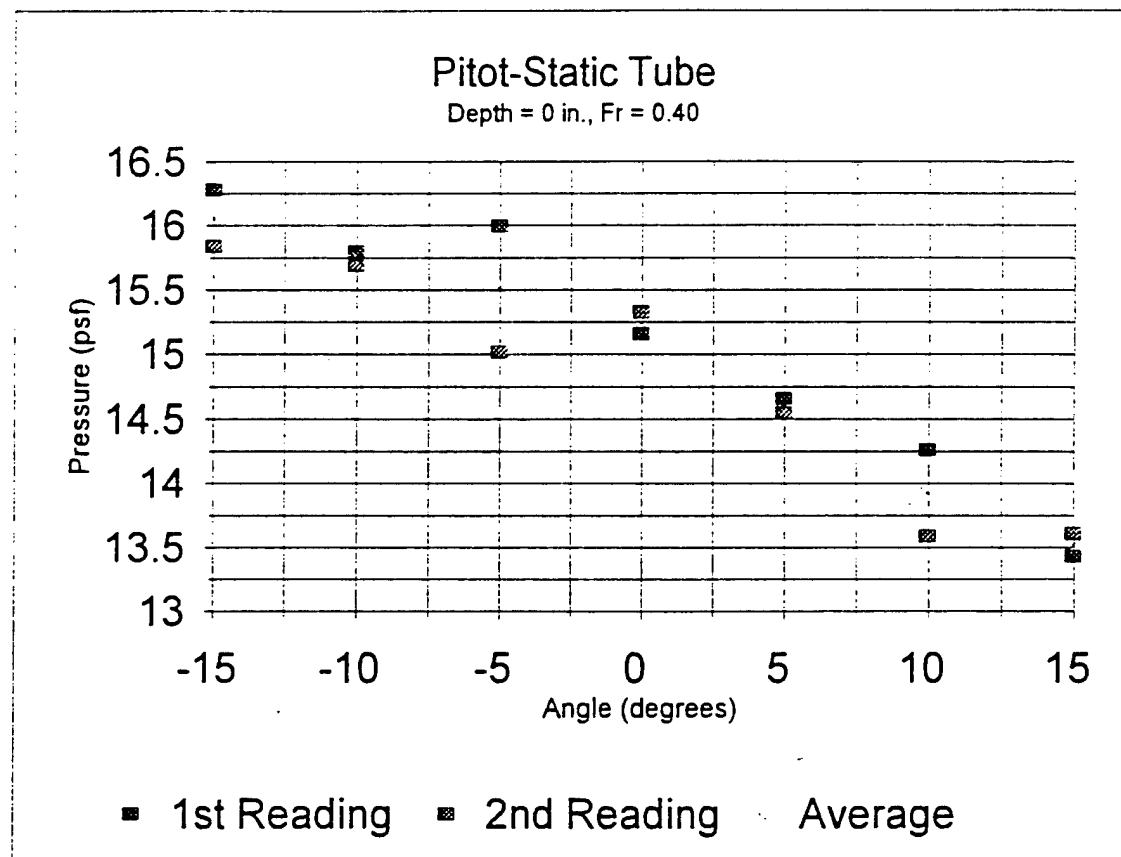Dotted line represents theoretical velocity profile.

Figure 101: Pitot-static tube data for depth = 0.0 in at Fr = 0.40.

Figure 102: Pitot-static tube data for depth = 0.5 in. at Fr = 0.40.

Figure 103: Pitot-static tube data for depth = 1.0 in. at Fr = 0.40.

Figure 104: Pitot-static tube data for depth = 1.5 in. at Fr = 0.40.

Figure 105: Pitot-static tube data for depth = 2 0 in. at Fr = 0.40.

Figure 106: Pitot-static tube data for depth = 2.5 in. at Fr = 0.40.

Figure 107: Pitot-static tube data for depth = 3.0 in. at Fr = 0.40.
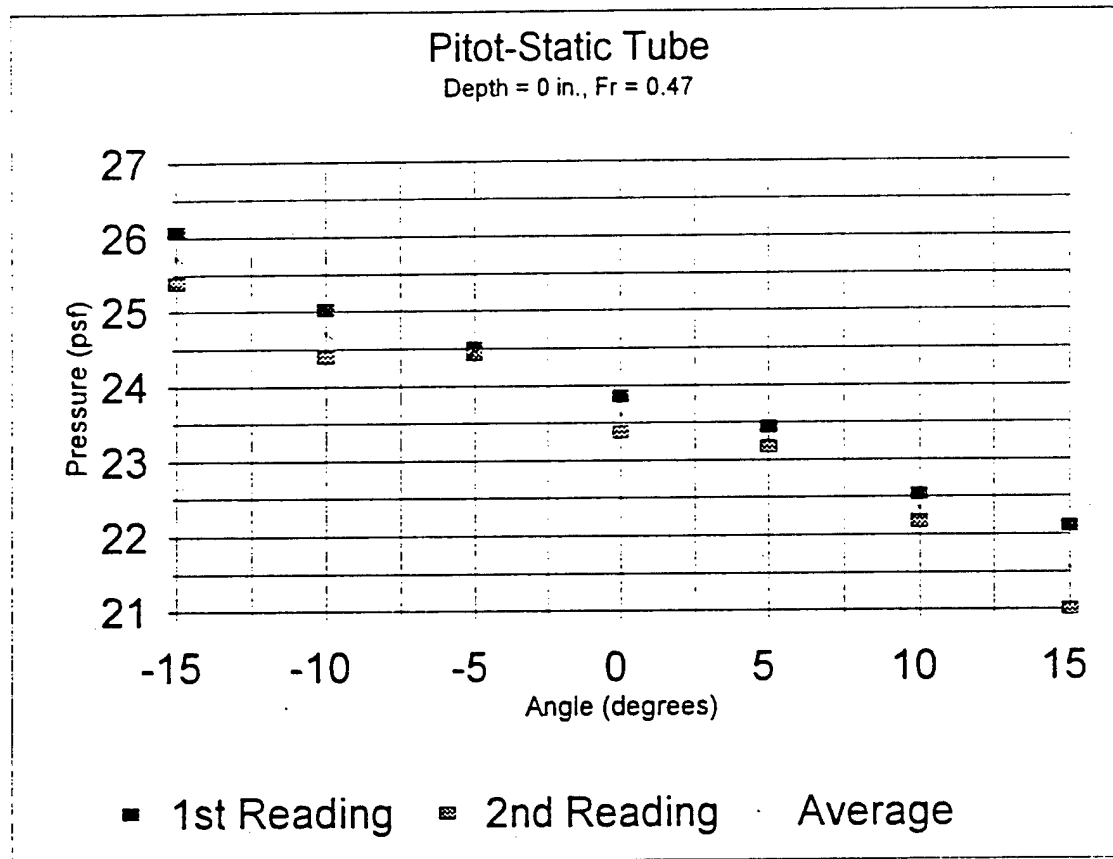
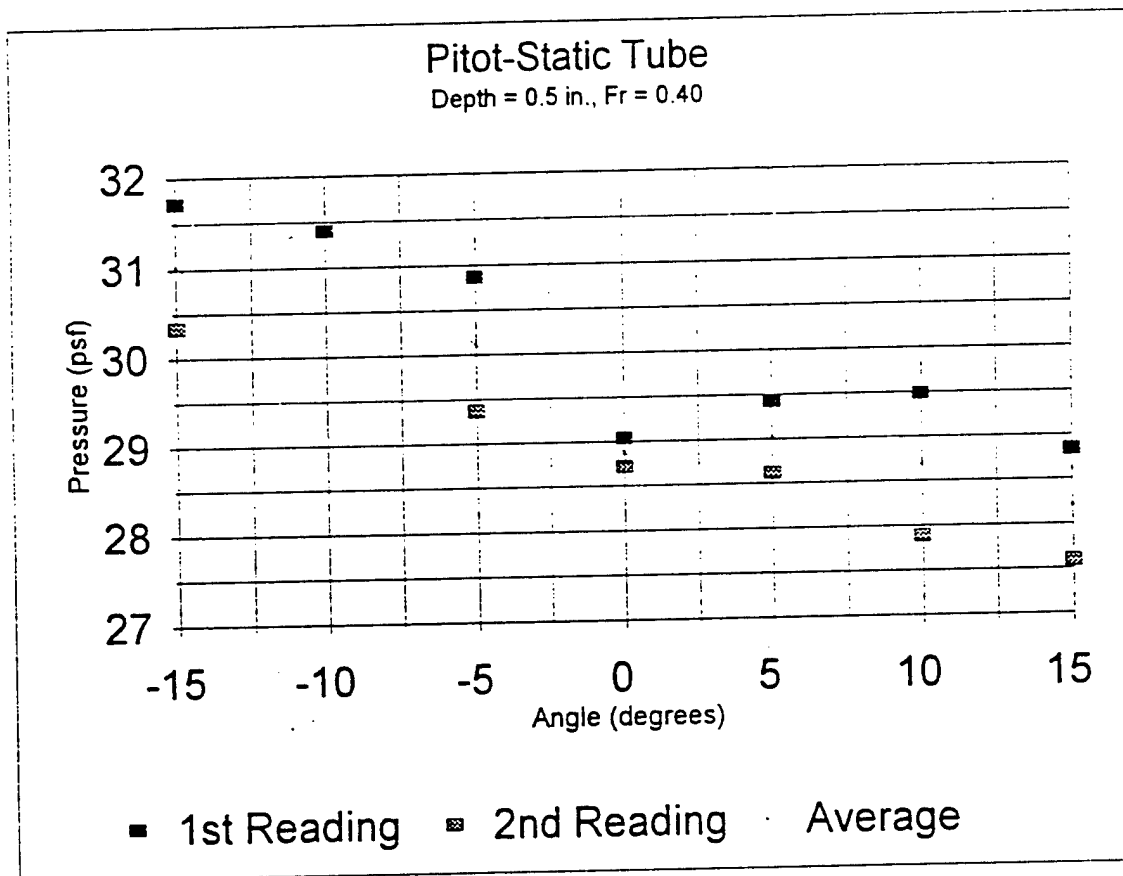Figure 108: Pitot-static tube data for depth = 0.0 at Fr = 0.47.
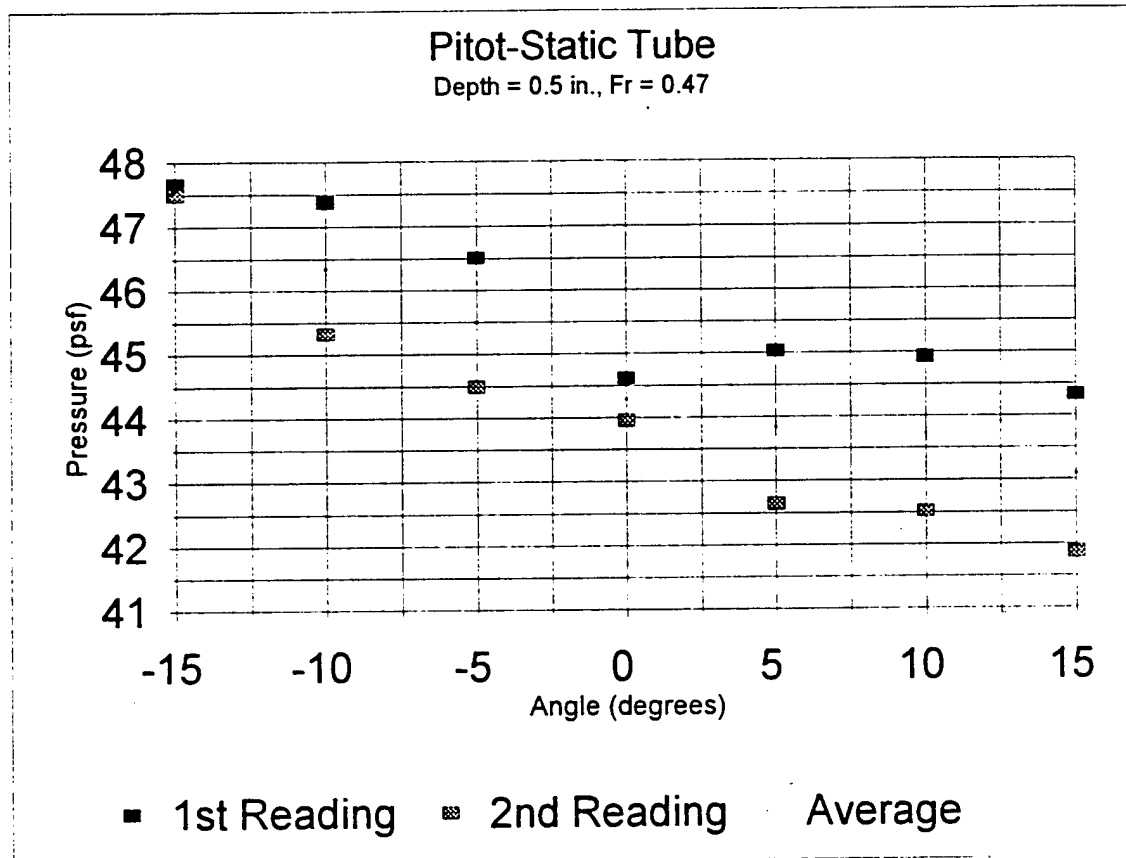
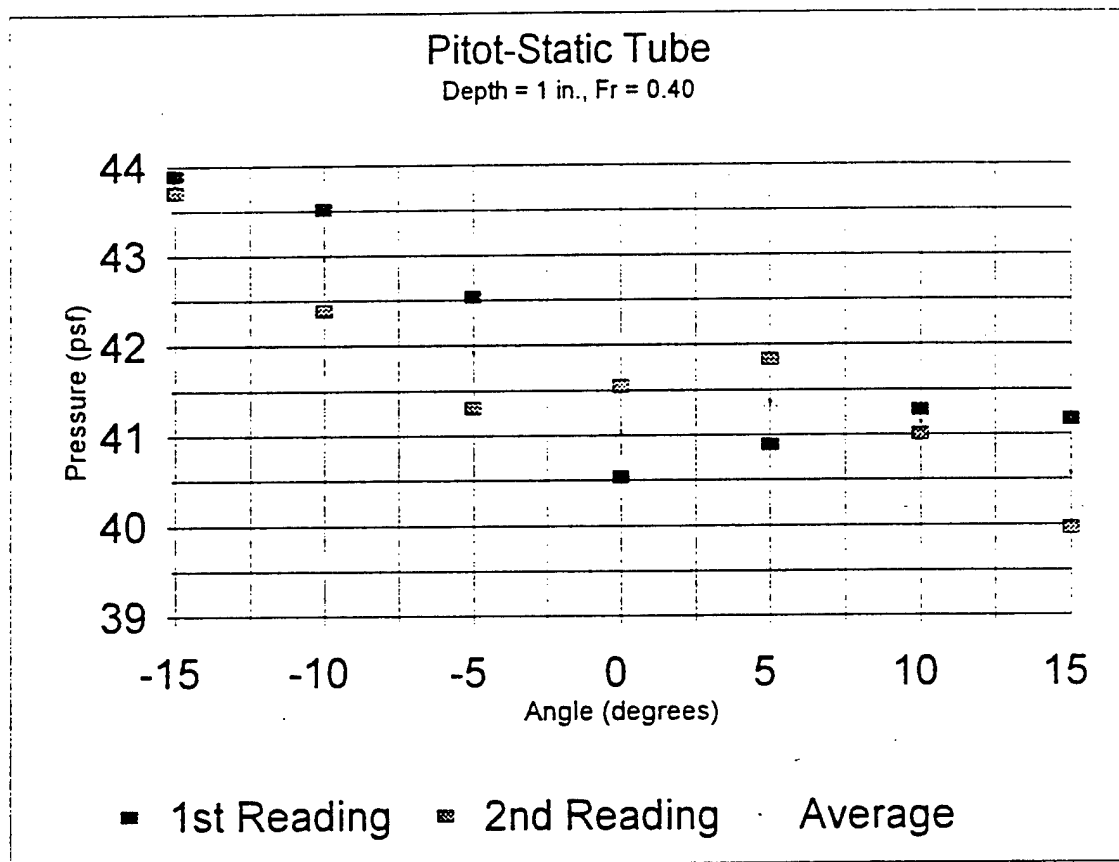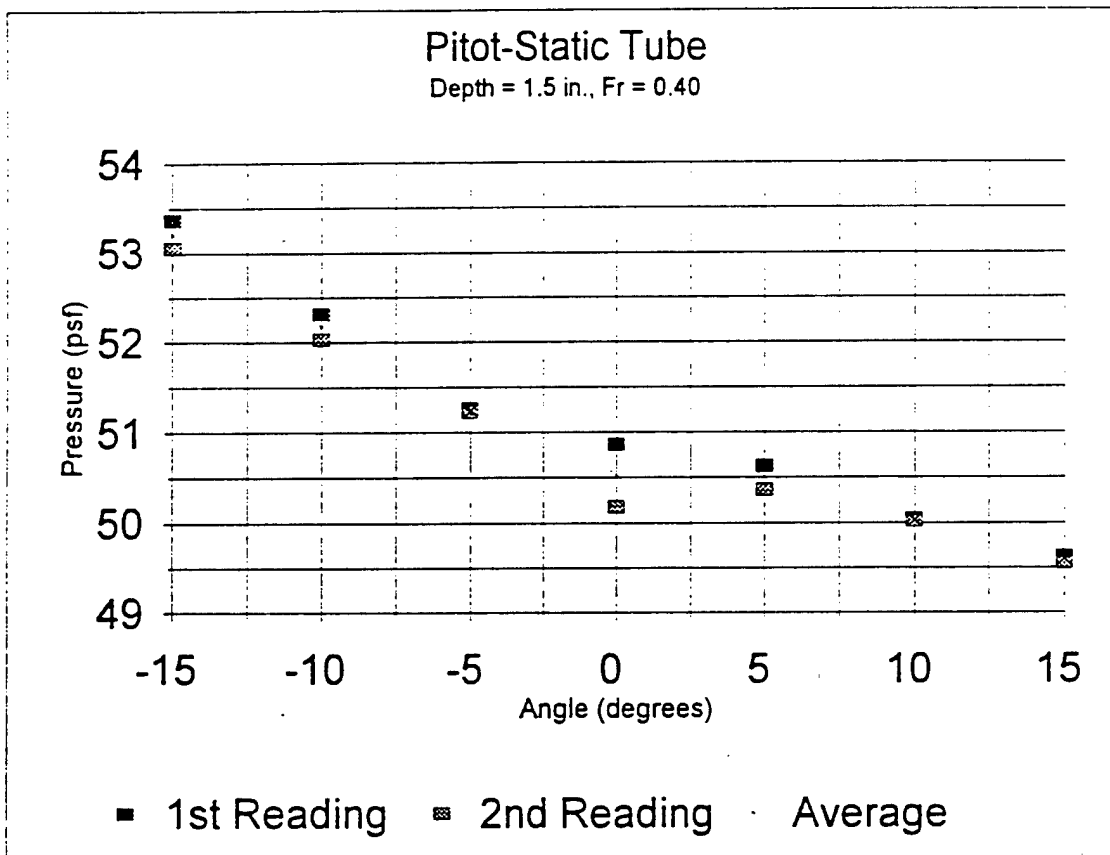Figure 109: Pitot-static tube data for depth = 0.5 in. at Fr = 0.47.
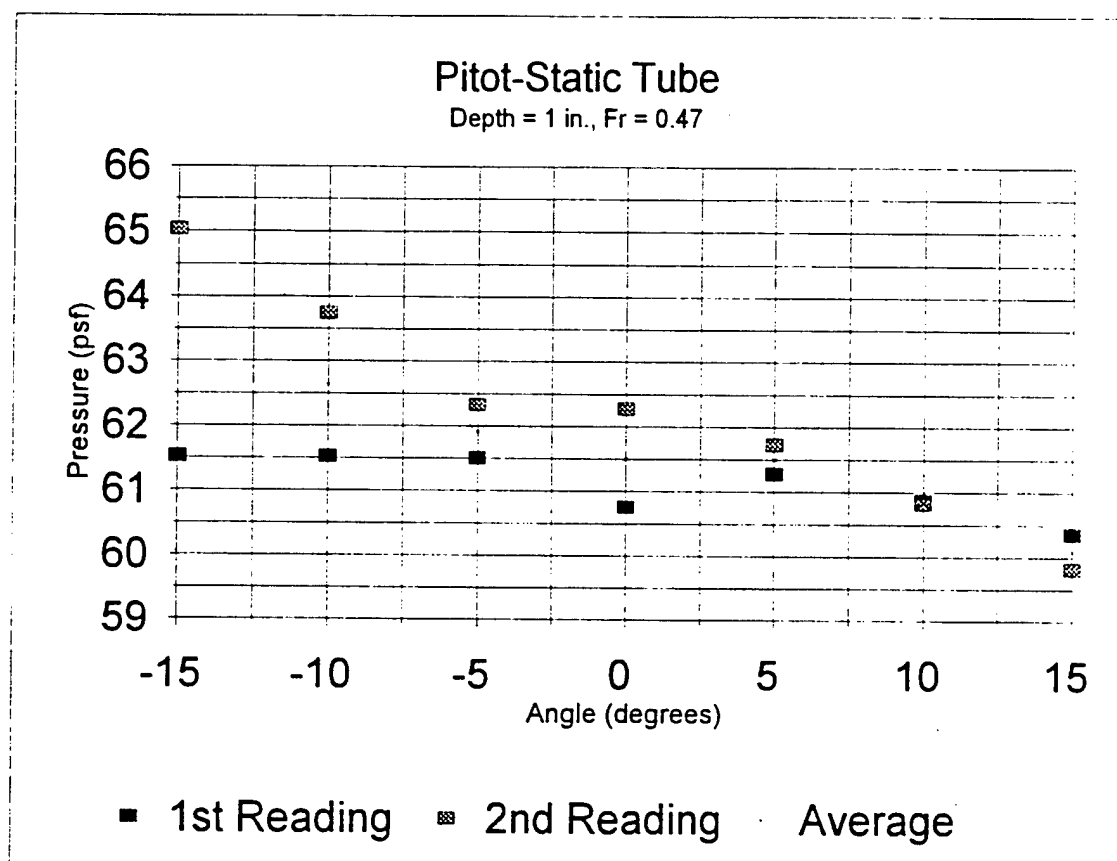
Figure 110: Pitot-static tube data for depth = 1.0 in. at Fr = 0.47.
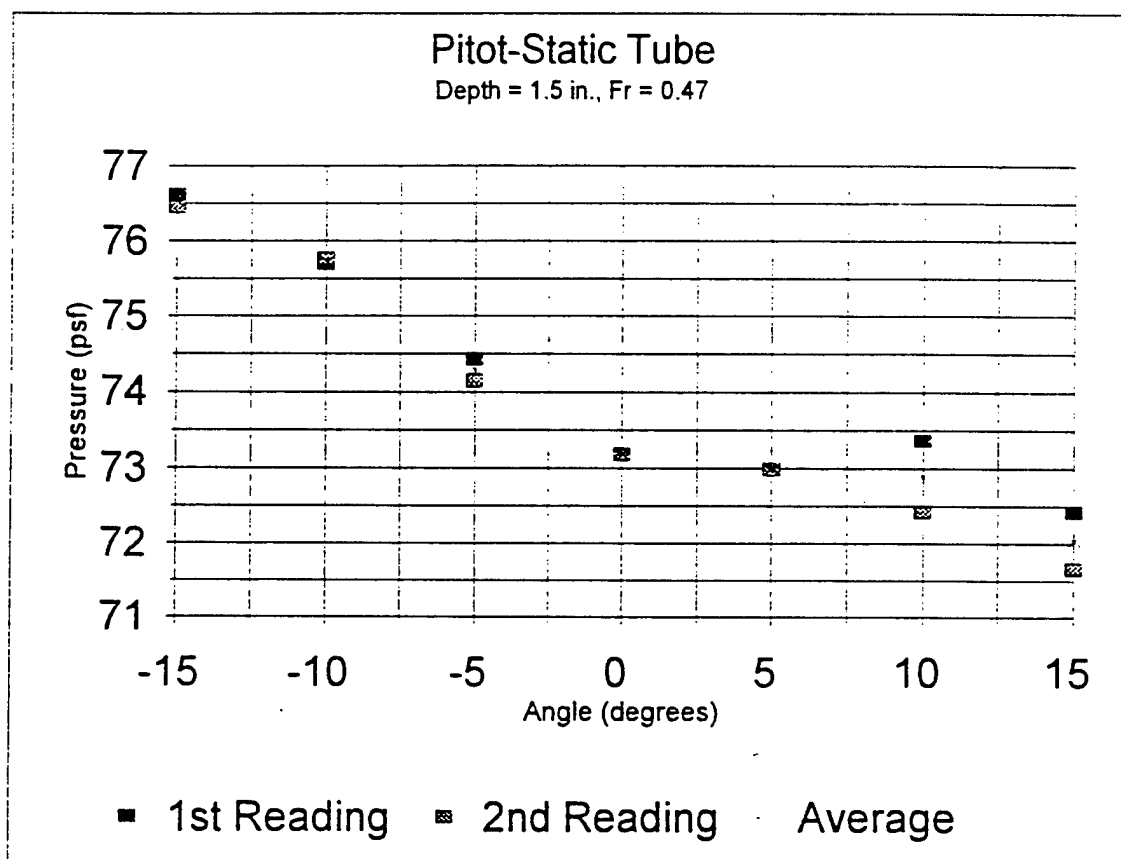
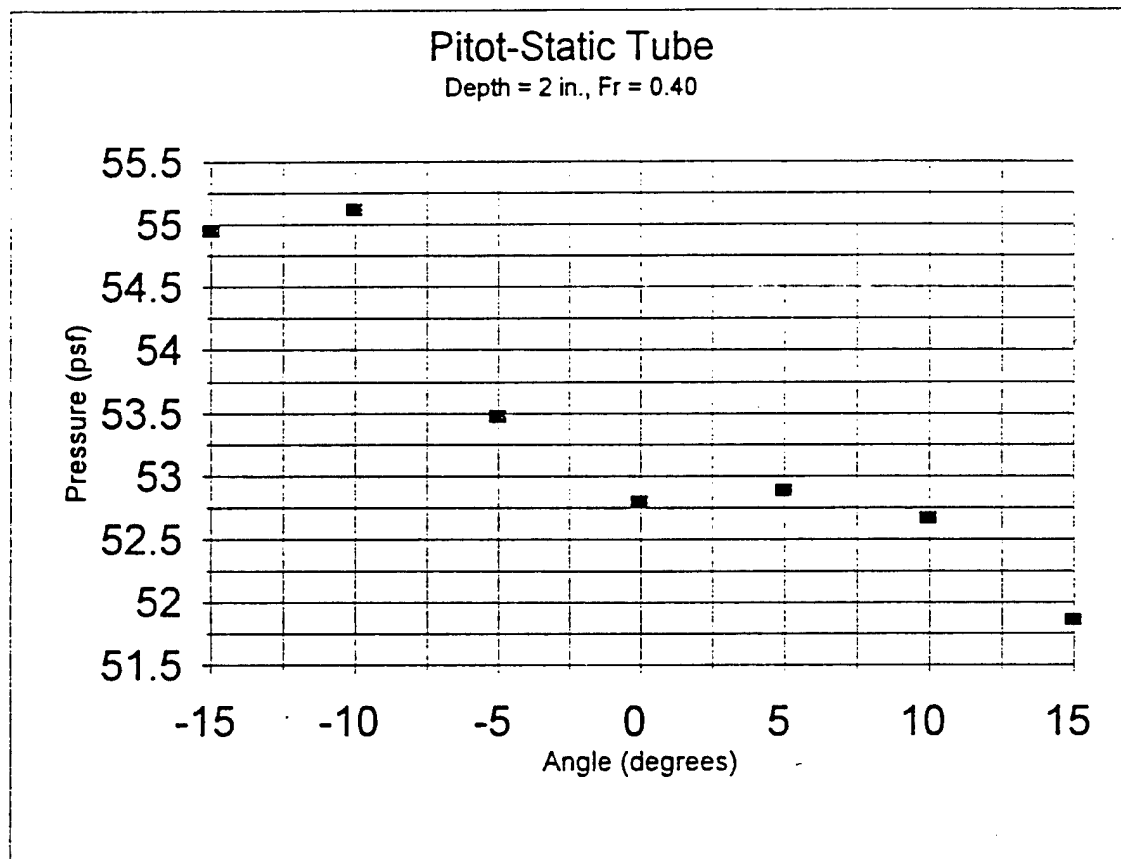Figure 111: Pitot-static tube data for depth = 1.5 in. at Fr = 0.47.
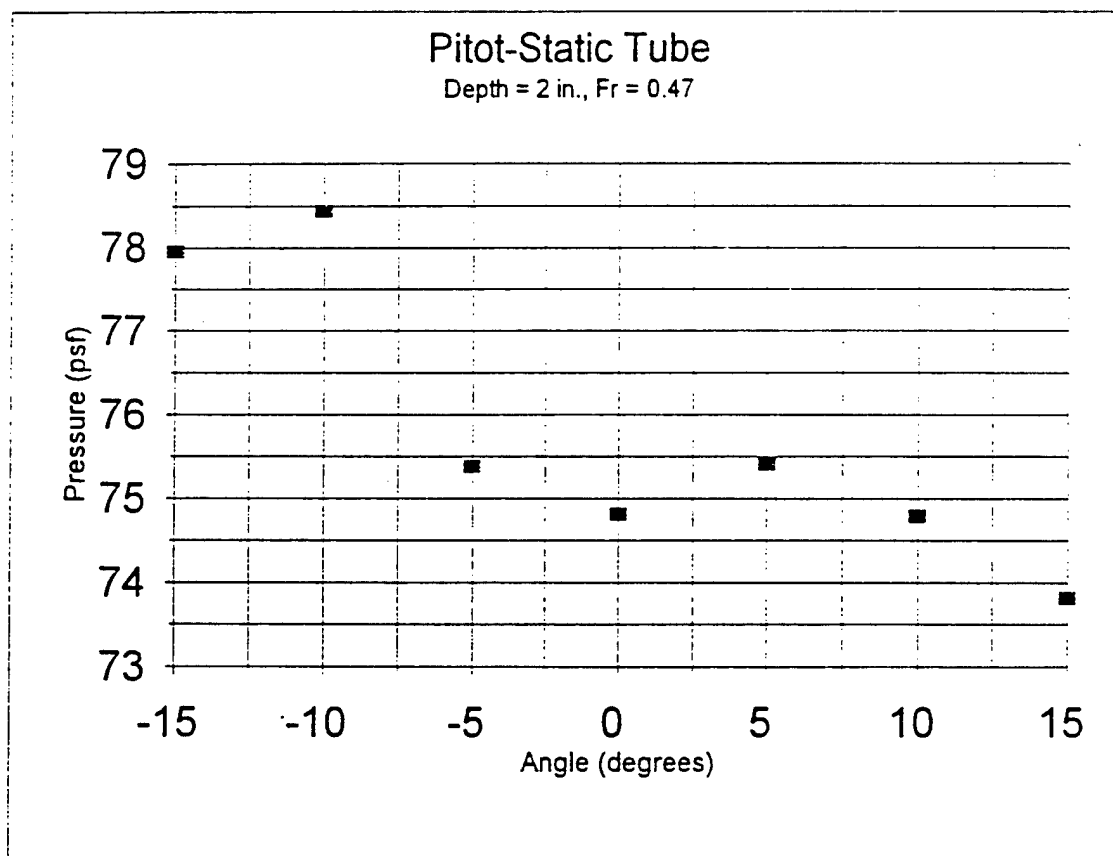
Figure 112: Pitot-static tube data for depth = 2.0 in. at Fr = 0.47.
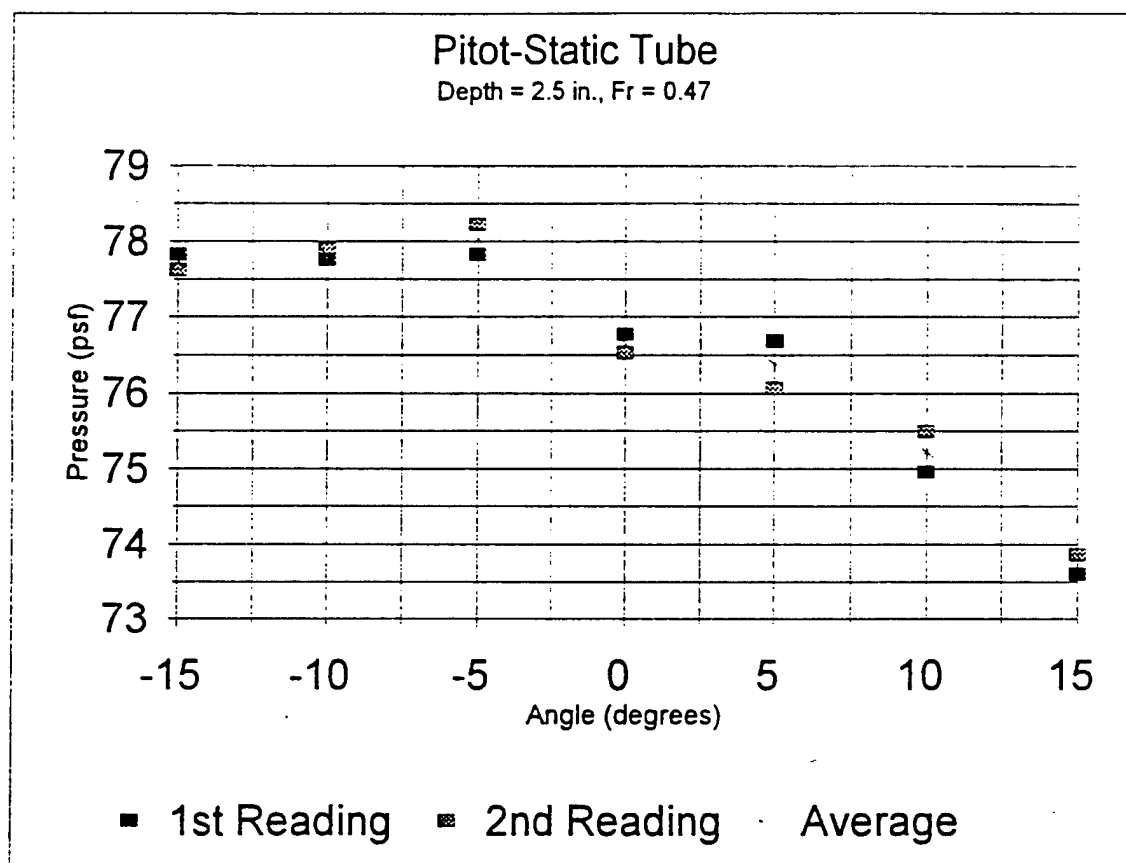
Figure 113: Pitot-static tube data for depth = 2.5 in. at Fr = 0.47.
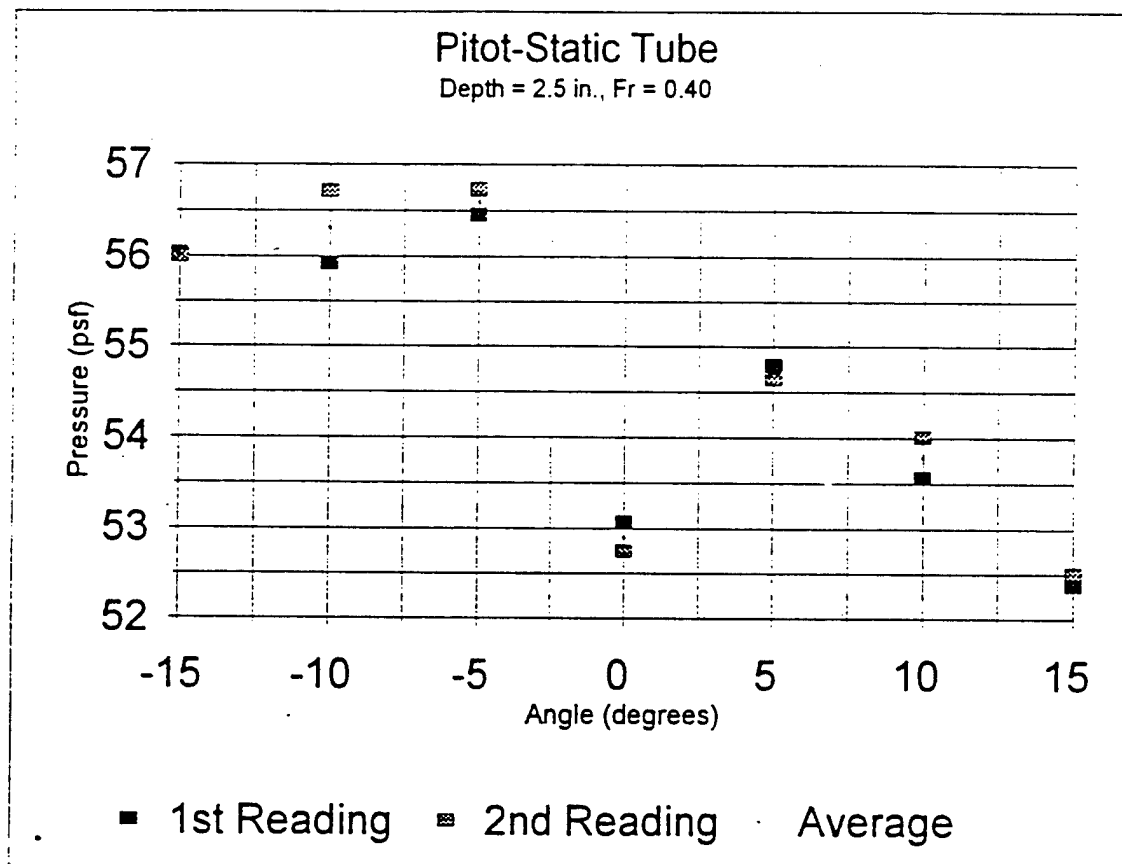
Pitot-Static Tube

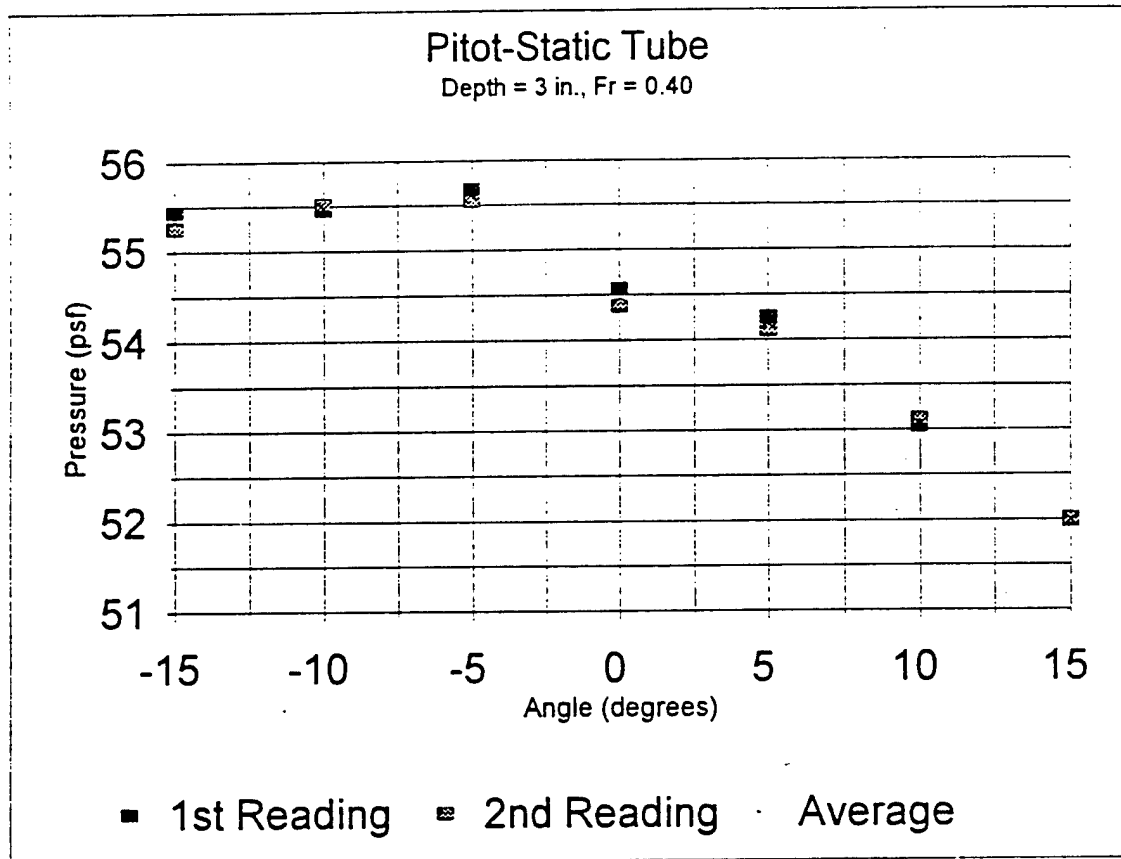Depth = 3 in., Fr = 0.47

- 1st Reading   2nd Reading   · Average

Figure 114: Pitot-static tube data for depth = 3.0 in. at Fr = 0.47.

Figure 115: Pitot-static tube data for angle = 0 degrees at Fr = 0.40.

Figure 116: Pitot-static tube data for angle = 5 degrees at Fr = 0.40.
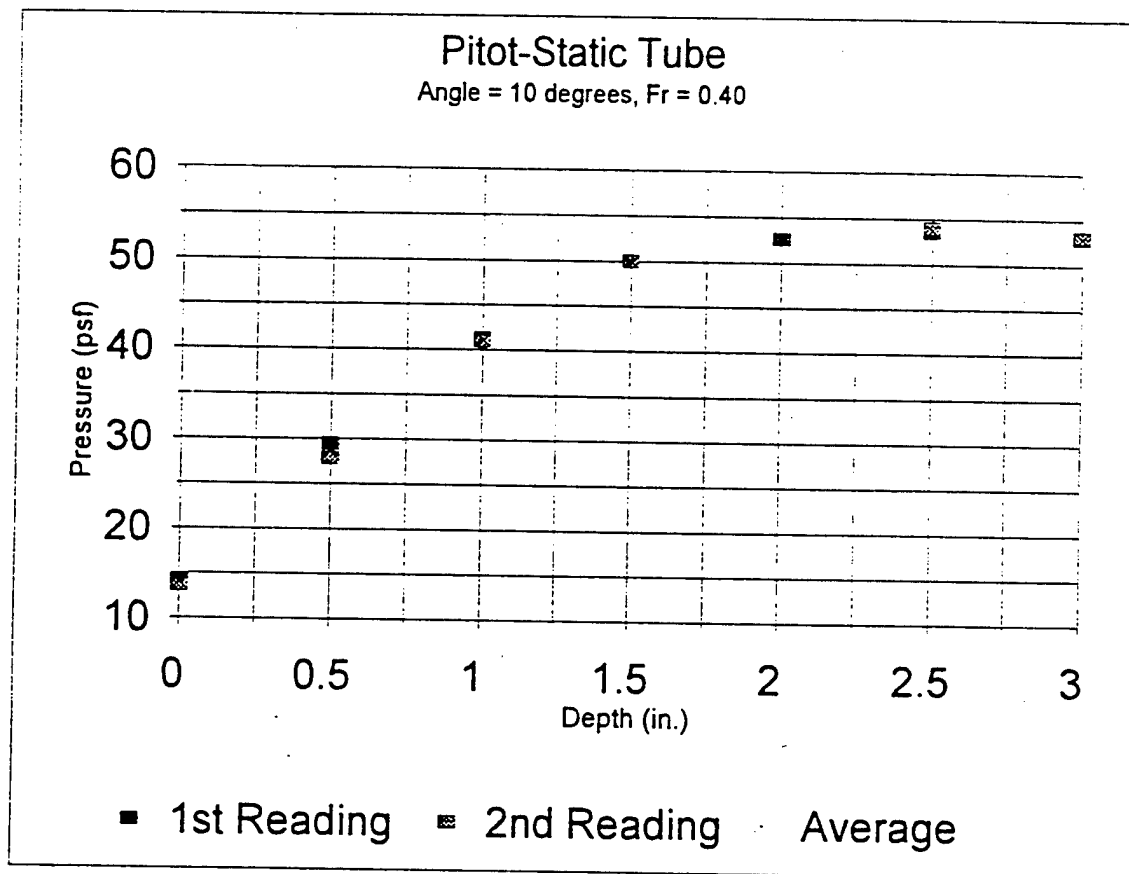
Figure 117: Pitot-static tube data for angle = 10 degrees at Fr = 0.40.
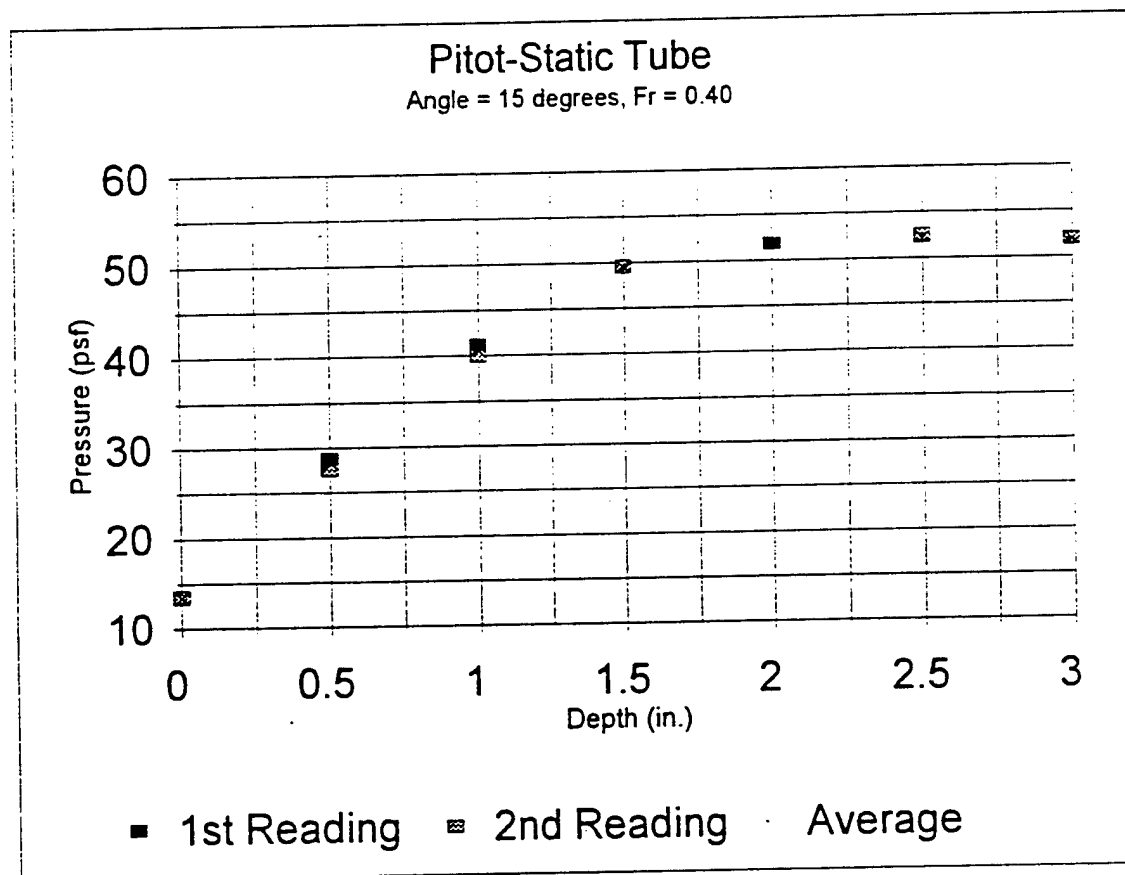
Figure 118: Pitot-static tube data for angle = 15 degrees at Fr = 0.40.

Pitot-Static Tube

Angle = -5 degrees, Fr = 0.40

- 1st Reading   2nd Reading   Average
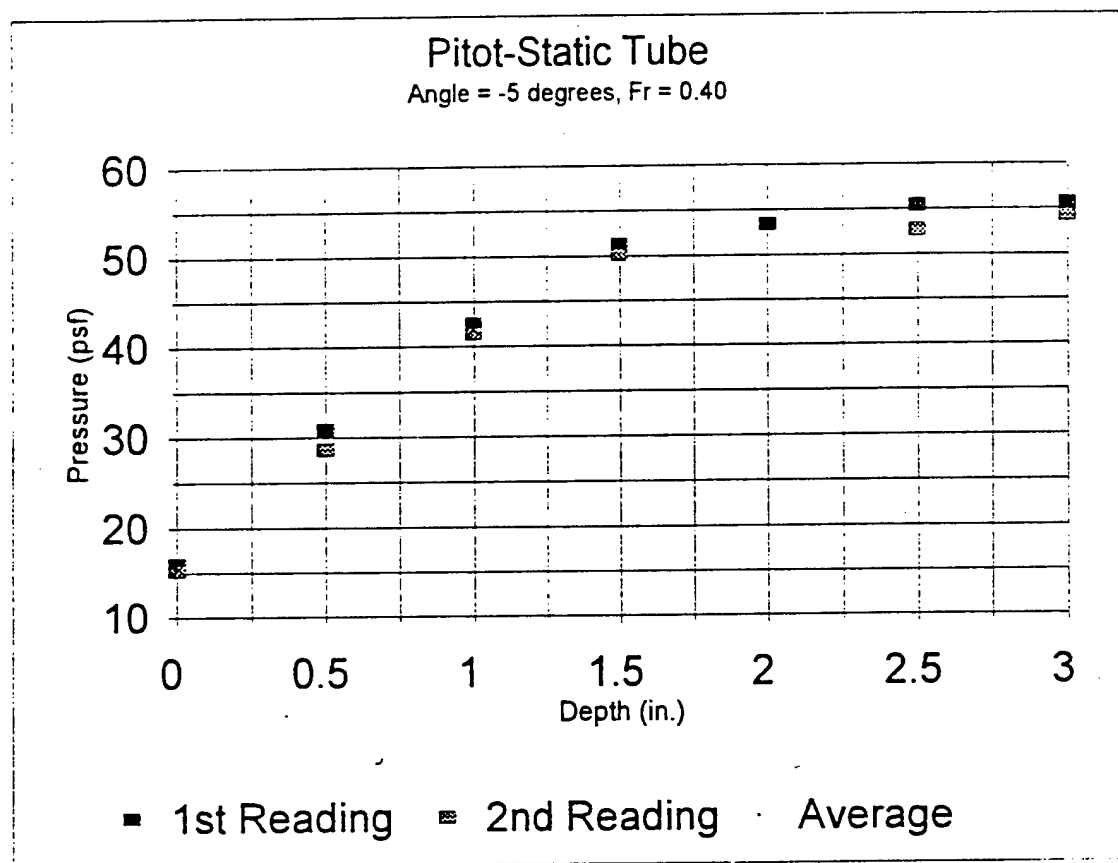
Figure 119: Pitot-static tube data for angle = -5 degrees at Fr = 0.40.
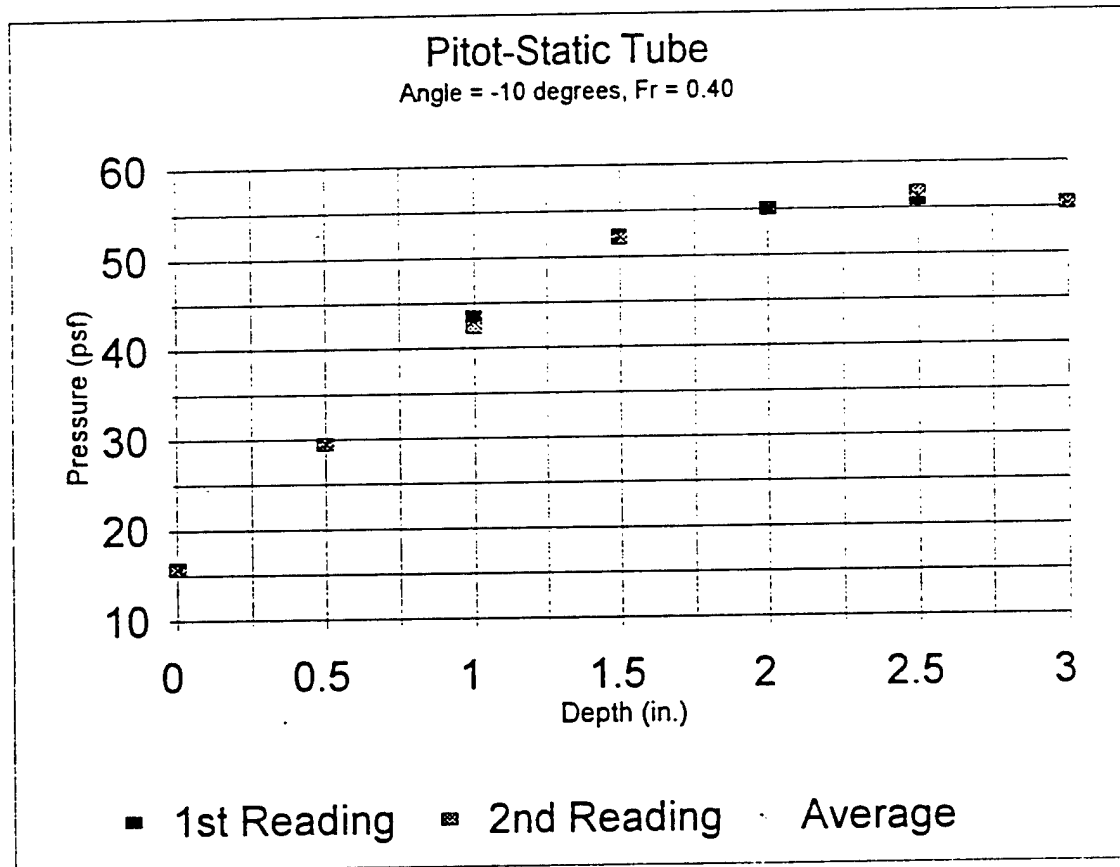
Figure 120: Pitot-static tube data for angle = -10 degrees at Fr = 0.40.
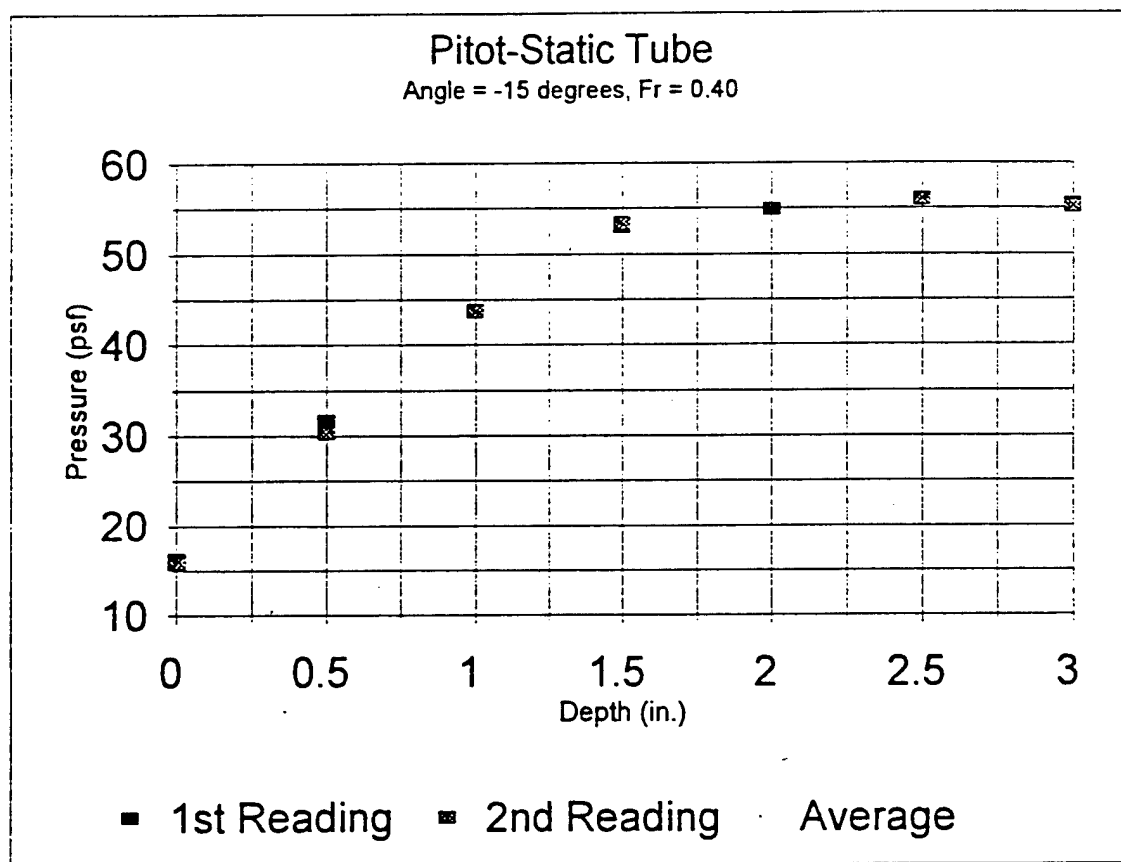
Figure 121: Pitot-static tube data for angle = -15 degrees at Fr = 0.40.
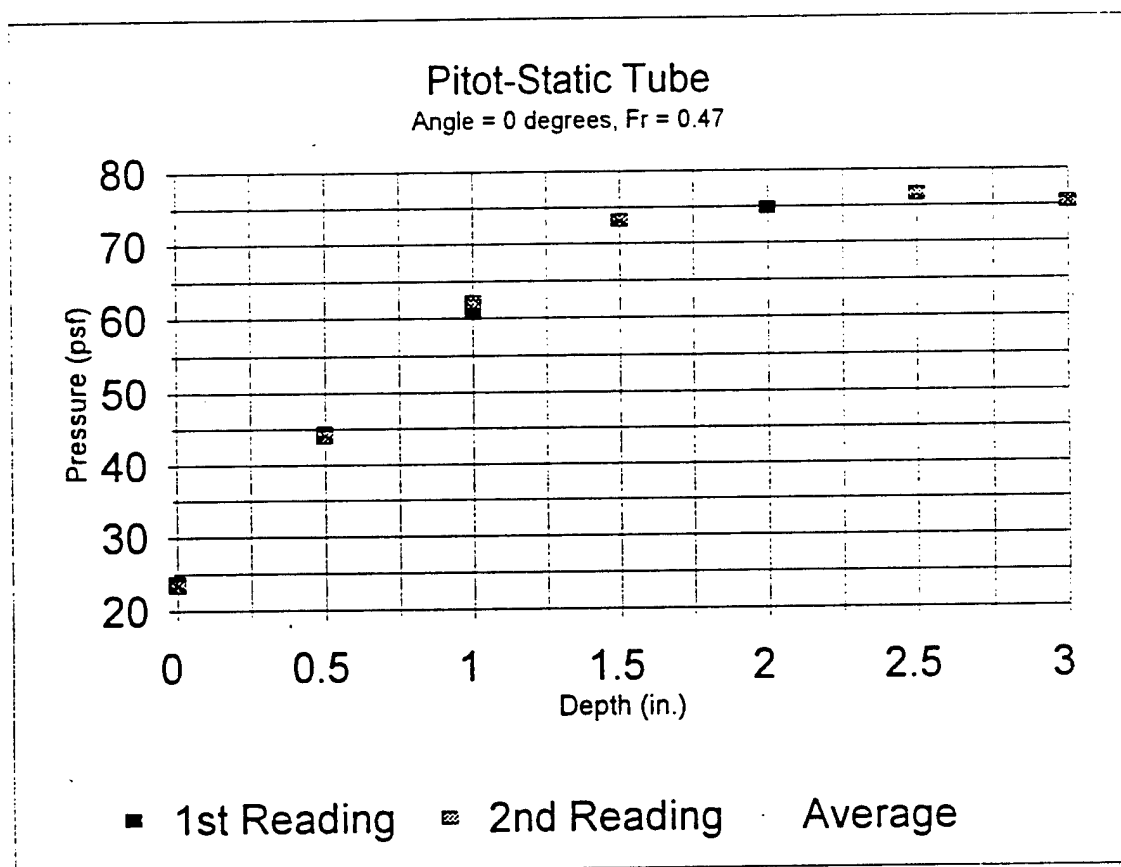
Figure 122: Pitot-static tube data for angle = 0 degrees at Fr = 0.47.
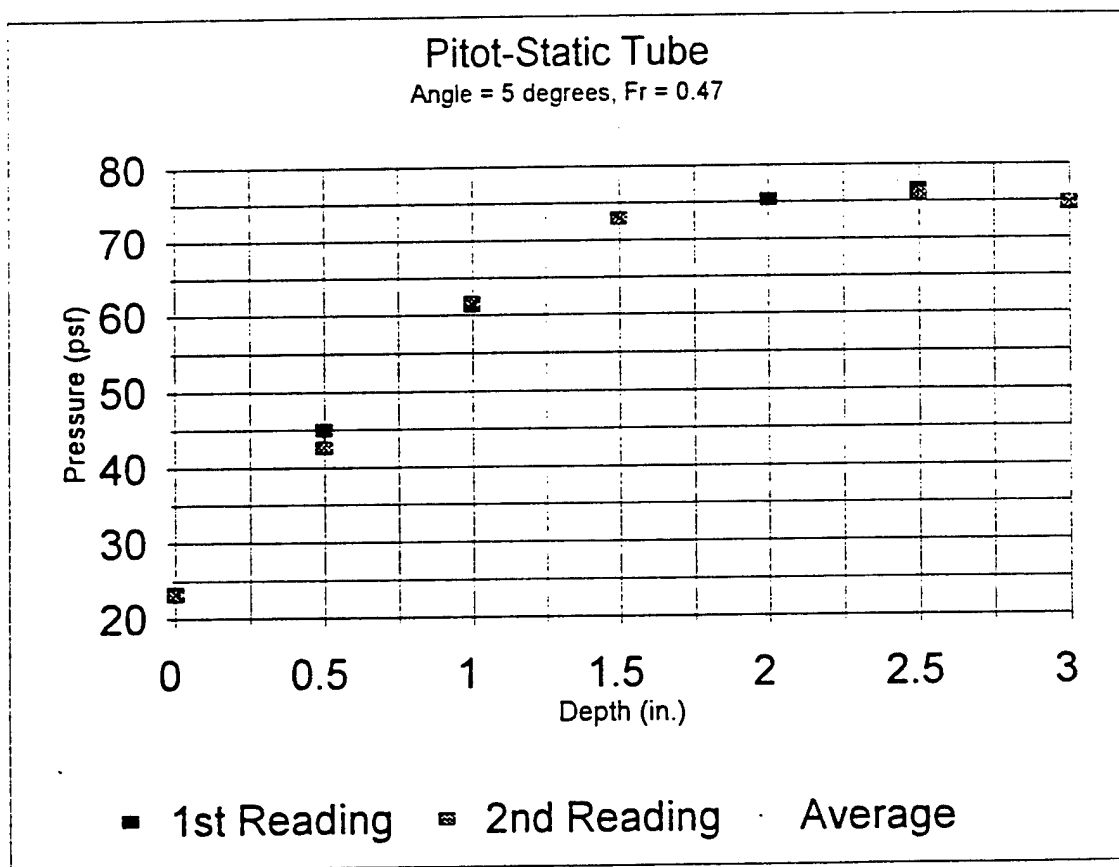
Figure 123: Pitot-static tube data for angle = 5 degrees at Fr = 0.47.
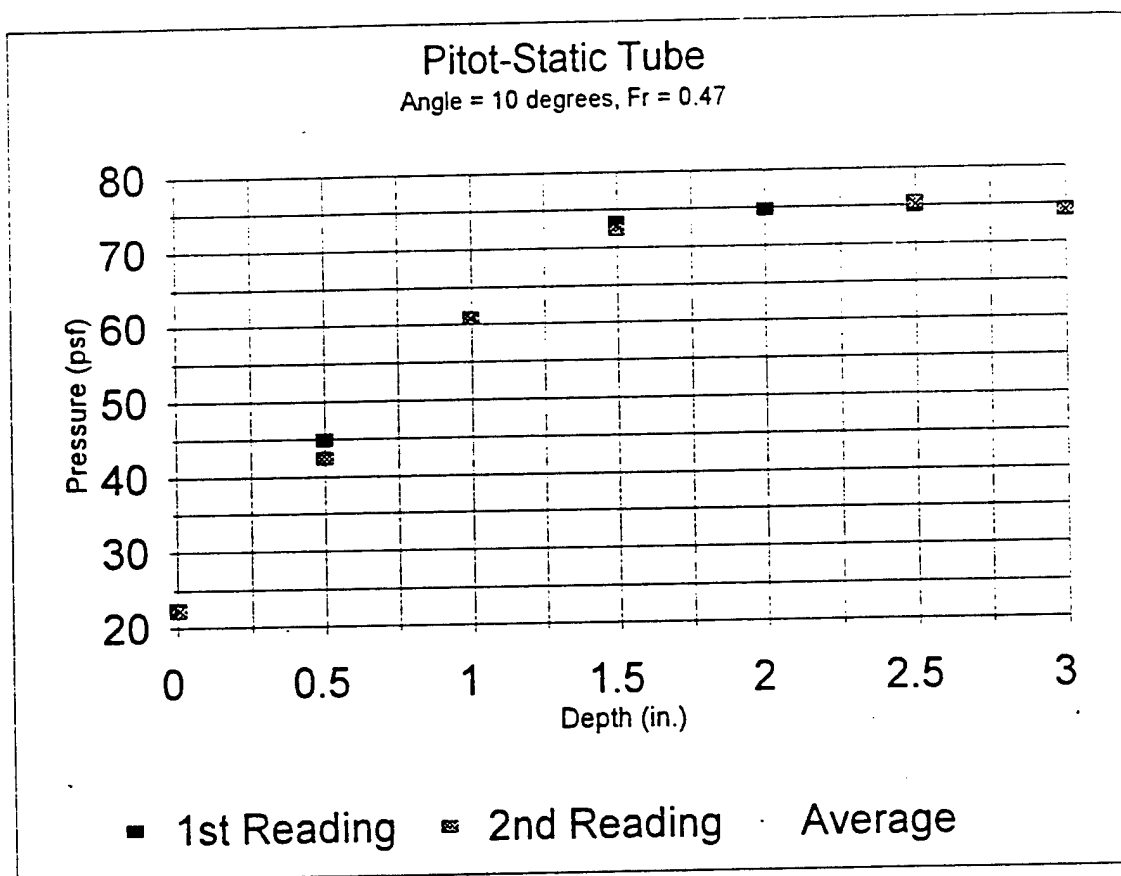
Figure 124: Pitot-static tube data for angle = 10 degrees at Fr = 0.47.
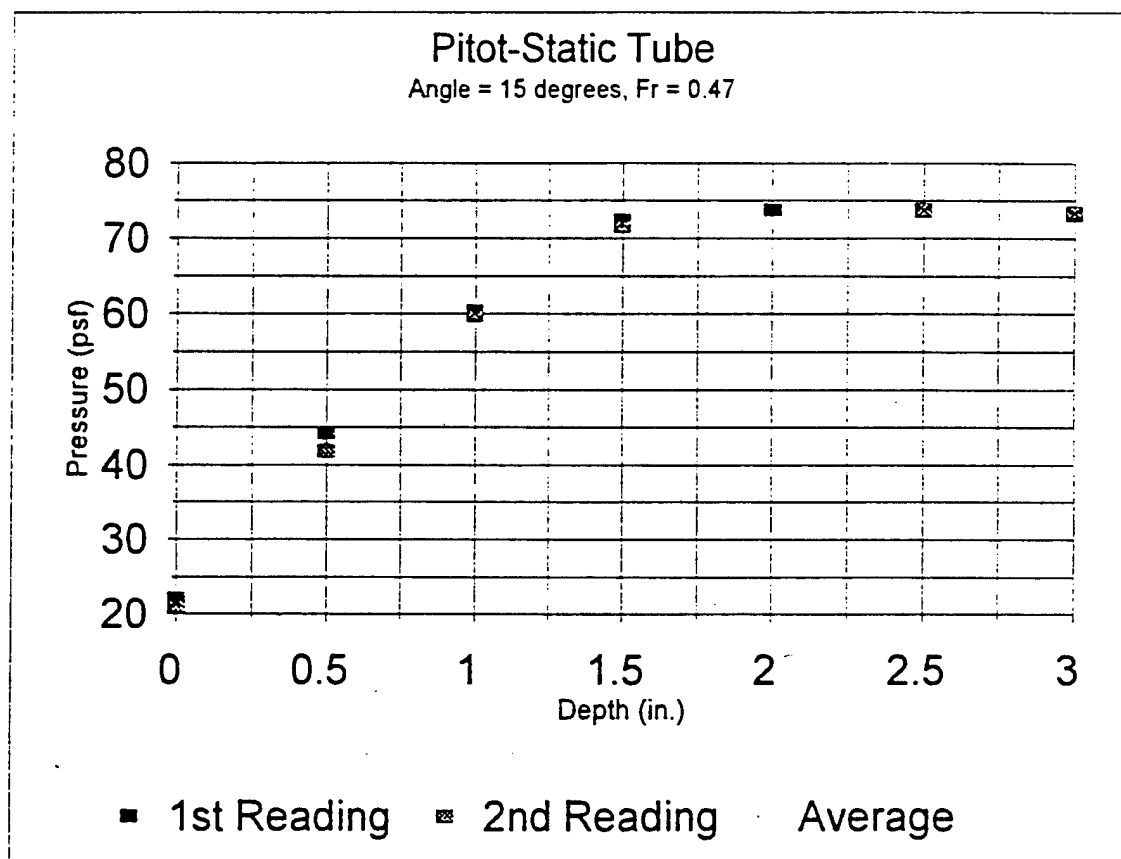
Figure 125: Pitot-static tube data for angle = 15 degrees at Fr = 0.47.
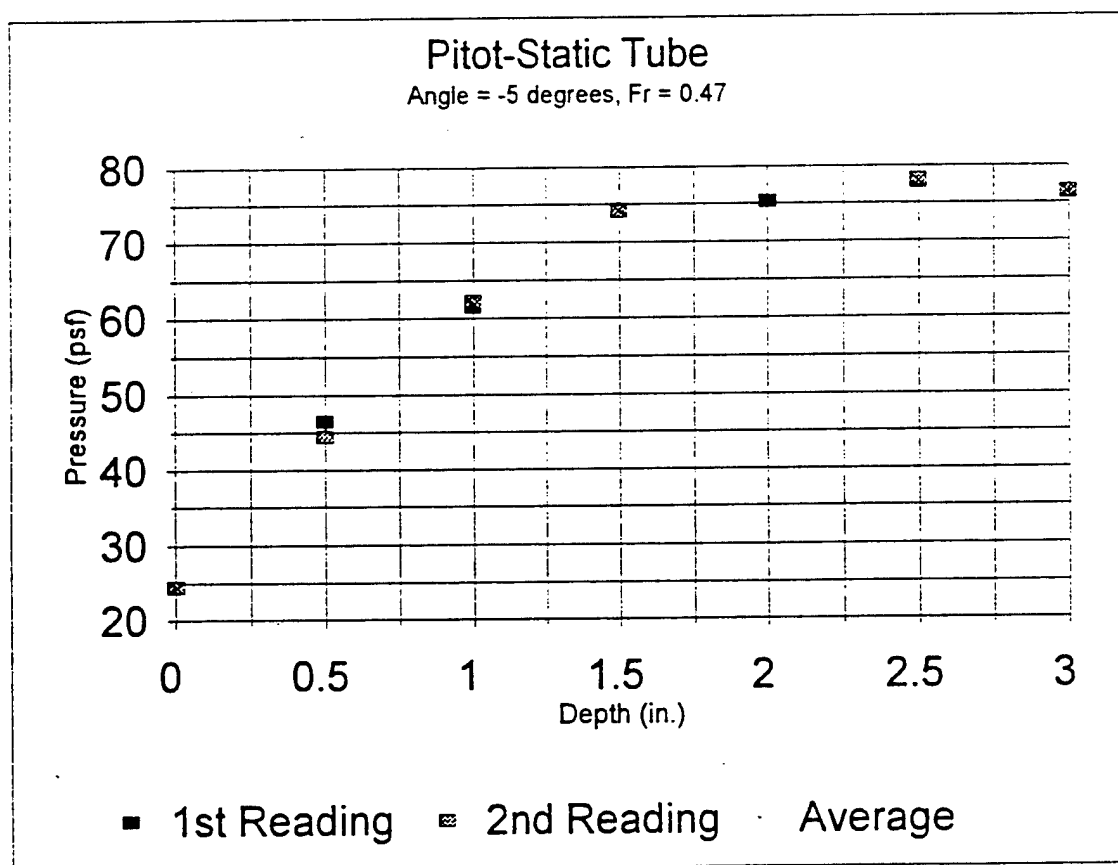
Figure 126: Pitot-static tube data for angle = -5 degrees at Fr = 0.47.
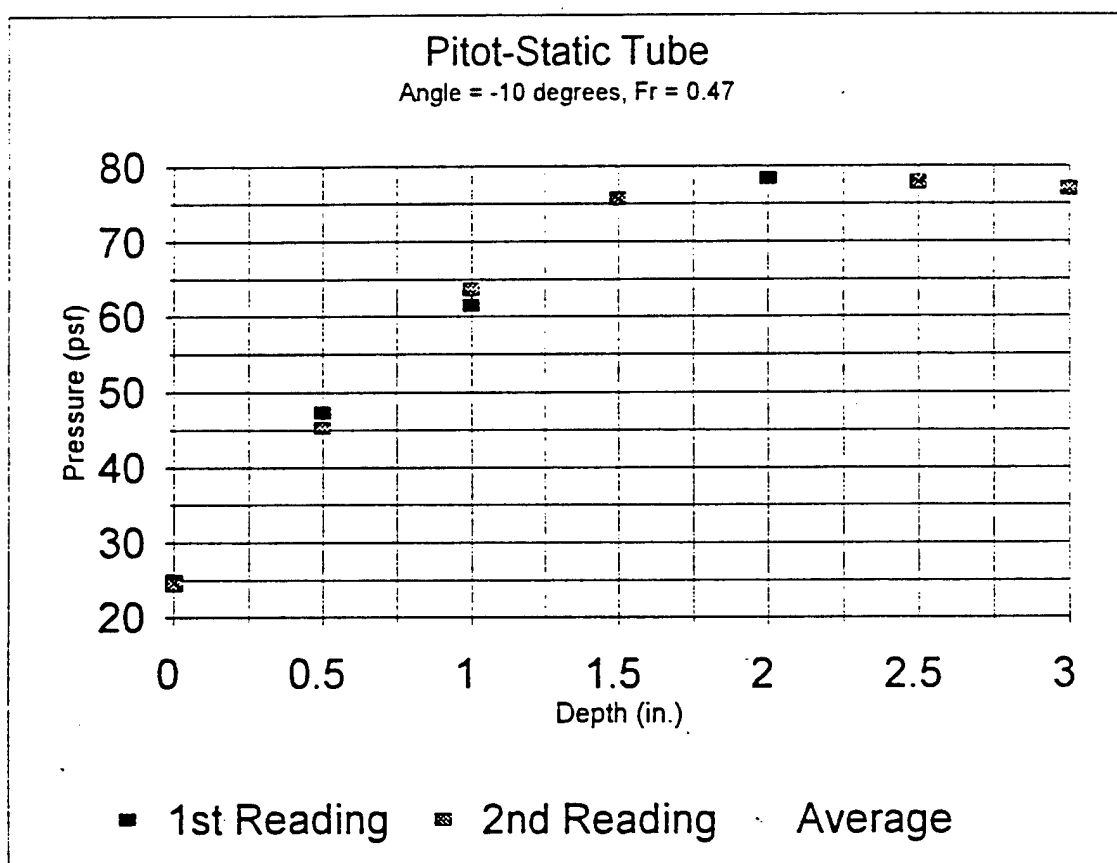
Figure 127: Pitot-static tube data for angle = -10 degrees at Fr = 0.47.

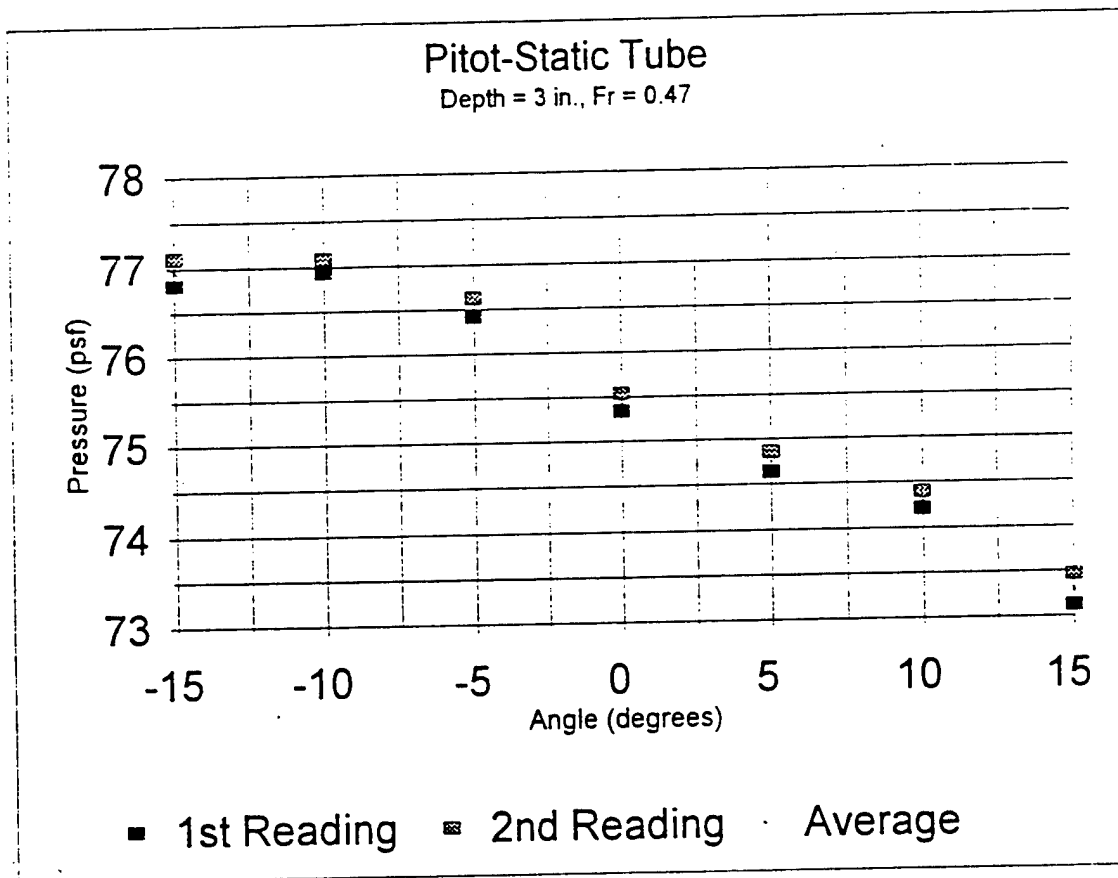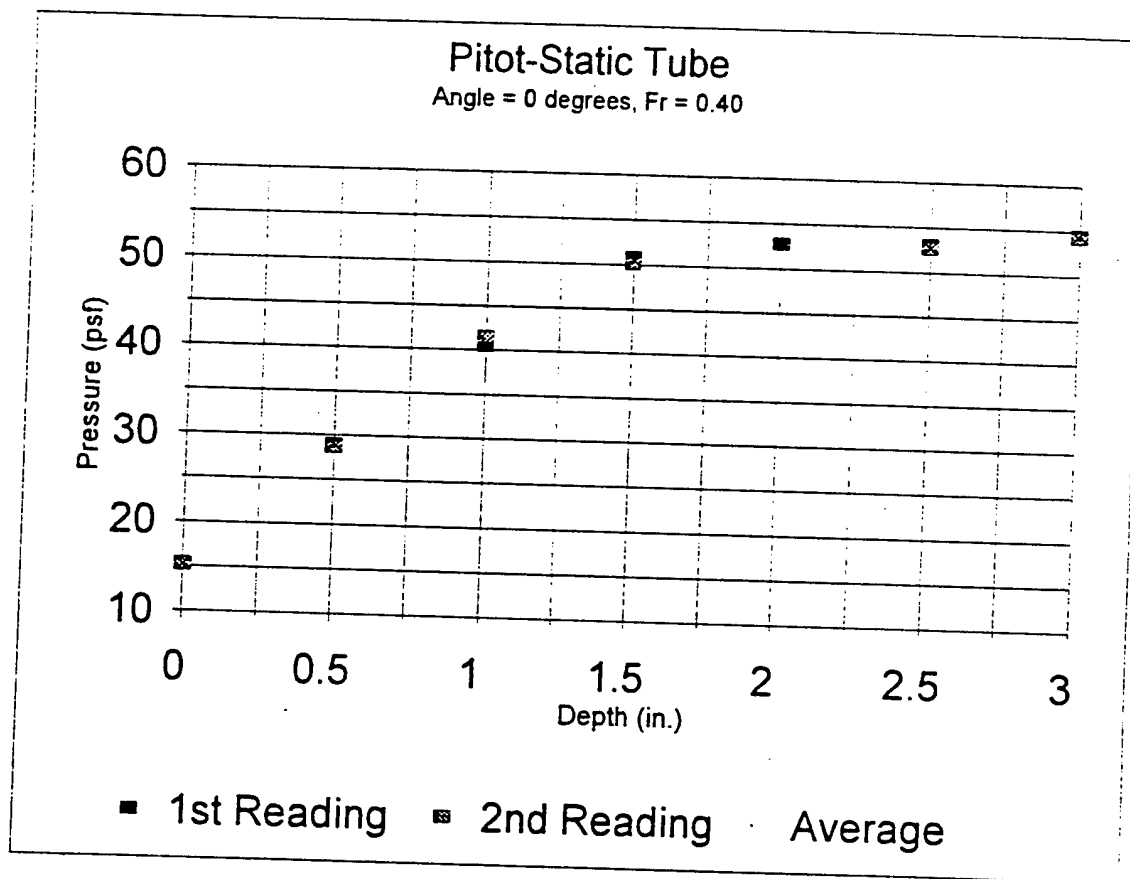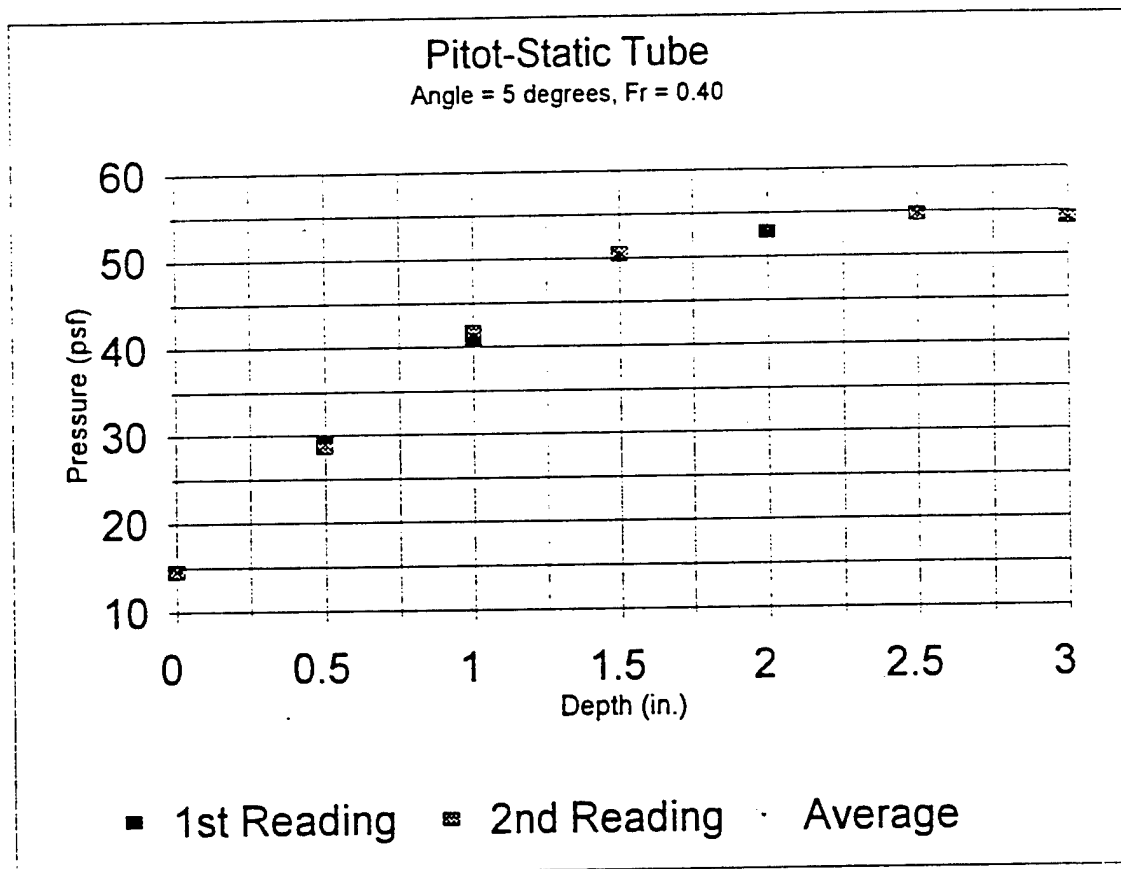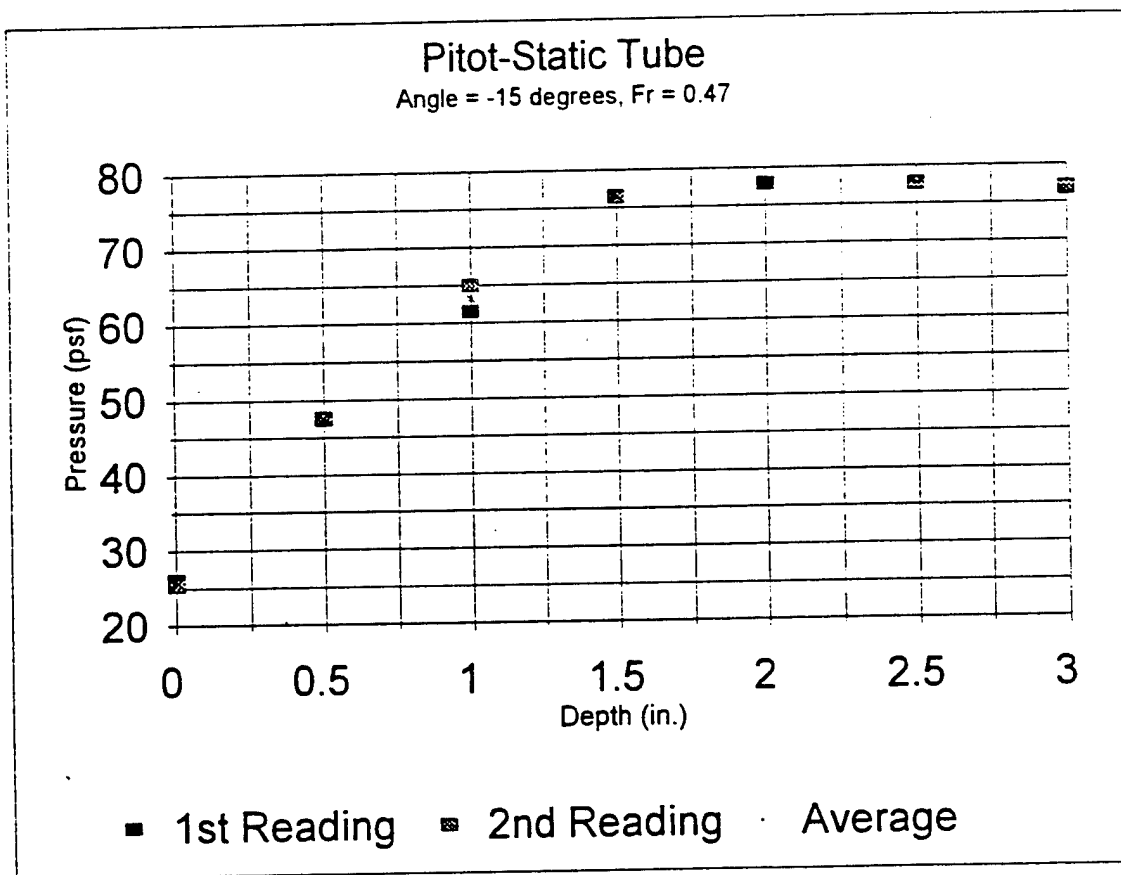Figure 128: Pitot-static tube data for angle = -15 degrees at Fr = 0.47
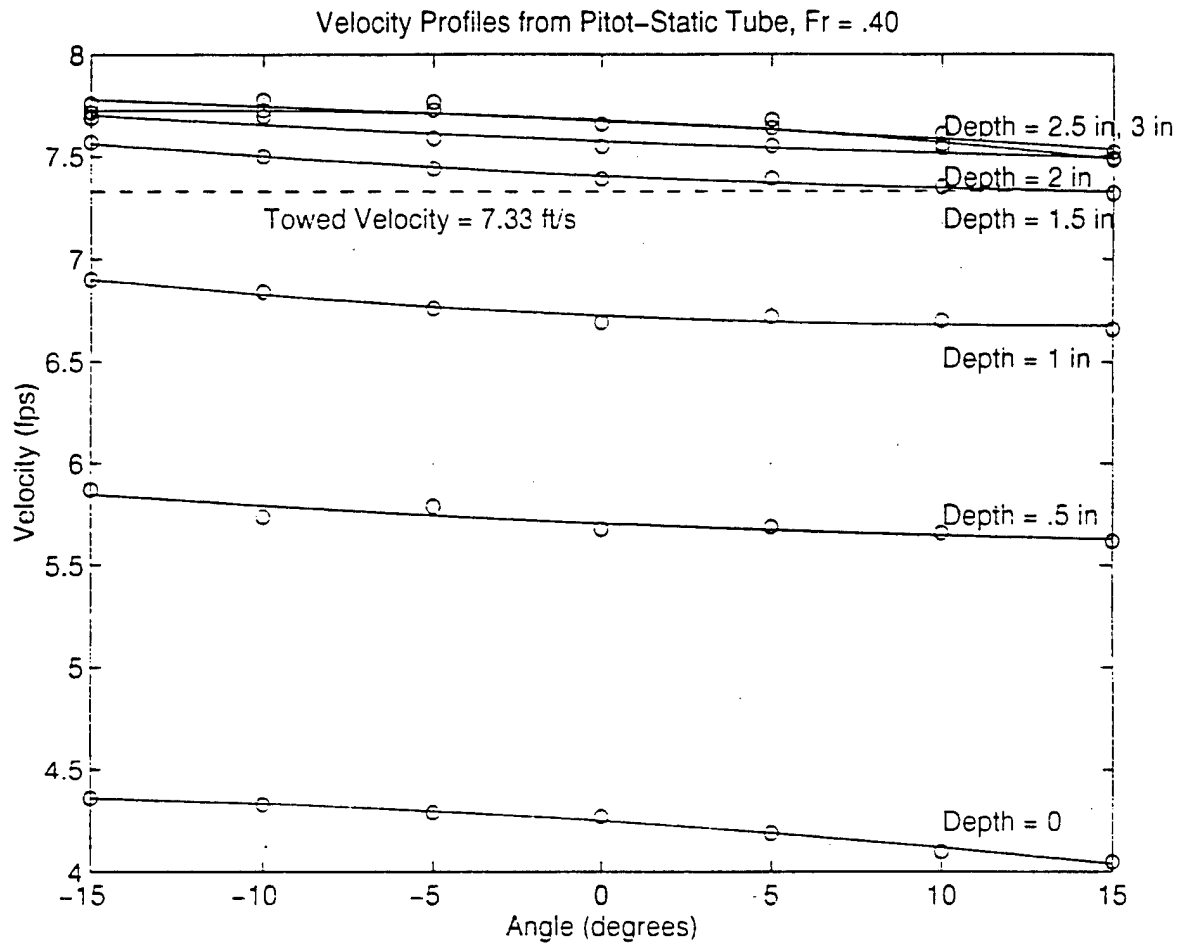
Figure 129. Velocity profiles from Pitot-static tube at Fr = 0.40.
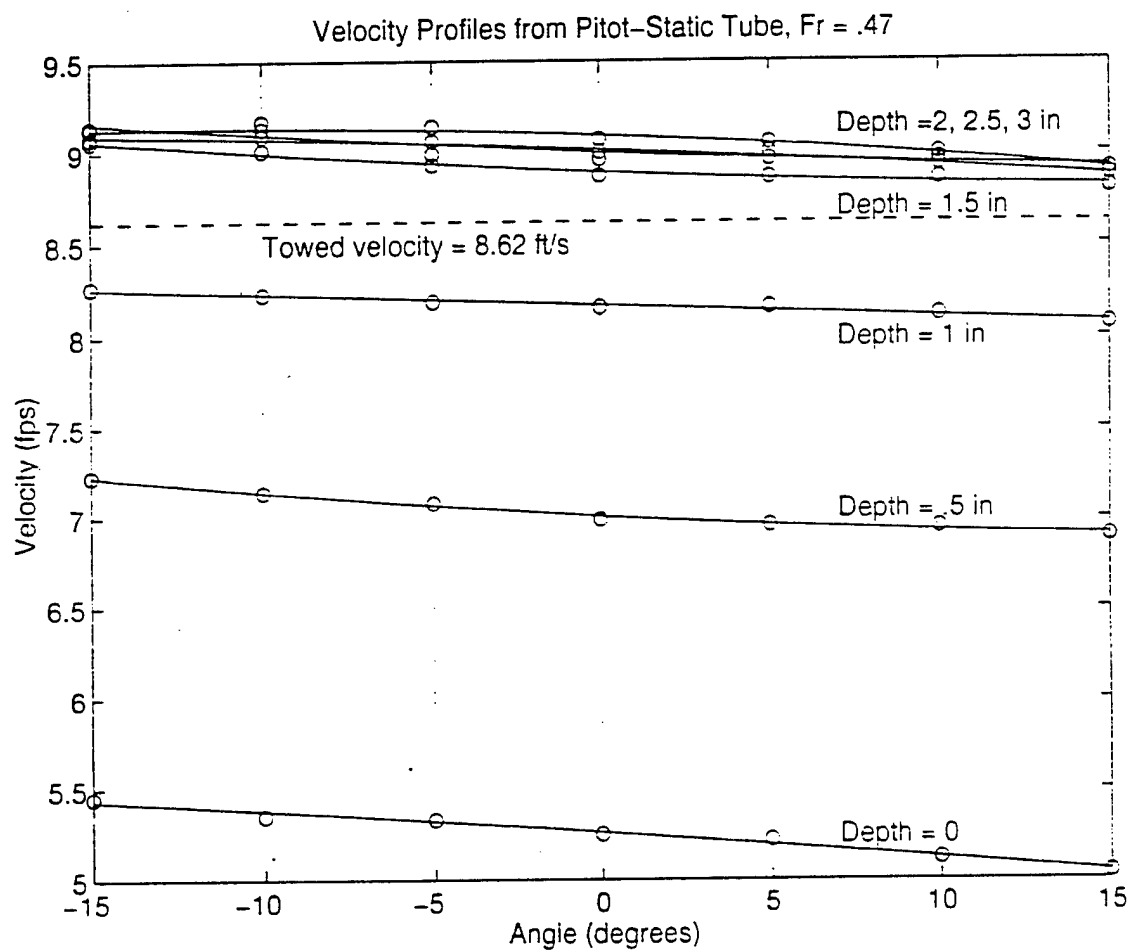
Figure 130. Velocity profiles from Pitot-static tube at Fr = 0.47.

10. NOTES

[1] Hines, Frank, "Waterjet Propulsors Promise Improved Performance," <u>NREC Newsletter</u> Fall 1994: 2.

[2] 21st International Towing Tank Conference Waterjet Group, Trondheim Norway, 15-21 Sept 1996.

[3] Granger, Robert, personal interview, 29 Nov. 1995.

[4] Hodges, Bill, "Strain-gage & Piezoresistive Pressure Transducers," <u>Measurements and Control</u> Apr. 1995: 243.

[5] Granger, Robert, <u>Fluid Mechanics</u> (New York: Dover Publications, Inc., 1995) 713.

[6] F.X. Wortman, <u>AGARD Conference Proceeding no. 224</u>, 1977.

[7] J.P Holman, <u>Experimental Methods for Engineers</u> (New York: McGraw-Hill, Inc., 1994) 73.

[8] Granger, 757.

11. BIBLIOGRAPHY

Granger, Robert A. Fluid Mechanics. New York: Dover Publications, Inc., 1995.

Hines, Frank. "Waterjet Propulsors Promise Improved Performance." NREC Newletter Fall 1994: 1-3.

Hodges, Bill. "Strain-gage & Piezoresistive Pressure Transducers." Measurements and Control Apr. 1995: 243.

Holman, J. P. Experimental Methods for Engineers. New York: McGraw-Hill, Inc., 1994.

Munson, Bruce R., Donald F. Young, Theodore H. Okiishi. Fundamentals of Fluid Mechanics. New York: John Wiley & Sons, Inc., 1994.

Wortman, F. X. AGARD Conference Proceedingno. 224. 1977.

United States. Stricker, John G., Alan J. Becnel, Robert L. Kiang, and John G. Purnell. David Taylor Research Center. Surface Ship Waterjet Propulsion S t u d i e s. Washington: GPO, 1991.

21st International Towing TAnk Conference Waterjet Group. Trondheim, Norway, 15-21 Sept. 1996.

APPENDIX A: UNCERTAINTY ANALYSIS

Since pressure measurements are always difficult to repeat, the readings from any given port are not all the same. In this project, the static ports all had a range of readings, as can be seen in Figures 18 - 57. An uncertainty analysis is a means of quantifying the range of the data.

Using the Student's t distribution to find the uncertainty, the standard deviation of the mean, σ_m, must be known. It can be found using all the data points, finding the standard deviation of the population, σ, and then using:

$$\sigma_m = \frac{\sigma}{\sqrt{n}} \qquad (A.1)$$

where n is the number of readings taken.

Next, the degrees of freedom, must be found. It is simply one less than the number of readings. Using this number, the t factor for any given confidence interval is found on a table of the Student's t Distribution. The uncertainty, or the range of values expected for each measurement, is determined by multiplying the t factor and the standard deviation of the mean.

The results of the uncertainty analysis are shown in Tables A.1 and A.2. The analysis is done using a 95% confidence interval, which means that 95% of the readings should fall within the range determined. The largest uncertainty is +/- 0.97 psf for port 23 at a Froude number of 0.47. This means the average for the population at large for this port is -2.25 ± 0.97 psf at a 95% confidence interval. The average for all the ports is -3.20 ± 0.461 psf at a 95% confidence interval.

Port	Average	# of readings	t95	stdm	delta
1	-2.64185	20	2.093	0.409646	0.85739
2	-0.828168	22	2.08	0.461865	0.960679
3	-1.385561	19	2.101	0.032474	0.068228
4	-1.326906	18	2.11	0.026087	0.055044
5	-2.09785	20	2.093	0.222017	0.464682
6	-0.958225	16	2.131	0.023233	0.049509
7	-2.092437	22	2.08	0.155532	0.323507
8	-1.482755	20	2.093	0.014837	0.031054
9	-2.321636	21	2.086	0.115069	0.240034
10	-2.370124	23	2.074	0.089412	0.18544
11	-0.392755	20	2.093	0.052642	0.11018
12	-1.257992	18	2.11	0.355664	0.750452
13	-2.47986	22	2.08	0.193632	0.402755
14	-2.385243	19	2.101	0.258647	0.543418
15	-2.968547	18	2.11	0.13266	0.279912
16	-2.414191	19	2.101	0.038299	0.080466
17	-4.297436	18	2.11	0.095052	0.200559
18	-2.787285	22	2.08	0.379441	0.789238
19	-2.847996	22	2.08	0.343469	0.714416
20	-1.293648	22	2.08	0.184983	0.384764
21	-1.315822	23	2.074	0.339799	0.704743
22	-2.624518	23	2.074	0.337475	0.699924
23	-2.264953	23	2.074	0.447664	0.928455
24	-3.161163	22	2.08	0.170361	0.354351
25	-1.85218	17	2.12	0.406608	0.862009
26	-3.44182	18	2.11	0.240873	0.508242
27	-3.748487	18	2.11	0.42263	0.89175
28	-4.245274	23	2.074	0.19876	0.412229
29	-2.025709	17	2.12	0.175178	0.371378
30	-3.040153	17	2.12	0.381877	0.809579
31	-3.807007	22	2.08	0.295312	0.614249
32	-5.673529	23	2.074	0.353003	0.732128
33	-3.817877	23	2.074	0.096179	0.199475
34	-5.255268	23	2.074	0.332526	0.689658
35	-5.595268	23	2.074	0.361847	0.75047
36					
37	-5.579682	14	2.16	0.089287	0.19286
38					
39	-7.73619	17	2.12	0.217519	0.461141
40	-7.528634	15	2.145	0.070474	0.151166
41	-7.076073	19	2.101	0.251128	0.52762
42	-7.626599	19	2.101	0.162248	0.340883

Table A.1 Uncertainty analysis for static pressure ports at Fr = 0.40.

Port	Average	# of readings	t95	stdm	delta
1	-6.306637	13	2.179	0.027554	0.06004
2	0.876156	19	2.101	0.091236	0.191687
3	-2.042791	16	2.131	0.036922	0.078681
4	-2.044458	18	2.11	0.01863	0.039309
5	-2.277166	16	2.131	0.102252	0.217899
6	-1.32668	18	2.11	0.044702	0.09432
7	-2.545974	21	2.086	0.047759	0.099626
8	-2.396255	22	2.08	0.018682	0.038859
9	-2.518165	20	2.093	0.051973	0.10878
10	-2.273528	22	2.08	0.099522	0.207006
11	-0.272165	20	2.093	0.120615	0.252447
12	-1.803105	18	2.11	0.207743	0.438339
13	-3.118307	22	2.08	0.179773	0.373929
14	-2.949772	18	2.11	0.180798	0.381483
15	-2.815327	18	2.11	0.110532	0.233221
16	-3.361275	17	2.12	0.07891	0.16729
17	-6.037073	14	2.16	0.058094	0.125483
18	-3.481131	20	2.093	0.328347	0.68723
19	-3.313702	20	2.093	0.218183	0.456656
20	-1.453988	21	2.086	0.204339	0.426251
21	-1.288793	22	2.08	0.355685	0.739824
22	-2.757884	22	2.08	0.337471	0.70194
23	-2.24652	22	2.08	0.466139	0.969568
24	-3.415477	22	2.08	0.160643	0.334137
25	-1.990073	18	2.11	0.288464	0.60866
26	-3.844517	18	2.11	0.232611	0.490809
27	-3.583962	18	2.11	0.336964	0.710993
28	-4.187295	22	2.08	0.111518	0.231958
29	-1.84292	16	2.131	0.11722	0.249796
30	-2.618406	18	2.11	0.360665	0.761004
31	-4.233105	21	2.086	0.259091	0.540464
32	-5.463581	22	2.08	0.287318	0.597622
33	-4.353126	22	2.08	0.105155	0.218723
34	-3.697866	7	2.447	0.036804	0.090059
35	-5.914944	22	2.08	0.31973	0.665037
36					
37	-6.441061	15	2.145	0.074058	0.158855
38					
39	-8.175414	17	2.12	0.117566	0.24924
40	-8.426811	16	2.131	0.058382	0.124413
41	-7.752093	30	2.045	0.142531	0.291476
42	-8.439311	16	2.131	0.053582	0.114183

Table A.2: Uncertainty analysis for static pressure ports at Fr = 0.47.